# THE STATISTICS OF FINITE BANDWIDTH MODULATED ACOUSTICS SIGNALS PROPAGATED TO LONG RANGES IN THE OCEAN, INCLUDING MULTIPLE SOURCE EFFECTS

Peter N. Mikhalevsky

UNCLASS

SECURITY CLASSIFICATION OF THIS PAGE (When Data Entered)

| REPORT DOCUMENTATION PAGE | | READ INSTRUCTIONS BEFORE COMPLETING FORM |
|---|---|---|
| 1. REPORT NUMBER | 2. GOVT ACCESSION NO. | 3. RECIPIENT'S CATALOG NUMBER |
| 4. TITLE (and Subtitle)<br>The Statistics of Finite Bandwidth Modulated Acoustic Signals Propagated to Long Ranges in the Ocean, Including Multiple Source Effects | | 5. TYPE OF REPORT & PERIOD COVERED<br>THESIS<br>6. PERFORMING ORG. REPORT NUMBER |
| 7. AUTHOR(s)<br>Peter N. Mikhalevsky | | 8. CONTRACT OR GRANT NUMBER(s) |
| 9. PERFORMING ORGANIZATION NAME AND ADDRESS<br>Massachusetts Institute of Technology<br>Cambridge, Massachusetts | | 10. PROGRAM ELEMENT, PROJECT, TASK AREA & WORK UNIT NUMBERS |
| 11. CONTROLLING OFFICE NAME AND ADDRESS<br>CODE 031<br>Naval Postgraduate School<br>Monterey, California 93940 | | 12. REPORT DATE<br>Feb 79<br>13. NUMBER OF PAGES<br>319 |
| 14. MONITORING AGENCY NAME & ADDRESS(if different from Controlling Office) | | 15. SECURITY CLASS. (of this report)<br>UNCLASS<br>15a. DECLASSIFICATION/DOWNGRADING SCHEDULE |

16. DISTRIBUTION STATEMENT (of this Report)

APPROVED FOR PUBLIC RELEASE; DISTRIBUTION UNLIMITED

17. DISTRIBUTION STATEMENT (of the abstract entered in Block 20, if different from Report)

18. SUPPLEMENTARY NOTES

19. KEY WORDS (Continue on reverse side if necessary and identify by block number)

Finite Bandwidth, Modulated Acoustic Signals, Propagation, Multiple Source Effects

20. ABSTRACT (Continue on reverse side if necessary and identify by block number)

SEE REVERSE

DD FORM 1 JAN 73 1473 EDITION OF 1 NOV 65 IS OBSOLETE
S/N 0102-014-6601

(Page 1)



UNCLASS

SECURITY CLASSIFICATION OF THIS PAGE (When Data Entered)

## ABSTRACT

The statistics of acoustic signals propagated to long ranges in the ocean are investigated in detail in this thesis. The phase random model of multipath propagation is extended to include finite bandwidth and/or modulated sources as well as multiple source configurations. The theoretical analyses include the derivation of many new probability density functions for these new cases as well as for the single narrowband source.

The probability density function for $\dot{\Lambda}$, the time rate of change of the level in decibels for the single narrowband source is derived. $P_{\dot{\Lambda}}(\dot{\Lambda})$ depends only upon $\nu^2$, the single path mean square phase rate, which can be related to certain ocean dynamical processes. The analysis of finite bandwidth and/or modulated sources reveals that the amplitude and amplitude rate densities (including $P_{\dot{\Lambda}}(\dot{\Lambda})$) are independent of the finite bandwidth and modulation effects, but the density of the time rate-of-change of the multipath phase $\dot{\phi}$ is sensitive to these effects. Thus, fitting $P_{\dot{\Lambda}}(\dot{\Lambda})$ to histograms from data to find $\nu^2$ is the preferred method for determining this important parameter. Bandwidth effects in $\dot{\phi}$ can be neglected however, if $B<<2\nu$ where B is the signal bandwidth. The analysis also reveals a potentially powerful technique for determining parameters of the modulation or bandwidth of a source from the received multipath signal.

The analysis of multiple sources, applicable to noise problems, includes important approximations to densities which are intractable analytically, and would involve significant computer time to solve exactly. In addition to studies of the amplitude densities, significant progress has been made in solving for the amplitude rate densities and the joint densities of amplitude and amplitude rate.

In addition to providing valuable confirmation of much of the theoretical analysis, a computer simulation of phase random multipath propagation also confirms that for $N \geq 4$ paths phase random multipath conditions begin to closely approach the asymptotic conditions for $N \rightarrow \infty$.

Data at 220Hz and 406Hz received by drifting sonobuoys in the Atlantic at approximately 300 km in range were analyzed. Values of $\nu^2$ obtained support an internal wave model for the relevant dynamical process. The modulation theory uncovered a heretofore unrecognized modulation in the data due to an error of the Doppler tracking system. Predictions of crossing rates including this modulation effect are in good agreement with the data.

Other data at 15Hz and 33Hz propagated to ranges between 250 km to 450 km in the Pacific in which deliberate modulation was introduced, once again provide excellent confirmation of the theory. Measured values of $\nu^2$ vary significantly from run to run and are not consistent with an internal wave model, indicating some other mechanism (i.e., tidal, rough scattering) must account for the fully saturated phase random nature of the data. The technique for determining modulation parameters was used, and for the 76 modulated runs analyzed, the average error in determining the actual bandwidth of the modulation of the source from the received multipath signal was 8%.

Approved for public release;
distribution unlimited.

# THE STATISTICS OF FINITE BANDWIDTH, MODULATED ACOUSTIC SIGNALS PROPAGATED TO LONG RANGES IN THE OCEAN, INCLUDING MULTIPLE SOURCE EFFECTS

by

PETER NICHOLAS MIKHALEVSKY

B.A., Harvard University
(1972)

M.S., Harvard University
(1972)

SUBMITTED IN PARTIAL FULFILLMENT
OF THE REQUIREMENTS FOR THE
DEGREE OF

DOCTOR OF PHILOSOPHY

at the

MASSACHUSETTS INSTITUTE OF TECHNOLOGY

February 1979

© M.I.T., 1979

Thesis
M58145
c.1

# THE STATISTICS OF FINITE BANDWIDTH, MODULATED ACOUSTIC SIGNALS PROPAGATED TO LONG RANGES IN THE OCEAN, INCLUDING MULTIPLE SOURCE EFFECTS

by

PETER NICHOLAS MIKHALEVSKY

Submitted to the Department of Ocean Engineering on February 5, 1979 , in partial fulfillment of the requirements for the degree of Doctor of Philosophy.

## ABSTRACT

The statistics of acoustic signals propagated to long ranges in the ocean are investigated in detail in this thesis. The phase random model of multipath propagation is extended to include finite bandwidth and/or modulated sources as well as multiple source configurations. The theoretical analyses include the derivation of many new probability density functions for these new cases as well as for the single narrowband source.

The probability density function for $\dot{\Lambda}$, the time rate of change of the level in decibels for the single narrowband source is derived. $P_{\dot{\Lambda}}(\dot{\Lambda})$ depends only upon $\nu^2$, the single path mean square phase rate, which can be related to certain ocean dynamical processes. The analysis of finite bandwidth and/or modulated sources reveals that the amplitude and amplitude rate densities (including $P_{\dot{\Lambda}}(\dot{\Lambda})$) are independent of the finite bandwidth and modulation effects, but the density of the time rate-of-change of the multipath phase $\dot{\phi}$ is sensitive to these effects. Thus, fitting $P_{\dot{\Lambda}}(\dot{\Lambda})$ to histograms from data to find $\nu^2$ is the preferred method for determining this important parameter. Bandwidth effects in $\dot{\phi}$ can be neglected, however, if $B << 2\nu$ where B is the signal bandwidth. The analysis also reveals a potentially powerful technique for determining parameters of the

modulation or bandwidth of a source from the received multipath signal.

The analysis of multiple sources, applicable to noise problems, includes important approximations to densities which are intractable analytically, and would involve significant computer time to solve exactly. In addition to studies of the amplitude densities, significant progress has been made in solving for the amplitude rate densities and the joint densities of amplitude and amplitude rate.

In addition to providing valuable confirmation of much of the theoretical analysis, a computer simulation of phase random multipath propagation also confirms that for $N \geq 4$ paths phase random multipath conditions begin to closely approach the asymptotic conditions for $N \rightarrow \infty$.

Data at 220Hz and 406Hz received by drifting sonobuoys in the Atlantic at approximately 300 km in range were analyzed. Values of $\nu^2$ obtained support an internal wave model for the relevant dynamical process. The modulation theory uncovered a heretofore unrecognized modulation in the data due to an error of the Doppler tracking system. Predictions of crossing rates including this modulation effect are in good agreement with the data.

Other data at 15Hz and 33Hz propagated to ranges between 250 km to 450 km in the Pacific in which deliberate modulation was introduced, once again provide excellent confirmation of the theory. Measured values of $\nu^2$ vary significantly from run to run and are not consistent with an internal wave model, indicating some other mechanism (i.e., tidal, rough scattering) must account for the fully saturated phase random nature of the data. The technique for determining modulation parameters was used, and for the 76 modulated runs analyzed, the average error in determining the actual bandwidth of the modulation of the source from the received multipath signal was 8%.

Thesis Supervisor: Ira Dyer

Title: Professor of Ocean Engineering

# ACKNOWLEDGEMENTS

I wish to express my deepest gratitude to Ira Dyer, whose guidance, understanding, and friendship were invaluable not only in the preparation of this thesis, but also during my course of study at M.I.T. I wish also to thank the other members of my thesis committee, Arthur B. Baggeroer and George V. Frisk for their interest and comments.

I am indebted to my office mates and fellow workers, particularly William R. Hamblen, and George Shepard, for their support and friendship these past years.

For their aid in obtaining and analyzing the data in this thesis, I owe thanks to Robert Spindel, John J. Anton, James B. McCrumb, James G. Smith, and Neil Miller.

Much thanks go to Debbie Schmitt for her unflinching endurance in the typing of the manuscript.

I wish also to thank the United States Navy for giving me the opportunity to return to graduate school to obtain my doctorate. Particular thanks are due to the Ocean Science division of the Office of Naval Research which funded a large portion of this research effort.

Finally, to my wife Litsa, words cannot express the love and support which she has given me during these years.

Our daughter Lara has been a source of joy and happiness for me, though my work has often precluded the attentions she and my wife deserve. A very special thanks to them both for years of patient understanding.

# TABLE OF CONTENTS

Page

Page

# LIST OF FIGURES

Page

Page

Page

Page

Page

Page

# LIST OF SYMBOLS AND NOTATION

| | |
|---|---|
| $A$ | maximum excursion of the carrier in Hz, $2A$ is therefore the bandwidth of the modulation |
| $a$ | the inverse of the mean of $\chi$ ($a = 1/\mu$) |
| $B$ | bandwidth of the signal |
| $b$ | the inverse of $2\sigma_1^2\nu$ |
| $\beta\sigma$ | product of the modulation amplitude and modulation frequency for sinusoidal phase modulation |
| $\Gamma(z)$ | gamma function |
| $\Gamma(a,z)$ | incomplete gamma function |
| $\gamma(a,z)$ | incomplete gamma function [$\gamma(a,z) = \Gamma(a) - \Gamma(a,z)$] |
| $\gamma_s$ | coefficient of skew |
| $\gamma_e$ | coefficient of excess |
| $\gamma$ | Euler's constant (= .5772...) |
| $(2n-1)!!$ | $\equiv 1\cdot3\cdot5\cdots(2n-1)$; $(-1)!! \equiv 1$ |
| $D_p(z)$ | parabolic cylinder function |
| $E[x]$ | defined as the expected value of random variable $\chi$ |
| $E_1(z)$ | the exponential integral |
| $E[\pi/2, k]$ | complete elliptic integral of the second kind |
| $\varepsilon$ | defined as $10 \log_{10} e = 4.34...$ |
| $F(a,b;c;z)$ | Gauss's hypergeometric series |
| $\zeta,t,z,u$ | variables of integration |

| | |
|---|---|
| $G(\rho_o)$ | amplitude crossing rate at axis level equal to $\rho_o$, or the conditional expection of $\lvert\dot{\rho}\rvert$ given $\rho = \rho_o$ $(= E[\dot{\rho} \mid \rho = \rho_o])$ |
| $G(\phi_o)$ | phase crossing rate |
| $\theta_n$ | single path phase for the nth path |
| $J_\nu(z)$ | Bessel's function of order $\nu$ |
| $K_\nu(z)$ | the modified Bessel function of order $\nu$ |
| $K[\pi/2, \gamma]$ | complete elliptic integral of the first kind |
| L | number of sources |
| LD | number of sources with different intensity and different mean square phase rates at the receiver |
| LE | number of sources with equal intensity and equal mean square phase rates at the receiver |
| $\Lambda$ | level in dB's of the short time average mean-square pressure $(\Lambda = 10 \log_{10}\chi)$ |
| $\dot{\Lambda}$ | time rate of change of $\Lambda$ |
| M(t) | temporal modulation function |
| $\dot{M}(t)$ | time rate of change of M(t) |
| $M_\chi(\omega)$ | characteristic function of random variable $\chi$ |
| $M_{\chi_1,\chi_2}(\omega,\sigma)$ | two-dimensional characteristic function of the joint pdf of random variables $\chi_1$ and $\chi_2$ |
| $M(\alpha,\delta,z)$ | the confluent hypergeometric function [sometimes written $\Phi(\alpha,\delta,z)$] |
| N | number of groups of sources, each group with $LE_i$ $(i = 1,2,\ldots,N)$ sources per group |
| $N$ | number of independent propagation paths |

| | |
|---|---|
| $\mu$ | the long time average mean square pressure at the receiver for a single source ($\mu = 2\sigma_1^2 \equiv E[\chi]$) |
| $\nu^2$ | the single path mean-square phase rate ($\nu^2 \equiv E[\dot{\theta}_n^2] \forall n$) |
| $P_\chi(\chi)$ | probability density function (pdf) of random variable $\chi$ |
| $P_{\chi_1,\chi_2}(\chi_1,\chi_2)$ | the joint pdf of random variables $\chi_1$ and $\chi_2$ |
| $P_{N\chi}(\chi)$ | the pdf of random variable $\chi$ for N groups |
| $\rho_\chi(s)$ | the Laplace transform of the pdf of random variable $\chi$ |
| $r$ | single path amplitude at the receiver |
| $\rho$ | short time average root-mean-square pressure |
| $\dot{\rho}$ | time rate of change of $\rho$ |
| $\sigma_G^2$ | variance of phase in Gaussian phase modulation |
| $\sigma_1^2$ | one half of the long time average mean-square pressure at the receiver ($\sigma_1^2 = Nr^2/2$) |
| $W_{\nu,\mu}(z)$ | Whittaker's function |
| $X,Y$ | quadrature components of the signal envelope |
| $\dot{X},\dot{Y}$ | time rate of change of the quadrature components |
| $\Phi_1(\alpha,\beta,\gamma;x,y)$ | degenerate hypergeometric series in two variables |
| $\chi$ | short time average mean-square pressure ($\chi = \rho^2$) |
| $\dot{\chi}$ | time rate of change of $\chi$ |
| $\phi$ | multipath phase |

| | |
|---|---|
| $\dot{\phi}$ | multipath phase rate |
| $\psi(\chi)$ | Euler psi function [$\psi(\chi) \equiv \ln\Gamma(\chi)$] |
| $\psi^1(\chi)$ | digamma function [$\psi^1(\chi) \equiv d/d\chi\ \psi(\chi)$] |

# INTRODUCTION

Acoustic signals propagated to long ranges in the ocean, tens to hundreds to thousands of kilometers, via all modes of propagation including surface ducts, the deep sound channel, or sea-surface and ocean-bottom reflections exhibit fluctuations in amplitude and phase which are now recognized to be dominated by the multipath interference of the acoustic field. The statistics of these fluctuations as well as their relationships to the dynamics of the ocean has been one focus of recent research in understanding this important physical process. The optimum design of sonars (e.g., the receiver operating characteristics), underwater communications devices, and in fact any system which operates via acoustic transmission in the sea depends upon the knowledge of the statistical behavior of these transmissions.

The recognition of the dominance of the multipath structure on the statistics, or the assertion that long range multipath acoustic propagation in the ocean can be modelled as a phase random process has been established only within the last ten years, although the phase random process or random walk problem has been under study since Rayleigh (1880) [1], and is one of the classical problems of mathematics and physics. Bergmann (1946) [2] was among

the first to speculate that observed fluctuations in signal intensity might be attributed to the interference of many paths summing in random phase. Dyer (1970) [3] formally applied the theory of a phase random process or random walk problem to long range acoustic multipath propagation in the ocean, and was the first to investigate the statistics of log transformed variables. Dyer also showed that even in the presence of scattering randomness multipath interference would dominate the statistics. This research in fact indicated a basic shift from the scattering models of earlier research which are more appropriate for high frequencies and short ranges when multipath effects are less important. Dyer also proposed a model of distant shipping noise based upon the precepts of phase random multipath propagation and continued this research in a later paper (1973) [4], and most recently in Mikhalevsky and Dyer (1978) [5], results of the latter being included as part of this thesis. This model, appropriate to distant shipping noise, assumes the noise in a band is dominated by narrowband lines discrete in frequency.

Mark (1972) [6] investigated the statistics of the multipath propagation of finite bandwidth signals. Employing a systems approach, he derived general expressions

for the mean and variance of the received signal energy in terms of the correlation function of the time varying impulse response of the medium. He also showed that the gamma or Erlang probability density function is often a good approximation to the real pdf of the received energy. Much earlier, Nakagami [7] had noted the utility of an appropriately transformed Erlang pdf in approximating the densities of received HF electromagnetic radiation undergoing rapid fading, indicating the broadness of scope of the phase random model and its general applicability. All these efforts, however, concentrated on the amplitude (or related quantities) of the signal and did not address the amplitude rate or phase rate of the signal.

Longuet-Higgins (1975) [8] in connection with research on random sea surface waves (another phase random process) introduced the joint pdf's of amplitude, amplitude rate, phase, and phase rate as well as the marginal densities to the growing body of knowledge of phase random processes. It remained for Hamblen (1977) [9] to formally extend the phase random analysis to the multipath acoustic propagation process, incorporating the results of Longuet-Higgins [8] and also S.O. Rice [10] whose extensive research on noise statistics were also applicable to the long range acoustic

propagation problem. Hamblen [9] also established the dependence of the probability density functions for a single narrowband acoustic source on the two parameters $\sigma_1^2$, one-half the mean square pressure at the receiver, and $\nu^2$, the single path mean square phase rate. He also verified the basic results with data from an ocean acoustic propagation experiment.

Concurrent with the development of the phase random model of multipath acoustic propagation, much research was and is being conducted on another important aspect of the problem, namely to discover what ocean dynamic processes are the driving mechanisms and how parameters of these ocean dynamic processes are related to the parameters of the acoustic field, $\sigma_1^2$ and $\nu^2$. Most notable perhaps is the recent research of Dyson, Munk, and Zetler (1976) [11] who have proposed a theoretical model relating the dynamics of internal waves in the ocean to the fluctuation of the acoustic field. However, this model appears to have serious limitations at low frequencies. In fact, little research has been reported on the low frequency cases.

In the following paragraphs I will introduce the research reported on in this thesis. There are three basic areas in which significant progress has been made in

understanding the statistical behavior of multipath acoustic propagation: (1) the single narrowband source, (2) finite bandwidth and/or modulated sources, and (3) multiple sources or receptions. An extensive analysis of data from acoustic experiments in the ocean as well as a computer simulation of phase random multipath acoustic propagation not only increase our confidence in this new understanding, but reveal new information for low frequency signals about the driving mechanism of $\nu^2$, the single path mean square phase rate.

The Single Narrowband Source

I derive for a single narrowband source the pdf's for the time rate of change of the sta (short time average) mean square pressure, $\dot{\chi}$, and the time rate of change of the level in decibels, $\dot{\Lambda}$, results which are unique to this thesis. The pdf for $\dot{\Lambda}$ is independent of $\sigma_1^2$ and is a function only of $\nu^2$. This result is of particular importance as it affords a method of measuring $\nu^2$ from ocean acoustic data without error due to uncertainties in the signal carrier. Included in this analysis are the joint densities $P_{\chi,\dot{\chi}}(\chi,\dot{\chi})$ and $P_{\Lambda,\dot{\Lambda}}(\Lambda,\dot{\Lambda})$ and their characteristic functions, also unique to this thesis. This analysis in fact completes the family of first order

and joint pdf's for a single narrowband source. Appendix A contains a list of all the first order pdf's, their characteristic functions, means, and variances as found by me, and earlier as found by others, so that a complete set can be referred to.

Finite Bandwidth and/or Modulated Sources

Many acoustic signals of interest received in the ocean have bandwidths which are not narrow, and carriers that may not be stable or may be deliberately modulated. In applying the phase random model of multipath acoustic propagation, it is necessary to assume that the spectrum of the received signal is narrow, and that in homodyning the signal the spectral mean is zero [8,9]. Clearly, the signals mentioned in the beginning of this paragraph would violate these assumptions. I show, however, that the amplitude and amplitude rate statistics (including $P_{\dot{\Lambda}}(\dot{\Lambda})$ are independent of finite bandwidth and/or carrier modulation effects. The multipath phase rate, $\dot{\phi}$, is sensitive to these effects, and it is the pdf for $\dot{\phi}$ which must be modified.

The pdf for $\dot{\phi}$ is in fact a function of $v^2$, as well as the bandwidth, and/or parameters of the modulation. Bandwidth effects can be neglected when $B << 2v$, which is

therefore a criterion for what is meant by "narrowband" in the ocean. Furthermore, this analysis reveals a method of separating and understanding the source induced modulation independent of the ocean induced modulation or vice versa. In addition to solving for the pdf's of $\dot{\phi}$ in the presence of bandwidth and/or modulation, I solve for the crossing rate statistics of phase for these cases as well.

Multiple Sources or Receptions

The statistics of the received signal amplitude and amplitude rate when there is multiple source structure depends on the exact nature of the received multi-source signal and the analysis performed by the receiver. I consider two basic cases. First, I assume the receptions (one per source) are disjoint in frequency in the analysis band and can be separated and summed incoherently (that is, without concern for phase). I assume, therefore, that each of the receptions/sources are independent, thus the analysis band should not include harmonics of a signal already in the band. This type of analysis is motivated by the structure of distant shipping noise [4,5]. For the second case, I consider the receptions to be at or so close in frequency that they

must be summed coherently. Note that the dividing line between case one and case two depends upon the resolution of the receiver. Most all of the pdf's I derive for the amplitude and particularly the amplitude rate for these cases are unique to this thesis. Where I have been unable to derive the exact pdf analytically or in which the exact solution is extremely time consuming to obtain even with the aid of a computer, I have in most cases found an approximation based upon Edgeworth's series. This approximation is shown to be excellent in the main lobe of the density but performance is degraded in the tails.

I use the analysis of coherent sources to model the effect of ocean ambient noise on the pdf's for a single narrowband source. The pdf's are expressed in terms of the SNR (signal to noise ratio). In light of this analysis, I am able, as well, to extend with only slight modification all the frequency disjoint multiple source solutions to include the cases when both coherent and disjoint source structure is present in the analysis band, or for noise which is continuously distributed over the passband.

The reader is forewarned that the sections of this thesis on multiple sources (see Table of Contents) are

lengthy and in many cases quite tedious due to the complexity of the analysis. Table III is provided (page 143) to aid in understanding the organization of this material and to aid the reader in finding that analysis which is most pertinent to his problem. The analysis of the statistics of multiple sources which is not immediately motivated by any current ocean acoustics problem of interest is presented for completeness with potential for application to future problems, even perhaps in areas unrelated to acoustics. For example, the solutions for $P_{\chi}(\chi)$, using the terminology of Queuing Theory, are in fact the pdf's for the interarrival times of cascaded Poisson processes which are unique to this thesis and, to my knowledge, not to be found in Queuing Theory literature.

Computer Simulation and Data Analysis

A computer simulation of phase random multipath propagation is developed to assist in and to check the theoretical analysis. The simulation demonstrates the independence of the exact nature of the pdf for $\dot{\theta}_n$ (the single path phase) to the statistics when there are at least four propagation paths from the source to the receiver. Of importance is the confirmation of the

generally accepted criterion that $N \geq 4$ paths results in an almost fully saturated phase random process, and pdf's for the limiting case as $N \to \infty$ suffice. The simulation allows me in Appendix C to compare the theoretical pdf's, many which I derived, for $N \leq 3$ to the computer generated histograms with excellent results.

I analyze data from two ocean acoustic experiments. One was conducted near Eleuthera in which two CW signals at 220Hz and 406Hz were transmitted approximately 300 km northeast towards Bermuda and received by drifting sonobuoys [12]. These data support the theoretical pdf's derived in Chapter 1. Furthermore, the modulation theory uncovered a heretofore unrecognized modulation in the phase rate data due to errors in the sonobuoy tracking system that has dramatic results on the statistics for the phase crossing rates. These data are also consistent with a model of phase random multipath propagation resulting from the interaction of the acoustic field with internal waves [11].

I also analyze data taken in the Pacific in 1973 known collectively as the CASE experiment [13] in which CW signals at 15Hz and 33Hz were propagated to ranges varying from 250 km to 450 km. These data were deliberately modulated and the predictions derived

theoretically in Chapter 1 are once again confirmed. The analysis I used was capable of determining the bandwidth of the modulation from the received multipath signal with an average error of 8%. Where previously there had been some problems in the consistency of the data with the phase random model, the modulation theory successfully lays these problems to rest. These data, however, are not consistent with the internal wave model and this analysis has brought sharply into focus a shortcoming in our current understanding of the driving mechanisms of $v^2$, particularly for low frequency signals. Correlations I have derived appear to support, though tenuously without additional research, either a rough scattering or tidal mechanism to account for the fully saturated nature of the CASE data.

In Appendix D, the effects of amplitude parameter variation are discussed. This analysis is aimed at uncovering the effects of temporal variations in the total energy of the signal during the observation period on the statistics of the received multipath signal.

# CHAPTER 1

# ANALYTICAL TREATMENT

## 1.1 Single Narrowband Source

For a narrowband signal the phase-random model of multipath acoustic propagation predicts that the sta root-mean-square pressure, $\rho$, is a Rayleigh distributed random variable [3,9], its rate, $\dot{\rho}$, is Gaussian [9], the multipath phase, $\phi$, is uniform, and its rate, $\dot{\phi}$, is distributed according to a density first given by M.S. Longuet-Higgins [8,9]. The transformation $\chi = \rho^2$ yields the density for the sta mean-square pressure which is exponential [3], and following Dyer [3] the transformation $\Lambda = 10 \log_{10} \chi$ gives the density for the level in decibels which is Log-Rayleigh. To complete the family of first order densities for a single narrowband source, I have derived the densities for $\dot{\chi}$ and $\dot{\Lambda}$.

### 1.1.1 Derivation of $P_{\chi}(\dot{\chi})$ and $P_{\Lambda}(\dot{\Lambda})$

For phase random multipath propagation the joint density of the sta rms pressure $\rho$ and its rate $\dot{\rho}$ is given by [8,9],

$$P_{\rho,\dot{\rho}}(\rho,\dot{\rho}) = \frac{o}{\sigma_1^2 \sqrt{\pi \sigma_1^2 \overline{\nu^2}}} \exp\left[ - \frac{\rho^2}{2\sigma_1^2} - \frac{\dot{\rho}^2}{2\sigma_1^2 \nu^2} \right] \quad (1.1)$$

where $\nu^2$ is the single path mean-square phase rate,

$$\sigma_1^2 = \frac{Nr^2}{2} = \frac{\mu}{2} \tag{1.2}$$

and $N$ is the number of propagation paths, $r$ is the single path amplitude, and $\mu$ is the long-time average mean-square pressure.

For $\chi = \rho^2$ we have $\dot{\chi} = 2\rho\dot{\rho}$. To find the pdf (probability density function) for $\dot{\chi}$ I first solve for the cumulative distribution function [14] of $\dot{\chi}$ by integrating over the joint density of $\rho$ and $\dot{\rho}$, Equation (1.1).

$$P_{<\dot{\chi}}(\dot{\chi}) = \int_0^\infty \int_{-\infty}^{\frac{\dot{\chi}}{2\rho}} P_{\rho,\dot{\rho}}(\rho,\dot{\rho})\, d\rho d\dot{\rho} \quad , \quad \dot{\chi} > 0 \tag{1.3}$$

The pdf for $\dot{\chi}$ will be given by $\frac{\partial}{\partial\dot{\chi}} P_{<\dot{\chi}}(\dot{\chi})$. Combining this result with Equations (1.1) and (1.3) differentiating under the integral sign and integrating once, I obtain the result

$$P_{\dot{\chi}}(\dot{\chi}) = \frac{1}{4\sigma_1^2\nu} \exp\left\{-\frac{|\dot{\chi}|}{2\sigma_1^2\nu}\right\} \quad , \quad -\infty<\dot{\chi}<\infty \tag{1.4}$$

The absolute value results from the analysis for $\dot{\chi} < 0$. Equation (1.4) is the Laplace pdf [14]. The variance of $\dot{\chi}$ is given by

$$\sigma_{\dot{\chi}}^2 = 8\sigma_1^4\nu^2$$

The pdf for $\dot{\Lambda}$ is solved in the same manner. First I find the pdf for $\dot{y}$ where $y = \ln\rho^2$ and thus $\dot{y} = 2\dot{\rho}/\rho$, therefore,

$$P_{\dot{y}}(\dot{y}) = \frac{\partial}{\partial \dot{y}} \int_0^{\infty} \int_0^{\frac{\dot{y}\rho}{2}} P_{\rho,\dot{\rho}}(\rho,\dot{\rho})\, d\rho d\dot{\rho} \quad , \quad \dot{y} > 0 \tag{1.5}$$

As before, I differentiate under the integral sign and perform the remaining integration to obtain

$$P_{\dot{y}}(\dot{y}) = \frac{1/2\nu}{2\left[1 + \frac{\dot{y}^2}{4\nu^2}\right]^{3/2}} \quad , \quad -\infty < \dot{y} < \infty \tag{1.6}$$

Making the final transformation $\dot{\Lambda} = \varepsilon\dot{y}$, where $\varepsilon = 10 \log_{10} e = 4.34...$ (this notation will be adhered to in the remainder of the thesis), I obtain the final result

$$P_{\dot{\Lambda}}(\dot{\Lambda}) = \frac{1}{\varepsilon} P_{\dot{y}}(\dot{y})\Big|_{\dot{y} = \dot{\Lambda}/\varepsilon} \quad , \quad -\infty<\dot{\Lambda}<\infty \tag{1.7}$$

This density is in fact of the same form as $P_{\dot{\phi}}(\dot{\phi})$ (see Equation A8 in Appendix A). The second moment of this density is infinite. Physical insight of this phenomenon can be obtained if one visualizes the random walk problem. The amplitude of the vector is $\rho$ and its phase $\phi$. When the amplitude of $\rho$ goes to zero as in a deep fade it is easily seen that the phase can undergo very rapid changes. Likewise because $\dot{\Lambda} = \varepsilon 2\dot{\rho}/\rho$ it is also clear that $\dot{\Lambda}$ can assume very large values when $\rho$ is small. Thus both $\dot{\Lambda}$ and $\dot{\phi}$ are governed by the same form of pdf and their variances are infinite. It is also noteworthy that while the pdf's for $\dot{\rho}$ and $\dot{\chi}$ depend upon both $\sigma_1$ and $\nu$, Equation (1.7) depends only on $\nu$.

### 1.1.2 Joint Densities of Amplitude and Amplitude Rate and Crossing Rate Statistics

In order to complete the family of joint densities of amplitude and amplitude rate for a single source, I have derived $P_{\chi,\dot{\chi}}(\chi,\dot{\chi})$ and $P_{\Lambda,\dot{\Lambda}}(\Lambda,\dot{\Lambda})$. This analysis also provides an alternative method for deriving $P_{\dot{\chi}}(\dot{\chi})$ and $P_{\dot{\Lambda}}(\dot{\Lambda})$ to check the calculations of the previous section. In addition, I derive the two-dimensional characteristic

functions [14] which will be of significant importance when I investigate multiple sources.

For $\chi = \rho^2$ we have $\rho = \chi^{1/2}$ and $\dot{\rho} = \frac{1}{2}\dot{\chi}\chi^{-1/2}$. In order to solve for $P_{\chi,\dot{\chi}}(\chi,\dot{\chi})$ I make a two dimensional transformation on $P_{\rho,\dot{\rho}}(\rho,\dot{\rho})$ (Equation 1.1) as follows:

$$P_{\chi,\dot{\chi}}(\chi,\dot{\chi}) = \frac{\partial^2}{\partial\chi\partial\dot{\chi}} \int_0^{\chi^{1/2}} \int_{-\infty}^{\frac{1}{2}\chi,\chi^{-1/2}} P_{\rho,\dot{\rho}}(\rho,\dot{\rho})\,d\rho\,d\dot{\rho} \qquad (1.8)$$

By differentiating under the integrals in Equation (1.8) I obtain

$$P_{\chi,\dot{\chi}}(\chi,\dot{\chi}) = \frac{1}{4\sigma_1^3\nu\sqrt{2\pi\chi}} \exp\left[-\frac{\chi}{2\sigma_1^2} - \frac{\dot{\chi}^2}{8\chi\sigma_1^2\nu^2}\right],$$

$$\chi > 0, \text{ and } -\infty<\dot{\chi}<\infty \qquad (1.9)$$

The two dimensional characteristic function or two dimensional Fourier transform can be defined as

$$M_{\chi_1,\chi_2}(\omega,\sigma) = \int_{-\infty}^{\infty}\int_{-\infty}^{\infty} P_{\chi_1,\chi_2}(\chi_1,\chi_2)e^{i\omega\chi_1 + i\sigma\chi_2}d\chi_1 d\chi_2 \qquad (1.10)$$

For $P_{\chi,\dot{\chi}}(\chi,\dot{\chi})$

$$M_{\chi,\dot{\chi}}(\omega,\sigma) = \int_{-\infty}^{\infty}\int_{0}^{\infty} P_{\chi,\dot{\chi}}(\chi,\dot{\chi})e^{i\omega\chi + i\sigma\dot{\chi}}\, d\chi d\dot{\chi} \qquad (1.11)$$

Performing the double integration yields

$$M_{\chi,\dot{\chi}}(\omega,\sigma) = \frac{1}{1 - i2\sigma_1{}^2\omega + 4\sigma_1{}^4\nu^2\sigma^2} \qquad (1.12)$$

Recalling that $y = \ln\chi$, we have $\chi = e^y$ and $\dot{\chi} = \dot{y}e^y$. Thus,

$$P_{y,\dot{y}}(y,\dot{y}) = \frac{\partial^2}{\partial y\partial\dot{y}}\int_{0}^{e^y}\int_{-\infty}^{\dot{y}e^y} P_{\chi,\dot{\chi}}(\chi,\dot{\chi})d\chi d\dot{\chi} \qquad (1.13)$$

As before I differentiate under the integrals, and make the final transformations $\Lambda = \varepsilon y$ and $\dot{\Lambda} = \varepsilon\dot{y}$ to obtain,

$$P_{\Lambda,\dot{\Lambda}}(\Lambda,\dot{\Lambda}) = \frac{\exp\ (\frac{3}{2\varepsilon}\ \Lambda)}{4\varepsilon^2\sigma_1{}^3\nu\sqrt{2\pi}} \exp\left\{-\exp(\frac{\Lambda}{\varepsilon})\ [\frac{1}{2\sigma_1{}^2} + \frac{\dot{\Lambda}^2}{8\varepsilon^2\sigma_1{}^2\nu^2}]\right\}$$

$$-\infty<\Lambda<\infty, \text{ and } -\infty<\dot{\Lambda}<\infty \qquad (1.14)$$

The two dimensional characteristic function of $P_{\Lambda,\dot{\Lambda}}(\Lambda,\dot{\Lambda})$ (Equation 1.14) is

$$M_{\Lambda,\dot{\Lambda}}(\omega,\sigma) = 2\varepsilon\nu|\sigma|(8\varepsilon^3|\sigma|\sigma_1{}^2\nu^2)^{i\varepsilon\omega}K_{1+i\varepsilon\omega}(2\varepsilon\nu|\sigma|)$$

. . .(1.15)

where $K_z(x)$ is the modified Bessel function of order z.

Performing the integrals over $\chi$ and $\Lambda$ in Equations (1.9) and (1.14) respectively yields the marginal densities of $\dot{\chi}$ and $\dot{\Lambda}$ which are given by Equations (1.4) and (1.7) respectively as expected.

Following Rice [10] and using Equation (1.14) I derive the mean axis crossing rate for the amplitude of the signal expressed in decibels.

$$G(\Lambda_o) = 2\int_o^\infty \dot{\Lambda}P_{\Lambda,\dot{\Lambda}}(\Lambda_o,\dot{\Lambda})d\dot{\Lambda} \equiv E[\dot{\Lambda}|\Lambda=\Lambda_o] \qquad (1.16)$$

Thus,

$$G(\Lambda_o) = \int_o^\infty 2 \frac{\dot{\Lambda}\exp(\frac{3}{2\varepsilon}\Lambda_o)}{4\varepsilon^2\sigma_1^3\nu\sqrt{2\pi}} \exp\left\{-\exp(\frac{\Lambda_o}{\varepsilon}) [\frac{1}{2\sigma_1^2} + \frac{\dot{\Lambda}^2}{8\varepsilon^2\sigma_1^2\nu^2}]\right\} d\dot{\Lambda}$$

and

$$G(\Lambda_o) = \frac{2\nu\exp(\frac{\Lambda_o}{2\varepsilon})}{\sigma_1\sqrt{2\pi}} \exp\left[-\frac{\exp(\frac{\Lambda_o}{\varepsilon})}{2\sigma_1^2}\right] \quad (1.17)$$

If we transform Equation (1.17) to determine the axis crossing rate for $\rho_o \equiv \exp(\Lambda_o/2\varepsilon)$

$$G(\rho_o) = \frac{2\nu\rho_o}{\sigma_1\sqrt{2\pi}} \exp\left[-\frac{\rho_o^2}{2\sigma_1^2}\right] \quad (1.18)$$

Equation (1.18) was previously obtained by Dyer and Shepard [15], and Hamblen [9].

## 1.2 Multiple Sources

In this section the statistics of the amplitude and amplitude rate variables are analyzed when the source

structure consists of many independent acoustic generators distributed at various frequencies across the bandwidth of the receiver. It is assumed that propagation from each source is phase random and multipath. An initial assumption is also made that each source radiates at a different frequency. This problem is applicable to the case of deep ocean ambient noise due to distant shipping [4]. For this case the spectrum of ship radiation is assumed to be dominated by lines disjoint in frequency, so that each ship contributes as many independent sources as there are lines within the observational bandwidth. (Note, the observational bandwidth cannot be so large as to include harmonics.) Henceforth line and source will be used interchangeably. Furthermore, the analysis assumes that the Fourier components of the received signal over the observational bandwidth are squared and summed. Thus, by Parseval's theorem it is the square of the signal amplitude, in this case $\chi = \rho^2$ which is summed for each source, or $\chi_{total} = \sum_{n=1}^{L} \chi_n$ for L sources. As noted in Reference [4], this model breaks down when sources cannot be separated in frequency, and then the model must be modified to include the effect of two or more sources which may be radiating at the same frequency. This coherent problem is treated in Section 1.2.3.

### 1.2.1 Amplitude Densities

Dyer [4] first investigated the amplitude statistics for the multicomponent case and developed the framework for the problem which will be followed here. Three categories are defined: (a) all line components, L in number, arrive with the same long-time average intensity; (b) all line components, M in number, arrive with different intensities; and (c) N groups arrive, each with $L_i$ equal intensity components. As an example, Case (c) was applied in Reference [4] to noise as might be measured at low frequencies in deep water near Bermuda.

As pointed out in Reference [4], and as will be shown in Section 1.2.1.3, use of the models describing line component noise often entails considerable computational tedium. This complexity often motivates adoption of approximate methods, which will be discussed in Section 1.2.1.4. Cases (a) and (b) are treated in Reference [4]. Exact solutions for $N = 2$ and $N = 3$ of Case (c) are derived in Sections 1.2.1.1 and 1.2.1.2 respectively. It is true that the exact solutions of $N = 2$ and $N = 3$ may be of little practical value as most cases of interest will probably contain many more than three groups. The analysis is performed, however, to build the theoretical framework of this problem, perhaps

enabling someone else to solve it exactly in all generality, and more importantly in relation to this thesis research these exact solutions will provide a check for the approximate solution which is presented in Section 1.2.1.4.

1.2.1.1 Exact Solution for N = 2, Case (c)

Consider L line components, each with the same long-time average mean square pressure $\mu$. The probability of the sta mean square $\chi$ is [3 ,4 ]

$$P_{\chi_{LE}}(\chi) = \frac{a^L \chi^{L-1} e^{-a\chi}}{(L-1)!} \quad , \quad \chi > 0, \; a > 0 \quad ;$$

$$L = 1,2,... \tag{1.19}$$

where $a = 1/\mu$, the mean $\mu_{\chi_L} = L\mu_\chi$, and the variance $\sigma^2_{\chi_L} = L\mu^2 = \mu^2_{\chi_L}/L$. Equation (1.19) is the Erlang or gamma pdf (see Appendix B).

Let $\chi_1$ and $\chi_2$ be distributed according to Equation (1.19) but with different $\mu_i$ and different $L_i$ $(i = 1,2)$. Further, let $_2\chi = \chi_1 + \chi_2$. Then $P_{2\chi}(\chi) = \int_o^\chi P_1(\zeta)\, P_2(\chi-\zeta)d\zeta$. If we make the change of

variables $\zeta = \chi t$,

$$P_{2\chi}(\chi) = \frac{a_1^{L_1} a_2^{L_2} e^{-a_2\chi}}{\Gamma(L_1)\,\Gamma(L_2)}\,\chi^{L_2+L_1-1}\int_0^1 t^{L_1-1}(1-t)^{L_2-1}e^{t\chi(a_2-a_1)}\,dt$$

. . .(1.20)

The integral is the confluent hypergeometric function defined in its integral form [16,17]:

$$M(\alpha,\delta,Z) = \frac{\Gamma(\delta)}{\Gamma(\delta-\alpha)\Gamma(\alpha)}\int_0^1 e^{Zt}\,t^{\alpha-1}(1-t)^{\delta-\alpha-1}\,dt \qquad (1.21)$$

This is a well tabulated function [18,19,20] alternatively defined by Kummers series (absolutely convergent):

$$M(\alpha,\delta,Z) = 1 + \frac{\alpha Z}{\delta} + \frac{(\alpha)_2}{(\delta)_2}\frac{Z^2}{2!} + \ldots + \frac{(\alpha)_n}{(\delta)_n}\frac{Z^n}{n!} + \ldots \qquad (1.22)$$

where $(\alpha)_n = \alpha(\alpha+1)(\alpha+2)\ldots(\alpha+n-1)$, $(\alpha)_o \equiv 1$.

Applying Equation (1.21) to Equation (1.20) I obtain

the desired result:

$$P_{2\chi}(\chi) = \frac{a_1^{L_1} a_2^{L_2} \chi^{L_2+L_1-1} e^{-\chi a_2}}{\Gamma(L_1+L_2)} M\,[L_1, L_1+L_2, \chi(a_2-a_1)] \qquad (1.23)$$

with

$$\mu_{2\chi} = \mu_{\chi_1} + \mu_{\chi_2} = L_1\mu_1 + L_2\mu_2$$

$$\sigma^2_{2\chi} = \sigma^2_{\chi_1} + \sigma^2_{\chi_2} = L_1\mu_1^2 + L_2\mu_2^2$$

If $a_1 = a_2$ then as expected, Equation (1.23) reduces to Equation (1.19) with $L = L_1 + L_2$, upon noting from Equation (1.22) that $M(\alpha,\delta,0) = 1$.

To obtain the density of the level in dB I make the now familiar transformation $\Lambda = \varepsilon \ln\chi$ in Equation (1.23):

$$P_{2\Lambda}(\Lambda) = \frac{a_1^{L_1} a_2^{L_2}}{\varepsilon\Gamma(L_1+L_2)} M\,[L_1, L_1+L_2, (a_2-a_1)e^{(\Lambda/\varepsilon)}]$$

$$\exp\left[\frac{\Lambda}{\varepsilon}(L_2+L_1) - a_2 e^{(\Lambda/\varepsilon)}\right] \qquad (1.24)$$

The statistics for $\Lambda$ are:

$$\mu_\Lambda = \varepsilon[\ln\mu_2 - \gamma + S_1(L_1 + L_2) + Q_1(a_1,a_2,L_1,L_2)]$$

(1.25)

$$\sigma_\Lambda^2 = \varepsilon^2\left[\frac{\pi^2}{6} - S_2(L_1 + L_2) - Q_1^2(a_1,a_2,L_1,L_2) + Q_2(a_1,a_2,L_1,L_2)\right]$$

where

$$S_1(1) = 0,\ S_1(L) = \sum_{w=1}^{L-1} \frac{1}{w}$$

$$S_2(1) = 0,\ S_2(L) = \sum_{w=1}^{L-1} \frac{1}{w^2}$$

$$Q_1(a_1,a_2,L_1,L_2) = \left(\frac{a_1}{a_2}\right)^{L_1} \sum_{n=1}^{\infty} \frac{(L_1)_n}{n!} \left(\frac{a_2-a_1}{a_2}\right)^n \sum_{k=0}^{n-1} \frac{1}{L_1+L_2+k}$$

$$Q_2(a_1,a_2,L_1,L_2) = 2\left(\frac{a_1}{a_2}\right)^{L_1} \sum_{n=2}^{\infty} \frac{(L_1)_n}{n!} \left(\frac{a_2-a_1}{a_2}\right)^n \sum_{k=M+1}^{M+n-1} \sum_{p=M}^{k-1} \frac{1}{pk}$$

where $M = L_1 + L_2$, and $\gamma \equiv$ Euler's constant = .5772... .
Note that if $a_1 = a_2$, Equations (1.25) reduce to
Equations (4) of Reference [4] as expected.

For non-integer values of $L_1$ and $L_2$, Equations (1.25) can be expressed as follows:

$$\mu_\Lambda/\varepsilon = \ln\mu_2 + \left(\frac{a_1}{a_2}\right)^{L_1} \sum_{n=0}^{\infty} \frac{(L_1)_n}{n!} \left(\frac{a_2-a_1}{a_2}\right)^n [\psi(L_2+L_1+n)]$$

(1.26)

$$(\sigma_\Lambda^2 + \mu_\Lambda^2)/\varepsilon^2 = \left(\frac{a_1}{a_2}\right)^{L_1} \sum_{n=0}^{\infty} \frac{(L_1)_n}{n!} \left(\frac{a_2-a_1}{a_2}\right)^n \left\{ [\psi(L_2+L_1+n) - \ln a_2]^2 + \psi^1(L_1+L_2+n) \right\}$$

where

$\psi(x)$ is the Euler Psi function [21]

and where

$$\psi^1(\chi) = \frac{d}{dx}\psi(\chi).$$

Equation (1.23) can also be expressed in terms of the incomplete gamma function [22,23] which is a special case of the confluent hypergeometric function.

1.2.1.2 Exact Solution for N = 3, Case (c)

I now consider three groups with $L_i$ (i = 1,2,3) sources in each group. Let ${}_3\chi = \chi_1 + \chi_2 + \chi_3 = {}_2\chi + \chi_3$ where the $\chi_i$ (i = 1,2,3) are distributed according to Equation (1.19) (with different means and $L_i$) and ${}_2\chi$ is distributed according to Equation (1.23). Then:

$$P_{{}_3\chi}(\chi) = \int_0^{\chi} P_{{}_2\chi}(\zeta)\ P_{\chi_3}(\chi-\zeta)\,d\zeta$$

As before, let $\zeta = \chi t$ and

$$P_{{}_3\chi}(\chi) = \frac{a_1^{L_1} a_2^{L_2} a_3^{L_3}\ \chi^{L_1+L_2+L_3-1}\ e^{-a_3\chi}}{\Gamma(L_1+L_2)\ \Gamma(L_3)} \cdot I \qquad (1.27)$$

and

$$I = \int_0^1 (1-t)^{L_3-1} t^{L_1+L_2-1} e^{t\chi(a_3-a_2)} \cdot M[L_1, L_1+L_2, t\chi(a_2-a_1)]dt$$

. . .(1.28)

Equation (1.28) is evaluated by expanding the confluent hypergeometric junction in its series form (Equation 1.22), and integrating term by term. When I combine this result with Equation (1.27) I obtain the result

$$P_{3\chi}(\chi) = \frac{a_1^{L_1} a_2^{L_2} a_3^{L_3} \chi^{L_1+L_2+L_3-1} e^{-a_3\chi}}{\Gamma(L_1+L_2+L_3)} \sum_{n=0}^{\infty} \frac{\chi^n (a_2-a_1)^n}{n!} \frac{(L_1)_n}{(L_1+L_2+L_3)_n}$$

$$\cdot M[L_1+L_2+n,\ L_1+L_2+L_3+n,\ \chi(a_3-a_2)] \qquad (1.29)$$

with

$$\mu_{3\chi} = L_1\mu_1 + L_2\mu_2 + L_3\mu_3$$

$$\sigma^2_{3\chi} = L_1\mu_1^2 + L_2\mu_2^2 + L_3\mu_3^2$$

Deriving numerical results from Equation (1.29) is straightforward by rewriting the summation

$$\sum = \sum_{n=0}^{\infty} c_n m_n \tag{1.30}$$

where

$$c_n = \frac{\chi(a_2-a_1)}{n} \frac{L_1+n-1}{L_1+L_2+L_3+n-1} c_{n-1} \; ; \quad c_o = 1 \tag{1.31}$$

and [18],

$$m_n = \frac{b(1+b-z)}{az} m_{n-1} + \frac{b(b-1)}{az} m_{n-2}. \tag{1.32}$$

In these I define $m_n \equiv M(a+n, b+n, z)$ and, $a = L_1+L_2$, $b = L_1+L_2+L_3$, and $z = \chi(a_3 - a_2)$.

From Equation (1.29) the density of the level in dB is obtained as before:

$$P_{3\Lambda}(\Lambda) = \frac{1}{\varepsilon} e^y P_{3\chi}(e^y) \Big|_{y = \Lambda/\varepsilon} \tag{1.33}$$

The statistics of the level are:

$$\mu_{3\Lambda} = \varepsilon[\ln\mu_3 - \gamma + S_1(L_1+L_2+L_3) + R_1(a_1,a_2,a_3,L_1,L_2,L_3)]$$

$$\sigma^2_{3\Lambda} = \varepsilon^2\left[\frac{\pi^2}{6} - S_2(L_1+L_2+L_3) - R_1^2(a_1,a_2,a_3,L_1,L_2,L_3)\right.$$

$$\left. + R_2(a_1,a_2,a_3,L_1,L_2,L_3)\right] \qquad (1.34)$$

where:

$$R_1(a_1,a_2,a_3,L_1,L_2,L_3) = \left(\frac{a_1}{a_3}\right)^{L_1}\left(\frac{a_2}{a_3}\right)^{L_2}\sum_{p=0}^{\infty}\frac{(L_1)_p}{p!}\left(\frac{a_2-a_1}{a_3}\right)^p$$

$$\cdot \sum_{n=0}^{\infty}\frac{(L_1+L_2+p)_n}{n!}\left(\frac{a_3-a_2}{a_3}\right)^n \sum_{k=0}^{p+n-1}\frac{1}{L_1+L_2+L_3+k}$$

for $p+n > 0$, and

$$R_2(a_1,a_2,a_3,L_1,L_2,L_3) = 2\left(\frac{a_1}{a_3}\right)^{L_1}\left(\frac{a_2}{a_3}\right)^{L_2}\sum_{p=0}^{\infty}\frac{(L_1)_p}{p!}\left(\frac{a_2-a_1}{a_3}\right)^p$$

$$\cdot \sum_{n=0}^{\infty}\frac{(L_1+L_2+p)_n}{n!}\left(\frac{a_3-a_2}{a_3}\right)^n \sum_{\ell=\mathcal{L}+1}^{\mathcal{L}+p+n-1}\sum_{m=\mathcal{L}}^{\ell-1}\frac{1}{\ell m}$$

for $p+n > 1$, in which $\mathcal{L} = L_1+L_2+L_3$.

Note that for both $N = 2$ and $N = 3$ one can judiciously choose which $a_i, L_i$ will be designated $a_1, L_1$; $a_2, L_2$; or $a_3, L_3$ so as to insure the fastest convergence of the terms involving infinite series.

1.2.1.3 Solution for Arbitrary N, Case (c)

In this section I will derive an expression for the pdf of the sta mean square pressure $\chi$, for an arbitrary number of groups N, using Laplace transform techniques.

Let

$$ {}_N\chi = \sum_{n=1}^{N} \chi_n \tag{1.35}$$

where ${}_N\chi$ denotes the random variable whose pdf we seek and the $\chi_n$ are Erlang distributed random variables, distributed according to Equation (1.19) with arbitrary order $L_n$. The Laplace transform of $\chi_n$ is

$$ \mathcal{P}_{\chi_n}(s) = \left( \frac{a_n}{s + a_n} \right)^{L_n}, \quad s > -a_n \tag{1.36}$$

where $a_n = 1/\mu_n$. From the properties of Laplace transforms

and independent random variables

$$\varphi_{N\chi}(s) = \prod_{n=1}^{N} \left(\frac{a_n}{s + a_n}\right)^{L_n} \tag{1.37}$$

and thus,

$$P_{N\chi}(\chi) = \frac{1}{2\pi j} \int_{-j\infty}^{j\infty} \prod_{n=1}^{N} \left(\frac{a_n}{s + a_n}\right)^{L_n} e^{s\chi}\, ds \tag{1.38}$$

Though Equation (1.38) is attractively compact, it is computationally tedious for most cases of interest, i.e., large N and large $L_n$ as you might expect with many ships and many lines. To carry the analysis a bit further, I make a partial fraction expansion of Equation (1.37),

$$\varphi_{N\chi}(s) = \left(\prod_{n=1}^{N} a_n^{L_n}\right)\left\{\sum_{n=1}^{N}\sum_{k=1}^{L_n} \frac{C_{nk}}{(s + a_n)^k}\right\} \tag{1.39}$$

It is clear from this expression that $P_{N\chi}(\chi)$ is a linear sum of weighted Erlang distributions, and the problem is

reduced to finding the coefficients $C_{nk}$. I take the inverse transform of Equation (1.39) by applying the calculus of residues to obtain

$$C_{nk} = \left\{ \frac{1}{(k-1)!} \frac{d^{k-1}}{ds^{k-1}} \left[ (s+a_n)^k \, \Phi_{N\chi}(s) \right] \right\} \Bigg|_{s=-a_n} \tag{1.40}$$

and finally,

$$P_{N\chi}(\chi) = \left( \prod_{n=1}^{N} a_n^{L_n} \right) \sum_{n=1}^{N} \sum_{k=1}^{L_n} \frac{C_{nk} \chi^{k-1} e^{-a_n \chi}}{(k-1)!} \tag{1.41}$$

The generally intractable nature of Equation (1.40) leads to the introduction of approximate methods discussed in the following section.

1.2.1.4 Edgeworth's Series Approximation, Case (c)

As before,

$$N\chi = \sum_{i=1}^{N} \chi_i$$

where the $\chi_i$ are independent random variables distributed

according to Equation (1.19) and in general with different long term average means $\mu_i$ and different number of line components $L_i$. Although $P_{N\chi}(\chi)$ cannot be solved exactly for N > 3 without considerable computational tedium, it can be approximated in the main lobe, and as we shall see, quite accurately and easily by an Edgeworth's series [14]:

$$P_{N\chi}(\chi) = \frac{1}{\sigma_{N\chi}} \left\{ Z(\xi) - \frac{1}{3!}\gamma_s Z^{(3)}(\xi) + \frac{1}{4!}\gamma_e Z^{(4)}(\xi) \right.$$

$$+ \frac{10}{6!}\gamma_s^2 Z^{(6)}(\xi) - \frac{1}{5!}\frac{K_5}{\sigma_\chi^5} Z^{(5)}(\xi)$$

$$- \frac{37}{7!}\gamma_s\gamma_e Z^{(7)}(\xi)$$

$$\left. - \frac{280}{9!}\gamma_s^3 Z^{(9)}(\xi) + \ldots \text{terms in higher order moments} \right\} \quad \ldots (1.42)$$

where

$$\xi = \frac{\chi - \mu_{N\chi}}{\sigma_{N\chi}} , \qquad Z(\xi) = \frac{1}{(2\pi)^{1/2}} e^{-\frac{1}{2}\xi^2} ,$$

$Z^{(n)}(\xi)$ = $n^{th}$ derivative of the Gaussian pdf,

$$\gamma_s \equiv \text{coefficient of skew} = \frac{^3\mu_\chi}{\sigma_\chi^3} = \frac{K_3}{\sigma_\chi^3} \tag{1.43}$$

$$\gamma_e \equiv \text{coefficient of excess} = \frac{^4\mu_\chi}{\sigma_\chi^4} - 3 = \frac{K_4}{\sigma_\chi^4} \tag{1.44}$$

$^n\mu_\chi \equiv n^{th}$ central moment, and

$K_n \equiv n^{th}$ order cumulant or semi-invariant.

The point-by-point error in the approximation of Equation (1.42) is of the same order as the first term neglected [14].

A computationally more efficient expression of Equation (1.42) can be derived by actually taking the derivatives of $Z(\xi)$ as indicated with respect to $\xi$ and collect terms in powers of $\xi$. I have used only the first four terms in Equation (1.42) and as will be demonstrated later, this will be entirely adequate for practical

computations.

$$P_{N^{\chi}}(\chi) \simeq \frac{1}{\sigma_{N^{\chi}}} Z(\xi)\left\{1 + \frac{3\gamma_e}{4!} - \frac{5\gamma_s^2}{24} - \frac{\gamma_s}{2}\xi + \left[\frac{5\gamma_s^2}{8} - \frac{\gamma_e}{4}\right]\xi^2 + \frac{\gamma_s}{3!}\xi^3 + \left[\frac{\gamma_e}{4!} - \frac{5\gamma_s^2}{24}\right]\xi^4 + \frac{10\gamma_s^2}{6!}\xi^6\right\} \tag{1.45}$$

It should be noted that because Equation (1.45) is an approximation, negative values may be obtained for some regions in the tails. In fact, the Edgeworth's series performs best in the main lobe of the density and worse in the tails. The mean and variance is respectively (evoking the properties of sums of independent random variables [14]):

$$\mu_{N^{\chi}} = \sum_{i=1}^{N} L_i \mu_i \tag{1.46}$$

$$\sigma^2_{N^{\chi}} = \sum_{i=1}^{N} L_i \mu_i^2 \tag{1.47}$$

For the gamma pdf [14]:

$$K_n = \mu^n L\Gamma(n) \tag{1.48}$$

Furthermore, for a sum of independent random variables [14]:

$$K_n = {}_1K_n + {}_2K_n + {}_3K_n + \ldots + {}_NK_n \tag{1.49}$$

I use Equations (1.46) through (1.49) to obtain the coefficients of skew and excess for $P_{N\chi}(\chi)$:

$$\gamma_s = \frac{1}{\sigma_\chi^3} \sum_{i=1}^{N} 2L_i\mu_i^3 , \tag{1.50}$$

$$\gamma_e = \frac{1}{\sigma_\chi^4} \sum_{i=1}^{N} 6L_i\mu_i^4 . \tag{1.51}$$

$\gamma_s$ and $\gamma_e$ are zero for the Gaussian pdf and attain maximum values of 2 and 6 respectively for the exponential pdf (which is the case of $N = 1$ and $L = 1$).

Before examining the nature of $\gamma_s$ and $\gamma_e$ more closely, let me return to Equation (1.42) and make the log transformation to obtain the Edgeworth's approximation for

the level in dB:

$$P_{N^{\Lambda}}(\Lambda) \approx \frac{1}{\varepsilon\sigma_{N^{\chi}}} e^{\Lambda/\varepsilon} \left\{ Z(\eta) - \frac{\gamma_s}{3!} Z^{(3)}(\eta) + \frac{\gamma_e}{4!} Z^{(4)}(\eta) + \frac{\gamma_s^2 \cdot 10}{6!} Z(\eta) \right\}$$

. . .(1.52)

or alternatively,

$$P_{N^{\Lambda}}(\Lambda) \approx \frac{1}{\varepsilon\sigma_{N^{\chi}}} e^{\Lambda/\varepsilon} Z(\eta) \left\{ 1 + \frac{3\gamma_e}{4!} - \frac{5\gamma_s^2}{24} - \frac{\gamma_s}{2}\eta + (\frac{5\gamma_s^2}{8} - \frac{\gamma_e}{4})\eta^2 \right.$$

$$\left. + \frac{\gamma_s}{3!}\eta^3 + (\frac{\gamma_e}{4!} - \frac{5\gamma_s^2}{24})\eta^4 + \frac{10\gamma_s^2}{6!}\eta^6 \right\} \qquad (1.53)$$

where

$$\eta\sigma_{N^{\chi}} = \exp(\Lambda/\varepsilon) - \mu_{N^{\chi}}.$$

As a result of the fact that the transformation $\Lambda = 10 \log_{10}\chi$ is nonlinear, the statistics of $\Lambda$ cannot be found without exact knowledge of $P_{N^{\Lambda}}(\Lambda)$:

$$\mu_{N^{\Lambda}} = \varepsilon \int_{o}^{\infty} \ln\chi \; P_{N^{\chi}}(\chi) d\chi$$

$$\sigma^2_{N^{\Lambda}} + \mu^2_{N^{\Lambda}} = \varepsilon^2 \int_{o}^{\infty} (\ln\chi)^2 \; P_{N^{\chi}}(\chi) d\chi \qquad (1.54)$$

Using Equation (1.41) in the previous section and interchanging the order of summation and integration I obtain:

$$\mu_{N^{\Lambda}} = (\varepsilon \prod_{n=1}^{N} a_n^{L_n}) \sum_{n=1}^{N} \sum_{k=1}^{L_n} \frac{C_{nk}}{(k-1)!} \int_{o}^{\infty} \ln\chi \cdot \chi^{k-1} \; e^{-a_n\chi} d\chi$$

$$\sigma^2_{N^{\Lambda}} + \mu^2_{N^{\Lambda}} = (\varepsilon^2 \prod_{n=1}^{N} a_n^{L_n}) \sum_{n=1}^{N} \sum_{k=1}^{L_n} \frac{C_{nk}}{(k-1)!} (\ln\chi)^2 \chi^{k-1} \; e^{-a_n\chi} d\chi \qquad (1.55)$$

Evaluating Equations (1.55) yields [24]:

$$\mu_{N^{\Lambda}} = (\varepsilon \prod_{n=1}^{N} a_n^{L_n}) \sum_{n=1}^{N} \sum_{k=1}^{L_n} \frac{C_{nk}}{a_n^k} [\psi(k) - \ln a_n]$$

$$\sigma^2_{N^{\Lambda}} + \mu^2_{N^{\Lambda}} = (\varepsilon^2 \prod_{n=1}^{N} a_n^{L_n}) \sum_{n=1}^{N} \sum_{k=1}^{L_n} \frac{C_{nk}}{a_n^k} \left\{ [\psi(k) - \ln a_n]^2 + \psi^1(k) \right\} \qquad (1.56)$$

Though Equations (1.56) are exact, they are predicated on the knowledge of the $C_{nk}$'s given by Equation (1.40), which in turn motivates an approximate solution. Unfortunately, direct integration of the Edgeworth's series is not possible because term by term the integrals diverge. An approximation can be made, however, using the first term only, that is, to integrate the log transformed Gaussian. Thus,

$$\mu_{N^{\Lambda}} \approx \frac{\varepsilon}{\sigma_{\chi}\sqrt{2\pi}} \int_{o}^{\infty} \ln\chi \exp\left[-\frac{(\chi-\mu_{\chi})^2}{2\sigma_{\chi}^2}\right] d\chi$$

$$\sigma^2_{N^{\Lambda}} + \mu^2_{N^{\Lambda}} \approx \frac{\varepsilon^2}{\sigma_{\chi}\sqrt{2\pi}} \int_{o}^{\infty} (\ln\chi)^2 \exp\left[-\frac{(\chi-\mu_{\chi})^2}{2\sigma_{\chi}^2}\right] d\chi \qquad (1.57)$$

The integrals in Equations (1.57) are not straightforward but can be evaluated as follows. First, the square in the exponential is expanded, and the constant term removed from under the integral sign. Second, the change of variables $\chi = u^{1/2}$ is made:

$$\mu_{N^{\Lambda}} \approx \frac{\varepsilon e^{-\frac{\mu_\chi^2}{2\sigma_\chi^2}}}{2\sigma_\chi\sqrt{2\pi}} \int_0^\infty u^{-\frac{1}{2}} \ln\sqrt{u}\, \exp\left(-\frac{u}{2\sigma_\chi^2} + \frac{\mu_\chi}{\sigma_\chi^2}\sqrt{u}\right) du$$

$$\sigma^2_{N^{\Lambda}} + \mu^2_{N^{\Lambda}} \approx \frac{\varepsilon^2 e^{-\frac{\mu_\chi^2}{2\sigma_\chi^2}}}{2\sigma_\chi\sqrt{2\pi}} \int_0^\infty u^{-\frac{1}{2}} (\ln\sqrt{u})^2 \exp\left(-\frac{u}{2\sigma_\chi^2} + \frac{\mu_\chi}{\sigma_\chi^2}\sqrt{u}\right) du \qquad (1.58)$$

Third, the radical is removed from the ln and the exponential of $\sqrt{u}$ is expanded in its power series. Fourth, the order of integration and summation are interchanged and finally I have,

$$\mu_{N^{\Lambda}} \approx \frac{\varepsilon e^{-\frac{\mu_\chi^2}{2\sigma_\chi^2}}}{4\sigma_\chi\sqrt{2\pi}} \sum_{m=0}^{\infty} \frac{1}{m!} \left(\frac{\mu_\chi}{\sigma_\chi^2}\right)^m \int_0^\infty u^{\left(\frac{1}{2}m-\frac{1}{2}\right)} \ln u\, \exp\left(-\frac{u}{2\sigma_\chi^2}\right) du$$

$$\sigma^2_{N^{\Lambda}} + \mu^2_{N^{\Lambda}} \approx \frac{\varepsilon^2 e^{-\frac{\mu_\chi^2}{2\sigma_\chi^2}}}{8\sigma_\chi\sqrt{2\pi}} \sum_{m=0}^{\infty} \frac{1}{m!} \left(\frac{\mu_\chi}{\sigma_\chi^2}\right)^m \int_0^\infty u^{\left(\frac{1}{2}m-\frac{1}{2}\right)} (\ln u)^2 \exp\left(-\frac{u}{2\sigma_\chi^2}\right) du \qquad (1.59)$$

The integral in Equations (1.59) can be evaluated [24] and the final result is obtained:

$$\mu_{N^\Lambda} = \frac{\varepsilon e^{-\frac{\mu_\chi^2}{2\sigma_\chi^2}}}{4\sqrt{\pi}} \sum_{m=0}^{\infty} \frac{1}{m!} \left(\frac{\sqrt{2}\mu_\chi}{\sigma_\chi}\right)^m \Gamma\left(\tfrac{1}{2}m + \tfrac{1}{2}\right) \left\{\psi\left(\tfrac{1}{2}m + \tfrac{1}{2}\right) + \ln\, 2\sigma_\chi^2\right\}$$

and (1.60a)

$$\sigma^2_{N^\Lambda} + \mu^2_{N^\Lambda} = \frac{\varepsilon^2 e^{-\frac{\mu_\chi^2}{2\sigma_\chi^2}}}{8\sqrt{\pi}} \sum_{m=0}^{\infty} \frac{1}{m!} \left(\frac{\sqrt{2}\mu_\chi}{\sigma_\chi}\right)^m \Gamma\left(\tfrac{1}{2}m + \tfrac{1}{2}\right)$$

$$\cdot \left\{\left[\psi\left(\tfrac{1}{2}m + \tfrac{1}{2}\right) + \ln 2\sigma_\chi^2\right]^2 + \psi^1\left(\tfrac{1}{2}m + \tfrac{1}{2}\right)\right\}$$

Although the Edgeworth's series will provide an accurate approximation to the density we seek, the best approximation for the moments of $\Lambda$ are those of the log transformed Gaussian given by the statistics of Equations (1.60). Though not immediately derivable from Equations (1.60) when $\sigma_\chi^2$ is small, Dyer [4] obtains, by taking an expansion around the peak of the density,

$$\mu_{N^\Lambda} \simeq [\ln\mu_\chi - (\sigma_\chi^2/2\mu_\chi^2)]\varepsilon$$

$$\sigma^2_{N^\Lambda} \simeq (\sigma_\chi^2/\mu_\chi^2)\,\varepsilon^2 \qquad (1.60b)$$

Returning to the Edgeworth's series, and to gain more insight into the way the coefficients of skew and excess ($\gamma_s$ and $\gamma_e$) behave, depending upon the number of groups N, and number of line components in each group $L_i$, I have plotted $\gamma_s$ vs L in Figure 1 for N = 1 and N $\geq$ 3. In like manner, $\gamma_e$ is plotted in Figure 2. Each was constructed as follows: Each group N has the same number of line components L, and the long term average mean $\mu_i$ of each group is quantitized in 3dB steps, i.e.:

$$\left.\begin{aligned} \mu_i &= \left(\frac{1}{2}\right)^{i-1} \text{ relative units} \\ L_i &= L \end{aligned}\right\} \; i = 1,2,3,\ldots,N$$

For the case N = 1, Equations (1.50) and (1.51) yield:

$$\gamma_s = 2L^{-1/2}$$

$$\gamma_e = 6L^{-1}$$

In the limit as N $\to \infty$, Equations (1.50) and (1.51) converge to:

$$\gamma_s = [1.48]L^{-1/2}$$

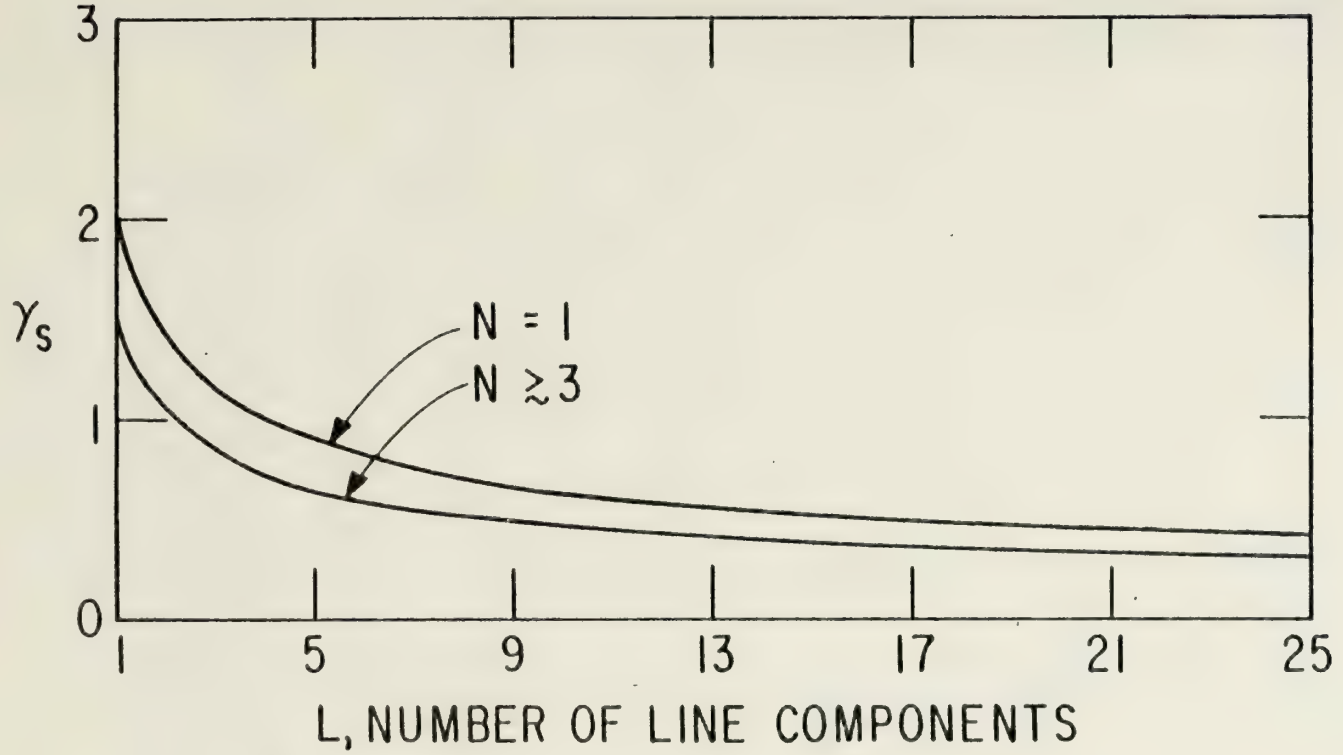


Fig. 1 The coefficient of skew, $\gamma_s$, for one group (N=1) and three or more groups (N≥3) as a function of L, the number of line components in each group.

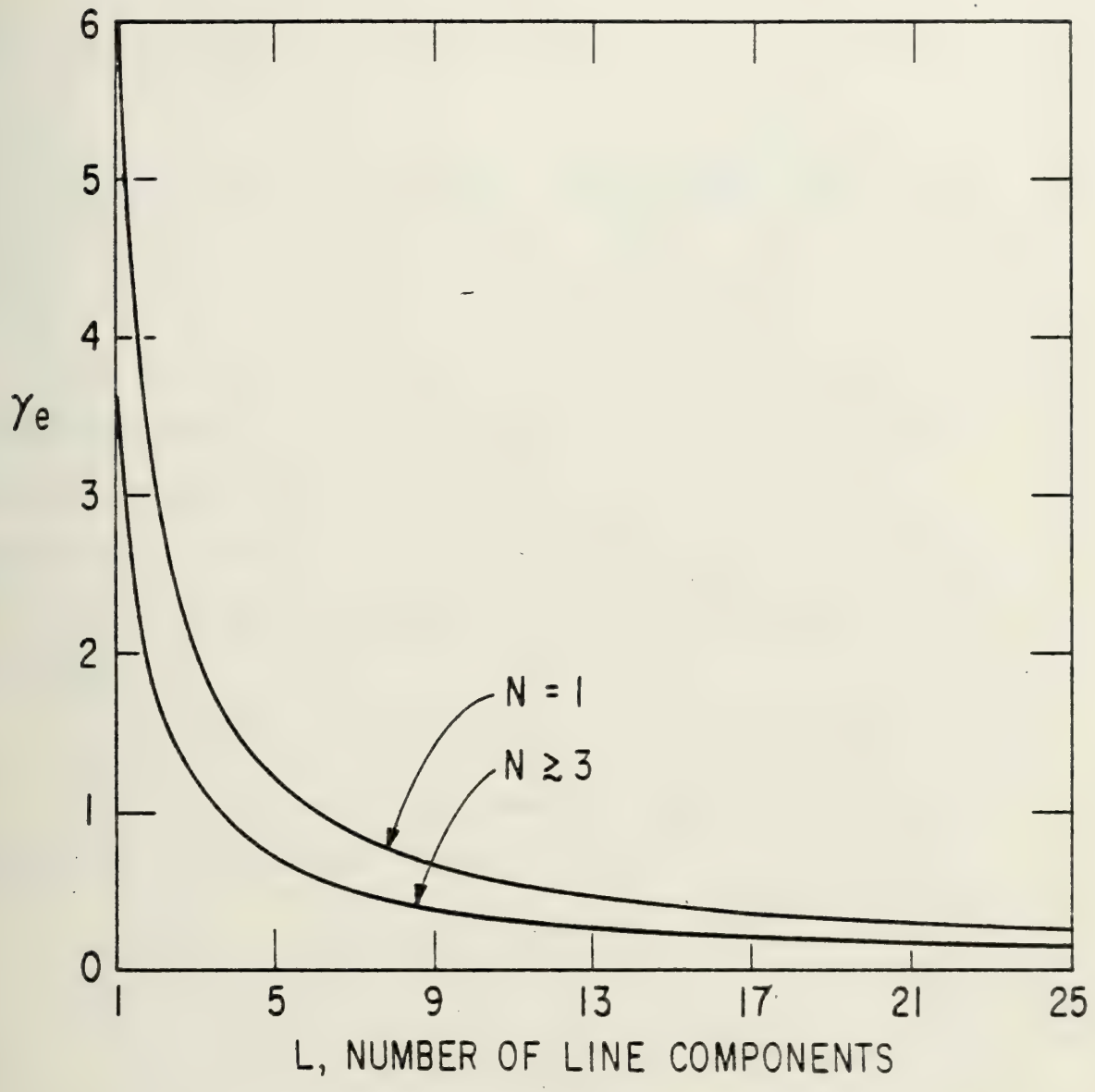


Fig. 2 The coefficient of excess, $\gamma_e$, for one group (N=1) and three or more groups (N≥3) as a function of L, the number of line components in each group.

$$\gamma_e = [3.60]L^{-1}$$

The convergence is very rapid. As evidence, the exact value for $N = 3$ is only about 10% greater than the limiting value.

From Figures 1 and 2 it can be seen that when $N = 1$, the coefficient of skew and excess closely approximate Gaussian values when $L \geq 6$. When $N \geq 3$ they closely approximate Gaussian values for $L \geq 3$. More justification for this conclusion is given in the next several paragraphs.

For further illustration of significance of the value of $\gamma_s$ and $\gamma_e$ I consider the case $N = 1$ and $L = 2$. For simplicity, I let $\mu = 1$. Then,

$$P_\chi(\chi) = \chi e^{-\chi} \tag{1.61}$$

$$\mu_\chi = 2$$

$$\sigma_\chi^2 = 2$$

$$\gamma_s = \sqrt{2}$$

$$\gamma_e = 3$$

Equation (1.61) is plotted with the Edgeworth's series,

Equation (1.45), and its corresponding Gaussian in Figure 3. Note that the large values of $\gamma_s$ and $\gamma_e$ would predict the Gaussian to be a poor approximation, and so it is. The Edgeworth's series, on the other hand, is quite good except at the tails.

Taking the log transformation of Equation (1.61) for the same simple case (N = 1 and L = 2), I have the density of the level in dB:

$$P_{\Lambda}(\Lambda) = \frac{1}{\varepsilon} \exp\left\{\frac{2\Lambda}{\varepsilon} - \exp\ (\Lambda/\varepsilon)\right\} \qquad (1.62)$$

Equation (1.62) is plotted with the Edgeworth's series as given by Equation (1.53) in Figure 4. Again, the values for $\gamma_s$ and $\gamma_e$ suggest the log transform of the Gaussian to be a poor approximation, and indeed it is. But the Edgeworth's series for the density of the level is remarkably close. Thus, I conclude than when $\gamma_s$ and $\gamma_e$ are large, the Gaussian is not a useful approximation, but the Edgeworth is, especially when dealing with the pdf of the level. Also, it is interesting to compare estimates of the mean level. Equation (1.60a) gives $\mu_{\Lambda}$ = 2.28dB while the exact value given by Equation (1.25),

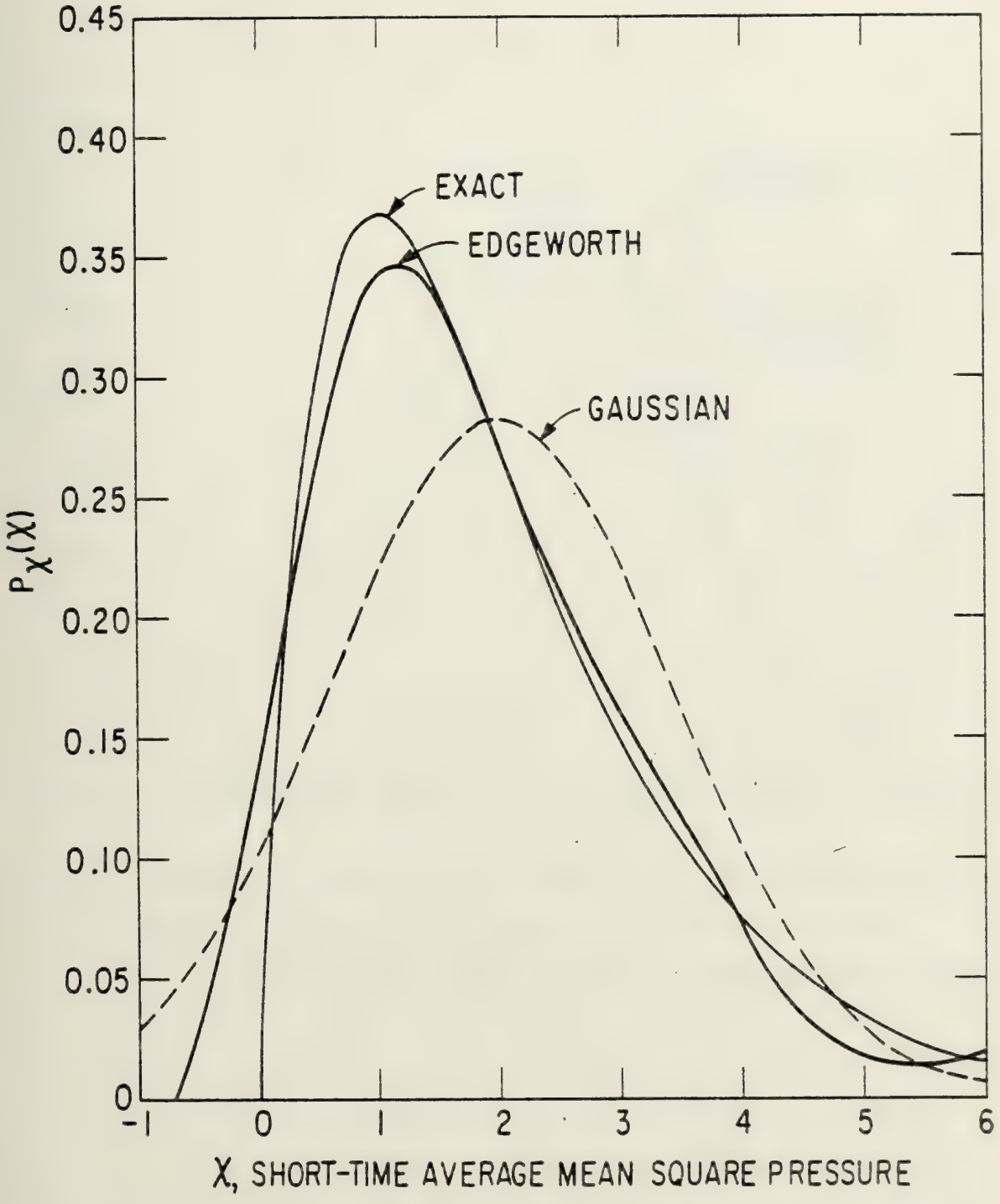


Fig. 3 Probability density for the case N=1, L=2, and $\mu$=1. $\gamma_s = \sqrt{2}$ and $\gamma_e = 3$. The exact density is shown with its Edgeworth approximation and its corresponding Gaussian.

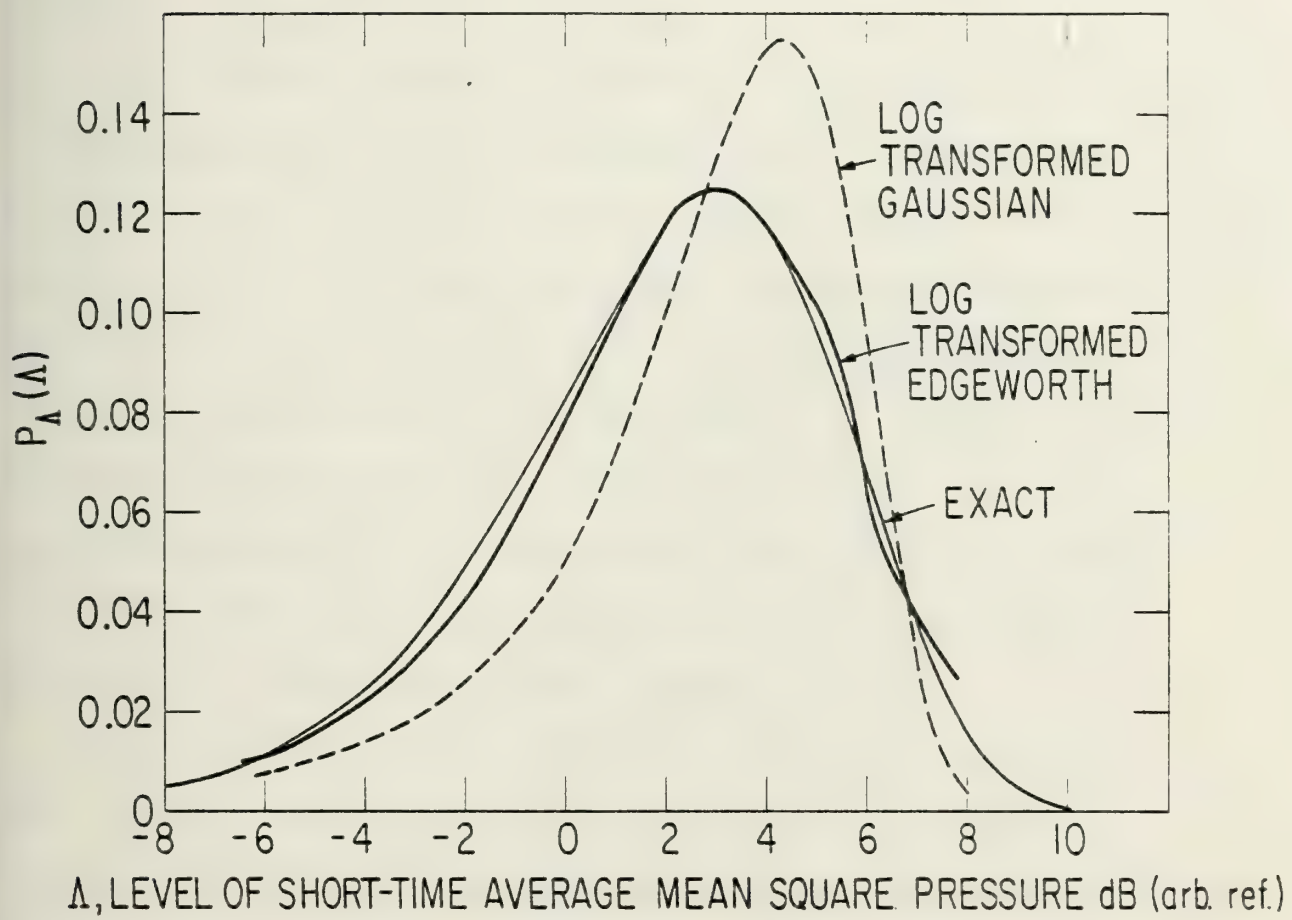


Fig. 4 Probability density of the level for the case plotted in Fig. 3. Shown with the exact density are its transformed Edgeworth approximation and its transformed Gaussian.

setting $L_1 = L_2 = a_1 = a_2 = 1$, is $\mu_\Lambda = 1.83$dB.

As a second example, I consider Case (c) of Figure 2 of Reference [4], with the specification N = 2, $a_1 = 0.3$, $a_2 = 0.6$, and $L_1 = L_2 = 2$. For this we have $\gamma_s = 1.14$ and $\gamma_e = 2.04$. The log transformed Edgeworth approximation, Equation (1.53), is plotted with the exact density in Figure 5. Here, Equation (1.60a) gives $\mu_\Lambda = 9.16$dB while the exact value given by Equation (1.25) is $\mu_\Lambda = 9.39$dB. The log transform of the Gaussian is not a good approximation, but here again the Edgeworth and the exact density are for all practical purposes identical.

For a final example I examine a three group problem (N = 3) using the results of Section 1.2.1.2 to compare with the Edgeworth's approximation and the Gaussian. In this example, $a_1 = 1$, $a_2 = 2$, $a_3 = 8$, $L_1 = 2$, $L_2 = 4$, and $L_3 = 16$. Using Equations (1.49) and (1.50), I find $\gamma_s = .86$ and $\gamma_e = 1.28$. Equation (1.53) and the exact density of the level as given by Equation (1.33) are plotted in Figure 6 with the transformed Gaussian. Once again, Equation (1.53) is exact for all practical purposes while the Gaussian assumption will result in some error.

Thus, from our examples for $\gamma_s$ and $\gamma_e$ not too large, i.e., $\leq 1.5$ and 3 respectively, the first four terms of the log transformed Edgeworth series adequately represents

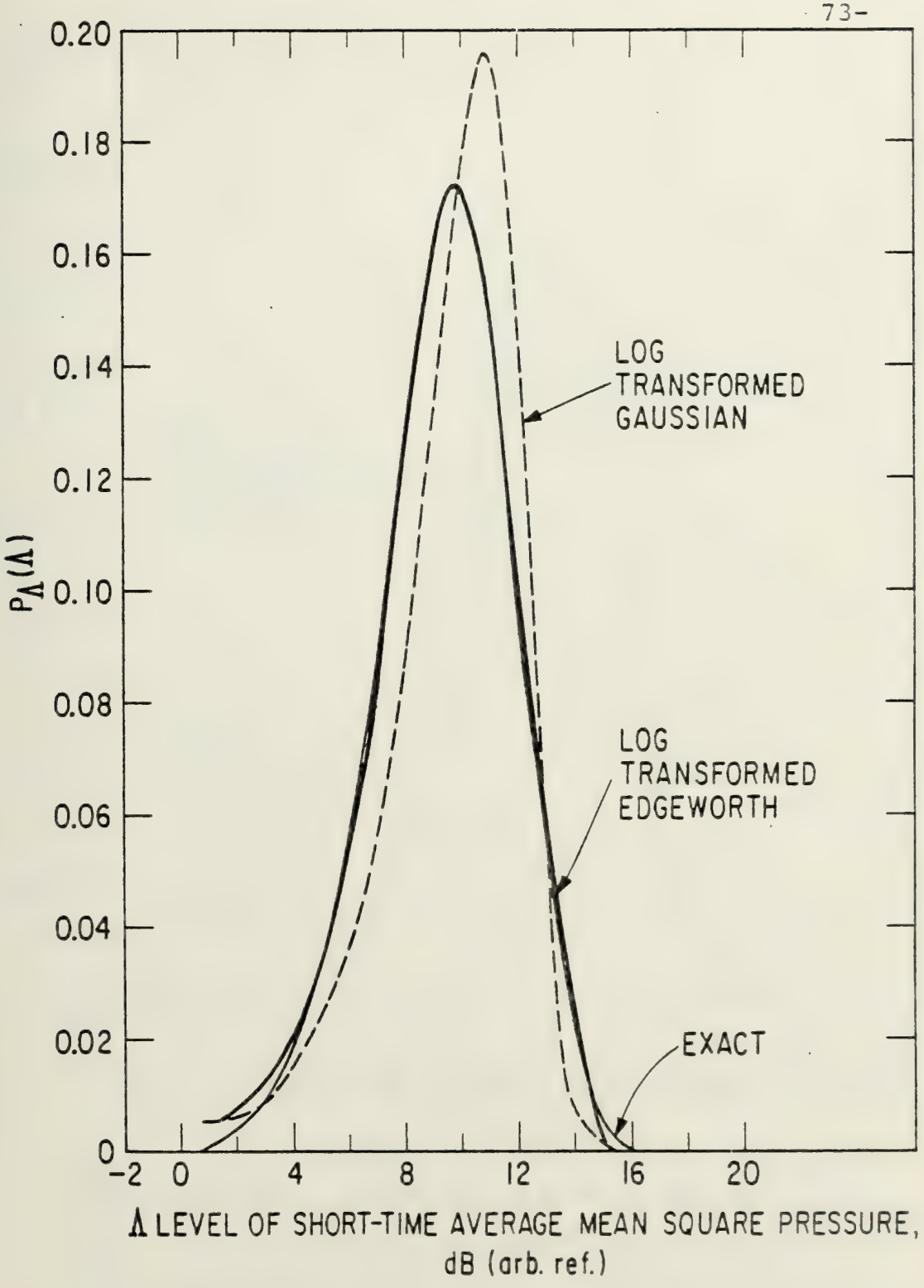


Fig. 5 Probability density of the level for the case $N=2$, $L_1=L_2=2$, $\mu_1=10/3$, and $\mu_2=5/3$, $\gamma_s=1.14$ and $\gamma_e=2.04$. Shown with the exact density are its transformed Edgeworth approximation and its transformed Gaussian.

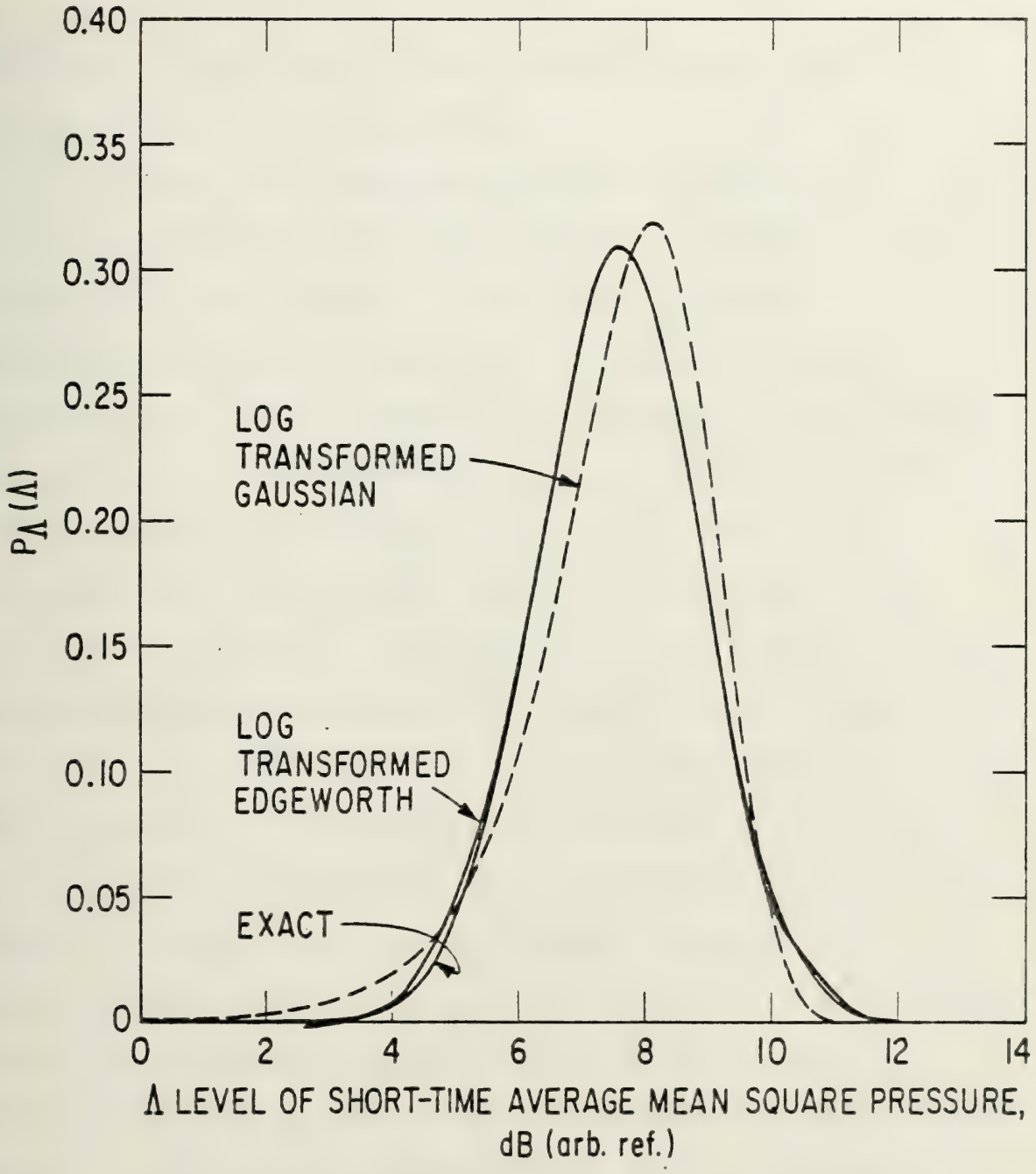


Fig. 6 Probability density of the level for the case $N=3$, $L_1=2$, $L_2=4$, $L_3=16$, $\mu_1=1$, $\mu_2=1/2$, and $\mu_3=1/8$. $\gamma_s=.86$ and $\gamma_e=1.28$. Shown with the exact density are its transformed Edgeworth approximation and its transformed Gaussian.

the levels, while the log transformed Gaussian requires $\gamma_s \approx \gamma_e \approx 0$ for it to be adequate.

I now apply the foregoing analysis to the N = 15 problem of Reference [4]. This problem involves estimates of ocean traffic in the North Atlantic. Components from each of the ships are grouped with 3dB quantitization in N = 15 steps, with components within each group numbering as high as $L_i = 57$, as is shown in the first three columns of Table I. With the use of Equations (1.50) and (1.51) I find $\gamma_s = 1.025$ and $\gamma_e = 1.743$. In Table I, the contributions of each of the groups to the mean, variance, and coefficients of skew and excess are also tabulated. As is clear from the table, groups 9-15 contribute very little to the overall density, since the variance, skew, and excess do not change (to within three decimal places) beyond N = 8. Reduction to an eight group problem, however, is not much of an improvement over the 15 group one. But, Equations (1.46), (1.47), (1.50), and (1.51) are very simple for any N, and in comparing $\gamma_s$ and $\gamma_e$ for this case with those of our previous examples, we can expect the density of the mean square pressure to be closely approximated by Equation (1.45). Similarly, Equation (1.53) should yield the density of the level in dB, which for all

TABLE I

| i | $\Lambda_R$(dB) | $L_i$ | $\mu_\chi$ | $\sigma_\chi^2$ | $\gamma_s$ | $\gamma_e$ |
|---|---|---|---|---|---|---|
| 1 | 0 | 2 | 2.000 | 2.000 | 0.897 | 1.634 |
| 2 | -3 | 2 | 3.000 | 2.500 | 1.009 | 1.736 |
| 3 | -6 | 2 | 3.500 | 2.625 | 1.023 | 1.742 |
| 4 | -9 | 2 | 3.750 | 2.656 | 1.025 | 1.743 |
| 5 | -12 | 6 | 4.125 | 2.679 | | |
| 6 | -15 | 17 | 4.656 | 2.696 | | |
| 7 | -18 | 44 | 5.344 | 2.707 | | |
| 8 | -21 | 48 | 5.719 | 2.710 | | |
| 9 | -24 | 15 | 5.778 | | | |
| 10 | -27 | 20 | 5.817 | | | |
| 11 | -30 | 57 | 5.873 | | | |
| 12 | -33 | 26 | 5.886 | | | |
| 13 | -36 | 28 | 5.893 | | | |
| 14 | -39 | 39 | 5.898 | | | |
| 15 | -42 | 31 | 5.900 | | | |

The contributions of each group of the N = 15 problem of Reference [4] to the overall mean, variance, coefficient of skew, and coefficient of excess of the density of the short-time average mean square pressure. The relative level ($\Lambda_R$) and the number of line components ($L_i$) is shown for each group i.

practical purposes would be exact. Equation (1.45) for this case is plotted along with the Gaussian in Figure 7, and Equation (1.53) is plotted with the transformed Gaussian in Figure 8. The Gaussian pdf is seen to depart significantly from the Edgeworth pdf, even for a case having a very large number of line components such as may be appropriate to an actual oceanic situation. However, with reference to the examples above and Figures 3-6, we are justified in expecting that the Edgeworth pdf is virtually exact.

As noted earlier, an analytical expression has not yet been derived for the statistics of the log transform for N > 3. However, I can estimate the mean from Figure 8 to be (supported by a numerical integration of Equation 1.53)

$$\mu_\Lambda \approx 7.2\text{dB}$$

The Gaussian assumption used in Reference [4] led to a slightly higher value for the mean ($\approx$ 7.5dB) as a glance at Figure 8 would explain. Equation (1.60a) gives $\mu_\Lambda \approx 7.51$dB affirming the result obtained by Dyer [4]. The standard deviation as computed in Reference [4] of 1.2dB appears reasonable, again by inspection of Figure 8, while Equation (1.60a) yields $\sigma_\Lambda \approx 1.40$dB.

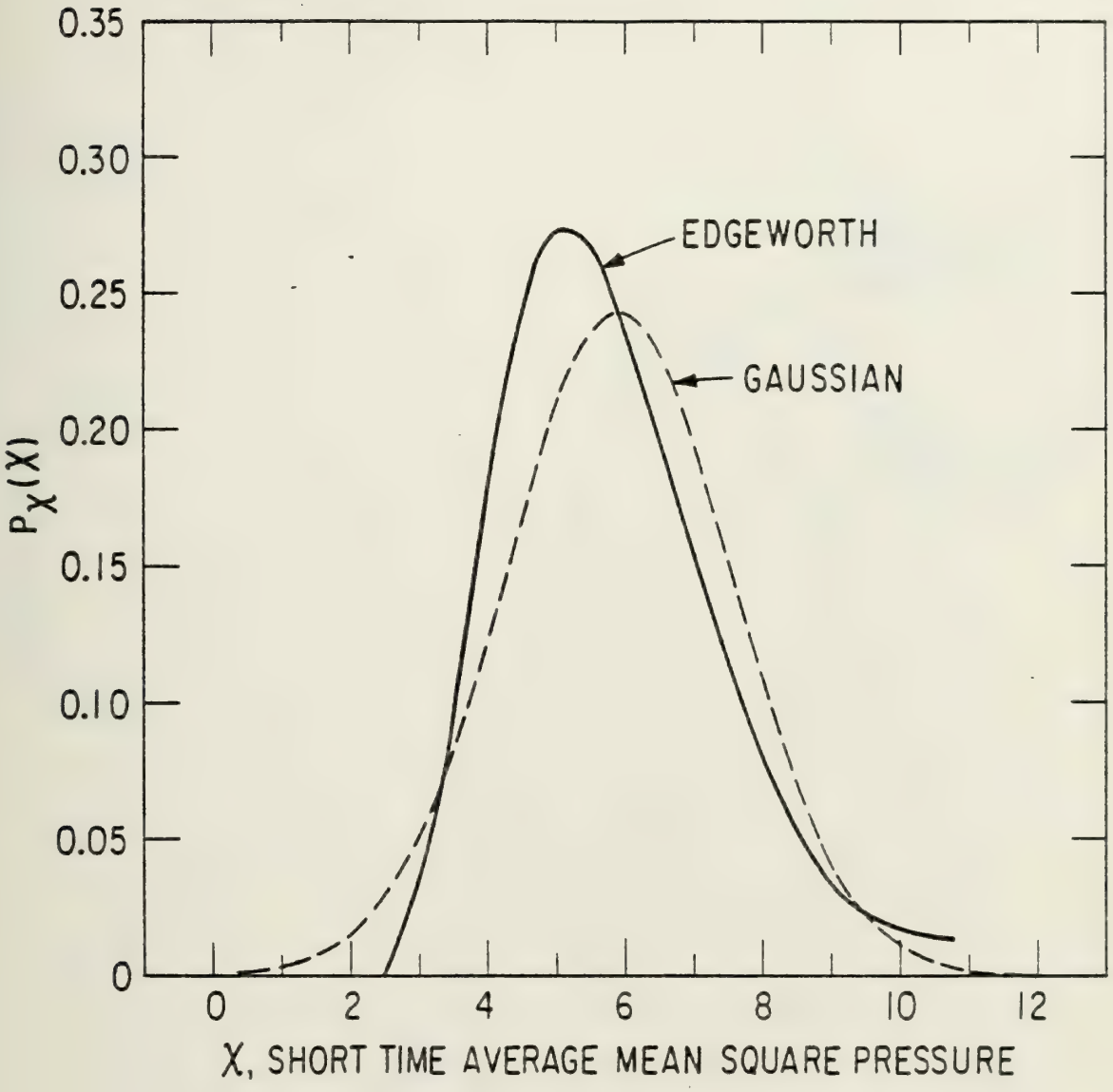


Fig. 7 The Gaussian and Edgeworth approximations of the probability density of the short-time average mean square pressure of the noise that may be sensed in deep water near Bermuda in winter, for a 1/3-oct band at 60 Hz and an omni-directional hydrophone. The ships have been grouped in 3dB steps in fifteen groups, with overall mean, variance, and coefficients of skew and excess as specified in Table I.

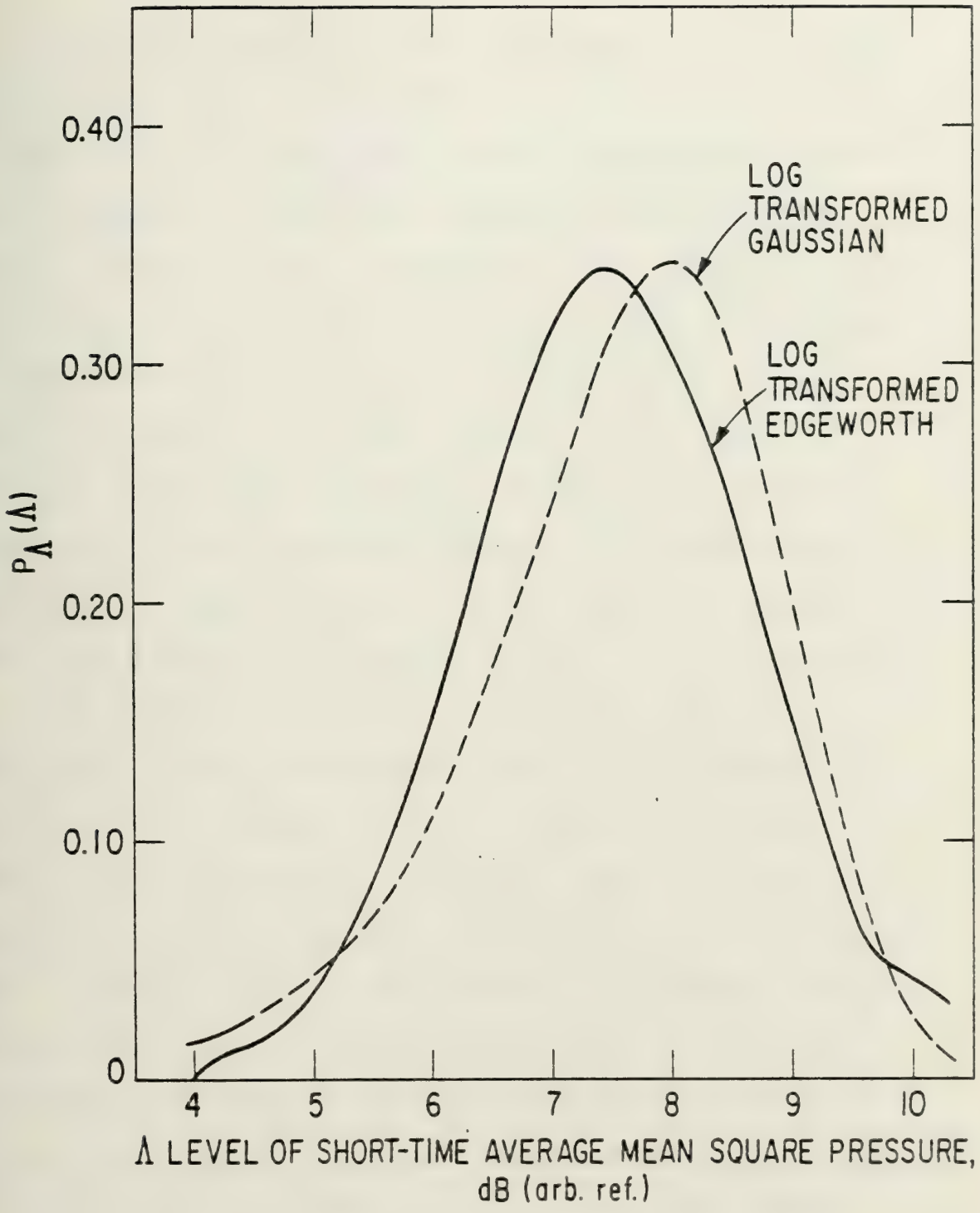


Fig. 8 The transformed Gaussian and the transformed Edgeworth approximation of the probability density of the level for the case plotted in Fig. 7.

We may conclude that when the number of groups which add significantly to the overall density is greater than 3, then use of the Edgeworth series approximation can be quite valuable in estimating the pdf of the received signal. While it may be tempting to use a Gaussian pdf for values of $\gamma_s \leq 1$ and $\gamma_e \lesssim 2$, significant differences in the pdf for the mean square pressure or the level should dissuade us from this course. It is true that the mean and standard deviation of the levels are less sensitive to the differences between the Edgeworth and the Gaussian approximations, but the Edgeworth is not much more difficult to use and is thus to be recommended.

The Edgeworth's series approximation therefore provides an easily implemented method of (1) estimating the statistics of the level in dB for even the most complicated realization of Case (c), and (2) revealing the extent to which the Gaussian assumption is a valid one. This is particularly valuable because one cannot merely assume on the basis that N is large that the Gaussian assumption will be a valid one. The critical factor is the amount of energy in each group. If one or two groups contain most of the energy, then the governing density will be significantly different from the Gaussian and, in fact, will more closely resemble the density that would be

associated with the most energetic group.

If the tails of the pdf are the primary regions of interest, then exact computer solution may be a viable alternative for a complicated realization of Case (c). It should be noted, however, that more terms in the Edgeworth's series can be taken to obtain any arbitrary accuracy desired, or alternative methods such as the Chernoff bound or "tilting" the density can be applied [25]. These methods will not be discussed in this work.

### 1.2.2 Amplitude Rate Densities

In this section of the thesis I will derive the pdf's of $\dot{\rho}$, $\dot{\chi}$, and $\dot{\Lambda}$ for the multiple source case. These rate variables are dependent variables with respect to the amplitude variables except for certain special cases. This fact introduces a great deal more complexity than has been encountered up to now. Solution for the joint densities of amplitude and amplitude rate are generally required before the marginal rate densities themselves can be found. Solution of the rate density for one variable does not lead by simple transformation to the solution for the rate densities for the other two variables as was the case for the amplitude.

In general, the rate variables depend upon both $\sigma_1^2$,

a measure of the intensity, and $\nu^2$, the single path mean square phase rate. This implies that there are a plethora of different possible combinations of multiple sources with different or same $\sigma_1^2$ and/or different or same $\nu^2$. The breakdown into the same cases employed in Section 1.2.1 will be followed here, though their definitions must be expanded to include $\nu^2$. In Section 1.2.2.1 I examine Case (a), the case of multiple sources or lines in which $\sigma_1^2$ and $\nu^2$ are the same for all source/receiver pairs. This would apply, for example, to noise which is flat across the passband of the receiver from a small geographical area or sector. In Section 1.2.2.2 I investigate various special cases when the $\sigma_1^2$'s and the $\nu^2$ may be different for each source/receiver pair, with more general applicability, including Cases (b) and (c).

### 1.2.2.1 Multiple Components of Equal Intensity and Equal Single Path Phase Rate

I will first solve for $P_{\dot{\chi}_{LE}}(\dot{\chi})$ which is the pdf for $\dot{\chi}$ from L sources or components of equal $\sigma_1^2$ and $\nu^2$. From $\chi_{total} = \sum_{n=1}^{L} \chi_n$, it is clear that $\dot{\chi}_{total} = \sum_{n=1}^{L} \dot{\chi}_n$. Thus for this, and only this variable, we can employ all the very nice properties of sums of independent random variables. For the pdf of $\dot{\chi}_{LE}$

$$P_{\dot{\chi}_{LE}}(\chi) = \int_{-\infty}^{y_1}\int_{-\infty}^{y_2}\cdots\int_{-\infty}^{\dot{\chi}} P_{\dot{\chi}}(y_1)P_{\dot{\chi}}(y_2-y_1)\cdots P_{\dot{\chi}}(\dot{\chi}-y_L)\,dy\cdots dy_L$$

. . .(1.63)

or

$$P_{\dot{\chi}_{LE}}(\dot{\chi}) = \frac{1}{2\pi}\int_{-\infty}^{\infty} \frac{b^{2L}}{(b^2+\omega^2)^L}\, e^{i\omega\dot{\chi}}\, d\omega \qquad (1.64)$$

by making use of $M_{\dot{\chi}}(\omega)$ (Equation A6), where $b = 1/2\sigma_1^2\nu$. For $\chi > 0$, therefore,

$$P_{\dot{\chi}_{LE}}(\dot{\chi}) = \frac{b^{2L}}{2\pi}\, 2\pi i \left\{\frac{1}{(L-1)!}\frac{d^{L-1}}{d\omega^{L-1}}\left[\frac{e^{i\omega\dot{\chi}}}{(\omega+ib)^L}\right]\right\}\Bigg|_{\omega = ib} \qquad (1.65)$$

Applying contour integration around the lower half plane for $\dot{\chi} < 0$ yields, as expected, the identical result given by Equation (1.65) because $\dot{\chi}$ is symmetric. Applying Equations (1.63) and (1.65) for L = 1-6, I obtain

$$P_{\dot{\chi}_{1E}}(\dot{\chi}) = \frac{b}{2}\exp(-b|\dot{\chi}|)$$

$$P_{\dot{\chi}_{2E}}(\dot{\chi}) = \frac{1}{4}\{b^2|\dot{\chi}| + b\}\exp(-b|\dot{\chi}|)$$

$$P_{\dot{\chi}_{3E}}(\dot{\chi}) = \frac{1}{16}\{b^3|\dot{\chi}|^2 + 3b^2|\dot{\chi}| + 3b\}\exp(-b|\dot{\chi}|)$$

$$P_{\dot{\chi}_{4E}}(\dot{\chi}) = \frac{1}{96}\{b^4|\dot{\chi}|^3 + 6b^3|\dot{\chi}|^2 + 15b^2|\dot{\chi}| + 15b\}\exp(-b|\dot{\chi}|)$$

$$P_{\dot{\chi}_{5E}}(\dot{\chi}) = \frac{1}{4!2^5}\{b^5|\dot{\chi}|^4 + 10b^4|\dot{\chi}|^3 + 45b^3|\dot{\chi}|^2 + 105b^2|\dot{\chi}| + 105b\}\exp(-b|\dot{\chi}|)$$

$$P_{\dot{\chi}_{6E}}(\dot{\chi}) = \frac{1}{5!2^6}\{b^6|\dot{\chi}|^5 + 15b^5|\dot{\chi}|^4 + 105b^4|\dot{\chi}|^3 + 420b^3|\dot{\chi}|^2 + 945b^2|\dot{\chi}| + 945b\}\exp(-b|\dot{\chi}|)$$

. . .(1.66a-f)

Upon inspection of Equations (1.66) the general form of the density for arbitrary L emerges (which will be proven below):

$$P_{\dot{\chi}_{LE}}(\dot{\chi}) = \frac{1}{(L-1)!2^L} e^{-b|\dot{\chi}|}\left\{\sum_{k=1}^{L} \frac{(L+k-2)!}{(k-1)!(L-k)!2^{k-1}} |\dot{\chi}|^{L-k} b^{L-k+1}\right\}$$

. . .(1.67)

Clearly, $\mu_{\dot{\chi}_{LE}} = 0$, and in general

$$E[\dot{\chi}_{LE}^n] = \frac{1}{(L-1)!2^{L-1}} \sum_{k=1}^{N} \frac{(L+k-2)!b^{L-k+1}}{(k-1)!(L-k)!2^{k-1}} \int_0^\infty \dot{\chi}^{L-k+n} e^{-b\dot{\chi}} d\dot{\chi} \quad \ldots (1.68)$$

which, for n odd is 0, and for n even:

$$E[\dot{\chi}_{LE}^n] = \frac{1}{(L-1)!2^{L-1}b^n} \sum_{k=1}^{N} \frac{(L+k-2)!(L-k+n)!}{(k-1)!(L-k)!2^{k-1}} \quad (1.69)$$

Using the independence property [14] I get

$$E[\dot{\chi}_{LE}^2] = \sigma_{\dot{\chi}_{LE}}^2 = 8L\sigma_1^4\nu^2 \quad (1.70)$$

This result is identical to Equation (1.69) when n=2.

A much more elegant solution for $P_{\dot{\chi}_{LE}}(\dot{\chi})$ will now be developed. The approach yields the complete solution for the equal $\sigma_1^2$ equal $\nu^2$ case including $P_{\dot{\rho}_{LE}}(\dot{\rho})$, $P_{\dot{\Lambda}_{LE}}(\dot{\Lambda})$, and all the joint densities of amplitude and amplitude rate.

I begin with Equation (1.12). Because $\chi_{LE} = \sum_{n=1}^{L} \chi_n$, $\dot{\chi}_{LE} = \sum_{n=1}^{L} \dot{\chi}_n$, the $\chi_n$'s are independent of each other, and the $\dot{\chi}_n$'s are likewise independent of each other the joint density $P_{\chi,\dot{\chi}_{LE}}(\chi,\dot{\chi})$ can be expressed as follows:

$$P_{\chi,\dot{\chi}_{LE}}(\chi,\dot{\chi}) = \left(\frac{i}{2\sigma_1^2}\right)^L \frac{1}{4\pi^2} \int_{-\infty}^{\infty}\int_{-\infty}^{\infty} \frac{e^{-i\omega\chi}\, e^{-i\sigma\chi} d\omega d\sigma}{[\omega + i(\frac{1}{2\sigma_1^2} + 2\sigma_1^2\nu^2\sigma^2)]^L} \quad (1.71)$$

which is just the inverse transform of the $L^{th}$ power of Equation (1.12). I use the calculus of residues and perform the integration over $\omega$ first, which has a pole of order L:

$$P_{\chi,\dot{\chi}_{LE}}(\chi,\dot{\chi}) = \left(\frac{i}{2\sigma_1^2}\right)^L \frac{2\pi i}{(L-1)!\,4\pi^2} \int_{-\infty}^{\infty} \frac{d^{L-1}}{d\omega^{L-1}} \left[e^{-i\omega\chi}\right] \Big| e^{-i\sigma\dot{\chi}}\, \sigma$$

$$\omega = -i\left(\frac{1}{2\sigma_1^2} + 2\sigma_1^2\nu^2\sigma^2\right) \quad (1.72)$$

and

$$P_{\chi,\dot{\chi}_{LE}}(\chi,\dot{\chi}) = \left[\frac{1}{2\sigma_1^2}\right]^L \frac{\chi^{L-1}}{2\pi(L-1)!} \int_{-\infty}^{\infty} e^{-(\frac{1}{2\sigma_1^2} + 2\sigma_1^2\nu^2\sigma^2)\chi - i\sigma\dot{\chi}} d\sigma$$

. . .(1.73)

Performing the final integration I obtain the desired result, the joint density of the sta mean square pressure $\chi$ and its rate $\dot{\chi}$ for L sources with equal $\sigma_1^2$ and equal $\nu$:

$$P_{\chi,\dot{\chi}_{LE}}(\chi,\dot{\chi}) = \frac{\chi^{L-\frac{3}{2}}}{(L-1)!\,2^{L+1}\sigma_1^{2L+1}\nu\sqrt{2\pi}} \exp\left[-\frac{\chi}{2\sigma_1^2} - \frac{\dot{\chi}^2}{8\sigma_1^2\nu^2\chi}\right]$$

. . .(1.74)

To find the marginal density $P_{\dot{\chi}_{LE}}(\dot{\chi})$ I integrate over $\chi$ in Equation (1.74):

$$P_{\dot{\chi}_{LE}}(\dot{\chi}) = \int_{-\infty}^{\infty} P_{\chi,\dot{\chi}_{LE}}(\chi,\dot{\chi})\,d\chi \qquad (1.75)$$

to obtain:

$$P_{\dot{\chi}_{LE}}(\dot{\chi}) = \left(\frac{1}{2\sigma_1^2}\right)^L \frac{1}{\Gamma(L)\sqrt{2\pi\sigma_1^2\nu^{2-}}} \left(\frac{\dot{\chi}^2}{4\nu^2}\right)^{\frac{L}{2}-\frac{1}{4}} \cdot K_{L-\frac{1}{2}}\left(\frac{|\dot{\chi}|}{2\sigma_1^2\nu}\right)$$

. . .(1.76)

where $\Gamma(L)$ is the Gamma function and $K_\nu(Z)$ is the modified Bessel function of order $\nu$. If we make use of the identity [20]

$$K_{L-\frac{1}{2}}(Z) = \sqrt{\frac{\pi}{2Z}}\ e^{-Z} \sum_{k=1}^{L} \frac{(L-2+k)!}{(k-1)!(L-k)!(2Z)^{k-1}}$$

it is easily proven that Equation (1.76) is identical to Equation (1.67). When $\dot{\chi}$ is integrated out in Equation (1.74), I obtain $P_{\chi_{LE}}(\chi)$ which confirms the result first obtained by Dyer [4].

The next step is to solve for the joint density of $\rho$ and $\dot{\rho}$. This is easily accomplished by the following two dimensional transformations of Equation (1.74):

$$P_{\rho,\dot{\rho}_{LE}}(\rho,\dot{\rho}) = \frac{\partial^2}{\partial\rho\partial\rho} \int_0^{\rho^2} \int_{-\infty}^{2\rho\dot{\rho}} P_{\chi,\dot{\chi}_{LE}}(\chi,\dot{\chi})\,d\chi d\dot{\chi} \qquad (1.77)$$

which yields:

$$P_{\rho,\dot{\rho}_{LE}}(\rho,\dot{\rho}) = \frac{\rho^{2L-1}}{(L-1)!\,2^{L-1}\sigma_1^{2L-1}\nu\sqrt{2\pi}} \exp\left[-\frac{\rho^2}{2\sigma_1^2} - \frac{\dot{\rho}^2}{2\sigma_1^2\nu}\right] \qquad (1.78)$$

This result is rather remarkable. One can see immediately that $\rho$ and $\dot{\rho}$ are independent as they are for the single source case and furthermore that $\dot{\rho}$ is independent of L, and $P_{\dot{\rho}_{LE}}(\dot{\rho})$, the density for L equal receptions is in fact identical to $P_{\dot{\rho}}(\dot{\rho})$, the density for the single source. Integrating over $\dot{\rho}$ and $\rho$ respectively in Equation (1.78), I obtain:

$$P_{\rho_{LE}}(\rho) = \frac{\rho^{2L-1}}{(L-1)!\,2^{L-1}\sigma_1^{2L}} \exp\left[-\frac{\rho^2}{2\sigma_1^2}\right] \qquad (1.79)$$

The mean and variance are respectively

$$\mu_{\rho_{LE}} = \frac{\sqrt{2\pi}\,\sigma_1\,(2L-1)!!}{2^L\,(L-1)!}$$

where $(2L-1)!! = 1\cdot 3\cdot 5\cdots(2L-1)$

$$\sigma^2_{\rho_{LE}} = 2\sigma_1^2 L - \mu^2_{\rho_{LE}}$$

and

$$P_{\dot{\rho}_{LE}}(\dot{\rho}) = \frac{1}{\sqrt{2\pi\sigma_1^2\bar{\nu}^2}} \exp\left[-\frac{\dot{\rho}^2}{2\sigma_1^2\nu^2}\right] \tag{1.80}$$

$$\mu_{\dot{\rho}_{LE}} = 0 \quad \text{and} \quad \sigma^2_{\dot{\rho}_{LE}} = \sigma_1^2\nu^2$$

To complete the statistics for this case, I make the final transformation $\Lambda = \varepsilon \ln \chi$ and $\dot{\Lambda} = \varepsilon\dot{\chi}/\chi$ in Equation (1.74):

$$P_{\Lambda,\dot{\Lambda}_{LE}}(\Lambda,\dot{\Lambda}) = \frac{\partial^2}{\partial\Lambda\partial\dot{\Lambda}} \int_0^{e^{\Lambda/\varepsilon}} \int_\infty^{\frac{\dot{\Lambda}}{\varepsilon} e^{\Lambda/\varepsilon}} P_{\chi,\dot{\chi}_{LE}}(\chi,\dot{\chi})\, d\chi d\dot{\chi} \tag{1.81}$$

to obtain:

$$P_{\Lambda,\dot{\Lambda}_{LE}}(\Lambda,\dot{\Lambda}) = \frac{\exp[(L+\frac{1}{2})\frac{\Lambda}{\varepsilon}]}{2^{L+1}\sigma_1^{2L+1}\nu\sqrt{2\pi}\ (L-1)!} \exp\left[-e^{\Lambda/\varepsilon}\left(\frac{1}{2\sigma_1^2} + \frac{\dot{\Lambda}^2}{\varepsilon^2 8\sigma_1^2\nu^2}\right)\right]$$

. . .(1.82)

Integrating over $\dot{\Lambda}$ in Equation (1.82) I obtain

$$P_{\Lambda_{LE}}(\Lambda) = \frac{1}{2^L\sigma_1^{2L}(L-1)!} \exp\left[\frac{L\Lambda}{\varepsilon} - \frac{1}{2\sigma_1^2}\exp(\frac{\Lambda}{\varepsilon})\right] \qquad (1.83)$$

$$\mu_{\Lambda_{LE}} = \varepsilon[\ln 2\sigma_1^2 - \gamma + S_1(L)]$$

and

$$\sigma^2_{\Lambda_{LE}} = \varepsilon^2\left[\frac{\pi^2}{6} - S_2(L)\right]$$

where

$$S_1(L) = \sum_{w=1}^{L-1}\frac{1}{w}\ ,\ S_1(1) \equiv 0$$

$$S_2(L) = \sum_{w=1}^{L-1} \frac{1}{w^2} \ , \ S_2(1) \equiv 0$$

Again this result was previously obtained by Dyer [4].

Integrating over $\Lambda$ in Equation (1.82), I obtain

$$P_{\dot{\Lambda}_{LE}}(\dot{\Lambda}) = \frac{1}{\varepsilon} \frac{(2L-1)!!}{2^L(L-1)!} \frac{1/2\nu}{(1 + \frac{\dot{\Lambda}^2}{4\varepsilon^2\nu^2})^{L+1/2}} \tag{1.84}$$

The moments of $\dot{\Lambda}$ for the equal reception case are interesting:

$$E[\dot{\Lambda}^n_{LE}] = \begin{cases} 0 & , \ n \text{ odd} \\ \varepsilon^n \frac{\nu^n 2^{n-L+\frac{1}{2}}\sqrt{\pi}\ (n-1)!!(2L-n-2)!!}{(L-1)!} & , \ \frac{n}{2} < L \\ \infty & , \ \frac{n}{2} \geq L \end{cases} \tag{1.85}$$

Note that the single source case yields an infinite second moment as reported in Section 1.1, however, for $L \geq 2$ the variance always exists.

### 1.2.2.2 Multiple Components with Different $\sigma_1^2$'s and Different $\nu^2$'s

The most general case of this problem is Case (c) of Section 1.2.1, i.e., there are many groups N, and within each group there are $L_i$ receptions with identical $\sigma_1^2$ and $\nu^2$. Because there are now two parameters which can vary for each source, this implies that in general for multiple sources the number of groups will be larger for the rate variables than the amplitude variables. I define $\sigma_{1j}^2$ and $\nu_j^2$ to be $\sigma_1^2$ and $\nu^2$ for the jth source receiver pair. Considering the most general case and using Equation (1.12) I find the characteristic function

$$M_{N\chi,\dot{\chi}}(\omega,\sigma) = \prod_{j=1}^{N} \left(\frac{1}{2i}\right)^{NL_j} \left(\frac{1}{\sigma_{1j}^2}\right) \frac{1}{\left(\omega - i\left[\frac{1}{2\sigma_{1j}^2} + 2\sigma_{1j}^2\nu_j^2\sigma^2\right]\right)^{L_j}} \quad (1.86)$$

Taking the inverse transform

$$P_{N\chi,\dot{\chi}}(\chi,\dot{\chi}) = \frac{1}{4\pi^2} \prod_{j=1}^{N} \left(\frac{1}{2i}\right)^{NL_j} \left(\frac{1}{\sigma_{1j}^2}\right) \int_{-\infty}^{\infty}\int_{-\infty}^{\infty} \frac{e^{i\omega\chi} e^{i\sigma\dot{\chi}} d\omega d\sigma}{\left(\omega - i\left[\frac{1}{2\sigma_{1j}^2} + 2\sigma_{1j}^2\nu_j^2\sigma^2\right]\right)^{L_j}} \quad (1.87)$$

Unfortunately, I have been unable to evaluate this integral; thus a retreat for the moment from the most general case

is in order. Much more progress can be made in solving for the density of $\dot{\chi}$ because here we are dealing with a sum of independent random variables, and it is not required that we know the joint density. This analysis will ultimately lead to a very simple and useful approximation of the density for $\dot{\chi}$ under the most general case. Upon completion of this analysis I will return to the problem of the joint densities and the pdf's of $\dot{\rho}$ and $\dot{\Lambda}$.

1.2.2.2.1 Solutions for $P_{\dot{\chi}}(\dot{\chi})$

First I will consider the exact solution when the product $\sigma_1^2\nu$ is different for each source/receiver pair, Case (b).. I apply Equation (1.63) for L = 2:

$$P_{\dot{\chi}_{2D}}(\dot{\chi}) = \frac{b_1}{2} e^{-b_1|\dot{\chi}|} * \frac{b_2}{2} e^{-b_2|\dot{\chi}|} \tag{1.88}$$

where $b_i = 1/2\sigma_{1i}^2\nu_i$, and the * denotes convolution. Performing the convolution

$$P_{\dot{\chi}_{2D}}(\dot{\chi}) = \frac{1}{2} \frac{b_1 b_2}{b_2^2 - b_1^2} \left\{ b_2 e^{-b_1|\dot{\chi}|} - b_1 e^{-b_2|\dot{\chi}|} \right\} \tag{1.89}$$

Rewriting Equation (1.89) in a slightly different way,

$$P_{\dot{\chi}_{2D}}(\dot{\chi}) = \frac{b_2^2}{b_2^2 - b_1^2}\left\{\frac{b_1}{2} e^{-b_1|\dot{\chi}|}\right\} - \frac{b_1^2}{b_2^2 - b_1^2}\left\{\frac{b_2}{2} e^{-b_2|\dot{\chi}|}\right\} \quad (1.90)$$

Now $P_{\dot{\chi}_{3D}}(\dot{\chi}) = P_{\dot{\chi}_{2D}}(\dot{\chi}) * \frac{b_3}{2} e^{-b_3|\dot{\chi}|}$. Examination of Equations (1.88 - 1.90) reveals that successive convolutions can be done by inspection:

$$P_{\dot{\chi}_{3D}}(\dot{\chi}) = \frac{b_2^2}{b_2^2 - b_1^2}\left\{\frac{1}{2}\frac{b_1 b_3}{b_3^2 - b_1^2}\left[b_3 e^{-b_1|\dot{\chi}|} - b_1 e^{-b_3|\dot{\chi}|}\right]\right\}$$

$$- \frac{b_1^2}{b_2^2 - b_1^2}\left\{\frac{1}{2}\frac{b_2 b_3}{b_3^2 - b_1^2}\left[b_3 e^{-b_2|\dot{\chi}|} - b_2 e^{-b_3|\dot{\chi}|}\right]\right\} \quad (1.91)$$

Rewriting this result so that the method of inspection can be applied again,

$$P_{\dot{\chi}_{3D}}(\dot{\chi}) = \frac{b_2^2 b_3^2}{(b_2^2 - b_1^2)(b_3^2 - b_1^2)}\left\{\frac{b_1}{2} e^{-b_1|\dot{\chi}|}\right\} -$$

$$- \frac{b_1^2 b_3^2}{(b_2^2 - b_1^2)(b_3^2 - b_2^2)} \left\{ \frac{b_2}{2} e^{-b_2|\dot{\chi}|} \right\}$$

$$+ \frac{b_1^2 b_2^2}{(b_3^2 - b_1^2)(b_3^2 - b_2^2)} \left\{ \frac{b_3}{2} e^{-b_3|\dot{\chi}|} \right\} \qquad (1.92)$$

and thus,

$$P_{\dot{\chi}_{4D}}(\dot{\chi}) = \frac{b_2^2 b_3^2 b_4^2}{(b_2^2 - b_1^2)(b_3^2 - b_1^2)(b_4^2 - b_1^2)} \left\{ \frac{b_1}{2} e^{-b_1|\dot{\chi}|} \right\}$$

$$- \frac{b_1^2 b_3^2 b_4^2}{(b_2^2 - b_1^2)(b_3^2 - b_2^2)(b_4^2 - b_2^2)} \left\{ \frac{b_2}{2} e^{-b_2|\dot{\chi}|} \right\}$$

$$+ \frac{b_1^2 b_2^2 b_4^2}{(b_3^2 - b_1^2)(b_3^2 - b_2^2)(b_4^2 - b_3^2)} \left\{ \frac{b_3}{2} e^{-b_3|\dot{\chi}|} \right\}$$

$$- \frac{b_1^2 b_2^2 b_3^2}{(b_4^2 - b_1^2)(b_4^2 - b_2^2)(b_4^2 - b_3^2)} \left\{ \frac{b_4}{2} e^{-b_4|\dot{\chi}|} \right\} \qquad (1.93)$$

etc....

Thus it can be seen that $P_{\dot{\chi}_{LD}}(\dot{\chi})$ is a weighted sum of the individual single source pdf's of $\dot{\chi}$. It is also

evident from the L = 2-4 cases that in general

$$P_{\dot{\chi}_{LD}}(\dot{\chi}) = \frac{1}{2} \sum_{i=1}^{L} \frac{1}{b_i} \frac{\prod_{j=1}^{L} b_j^2}{\prod_{\substack{m=1 \\ m\neq i}}^{L} (b_m^2 - b_i^2)} e^{-b_i|\dot{\chi}|} \tag{1.94}$$

or more simply in terms of $\sigma_{li}^2$ and $\nu_i$

$$P_{\dot{\chi}_{LD}}(\dot{\chi}) = \frac{1}{4} \sum_{i=1}^{L} \frac{\sigma_{li}^2 \nu_i}{\prod_{\substack{m=1 \\ m\neq i}}^{L} (\sigma_{li}^4 \nu_i^2 - \sigma_{lm}^4 \nu_m^2)} \exp\left(-\frac{|\dot{\chi}|}{2\sigma_{li}^2 \nu_i}\right) \tag{1.95}$$

Solving for the moments,

$$E[\dot{\chi}_{LD}^k] = \begin{cases} 0 & k \text{ odd} \\ k! \sum_{i=1}^{L} \frac{1}{b_i} \frac{\prod_{j=1}^{L} b_j^2}{\prod_{\substack{m=1 \\ m\neq i}}^{L} (b_m^2 - b_i^2)} \frac{1}{b_i^{k+1}} & k \text{ even} \end{cases} \tag{1.96}$$

Making use of the properties of sums of independent

random variables,

$$\sigma^2_{\dot{\chi}_{LD}} = 8 \sum_{i=1}^{L} \sigma_{1i}^4 \nu_i^2 \tag{1.97}$$

Equation (1.96) with k=2 confirms this result.

An exact solution for $P_{\dot{\chi}_N}(\dot{\chi})$ for the most general case considered in the beginning of this section would be an N-fold convolution of Equation (1.67) or (1.76) with itself. An exact solution for N=2 will now be presented.

$$P_{2\dot{\chi}}(\dot{\chi}) = \frac{1}{(L_1 - 1)!\,2^{L_1}} \sum_{k=1}^{L_1} \frac{(L_1+k-2)!}{(k-1)!\,(L_1 - k)!\,2^{k-1}} b_1^{L_1-k+1}$$

$$\cdot \frac{1}{(L_2 - 1)!\,2^{L_2}} \sum_{m=1}^{L_2} \frac{(L_2+m-2)!}{(m-1)!\,(L_2 - m)!\,2^{m-1}} b_2^{L_2-m+1}$$

$$\cdot \int_{-\infty}^{\infty} e^{-b_1|y|}\, e^{-b_2|\dot{\chi}-y|}\, |y|^{L_1-k}\, |\dot{\chi}-y|^{L_2-m}\, dy \tag{1.98}$$

I will now evaluate the integral. I consider $\dot{\chi} > 0$ (we know the result for $\dot{\chi} < 0$ must be identical), $y > 0$, and

then $y < 0$:

For $\dot{\chi} > 0$ and $y > 0$,

let $y = \dot{\chi}t$

$$\int_0^\infty = \dot{\chi}^{L_1+L_2-k-m+1} \int_0^\infty e^{-b_1\dot{\chi}t} e^{-b_2\dot{\chi}|1-t|} t^{L_1-k} |1-t|^{L_2-m} dt \quad \ldots(1.99)$$

To remove the absolute values this integral must be further subdivided for $t < 1$, and $t > 1$:

$$\int_0^\infty = \dot{\chi}^{L_1+L_2-k-m+1} \left\{ e^{-b_2\dot{\chi}} \int_0^1 e^{-(b_1-b_2)\dot{\chi}t} t^{L_1-k} (1-t)^{L_2-m} dt \right.$$

$$\left. + e^{b_2\dot{\chi}} \int_1^\infty e^{-(b_1+b_2)\dot{\chi}t} t^{L_1-k} (t-1)^{L_2-m} dt \right\} \quad (1.100)$$

The first integral in Equation (1.100) is the confluent hypergeometric function encountered in Section 1.2.1.1.

The second integral is a degenerate hypergeometric function known as Whittaker's function [18,24]. Performing a similar analysis for $y < 0$ also yields Whittaker's function. Simplifying to as much an extent as possible, I obtain for the final result:

$$P_{2\dot{X}}(\dot{\chi}) = \frac{1}{\Gamma(L_1)\Gamma(L_2)2^{L_1+L_2}} \sum_{k=1}^{L_1} \sum_{m=1}^{L_2} \frac{(L_1+k-2)!(L_2+m-2)!b_1^{\alpha}b_2^{\delta}|\dot{\chi}|^{\alpha+\delta-1}}{(k-1)!(L_1-k)!(m-1)!(L_2-m)!2^{k+m-2}}$$

$$\cdot \Bigg\{ \exp(-b_2|\dot{\chi}|) \frac{\Gamma(\alpha)\Gamma(\delta)}{\Gamma(\alpha+\delta)} M[\alpha,\alpha+\delta,\ (b_2-b_1)|\dot{\chi}|]$$

$$+ \exp[-\tfrac{1}{2}(b_1-b_2)|\dot{\chi}|][(b_1+b_2)|\dot{\chi}|]^{-(\frac{\alpha+\delta}{2})} \Gamma(\delta)$$

$$\cdot W_{\frac{\alpha-\delta}{2},\frac{1-\alpha-\delta}{2}}[(b_1+b_2)|\dot{\chi}|] + (-1)^{a-1} \exp[-\tfrac{1}{2}(b_2-b_1)|\dot{\chi}|]$$

$$\cdot [(b_1+b_2)|\dot{\chi}|]^{-(\frac{\alpha+\delta}{2})} \Gamma(\alpha) W_{\frac{\delta-\alpha}{2},\frac{\alpha+\delta-1}{2}}[(b_1+b_2)|\dot{\chi}|] \Bigg\} \qquad (1.101)$$

where,

$$\alpha = L_1 - k + 1$$

$$\delta = L_2 - m + 1$$

$M(\alpha,\delta,z)$ is the confluent hypergeometric function,

and $W_{\nu,\mu}(z)$ is Whittaker's function.

In order to check Equation (1.101), if I let $L_1 = L_2 = 1$, then I should obtain Equation (1.89). For $L_1 = L_2 = 1$

$$P_{2\dot{\chi}}(\dot{\chi}) = \frac{b_1 b_2 |\dot{\chi}|}{4} \left\{ \exp(-b_2|\dot{\chi}|) M[1,2,(b_2 - b_1)|\dot{\chi}|] \right.$$

$$+ \exp[-\tfrac{1}{2}(b_1 - b_2)|\dot{\chi}|][(b_1 + b_2)|\dot{\chi}|]^{-1} W_{0,-\frac{1}{2}}[(b_1 + b_2|\dot{\chi}|]$$

$$\left. + \exp[-\tfrac{1}{2}(b_2 - b_1)|\dot{\chi}|][(b_1 + b_2)|\dot{\chi}|]^{-1} W_{0,\frac{1}{2}}[(b_1 + b_2)|\dot{\chi}|] \right\}$$

. . .(1.101a)

I now make use of the following identities [18,24]:

$$M(1,2,2z) = \frac{e^z}{z} \sinh z \ ,$$

$$W_{\mu,\lambda}(z) = W_{\mu,-\lambda}(z) \ ,$$

$$W_{0,\lambda}(z) = \sqrt{z/\pi}\ K_\lambda(\tfrac{z}{2}) \ , \text{ and}$$

$$K_{1/2}(w) = \sqrt{\pi/2z}\ e^{-w}$$

where $K_\nu(z)$ is the modified Bessel function of order $\nu$.
I obtain

$$W_{0,-1/2}(z) = W_{0,1/2}(z) = \exp(-\tfrac{z}{2})$$

and applying these results to Equation (1.101a):

$$P_{2\dot{\chi}}(\dot{\chi}) = \frac{b_1 b_2}{4} \left\{ \frac{1}{b_2 - b_1} \left[ \exp(-b_1|\dot{\chi}|) - \exp(-b_2|\dot{\chi}|) \right] \right.$$

$$\left. + \frac{1}{b_1 + b_2} \left[ \exp(-b_1|\dot{\chi}|) + \exp(-b_2|\dot{\chi}|) \right] \right\}$$

It is easily shown that this result is identical to Equation (1.89). However, though Equation (1.101) may be exact, it is of significant complexity and thus of limited engineering value. For arbitrary N it is therefore clear that $P_{N\dot{\chi}}(\dot{\chi})$ is analytically out of hand at this time. The complexity of the result, however, once again motivates an approximate solution. An Edgeworth's approximation turns out to be quite simple and very useful for even the most general case. Recall the Edgeworth's series is given by Equation (1.42). In the present case, however, because $\dot{\chi}$ is symmetric about the origin, the coefficient of skew, $\gamma_s$, is identically 0. Thus it remains only for me to solve for $\gamma_e$, the coefficient of excess. First I solve for $K_4$, the fourth order cumulant or semi-invariant [14] of $\dot{\chi}$:

$$K_4 = E[\dot{\chi}^4] - 3(E[\dot{\chi}^2])^2 \tag{1.102}$$

Performing the required calculations on $P_{\dot{\chi}}(\dot{\chi})$ given by Equation (1.4) I obtain

$$K_4 = 192\sigma_1^8\nu^4 \tag{1.103}$$

Recalling Equation (1.49) and considering N groups of $L_i$

identical sources each, the most general case, I have:

$$K_{N^4} = 192 \sum_{i=1}^{N} L_i \sigma_{1i}^8 \nu_i^4 \tag{1.104}$$

From Equation (1.70) I have for N groups of $L_i$ sources,

$$\sigma^2_{N\dot{\chi}} = \sum_{i=1}^{N} 8L_i \sigma_{1i}^4 \nu_i^2 \tag{1.105}$$

Applying Equations (1.44), (1.104), and (1.105), I obtain the result

$$\gamma_e = 3 \frac{\sum_{i=1}^{N} L_i \sigma_{1i}^8 \nu_i^4}{\left( \sum_{j=1}^{N} L_j \sigma_{1j}^4 \nu_j^2 \right)^2} \tag{1.106}$$

and the Edgeworth's series is then:

$$P_{N\dot{\chi}}(\dot{\chi}) \simeq \frac{1}{\sigma_{N\dot{\chi}}} \left\{ Z(\eta) + \frac{1}{4!} \gamma_e Z^{(4)}(\eta) \right\} \tag{1.107}$$

or

$$P_{N\dot{\chi}}(\dot{\chi}) \simeq \frac{1}{\sigma_{N\dot{\chi}}} Z(\eta) \left\{ 1 + \frac{3\gamma_e}{4!} - \frac{\gamma_e}{4} \eta^2 + \frac{\gamma_e}{4!} \right\} \qquad (1.108)$$

where $\eta = \dot{\chi}/\sigma_{N\dot{\chi}}$ and

$$Z(\eta) = \frac{1}{\sqrt{2\pi}} \exp\left(-\frac{1}{2}\eta^2\right)$$

It is clear from Equation (1.106) that as N becomes large or the $L_i$ become large, $P_{N\dot{\chi}}(\dot{\chi})$ approaches a Gaussian. The maximum value of $\gamma_e$ is 3 for a single source/receiver pair and for L identical ones $\gamma_e$ goes to zero as 1/L. In Figure 9 I have plotted the exact density for N=1, L=1 given by Equation (1.4) with its Edgeworth's approximation given by Equation (1.108). This is clearly the worst case. I have let $\sigma_1^2\nu = 1$ for convenience. In order to gain some understanding of the behavior of $\gamma_e$ for this case, in Table II I have listed $\gamma_e$ and $P_{\dot{\chi}}(0)$ from the exact density, and its Edgeworth's approximation for various values of L identical sources. The percent error is also tabulated. From Figure 9 it is evident that the error shown in Table II will be the maximum error of the

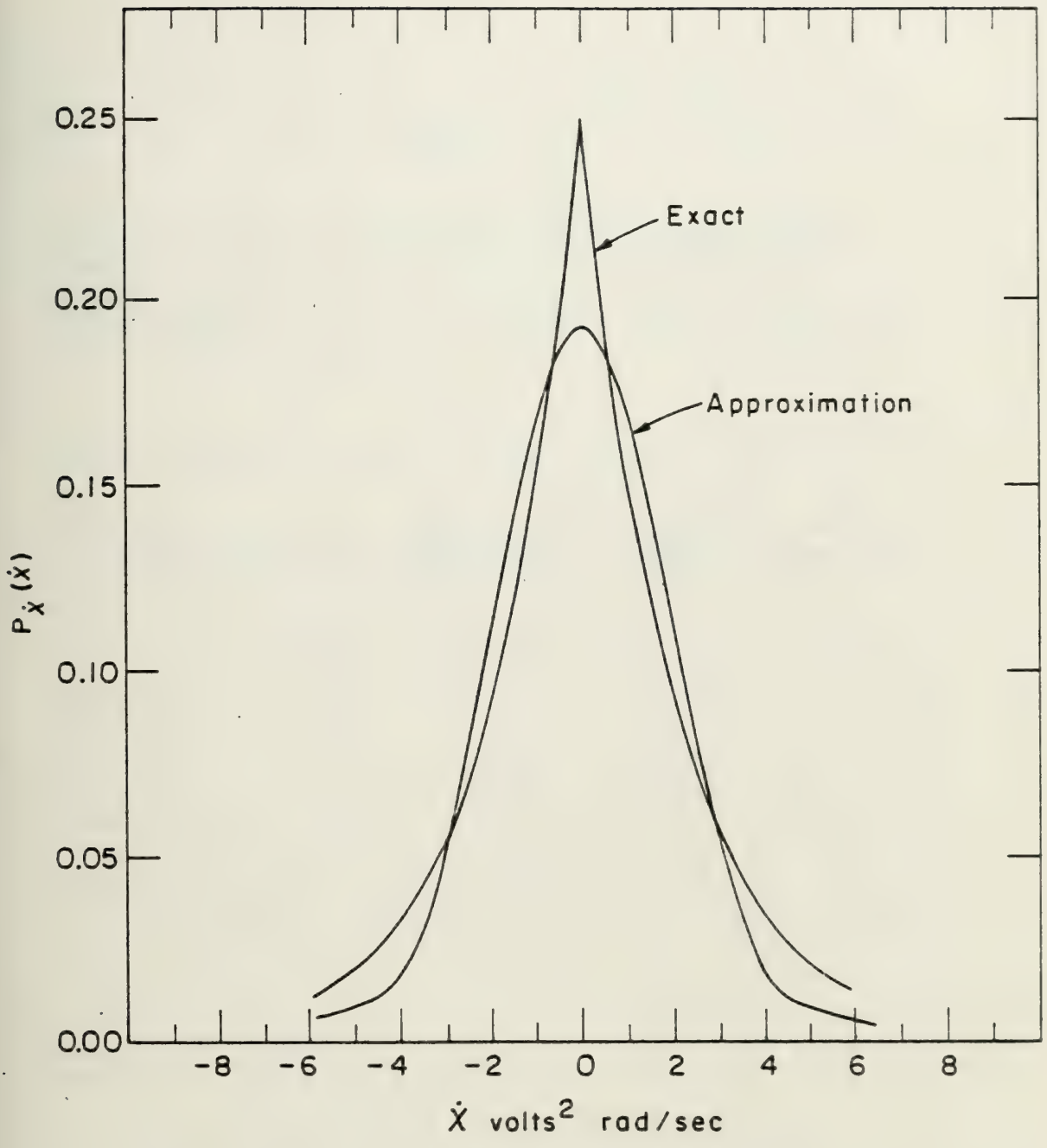


Fig. 9 Comparison of Edgeworth's approximation for $\dot{X}$ when N = L = 1 given by equ. (1.108) to the exact density for $\dot{X}$ given by equ. (1.4). This is the worst case.

TABLE II

The maximum point by point error of the Edgeworth's approximation to $P_{\chi_{LE}}^{(0)}(\chi)$ for various values of L.
Also listed is the value of $\gamma_e$, the coefficient of excess for each L.

| L | $\gamma_e$ | $P_{\chi_{LE}}^{(0)}$ | | % Error |
|---|---|---|---|---|
| | | Edgeworth | Exact | |
| 1 | 3.00 | .1939 | .2500 | 22 |
| 2 | 1.50 | .1184 | .1250 | 5 |
| 3 | 1.00 | .0916 | .0938 | 2 |
| 4 | 0.75 | .0771 | .0781 | 1 |
| 5 | 0.60 | .0678 | .0684 | 1 |
| 6 | 0.50 | .0612 | .0615 | .5 |
| 10 | 0.30 | .0463 | .0464 | .3 |

approximation in the main lobe. From the table convergence to the Edgeworth's is very rapid and it appears quite reasonable to assume that the Edgeworth's approximation will be a very good one when $\gamma_e \lesssim 1$. It is true that the Gaussian assumption will also be reasonable for $\gamma_e < 1$, however, because the corrections required by Equation (1.108) are trivial, accuracy need not be sacrificed for expediency.

#### 1.2.2.2.2 Solutions for the Joint pdf's, $P_{\dot{\rho}}(\dot{\rho})$ and $P_{\dot{\Lambda}}(\dot{\Lambda})$

In this section I will first solve the problem of two different source/receiver pairs, i.e., the $\sigma_1^2$ and $\nu^2$ are not the same. I will then generalize the analysis and solve for N=2 of Case (c). Finally, I will indicate the analysis required for arbitrary N.

For two independent pairs, the joint density of $\chi_1, \dot{\chi}_1, \chi_2$ and $\dot{\chi}_2$ is given by taking the product of Equation (1.9) with itself with different $\sigma_1^2$ and $\nu^2$:

$$P_{\chi_1,\dot{\chi}_1,\chi_2,\dot{\chi}_2}(\chi_1,\dot{\chi}_1,\chi_2,\dot{\chi}_2) = \frac{1}{4\sigma_1^2\sigma_2^2\sqrt{2\pi 4\chi_1\sigma_{11}^2\nu_1^2}\sqrt{2\pi 4\chi_2\sigma_{12}^2\nu_2^2}}$$

$$\cdot \exp\left[-\frac{\chi_1}{2\sigma_{11}^2} - \frac{\chi_2}{2\sigma_{12}^2}\right] \exp\left[-\frac{\dot{\chi}_1^2}{8\chi_1\sigma_{11}^2\nu_1^2} - \frac{\dot{\chi}_2^2}{8\chi_2\sigma_{12}^2\nu_2^2}\right] \qquad (1.109)$$

Now, the pdf we are after is the joint density of $\chi$ and $\dot{\chi}$ where $\chi = \chi_1 + \chi_2$ and $\dot{\chi} = \dot{\chi}_1 + \dot{\chi}_2$. I note that in Equation (1.109) $\dot{\chi}_1$ and $\dot{\chi}_2$ are jointly Gaussian. Because the density of their sum is given by convolution, the following can be done by inspection:

$$P_{\chi_1,\chi_2,\dot{\chi}}(\chi_1,\chi_2,\dot{\chi}) = \frac{1}{4\sigma_1^2\sigma_2^2\sqrt{2\pi(4\chi_1\sigma_{11}^2\nu_1^2 + 4\chi_2\sigma_{12}^2\nu_2^2)}}$$

$$\cdot \exp\left[-\frac{\chi_1}{2\sigma_{11}^2} - \frac{\chi_2}{2\sigma_{12}^2} - \frac{\dot{\chi}^2}{2(4\chi_1\sigma_{11}^2\nu_1^2 + 4\chi_2\sigma_{12}^2\nu_2^2)}\right] \qquad (1.110)$$

The final result is obtained using the convolution again:

$$P_{\chi,\dot{\chi}_{2D}}(\chi,\dot{\chi}) = \exp(-\frac{\chi}{2\sigma_{12}^2}) \int_0^{\chi} \frac{1}{4\sigma_{11}^2\sigma_{12}^2\sqrt{2\pi[4\chi_1\sigma_{11}^2\nu_1^2 + 4(\chi-\chi_1)\sigma_{12}^2\nu_2^2]}}$$

$$\cdot \exp\left[-\chi_1\left(\frac{1}{2\sigma_{11}^2} - \frac{1}{2\sigma_{12}^2}\right) - \frac{\dot{\chi}^2}{8[\chi_1\sigma_{11}^2\nu_1^2 + (\chi-\chi_1)\sigma_{12}^2\nu_2^2]}\right] d\chi_1 \qquad (1.111)$$

I now let $\chi_1 = \chi t$:

$$P_{\chi,\dot{\chi}_{2D}}(\chi,\dot{\chi}) = \frac{\chi^{\frac{1}{2}}\exp(-\chi/2\sigma_{12}^2)}{8\sigma_{11}^2\sigma_{12}^2\sqrt{2\pi}} \int_0^1 \frac{1}{\sqrt{\sigma_{12}^2\nu_2^2 + t(\sigma_{11}^2\nu_1^2 - \sigma_{12}^2\nu_2^2)}}$$

$$\cdot \exp\left[-t\left(\frac{\chi(\sigma_{12}^2 - \sigma_{11}^2)}{2\sigma_{11}^2\sigma_{12}^2}\right) - \frac{\dot{\chi}^2}{8\chi\sigma_{12}^2\nu_2^2 + 8\chi t(\sigma_{11}^2\nu_1^2 - \sigma_{12}^2\nu_2^2)}\right] dt \quad (1.112)$$

I have not been able to evaluate the remaining integral in Equation (1.112), however, as will be demonstrated below, numerical integration is very simple. Making the transformation to $\rho$ space I obtain:

$$P_{\rho,\dot{\rho}_{2D}}(\rho,\dot{\rho}) = \frac{\rho^3\exp(-\rho^2/2\sigma_{12}^2)}{2\sigma_{11}^2\sigma_{12}^2\sqrt{2\pi}} \int_0^1 \frac{1}{\sqrt{\sigma_{12}^2\nu_2^2 + t(\sigma_{11}^2\nu_1^2 - \sigma_{12}^2\nu_2^2)}}$$

$$\cdot \exp\left[-t\left(\frac{\rho^2(\sigma_{12}^2 - \sigma_{11}^2)}{2\sigma_{11}^2\sigma_{12}^2}\right) - \frac{\dot{\rho}^2}{2\sigma_{12}^2\nu_2^2 + 2t(\sigma_{11}^2\nu_1^2 - \sigma_{12}^2\nu_2^2)}\right] dt \quad (1.113)$$

Integrating Equation (1.113) over $\rho$ I obtain the marginal density of $\dot{\rho}$ for two different sources:

$$P_{\dot{\rho}_{2D}}(\dot{\rho}) = \frac{\sigma_{11}^2\sigma_{12}^2}{\sqrt{2\pi}} \int_0^1 \frac{1}{[\sigma_{11}^2 + t(\sigma_{12}^2 - \sigma_{11}^2)]^2 \sqrt{\sigma_{12}^2\nu_2^2 + t(\sigma_{11}^2\nu_1^2 - \sigma_{12}^2\nu_2^2)}}$$

$$\cdot \exp\left[-\frac{\dot{\rho}^2}{2\sigma_{12}^2\nu_2^2 + 2t(\sigma_{11}^2\nu_1^2 - \sigma_{12}^2\nu_2^2)}\right] dt \qquad (1.114)$$

The integral in Equation (1.114) can be evaluated by expanding the exponential in its power series and integrating term by term. After significant labor I obtain:

$$P_{\dot{\rho}_{2D}}(\dot{\rho}) = \frac{|\dot{\rho}|\sigma_{11}^2\sigma_{12}^2(\sigma_{11}^2\nu_1^2 - \sigma_{12}^2\nu_2^2)}{2\sqrt{\pi}\,(\sigma_{11}^4\nu_1^2 - \sigma_{12}^4\nu_2^2)^2} \sum_{n=0}^{\infty} (-1)^n(n+1)$$

$$\cdot \left[\frac{(\sigma_{12}^2 - \sigma_{11}^2)\dot{\rho}^2}{2\sigma_{11}^4\nu_1^2 - 2\sigma_{12}^4\nu_2^2}\right]^n \left\{\Gamma\left(-n - \frac{1}{2}, \frac{\dot{\rho}^2}{2\sigma_{11}^2\nu_1^2}\right) - \Gamma\left(-n - \frac{1}{2}, \frac{\dot{\rho}^2}{2\sigma_{12}^2\nu_2^2}\right)\right\}$$

. . . (1.115)

where $\Gamma(a,z)$ is the incomplete gamma function [23,24]. The appearance of $|\dot{\rho}|$ does not mean that $P_{\dot{\rho}_{2D}}(0) = 0$ because the limit as $\dot{\rho} \to 0$ of the incomplete gamma function is infinite. If the incomplete gamma function is expanded in

its power series, I get:

$$P_{\dot{\rho}_{2D}}(\dot{\rho}) = \frac{\sigma_{11}^2\sigma_{12}^2(\sigma_{11}^2\nu_1^2 - \sigma_{12}^2\nu_2^2)}{\sqrt{2\pi}\,(\sigma_{11}^4\nu_1^2 - \sigma_{12}^4\nu_2^2)^2} \sum_{n=0}^{\infty} (-1)^n(n+1)$$

$$\cdot \left[\frac{\sigma_{12}^2 - \sigma_{11}^2}{\sigma_{11}^4\nu_1^2 - \sigma_{12}^4\nu_2^2}\right]^n \sum_{m=0}^{\infty} \frac{(-1)^m}{m!(m-n-\frac{1}{2})} \left(\frac{\dot{\rho}^2}{2}\right)^m \left\{\sigma_{12}\nu_2^{2n-2m+1} - \sigma_{11}\nu_1^{2n-2m+1}\right\}$$

. . .(1.116)

In obtaining numerical results from Equation (1.116) I encountered overflow problems in computing successive terms of the series before an accurate result could be obtained. In order to avoid this problem, Equation (1.116) should be rewritten as follows:

$$P_{\dot{\rho}_{2D}}(\dot{\rho}) = \frac{\sigma_{11}^2\nu_{12}^2(\sigma_{11}^2\nu_1^2 - \sigma_{12}^2\nu_2^2)}{\sqrt{2\pi}\,(\sigma_{11}^4\nu_1^2 - \sigma_{12}^4\nu_2^2)^2}$$

$$\cdot \left\{\sigma_{12}\nu_2 \sum_{n=0}^{\infty} (-1)^n(n+1) \left[\frac{(\sigma_{12}^2 - \sigma_{11}^2)\sigma_{12}^2\nu_2^2}{\sigma_{11}^4\nu_1^2 - \sigma_{12}^4\nu_2^2}\right] \sum_{m=0}^{\infty} \frac{(-1)^m}{m!(m-n-\frac{1}{2})} \left(\frac{\dot{\rho}^2}{2\sigma_{12}^2\nu_2^2}\right)^m\right.$$

$$- \sigma_{11}\nu_1 \sum_{n=0}^{\infty} (-1)^n (n+1) \left[ \frac{(\sigma_{12}^2 - \sigma_{11}^2)\sigma_{11}^2\nu_1^2}{\sigma_{11}^4\nu_1^2 - \sigma_{12}^4\nu_2^2} \right] \sum_{m=0}^{\infty} \frac{(-1)^m}{m!(m-n-\frac{1}{2})} \left( \frac{\dot{\rho}^2}{2\sigma_{11}^2\nu_1^2} \right)^m \Bigg\}$$

. . .(1.117)

Values for $P_{\dot{\rho}_{2D}}(\dot{\rho})$ were computed by numerical integration of Equation (1.114) and from Equation (1.117). Depending upon the value of $\dot{\rho}$ desired, the numerical integration of Equation (1.114) to three place accuracy was about 40 times faster than use of Equation (1.117). The value for $\dot{\rho} = 0$ is obtained from Equation (1.114) analytically and exactly to aid in these comparisons. Performing the integration and simplifying as much as possible:

$$P_{\dot{\rho}_{2D}}(0) = \frac{1}{\sqrt{2\pi}} \left[ \frac{\sigma_{11}^3\nu_1 - \sigma_{12}^3\nu_2}{\sigma_{11}^4\nu_1^2 - \sigma_{12}^4\nu_2^2} \right]$$

$$+ \frac{\sigma_{11}^2\sigma_{12}^2(\sigma_{11}^2\nu_1^2 - \sigma_{12}^2\nu_2^2)}{(\sigma_{12}^2 - \sigma_{11}^2)2\sqrt{2\pi}\,(\sigma_{11}^4\nu_1^2 - \sigma_{12}^4\nu_2^2)} \sqrt{\frac{\sigma_{12}^2 - \sigma_{11}^2}{(\sigma_{12}^4\nu_2^2 - \sigma_{11}^4\nu_1^2)}}$$

$$\cdot \ln \left[ \frac{\sigma_{11}^4\sigma_{12}^2\nu_1^2 - 2\sigma_{12}^6\nu_2^2 + \sigma_{12}^4\sigma_{11}^2\nu_2^2 - \sigma_{12}^2(\sigma_{12}^2 - \sigma_{11}^2)2\sigma_{12}\nu_2 \sqrt{\frac{\sigma_{12}^4\nu_2^2 - \sigma_{11}^4\nu_1^2}{\sigma_{12}^2 - \sigma_{11}^2}}}{2\sigma_{11}^6\nu_1^2 - \sigma_{11}^2\sigma_{12}^4\nu_2^2 - \sigma_{11}^4\sigma_{12}^2\nu_1^2 - \sigma_{11}^2(\sigma_{12}^2 - \sigma_{11}^2)2\sigma_{11}\nu_1 \sqrt{\frac{\sigma_{12}^4\nu_2^2 - \sigma_{11}^4\nu_1^2}{\sigma_{12}^2 - \sigma_{11}^2}}} \right]$$

. . .(1.118)

The mean of $\dot{\rho}$ is zero and the variance of $\dot{\rho}$ is obtained by interchanging the order of integration in Equation (1.114), integrating over $\dot{\rho}$ first, then t:

$$\sigma^2_{\dot{\rho}_{2D}} = \frac{\sigma^2_{11}\sigma^2_{12}}{\sigma^2_{12} - \sigma^2_{11}} \left\{ \frac{\sigma^2_{12}\nu^2_2}{\sigma^2_{11}} - \frac{\sigma^2_{11}\nu^2_1}{\sigma^2_{12}} + \frac{\sigma^2_{11}\nu^2_1 - \sigma^2_{12}\nu^2_2}{\sigma^2_{12} - \sigma^2_{11}} \ln \frac{\sigma^2_{12}}{\sigma^2_{11}} \right\}$$

. . .(1.119)

Despite the complexity of Equations (1.114) and (1.117) it appears as though a Gaussian approximation is an exceptionally good one. For values of $\sigma^2_{11}$, $\nu^2_1$, $\sigma^2_{12}$, and $\nu^2_2$ taken from data, which will be discussed in more detail in Chapter III, the values of $P_{\dot{\rho}_{2D}}(\dot{\rho})$ from Equations (1.114) and (1.117) deviate from the Gaussian, using the value of $\sigma^2_{\dot{\rho}_{2D}}$ from Equation (1.119), only after the fourth significant figure. A more formal calculation with equivalent results is obtained if the coefficient of excess, $\gamma_e$, is solved for. I apply the definition of $\gamma_e$ from Equation (1.44 ), perform the two integrals required, and obtain $\gamma_e$ for $\dot{\rho}$ for two different sources.

$$\gamma_e = \frac{1}{\sigma_{12}^2 - \sigma_{11}^2}\left[3\sigma_{12}^6\nu_2^4 - 3\sigma_{11}^6\nu_1^4 + 6(\sigma_{11}^2\nu_1^2 - \sigma_{12}^2\nu_2^2)\sigma_{\dot{\rho}_{2D}}^2\right] - 3\sigma_{\dot{\rho}_{2D}}^4$$

. . .(1.120)

Applying the values of the parameters used above and Equation (1.119) in Equation (1.120) I obtain for this example that $\gamma_e = 2.4 \times 10^{-7}$ which certainly warrants the Gaussian assumption! Coupled with the result of Section 1.2.2.1 in which it is proven that $P_{\dot{\rho}_{LE}}(\dot{\rho})$ remains identically Gaussian and independent of the number of sources, it appears quite reasonable to state that even for the most general cases, $P_{\dot{\rho}}(\dot{\rho})$ will for all practical purposes be Gaussian.

Making the transformation $\Lambda = \varepsilon \ln\chi$ in Equation (1.112), I obtain

$$P_{\Lambda,\dot{\Lambda}_{2D}}(\Lambda,\dot{\Lambda}) = \frac{\exp\left[\frac{5}{2\varepsilon}\Lambda - \frac{e^{\Lambda/\varepsilon}}{2\sigma_{12}^2}\right]}{8\varepsilon^2\sigma_{11}^2\sigma_{12}^2\sqrt{2\pi}} \int_0^1 \frac{1}{\sqrt{\sigma_{12}^2\nu_2^2 + t(\sigma_{11}^2\nu_1^2 - \sigma_{12}^2\nu_2^2)}}$$

$$\cdot \exp\left[-t\left\{\frac{e^{\Lambda/\varepsilon}(\sigma_{12}^2 - \sigma_{11}^2)}{2\sigma_{11}^2\sigma_{12}^2}\right\} - \frac{e^{\Lambda/\varepsilon}\dot{\Lambda}^2}{8\varepsilon^2\sigma_{12}^2\nu_2^2 + 8\varepsilon^2 t(\sigma_{11}^2\nu_1^2 - \sigma_{12}^2\nu_2^2)}\right] dt$$

. . .(1.121)

Integrating over $\Lambda$ I obtain

$$P_{\dot{\Lambda}_{2D}}(\dot{\Lambda}) = \int_0^1 \frac{12[\sigma_{12}^2\nu_2^2 + t(\sigma_{11}^2\nu_1^2 - \sigma_{12}^2\nu_2^2)]^2 dt}{\varepsilon\sigma_{11}^2\sigma_{12}^2\left\{[\frac{1}{\sigma_{12}^2} + t(\frac{1}{\sigma_{11}^2} - \frac{1}{\sigma_{12}^2})][4\sigma_{12}^2\nu_2^2 + 4t(\sigma_{11}^2\nu_1^2 - \sigma_{12}^2\nu_2^2)] + \frac{\Lambda^2}{\varepsilon^2}\right\}^{5/2}}$$

. . .(1.122)

Making an enlightened change of variables allows the final integration to be performed, and

$$P_{\dot{\Lambda}_{2D}}(\dot{\Lambda}) = \frac{A}{(\frac{\dot{\Lambda}^2}{\varepsilon^2} + 4\nu_1^2)^{3/2}}\left\{-4\sigma_{11}^2\nu_1^2 + B + \frac{2\nu_1^2 - C}{D}E[1 + \frac{\dot{\Lambda}^2/\varepsilon^2 + 4\nu_1^2}{F}]\right\}$$

$$- \frac{A}{(\frac{\dot{\Lambda}^2}{\varepsilon^2} + 4\nu_2^2)^{3/2}}\left\{-4\sigma_{12}^2\nu_2^2 + B + \frac{C - 2\nu_2^2}{D}E[1 + \frac{\dot{\Lambda}^2/\varepsilon^2 + 4\nu_1^2}{F}]\right\}$$

. . .(1.123)

where:

$$A = \frac{3}{8\varepsilon}\frac{1}{\sigma_{12}^2 - \sigma_{11}^2}$$

$$B = \frac{2}{3}\left(\frac{\sigma_{11}^4\nu_1^2 - \sigma_{12}^4\nu_2^2}{\sigma_{12}^2 - \sigma_{11}^2}\right)$$

$$C = \frac{\sigma_{11}^4\nu_1^2 + \sigma_{12}^4\nu_2^2}{\sigma_{12}^2\sigma_{11}^2}$$

$$D = 4\left(\nu_1^2 - \frac{\sigma_{11}^2\nu_1^2}{\sigma_{12}^2} - \frac{\sigma_{12}^2\nu_2^2}{\sigma_{11}^2} + \nu_2^2\right)\frac{\dot{\Lambda}^2}{\varepsilon^2} - 4\left(\frac{\sigma_{11}^4\nu_1^2 - \sigma_{12}^4\nu_2^2}{\sigma_{11}^2\sigma_{12}^2}\right)^2$$

$$E = \frac{8}{3}\left[\frac{\left(\sigma_{11}^4\nu_1^2 - \sigma_{12}^4\nu_2^2\right)^2}{\sigma_{11}^2\sigma_{12}^4 - \sigma_{11}^4\sigma_{12}^2}\right] + \frac{8}{3}\left(\sigma_{11}^2\nu_1^2 - \sigma_{12}^2\nu_2^2\right)\frac{\Lambda^2}{\varepsilon^2}$$

$$F = \frac{\dot{\Lambda}^2}{2\varepsilon^2} - \frac{1}{2}\left[\frac{\left(\sigma_{11}^4\nu_1^2 - \sigma_{12}^4\nu_2^2\right)^2}{\sigma_{11}^2\sigma_{12}^2\left(\sigma_{12}^2 - \sigma_{11}^2\right)\left(\sigma_{11}^2\nu_1^2 - \sigma_{12}^2\nu_2^2\right)}\right]$$

Though arithmatically messy obtaining the exact solution from Equation (1.123) is approximately 50 times faster than numerical integration of Equation (1.122) which results in three place accuracy. The mean of $\dot{\Lambda}$ is of course zero and integrating Equation (1.121) first over $\dot{\Lambda}$ and then t, I obtain the variance,

$$\sigma^2_{\dot{\Lambda}_{2D}} = \frac{2\varepsilon^2}{\sigma^2_{11}\sigma^2_{12}} \left\{ \frac{\sigma^4_{11}\sigma^2_{12}\nu^2_1 - \sigma^4_{12}\sigma^2_{11}\nu^2_2}{\sigma^2_{12} - \sigma^2_{11}} + \frac{\sigma^6_{12}\sigma^2_{11}\nu^2_2 - \sigma^6_{11}\sigma^2_{12}\nu^2_1}{\sigma^4_{12} - 2\sigma^2_{11}\sigma^2_{12} + \sigma^4_{11}} 2\ln \frac{\sigma_{12}}{\sigma_{11}} \right\}$$

. . .(1.124)

Unlike the single source case, the variance is finite though the next nonzero moment $E[\dot{\Lambda}^4_{2D}]$ is infinite. The rule derived for equal source/receiver pairs appears to apply to unequal ones as well. Namely; $E[\dot{\Lambda}^n_{2D}]$ exists only for n even and $n < 2L$, where L is the number of sources. An example of $P_{\dot{\Lambda}_{2D}}(\dot{\Lambda})$ is plotted in Figure 10 using values for $\sigma^2_{11}$, $\nu^2_1$, $\sigma^2_{12}$, $\nu^2_2$ taken from data. The Gaussian using the variance given by Equation (1.124) is also plotted. The Gaussian assumption is clearly not warranted in this case, and in fact because densities for $\dot{\Lambda}$ for all cases are related to the Longuet-Higgins type density, the Gaussian assumption will be a poor one in general even when the densities are appropriately normalized (see Figure 1, Reference [9]), in which case the variance of the Gaussian will not be relevant to any of the source parameters.

I will now generalize the approach used to solve the two source/receiver case to solve the $N = 2$ case. That is two groups of pairs, with $L_i$ pairs each, with the same

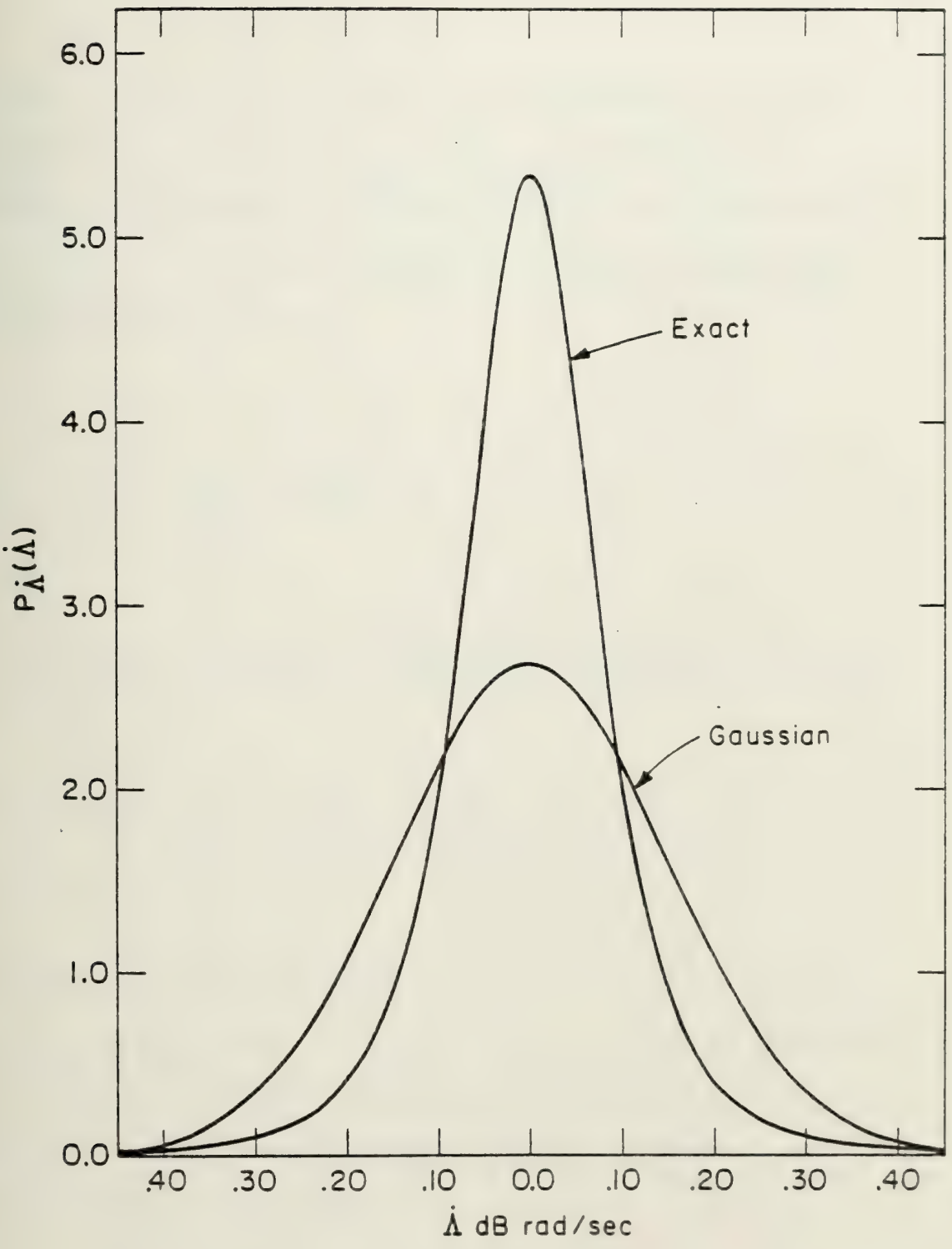


Fig. 10 The pdf of $\dot{A}$ for two different sources, equ. (1.123) is plotted with the Gaussian using the variance given by equ. (1.124).

$\sigma_{1i}^2$ and $\nu_i^2$ $(i = 1,2)$. I start by considering the joint density of $\chi_{L_1E}$, $\dot{\chi}_{L_1E}$, $\chi_{L_2E}$, and $\dot{\chi}_{L_2E}$ given by the product of Equation (1.74) with itself with different $L_i$, $\sigma_{1i}^2$ and $\nu_i^2$ $(i = 1,2)$, rewriting it slightly to make the first operation obvious:

$$p_{\chi_{L_1E},\dot{\chi}_{L_1E},\chi_{L_2E},\dot{\chi}_{L_2E}}(\chi_1,\dot{\chi}_1,\chi_2,\dot{\chi}_2) =$$

$$\frac{\chi_1^{L_1-1}\,\chi_2^{L_2-1}}{(L_1-1)!(L_2-1)!2^{L_1+L_2}\sqrt{2\pi^4\chi_1\sigma_{11}^2\nu_1^2}\sqrt{2\pi^4\chi_2\sigma_{12}^2\nu_2^2}\,\sigma_{11}^{2L_1}\sigma_{12}^{2L_2}}$$

$$\cdot \exp\left[-\frac{\chi_1}{2\sigma_{11}^2} - \frac{\chi_2}{2\sigma_{12}^2} - \frac{\dot{\chi}_1^2}{8\sigma_{11}^2\nu_1^2\chi_1} - \frac{\dot{\chi}_2^2}{8\sigma_{12}^2\nu_2^2\chi_2}\right] \qquad (1.125)$$

As before, I seek the joint density of $\chi$, and $\dot{\chi}$ where $\chi = \chi_{L_1E} + \chi_{L_2E}$, and $\dot{\chi} = \dot{\chi}_{L_1E} + \dot{\chi}_{L_2E}$. A double convolution will yield the desired density and because $\dot{\chi}_{L_1E}$ and $\dot{\chi}_{L_2E}$ are jointly Gaussian as before the first convolution can be done by inspection:

$$P_{\chi_{L_1E},\chi_{L_2E}}(\chi_1,\chi_2,\dot{\chi}) =$$

$$\frac{\chi_1^{L_1-1}\,\chi_2^{L_2-1}}{\Gamma(L_1)\Gamma(L_2)2^{L_1+L_2}\sigma_{11}^{2L_1}\sigma_{12}^{2L_2}\sqrt{2\pi(4\chi_1\sigma_{11}^2\nu_1^2+4\chi_2\sigma_{12}^2\nu_2^2)}}$$

$$\cdot\exp\left[-\frac{\chi_1}{2\sigma_{11}^2}-\frac{\chi_2}{2\sigma_{12}^2}-\frac{\chi^2}{2(4\chi_1\sigma_{11}^2\nu_1^2+4\chi_2\sigma_{12}^2\nu_2^2)}\right]$$

Setting up the final convolution after making a change of variables leaves the following result:

$$P_{2\chi,\dot{\chi}}(\chi,\dot{\chi}) = \frac{\chi^{L_1+L_2-\frac{3}{2}}\exp(-\frac{\chi}{2\sigma_{12}^2})}{\Gamma(L_1)\Gamma(L_2)2^{L_1+L_2+1}\sqrt{2\pi}\,\sigma_{11}^{2L_1}\,\sigma_{12}^{2L_2}}$$

$$\cdot\int_0^1\frac{t^{L_1-1}(1-t)^{L_2-1}}{\sqrt{\sigma_{12}^2\nu_2^2+t(\sigma_{11}^2\nu_1^2-\sigma_{12}^2\nu_2^2)}}$$

$$\cdot\exp\left[-t\left(\frac{\chi(\sigma_{12}^2-\sigma_{11}^2)}{2\sigma_{11}^2\sigma_{12}^2}\right)-\frac{\dot{\chi}^2}{8\chi\sigma_{12}^2\nu_2^2+8\chi t(\sigma_{11}^2\nu_1^2-\sigma_{12}^2\nu_2^2)}\right]dt$$

. . . (1.126)

This is a key result and is essentially the solution of the entire N = 2 problem because this joint pdf contains all the information required for the solution for the pdf's of $\chi$, $\rho$, $\Lambda$, $\dot{\chi}$, $\dot{\rho}$, $\dot{\Lambda}$. As a quick check, if I integrate Equation (1.126) over $\dot{\chi}$ (which can be done by inspection), I obtain Equation (1.20) and hence all the amplitude densities for N = 2 follow directly. Integrating over $\chi$ in Equation (1.126),

$$P_{2\dot{\chi}}(\dot{\chi}) = \frac{|\dot{\chi}|^M}{\Gamma(L_1)\Gamma(L_2)2^{M-\frac{1}{2}}\sqrt{\pi}\,\sigma_{11}^{2L_1}\sigma_{12}^{2L_2}\,8^{(M+1)/2}}$$

$$\cdot\int_0^1 \frac{t^{L_1-1}(1-t)^{L_2-1}}{[\sigma_{12}^2\nu_2^2 + t(\sigma_{11}^2\nu_1^2 - \sigma_{12}^2\nu_2^2)]^{(M+1)/2}\left[\frac{1}{2\sigma_{12}^2} + t\left(\frac{1}{2\sigma_{11}^2} - \frac{1}{2\sigma_{12}^2}\right)\right]^{M/2}}$$

$$\cdot K_M\left\{\frac{|\dot{\chi}|}{2}\left[\frac{\sigma_{11}^2 + t(\sigma_{12}^2 - \sigma_{11}^2)}{\sigma_{12}^4\sigma_{11}^2\nu_2^2 + t(\sigma_{11}^4\sigma_{12}^2\nu_1^2 - \sigma_{12}^4\sigma_{11}^2\nu_2^2)}\right]^{\frac{1}{2}}\right\}dt \qquad \ldots(1.127)$$

where $M = L_1 + L_2 - \frac{1}{2}$.

The remaining integral is clearly not a straight-

forward one, however, we have already solved for $P_{2\dot{\chi}}(\dot{\chi})$ in the previous section given by Equation (1.101) and its complexity has been noted. Clearly the $\dot{\chi}$ densities were handled by much more efficient means in the previous section. If I transform Equation (1.126) into $\rho,\dot{\rho}$ and $\Lambda,\dot{\Lambda}$ space, than I can obtain expressions for the densities $P_{2\dot{\rho}}(\dot{\rho})$ and $P_{2\dot{\Lambda}}(\dot{\Lambda})$ and their moments which have been unattainable until now.

$$P_{2\rho,\dot{\rho}}(\rho,\dot{\rho}) = \frac{\rho^{2L_1+2L_2-1} \exp(-\frac{\rho^2}{2\sigma_{12}^2})}{\Gamma(L_1)\Gamma(L_2)2^{L_1+L_2-1}\sqrt{2\pi}\,\sigma_{11}^{2L_1}\sigma_{12}^{2L_2}}$$

$$\cdot \int_0^1 \frac{t^{L_1-1}(1-t)^{L_2-1}}{\sqrt{\sigma_{12}^2\nu_2^2 + t(\sigma_{11}^2\nu_1^2 - \sigma_{12}^2\nu_2^2)}}$$

$$\cdot \exp\left[-t\left(\frac{\rho^2(\sigma_{12}^2 - \sigma_{11}^2)}{2\sigma_{11}^2\sigma_{12}^2}\right) - \frac{\dot{\rho}^2}{2\sigma_{12}^2\nu_2^2 + 2t(\sigma_{11}^2\nu_1^2 - \sigma_{12}^2\nu_2^2)}\right] dt$$

. . .(1.128)

Integrating over $\rho$ I obtain:

$$P_{2\dot{\rho}}(\dot{\rho}) = \frac{(L_1 + L_2 - 1)!\ \sigma_{11}^{2L_2}\sigma_{12}^{2L_1}}{\Gamma(L_1)\Gamma(L_2)\ \sqrt{2\pi}}$$

$$\cdot \int_0^1 \frac{t^{L_1-1}(1-t)^{L_2-1}}{\sqrt{\sigma_{12}^2\nu_2^2 + t(\sigma_{11}^2\nu_1^2 - \sigma_{12}^2\nu_2^2)}\ [\sigma_{11}^2 + t(\sigma_{12}^2 - \sigma_{11}^2)]^{L_1+L_2}}$$

$$\cdot \exp\left[-\frac{\dot{\rho}^2}{2\sigma_{12}^2\nu_2^2 + 2t(\sigma_{11}^2\nu_1^2 - \sigma_{12}^2\nu_2^2)}\right] dt \qquad (1.129)$$

As a check, if I let $L_1 = L_2 = 1$ I obtain Equation (1.114) as expected. Numerical integration of Equation (1.129) is not difficult. Solving for the variance, I obtain

$$\sigma^2_{2\dot{\rho}} = \frac{3(L_1 + L_2 - 1)!\sigma_{11}^{2L_2}\sigma_{12}^{2L_1}}{2\sqrt{2}\ \Gamma(L_1)\Gamma(L_2)} \int_0^1 \frac{t^{L_1-1}(1-t)^{L_2-1}[\sigma_{12}^2\nu_2^2 + t(\sigma_{11}^2\nu_1^2 - \sigma_{12}^2\nu_2^2)]^2}{[\sigma_{11}^2 + t(\sigma_{12}^2 - \sigma_{11}^2)]^{L_1+L_2}}\, dt$$

. . . (1.130)

To obtain the final rate density for this case, I transform to log variables:

$$P_{2\Lambda,\dot{\Lambda}}(\Lambda,\dot{\Lambda}) = \frac{\exp[\frac{\Lambda}{\varepsilon}(L_1+L_2+\frac{1}{2}) - \frac{e^{\Lambda/\varepsilon}}{2\sigma_{12}^2}]}{\varepsilon^2\Gamma(L_1)\Gamma(L_2)2^{L_1+L_2-1}\sqrt{2\pi}\,\sigma_{11}^{2L_1}\,\sigma_{12}^{2L_2}}$$

$$\cdot \int_0^1 \frac{t^{L_1-1}(1-t)^{L_2-1}}{\sqrt{\sigma_{12}^2\nu_2^2 + t(\sigma_{11}^2\nu_1^2 - \sigma_{12}^2\nu_2^2)}}$$

$$\cdot \exp\left\{-t\left[\frac{e^{\Lambda/\varepsilon}(\sigma_{12}^2 - \sigma_{11}^2)}{2\sigma_{11}^2\sigma_{12}^2}\right] - \frac{\dot{\Lambda}^2\, e^{\Lambda/\varepsilon}}{8\varepsilon^2\sigma_{12}^2\nu_2^2 + 8\varepsilon^2 t(\sigma_{11}^2\nu_1^2 - \sigma_{12}^2\nu_2^2)}\right\}dt$$

. . .(1.131)

and integrating once more over $\Lambda$, I obtain the desired result:

$$P_{2\dot{\Lambda}}(\dot{\Lambda}) = \frac{\Gamma(L_1 + L_2 + \frac{1}{2})}{\varepsilon\Gamma(L_1)\Gamma(L_2)2^{L_1+L_2+1}\sqrt{2\pi}\,\sigma_{11}^{2L_1}\,\sigma_{12}^{2L_2}} \int_0^1 \frac{t^{L_1-1}(1-t)^{L_2-1}}{\sqrt{\sigma_{12}^2\nu_2^2 + t(\sigma_{11}^2\nu_1^2 - \sigma_{12}^2\nu_2^2)}}$$

$$\cdot \left\{ \frac{1}{2\sigma_{12}^2} + t\,\frac{(\sigma_{12}^2-\sigma_{11}^2)}{2\sigma_{11}^2\sigma_{12}^2} + \frac{\dot{\Lambda}^2}{8\varepsilon^2\sigma_{12}^2\nu_2^2 + 8\varepsilon^2 t(\sigma_{11}^2\nu_1^2 - \sigma_{12}^2\nu_2^2)} \right\}^{-L_1-L_2-\frac{1}{2}} dt$$

. . .(1.132)

Equations (1.131) and (1.132) reduce to Equations (1.121) and (1.122) for $L_1 = L_2 = 1$. The integral for the variance of $\dot{\Lambda}_2$ is not straightforward and cannot be performed unless $L_1$ and $L_2$ are known. This completes the analysis for the rate densities for Case (c) when $N = 2$.

The solutions for arbitrary N are very complicated. Fortunately, an Edgeworth's series approximation has been derived for $P_{N\dot{\chi}}(\dot{\chi})$ (Equation 1.108) and it has been shown that $P_{N\dot{\rho}}(\dot{\rho})$ will be accurately approximated by a Gaussian. Unfortunately, $P_{N\dot{\Lambda}}(\dot{\Lambda})$ cannot be successfully approximated by either an Edgeworth's series or the Gaussian. The coefficients of skew and excess cannot be found for $\dot{\Lambda}$ for arbitrary N, thus ruling out the Edgeworth's series, and though one can certainly fit a Gaussian to $\dot{\Lambda}$, as

noted earlier, the fit will not be good, and the variance obtained from the Gaussian will not be relevant to any physical parameters of the problem. For realizations with $N > 2$ in which $P_{N\dot{\Lambda}}(\dot{\Lambda})$ is needed, and/or approximations for $P_{N\dot{\rho}}(\dot{\rho})$ or $P_{N\dot{\chi}}(\dot{\chi})$ are not good enough, the following procedure can be used for arbitrary N provided computer time is available.

For arbitrary N, following the approach used for $N = 2$, I can write:

$$P_{\chi_{L_1 E},\dot{\chi}_{L_1 E},\cdots,\chi_{L_N E},\dot{\chi}_{L_N E}}(\chi_1,\dot{\chi}_1,\cdots,\chi_N,\dot{\chi}_N) =$$

$$\prod_{n=1}^{N} \frac{\chi_n^{L_n-1}}{\Gamma(L_n)\,2^{L_n}\sqrt{2\pi 4\chi_n\sigma_{1n}^2\nu_n^2}\,\sigma_{1n}^{2L_n}}$$

$$\cdot \exp\left[-\frac{\chi_n}{2\sigma_{1n}^2} - \frac{\dot{\chi}_n^2}{8\sigma_{1n}^2\nu_n^2\chi_n}\right] \qquad (1.133)$$

As before, the sum of the $\dot{\chi}_n$'s involves the convolution of

Gaussians which can be done by inspection and

$$P_{\chi_{L_1E},\cdots,\chi_{L_NE},\dot{\chi}}(\chi_{L_1E},\cdots,\chi_{L_NE},\dot{\chi}) =$$

$$\frac{1}{\sqrt{8\pi \sum_{i=1}^{N} \chi_i \sigma_{1i}^2 \nu_i^2}} \exp\left[-\frac{\dot{\chi}^2}{8 \sum_{i=1}^{N} \chi_i \sigma_{1i}^2 \nu_i^2}\right]$$

$$\cdot \prod_{n=1}^{N} \frac{\chi_n^{L_n-1}}{\Gamma(L_n) 2^{L_n} \sigma_{1n}^{2L_n}} \exp\left[-\frac{\chi_n}{2\sigma_{1n}^2}\right] \qquad (1.134)$$

Unfortunately, this is as far as the analysis can be taken without considering a specific N. Thus, the procedure would be to numerically compute N convolutions with respect to the $\chi_n$'s to obtain $P_{N\chi,\dot{\chi}}(\chi,\dot{\chi})$. Then one more integration over $\chi$ yields the exact density for $\dot{\chi}_N$; likewise, integration over $\rho$ and $\Lambda$ after simple transformation yields the exact density for $\dot{\rho}_N$ and $\dot{\Lambda}_N$ respectively. Perhaps an easier route to $P_{N\chi,\dot{\chi}}(\chi,\dot{\chi})$ can be taken by numerically performing the two integrations required by Equation (1.87).

In summary, the solutions for the rate densities for Case (c) with $N > 2$ are of sufficient analytical complexity that approximate methods or numerical techniques must be employed. The densities for even the most complicated realizations of Case (c) for $\dot{\rho}$ and $\dot{\chi}$ are well in hand with the Gaussian and Edgeworth's series approximations respectively. For $\dot{\Lambda}$, however, complicated multiple source configurations must be handled numerically.

### 1.2.3 Coherent Source Addition

In this section of the thesis, I investigate the statistics of the received signal when two or more sources are radiating at the same frequency or so near in frequency that the receiver is unable to resolve them. The application of this analysis is therefore dependent upon parameters of the receiver; i.e., its resolution R, which is a function of its averaging time T ($R \gtrsim 1/T$), and the source bandwidths, specifically $R > \Delta f$, and $R > B_i, \forall_i$, where $\Delta f$ is the frequency separation, if any, of the sources and $B_i$ is the source bandwidth of the ith source. With these conditions, the procedures used in previous sections are not applicable, and coherent addition of the signals must be considered. This analysis will

model random, narrowband, sea noise from biologics, weather, distant shipping, etc. that overlap in frequency in a small band of interest.

The multipath signal, p(t), under the assumptions of phase random propagation can be written for a single source as

$$p(t) = r \sum_{n=1}^{N} \cos(\omega t + \theta_n) \tag{1.135}$$

where r is the single path amplitude, $N$ is the number of paths, and $\theta_n$ is the single path phase, which is distributed uniformly between 0 and $2\pi$. For many sources at or very near in frequency as indicated above,

$$p(t) = \sum_{i=1}^{L_c} r_i \sum_{n=1}^{N_i} \cos(\omega t + \theta_n) \tag{1.136}$$

where $L_c$ is the number of coherent sources. If this analysis is applied to random sea noise, then Equations (1.135) and (1.136) imply that each radiator

is CW with essentially constant mean output levels. This is perhaps not too bad an assumption if integration times and record lengths are not very long. It is assumed that $N_i \geq 4$, $\forall_i$, such that phase random propagation is obtained for each source. Thus, Equation (1.136) reveals that the problem is one of solving for the statistics of a random vector which is the sum of $L_c$ random vectors, each with Rayleigh distributed magnitudes with different means, and uniformly distributed phases. Forming the envelope of Equation (1.135), I obtain the quadrature components for one source, and applying Equation (1.136), I obtain for the quadrature components of the total vector:

$$X = \rho\cos\phi = \sum_{n=1}^{L_c} \rho_n \cos\phi_n$$

and (1.137)

$$Y = \rho\sin\phi = \sum_{n=1}^{L_c} \rho_n \sin\phi_n$$

where $\rho$ is the rms amplitude of the total vector, $\phi$ is the total multipath phase, $\rho_n$ is the rms amplitude of the nth source, and $\phi_n$ the multipath phase of the nth source.

The quadrature components for the single source are Gaussian [8,9], thus from Eqn (1.137) it is clear that X and Y are Gaussian as well:

$$P_X(X) = \frac{1}{\sqrt{2\pi\sigma_I^2}} \exp\left(-\frac{X}{2\sigma_I^2}\right)$$

$$P_Y(Y) = P_X(Y) \tag{1.138}$$

where $\sigma_I^2 = \sum_{n=1}^{L_c} \sigma_{ln}^2$, and

$$P_{\dot{X}}(\dot{X}) = \frac{1}{\sqrt{2\pi\sigma_{II}^2}} \exp\left(-\frac{\dot{X}^2}{2\sigma_{II}^2}\right)$$

$$P_{\dot{Y}}(\dot{Y}) = P_{\dot{X}}(\dot{Y}) \tag{1.139}$$

where $\sigma_{II}^2 = \sum_{n=1}^{L_c} \sigma_{ln}^2 \nu_n^2$

Note that the short hand notation for Y and $\dot{Y}$ is meant to show that the form of the densities is identical. The quadrature components are in fact independent. Eqns (1.138) and (1.139) illustrate that no conditions need be placed on the strengths of the sources or relative values of the $\nu_n^2$'s. At this point, however, I should caution that if one or two sources are propagating energy via 3 or fewer

paths, and they are strong relative to the other sources, dominant path affects must be considered. Please refer to Appendix C, and for dominant paths plus diffuse (Rayleigh) noise see Reference [26].

Continuing from Equations (1.138) and (1.139), the analysis is straightforward. The resulting densities are in fact identical in form to the densities for the single narrowband source as given in Appendix A. The functional difference is that wherever $\sigma_I^2$ and $\nu^2$ appear in Equations (A1-A8) they must be replaced by $\sigma_I^2$ and $\sigma_{II}^2/\sigma_I^2$ respectively, e.g.,

$$P_{\rho_{L_c}}(\rho) = \frac{\rho}{\sigma_I^2} \exp\left(-\frac{\rho^2}{2\sigma_I^2}\right) \quad , \quad \rho > 0$$

$$\mu_{\rho_{L_c}} = \frac{\sqrt{2\pi}}{2}\sigma_I \quad , \quad \sigma^2_{\rho_{L_c}} = \sigma_I^2(2 - \frac{\pi}{2}) \tag{1.140}$$

$$P_{\dot{\Lambda}_{L_c}}(\dot{\Lambda}) = \frac{1}{4\varepsilon} \frac{\sigma_I/\sigma_{II}}{[1 + \frac{1}{4\varepsilon^2}(\frac{\sigma_I}{\sigma_{II}})^2 \dot{\Lambda}^2]^{3/2}} \quad , \quad |\dot{\Lambda}| < \infty$$

$$\mu_{\dot{\Lambda}_{L_c}} = 0 \quad , \quad \sigma^2_{\dot{\Lambda}_{L_c}} = \infty \tag{1.141}$$

The most important difference, however, is that now the densities for $\dot{\Lambda}$ and $\dot{\phi}$ depend upon the $\sigma_{ln}^2$'s while for a single source they do not. It should be noted, however, that if $\nu^2$ is the same for all the source/receiver pairs,

then once again $\dot{\Lambda}$ and $\dot{\phi}$ are independent of the amplitude parameters, $\sigma_{1n}^2$'s, and are in fact equivalent to the densities of $\dot{\Lambda}$ and $\dot{\phi}$ for a single source. Even though all the sources are at the same or near in frequency the likelihood that $\nu^2$ is the same or almost the same may not be a good one given $\nu^2$'s range dependence [11] (when the internal wave model applies, see Section 3.2).

I now consider a narrowband experiment in which random, background sea noise is present. From the analysis above, I can write:

$$\sigma_I^2 = \sigma_1^2 + \sum_{n=1}^{L_c} \sigma_{1n}^2$$

and (1.142)

$$\sigma_{II}^2 = \sigma_1^2\nu^2 + \sum_{n=1}^{L_c} \sigma_{1n}^2\nu_n^2$$

where $L_c$ is now the number of noise sources in the analysis band and $\sigma_1^2$ and $\nu^2$ are the signal parameters, and the $\sigma_{1n}^2$ and $\nu_n^2$ are the noise related parameters. I now make the assumption (perhaps bad) that $\nu^2$ is a constant for the signal and the noise. Thus, $\sigma_{II}^2 = \sigma_I^2\nu^2$, and I define $\sigma_{N_o}^2 = \sum_{n=1}^{L_c} \sigma_{1n}^2$, which is one half the sta mean square noise, and therefore:

$$\sigma_I^2 = \sigma_1^2 + \sigma_{N_o}^2$$

$$\sigma_{II}^2 = \sigma_1^2 \nu^2 + \sigma_{N_o}^2 \nu^2 \tag{1.143}$$

or

$$\sigma_I^2 = \sigma_1^2 \left(\frac{1}{SNR} + 1\right)$$

$$\sigma_{II}^2 = \sigma_1^2 \nu^2 \left(\frac{1}{SNR} + 1\right) \tag{1.144}$$

where $SNR \equiv \frac{\sigma_1^2}{\sigma_{N_o}^2} = \frac{\text{long time average mean square signal}}{\text{long time average mean square noise}}$ .

Applying Equations (1.144) to the densities and statistics, e.g., Eqns. (1.140) and (1.141), the effect of background noise can be accounted for. It is clear that SNR will be a function of the analysis bandwidth, and that noise levels should be measured in the absence of the signal. By narrowband I mean the signal bandwidth B should be $<<2\nu$ which in turn should be $<< 1/T$ where T is the observation time and the analysis bandwidth $B_A$ should not be so large that the frequency dependence of $\nu^2$ would cause $\nu^2$ to vary significantly across the band.

If for other reasons, i.e., range dependence, the $\nu_n^2 \neq \nu^2$, then

$$\sigma_I^2 = \sigma_1^2 \left(\frac{1}{SNR}\right) + 1$$

but

$$\sigma_{II}^2 = \sigma_1^2 \nu^2 \left(\frac{1}{SNR'} + 1\right) \tag{1.145}$$

where $SNR' \equiv \sigma_1^2 \nu^2 / \sum_{n=1}^{L_c} \sigma_{1n}^2 \nu_n^2$ .

Finally, if one is analyzing over a wide band and the components are disjoint but each is a sum of one or more sources at that frequency, then all the results of the frequency disjoint analysis can be applied with $\sigma_1^2$ replaced by $\sigma_I^2$ and $\nu^2$ replaced by $\sigma_{II}^2/\sigma_I^2$ where these parameters are defined as given in Equations (1.138) and (1.139).

For noise which is continuous over the analysis band, the statistics will be a function of the total bandwidth and the receiver resolution. All the analysis of coherent and incoherent (or more correctly, frequency disjoint and independent) sources apply except now the number of groups N is given by $B_A/R$ where $B_A$ is the analysis bandwidth and R is the receiver resolution. Because the sources within each group are coherent $\sigma_I^2$ and $\sigma_{II}^2$ must be found for each group using Equations (1.138) and (1.139). The groups can now be considered for purposes of applying the results of Sections 1.2.1 and 1.2.2 as individual source/receiver pairs, with the $\sigma_1^2$'s given by the $\sigma_I^2$'s and $\nu^2$'s given by the $\sigma_{II}^2/\sigma_I^2$'s. In conclusion, therefore, the statistics of the received signal are a function of receiver parameters as well as source parameters. For large observation or analysis time T, and consequently higher receiver resolution, the analysis of Sections 1.2.1 and 1.2.2 will most probably apply.

As T becomes smaller, however, coherent effects must be considered as developed in this section. Careful regard for the inequalities stated in the beginning of this section must be applied, case by case, to the data set of interest and the receiver characteristics, in determining which analysis applies.

### 1.2.4 Crossing Rate Statistics

In previous sections I have solved for the joint densities of amplitude, and amplitude rate for many multiple source cases. This allows me, therefore, to solve for the theoretical amplitude crossing rates for these cases as well.

Following Rice [10] and Dyer and Shepard [15], the mean crossing rate for the sta rms pressure $\rho$ can be defined as

$$G(\rho_o) = \int_{-\infty}^{\infty} |\dot{\rho}| P_{\rho,\dot{\rho}}(\rho_o, \dot{\rho}) d\dot{\rho} \qquad (1.146)$$

where $\rho_o$ is the axis crossing level. For L equal source/receiver pairs, Equation (1.78) is used in Equation (1.146) and I obtain:

$$G_{LE}(\rho_o) = \frac{\nu \rho_o^{2L-1} \exp(-\frac{\rho_o^2}{2\sigma_1})}{2^{L-(3/2)} \Gamma(L) \sigma_1^{2L-1} \sqrt{\pi}} \qquad (1.147)$$

Equation (9) of Reference [15] is obtained for L = 1. (Note that $\mu_o \equiv \sigma_1^2$, $\mu_2 \equiv \sigma_1^2\nu^2$.) For two different sources/receptions Equation (1.146) is applied to Equation (1.113):

$$G_{2D}(\rho_o) = \frac{\rho_o^3 \exp(-\frac{\rho_o^2}{2\sigma_{12}^2})}{\sigma_{11}^2\sigma_{12}^2\sqrt{2\pi}} \int_0^1 (\alpha + \delta t)^{\frac{1}{2}} \exp(-ct)dt \qquad (1.148)$$

where $\alpha = \sigma_{12}^2\nu_2^2$ ,

$\delta = \sigma_{11}^2\nu_1^2 - \sigma_{12}^2\nu_2^2$ , and

$c = \rho_o^2(\frac{1}{2\sigma_{11}^2} - \frac{1}{2\sigma_{12}^2})$

If I make the change of variables $Z = \alpha + \delta t$ the integral in Equation (1.148) can be evaluated:

$$G_{2D}(\rho_o) = \frac{(\sigma_{11}^2\nu_1^2 - \sigma_{12}^2\nu_2^2)^{\frac{1}{2}}}{\sigma_{11}^2\sigma_{12}^2\sqrt{2\pi}} \exp\left[\frac{\rho_o^2}{2}\left(\frac{\sigma_{12}^2\nu_2^2/\sigma_{11}^2 - \nu_2^2}{\sigma_{11}^2\nu_1^2 - \sigma_{12}^2\nu_2^2} - \frac{1}{\sigma_{12}^2}\right)\right]$$

$$\cdot \left(\frac{1}{2\sigma_{11}^2} - \frac{1}{2\sigma_{12}^2}\right)^{-\frac{3}{2}} \left\{\gamma\left[\frac{3}{2}, \frac{\rho_o^2}{2}(\frac{1}{\sigma_{11}^2} - \frac{1}{\sigma_{12}^2})\frac{\sigma_{11}^2\nu_1^2}{\sigma_{11}^2\nu_1^2 - \sigma_{12}^2\nu_2^2}\right] -\right.$$

$$- \gamma\left[\frac{3}{2}\ ,\ \frac{\rho_o^2}{2}\left(\frac{1}{\sigma_{11}^2} - \frac{1}{\sigma_{12}^2}\right)\ \frac{\sigma_{12}^2\nu_2^2}{\sigma_{11}^2\nu_1^2 - \sigma_{12}^2\nu_2^2}\right]\Bigg\} \qquad (1.149)$$

where $\gamma(\nu,\mu)$ is the incomplete gamma function [23,24]. Finally, for Case (c) N = 2 I apply Equation (1.146) to Equation (1.128) and

$$G_2(\rho_o) = \frac{\rho_o^{2L_1+2L_2-1}\ \exp\left(-\frac{\rho_o^2}{2\sigma_{12}^2}\right)}{\Gamma(L_1)\Gamma(L_2)2^{L_1+L_2-2}\ \sqrt{2\pi}\ \sigma_{11}^{2L_1}\ \sigma_{12}^{2L_2}}$$

$$\cdot \int_0^1 t^{L_1-1}(1-t)^{L_2-1}(\alpha+\delta t)^{\frac{1}{2}}\exp(-ct)\,dt \qquad (1.150)$$

where $\alpha$, $\delta$, and c are the same as above.

Integrating I obtain [24]:

$$G_2(\rho_o) = \frac{\rho_o^{2L_1+2L_2-1}\ \exp\left(-\frac{\rho_o^2}{2\sigma_{12}^2}\right)}{\Gamma(L_1+L_2)2^{L_1+L_2-2}\ \sqrt{2\pi}\ \sigma_{11}^{2L_1}\ \sigma_{12}^{2L_2}}$$

$$\cdot \Phi_1\left[L_1, -\frac{1}{2}, L_1+L_2; 1-\frac{\sigma_{11}^2\nu_1^2}{\sigma_{12}^2\nu_2^2}, \frac{\rho_o^2}{2}\left(\frac{1}{\sigma_{12}^2} - \frac{1}{\sigma_{11}^2}\right)\right]$$

. . . (1.151)

where $\Gamma(x)$ is the gamma function [24], and $\Phi_1(\alpha,\beta,\gamma;x,y)$ is a degenerate hypergeometric series in two variables [24].

For coherent sources, phase crossing rates as well as amplitude crossing rates can be found. As with amplitude, for the multipath phase [10,15]

$$G(\phi_o) = \int_{-\infty}^{\infty} |\dot{\phi}| P_{\phi,\dot{\phi}}(\phi_o,\dot{\phi}) d\dot{\phi} \tag{1.152}$$

Following Dyer and Shepard [15] but allowing for the effect of many sources at the same frequency, it is easily shown that

$$G_{L_c}(\rho_o) = \sqrt{2/\pi}\ \frac{\sigma_{II}}{\sigma_I^2}\ \rho_o \exp(-\frac{\rho_o^2}{2\sigma_I^2}) \tag{1.153}$$

and

$$G_{L_c}(\phi_o) = \frac{\sigma_{II}}{\sigma_I}\ \frac{1}{2\pi} \tag{1.154}$$

Thus,

$$\frac{G(\rho_o)}{G(\phi_o)} = (8\pi)^{\frac{1}{2}}\ \frac{\rho_o}{\sigma_I} \exp(-\frac{\rho_o^2}{2\sigma_I^2}) \tag{1.155}$$

where $\sigma_I^2$ and $\sigma_{II}^2$ are given below Equations (1.138) and (1.139) respectively. Allowing for the normalization

employed in Reference [15], and the parameters $\sigma_I^2$ and $\sigma_{II}^2$, the form of Equations (1.153 - 1.155) are identical to Equations (9) and (10) in Reference [15]. It is also noteworthy that Equation (1.153) remains unchanged whether the $\nu^2$'s for all the coherent sources are the same or not. In terms of the SNR then

$$\frac{G(\rho_o)}{G(\phi_o)} = (8\pi)^{\frac{1}{2}} \left(\frac{SNR}{1+SNR}\right)\frac{\rho_o}{\sigma_1} \exp\left[-\frac{\rho_o^2}{2\sigma_1}\left(\frac{SNR}{1+SNR}\right)\right] \qquad (1.156)$$

I now consider the ratio of Equation (1.155) with Equation (10) of Reference [15] (the limit of Equation 1.156 as SNR $\to \infty$),

$$R = \frac{SNR}{1+SNR} \exp\left[\frac{\rho_o^2}{2\sigma_1^2}\left(\frac{1}{1+SNR}\right)\right] \qquad (1.157)$$

Thus the effect of noise on the ratio of amplitude crossing rates to phase crossing rates is a multiplicative factor given by Equation (1.157) which depends on both the SNR and the axis crossing level selected.

Finally, if one desires the crossing rates for the mean square pressure $\chi$ or the level in decibels $\Lambda$, the simple substitutions $\rho_o = \chi_o^{\frac{1}{2}}$, and $\rho_o = \exp(\Delta_o/2\varepsilon)$, respectively is all that is required.

### 1.2.5 Summary of Results

Because of the many cases, the notational difficulties, the complexity of the equations, and the plethora of random variables involved, I will attempt a summary in the form of a table of the multiple source section to aid the reader in gaining a little perspective on what exactly has been accomplished. In Table III, I have compiled the overall results of the analysis for the various pdf's of interest in the multicomponent and single source cases. On the left is the breakdown into cases based on source structure and signal analysis. Across the top are the random variables whose pdf's we seek. When a number appears alone in a box, it indicates the equation number of the pdf and also that the result is unique to this thesis. Superscripts (circled numbers) appear in boxes for comments below, and numbers in brackets refer the reader to those references in which the equation appeared previous to this work.

## 1.3 Finite Bandwidth and/or Modulated Source

In many actual oceanic situations the source does not exhibit stability in frequency but in fact oscillates or wobbles about a center frequency which can be characterized by either frequency or phase modulation. The effect of

TABLE III

Summary of Results

| | $\rho$ | $\chi$ | $\Lambda$ | $\dot{\rho}$ | $\dot{\chi}$ | $\dot{\Lambda}$ | $\dot{\phi}$ | $\rho\dot{\rho}$ | $\chi\dot{\chi}$ | $\Lambda\dot{\Lambda}$ |
|---|---|---|---|---|---|---|---|---|---|---|
| Single Source | A1[1] [3,8,9] | A2 [3] | A3 [3] | .5 [8,9] | 1.4 | 1.7 | A8 [8,9] | 1.1 [8,9] | 1.9 | 1.14 |
| Multiple Sources All Equal, Case (a) | 1.79 | 1.19 [4] | 1.83 [4] | 1.80 | 1.67 or 1.76 | 1.64 | NA[2] | 1.78 | 1.74 | 1.82 |
| Multiple Sources All Different, Case (b) | [4][3] | [4] | [4] | 1.114[4] or 1.117[6] | 1.95 | 1.122[4] or 1.123 | NA | 1.113[4] | 1.112[4] | 1.121[4] |
| Multiple Sources N Groups with $L_i$ Equal Sources Each Case (c) | (7) | N=2, 1.23 N=3, 1.29 N≥4, 1.41 or 1.45[5] | N=2, 1.24 N=3, 1.33 N≥4 1.53[5] | N=2, 1.129 N≥3, (8) | N=2, 1.101 or 1.127 N≥3, 1.108[5] | N=2, 1.132 N≥3, (8) | NA | N=2, 1.128 N≥3, (8) | N=2, 1.126 N≥3, 1.87 or 1.134 | N=2, 1.131 N≥3, (8) |
| Coherent Sources | 1.140 | (9) | (9) | (9) | (9) | 1.141 | (9) | (9) | (9) | (9) |

(1)The A refers to Appendix A.
(2)Not applicable.
(3)A simple transformation of the $\chi$ density in Ref. [4].
(4)Only for two different sources.
(5)Ellsworth's approximation.
(6)This density can be accurately approximated by a Gaussian for an arbitrary number of sources, or groups.
(7)Simple transformation of the $\chi$ densities.
(8)Unknown analytically until the integrals in equs. (1.87) or (1.114) can be evaluated. Numerical methods must be applied.
(9)Same as single source with $\sigma_I^2$, and $\sigma_{II}^2/\sigma_I^2$ replacing $\sigma_i^2$ and $\nu^2$ respectively.

this modulation on the family of single source densities is analyzed. Even "narrowband" signals have finite though small bandwidths. I have determined a criterion for smallness, as well as the bandwidth effect when this criterion is not met. Furthermore, the analysis presented in this section reveals a method by which finite bandwidths and/or source induced modulation can be determined from the received signal.

### 1.3.1 Amplitude and Amplitude Rate Densities

In the absence of modulation we can write the multipath signal, p(t), under the assumptions of the phase random model as given by Equation (1.135). When the source is frequency or phase modulated, we can write p(t) as

$$p(t) = r \sum_{n=1}^{N} \cos[\omega t - M(t) - \theta_n] \qquad (1.158)$$

where M(t) is a function of time which may be random that represents the modulation. As indicated in Equation (1.158), it is assumed that source induced modulation will be path independent which implies that any change in signal propagation characteristics (i.e., path structure, or volumetric absorbtion) will be independent of the

"instantaneous" carrier. This is apt to be so unless the modulation is extreme. This assumption also applies to the finite bandwidth effect. The bandwidth cannot be so large that different propagation characteristics obtain for the extremities of the signal. Further, it is assumed that none of the energy in the signal is rejected because the "instantaneous" carrier is outside the bandwidth of the receiver. Likewise, for a finite bandwidth source, it is assumed that the entire signal bandwidth is within the bandwidth of the receiver. Note that depending upon the specific temporal dependence of M(t) the modulation would be classified as either frequency modulation or phase modulation. This distinction, however, does not alter the analysis to follow.

I perform quadrature demodulation on p(t) and obtain the quadrature components:

$$X = \rho\cos[M(t) + \phi] = r \sum_{n=1}^{N} \cos[M(t) + \theta_n]$$
$$Y = \rho\sin[M(t) + \phi] = r \sum_{n=1}^{N} \sin[M(t) + \theta_n] \qquad (1.159)$$

where $\rho$ and $\phi$ are the amplitude and phase respectively of the complex envelope, or alternatively in the terminology of phase random acoustic propagation the sta rms pressure

and multipath phase. Taking the derivatives with respect to time,

$$\dot{X} = -r \sum_{n=1}^{N} [\dot{M}(t) + \dot{\theta}_n] \sin[M(t) + \theta_n]$$

$$\dot{Y} = r \sum_{n=1}^{N} [\dot{M}(t) + \dot{\theta}_n] \cos[M(t) + \theta_n] \tag{1.160}$$

In terms of the quadrature components, Equations (1.159) and their derivatives, Equations (1.160), I can write:

$$\rho = (X^2 + Y^2)^{1/2}$$

$$\dot{\rho} = (X\dot{X} + Y\dot{Y})(X^2 + Y^2)^{-1/2} \tag{1.161}$$

As given in Section 1.1, $\chi$, $\dot{\chi}$, $\Lambda$, and $\dot{\Lambda}$ can be expressed in terms of $\rho$ and $\dot{\rho}$. By applying Equations (1.159) and (1.160) to Equations (1.161) and making use of trigonometric identities, it is easily proven that Equations (1.161) are independent of $M(t)$ and, in fact, are equal to the result obtained when $M(t) = \dot{M}(t) = 0$. Thus, the amplitude, and amplitude rate variables are in fact independent of the modulation. It also follows, therefore, that the joint densities of amplitude and amplitude rate are independent of the modulation.

1.3.2 Multipath Phase Rate Densities

For the multipath phase rate, the modulation plays a critical role. From Equations (1.159) it is clear that the multipath phase with modulation, $\phi_M$, is given by:

$$\phi_M = \tan^{-1}\frac{Y}{X} = M(t) + \phi \tag{1.162}$$

and, therefore:

$$\dot{\phi}_M = \dot{M}(t) + \dot{\phi} \tag{1.163}$$

This result can also be obtained from the single path variables alone [the extreme right-hand side of Equations (1.159)] from which,

$$\dot{\phi}_M = \frac{r^2}{X^2 + Y^2}\left\{\sum_{n=1}^{N}\cos[M(t) + \theta_n]\sum_{n=1}^{N}[\dot{M}(t) + \dot{\theta}_n]\cos\theta_n\right.$$

$$\left. + \sum_{n=1}^{N}\sin[M(t) + \theta_n]\sum_{n=1}^{N}[\dot{M}(t) + \dot{\theta}_n]\sin\theta_n\right\} \tag{1.164}$$

Again, using trigonometric identities, I find that Equation (1.164) is equivalent to Equation (1.163), in which $\dot{\phi}$ is given by Equation (1.164) with $M(t) = \dot{M}(t) = 0$. Note that from Equations (1.159), Equation (1.164) is

independent of r.

M(t) can be either a known deterministic function of time or a random process governed by a pdf $P_{\dot{M}}(\dot{M})$. In the latter case, because $\dot{M}(t)$ is independent of ocean parameters, Equation (1.163) reveals that $\dot{\phi}_M$ is the sum of two independent random variables. Therefore [14],

$$P_{\dot{\phi}_M}(\dot{\phi}) = P_{\dot{M}}(\dot{M}) * P_{\dot{\phi}}(\dot{\phi}) \tag{1.165}$$

where * denotes convolution. The mean $\mu_{\dot{\phi}_M} = \mu_{\dot{M}}$, and as with an unmodulated source, the variance $\sigma^2_{\dot{\phi}_M} = \infty$.

If $\dot{M}(t)$ is a known deterministic function of time, I define:

$$H_{\dot{\phi}_M}(\dot{\phi}) = \frac{1}{T_s} \int_0^{T_s} \frac{1/2\nu}{\left\{1 + \frac{[\dot{\phi} - \dot{M}(t)]^2}{\nu^2}\right\}^{3/2}} dt \tag{1.166}$$

where $T_s$ is the length of the time series (not to be confused with T, the averaging time of the receiver). $H_{\dot{\phi}_M}(\dot{\phi})$ is a continuous histogram and has all the properties of a pdf, i.e., it is always positive and integrates to one. This function or pseudo pdf can be employed when $\dot{M}(t)$ is deterministic but not periodic for a given ensemble of time series. Equation (1.166) also applies for periodic deterministic $\dot{M}(t)$. However, for periodic

deterministic $\dot{M}(t)$ in which there is exactly one or n integral number of periods $\dot{M}(t)$ can be randomized, treated as if it were a random variable, and its pdf found enabling use of Equation (1.165). If there are many periods in the record, then an integral number is not required; however, some error will be introduced. As will be demonstrated by examples below and in Section 1.3.3 for periodic modulation functions, Equations (1.165) and (1.166) yield identical results. For many interesting problems in the ocean, $\dot{M}(t)$ may be deterministic but unknown, the real (nonrandom) parameter estimation problem [25]. In these situations one will obtain experimental realizations of $H_{\dot{\phi}_M}(\dot{\phi})$ from which one is able to learn characteristics of $\dot{M}(t)$, as will be demonstrated in Chapter 3. Also, as will be shown in the figures, some deterministic modulation functions will have easily recognizable histograms, $H_{\dot{\phi}_M}(\dot{\phi})$, and in fact knowledge of $H_{\dot{\phi}_M}(\dot{\phi})$ is by itself a valuable piece of information to have.

I shall now consider three analytical examples illustrating the effect first of sinusoidal phase modulation, second of uniform frequency modulation, and third of Gaussian frequency modulation on the pdf for $\dot{\phi}$.

For sinusoidal phase modulation,

$$M(t) = \beta\sin(\sigma t + \phi_s)$$

and thus, (1.167)

$$\dot{M}(t) = \beta\sigma\cos(\sigma t + \phi_s)$$

I have randomized the phase with $\phi_s$ (uniformly distributed between 0 and $2\pi$), which indicates uncertainty in initial conditions. I obtain the pdf for $\dot{M}(t)$ [3],

$$P_{\dot{M}}(\dot{M}) = \frac{1}{\pi} \frac{1}{(\beta^2\sigma^2 - \dot{M}^2)^{1/2}}, \quad |\dot{M}| < \beta\sigma \tag{1.168}$$

Combining Equations (1.168) and (A8) in Equation (1.165), I find

$$P_{\dot{\phi}_M}(x) = \frac{\nu^2}{2\pi} \int_{-\beta\sigma}^{\beta\sigma} \frac{dy}{\sqrt{(\nu^2 + (x-y)^2)^3(\beta^2\sigma^2 - y^2)}} \tag{1.169}$$

An analytical expression has not been found for this integral; however, numerical integration is straightforward. Applying Equation (1.166) with $T_s \equiv 2\pi n/\sigma$ (n is any integer) and $\dot{M}(t)$ as given by Equation (1.167) with $\phi_s = 0$ (don't forget to exploit the symmetry of the cosine)

yields Equation (1.169) as well. When $x = 0$ in Equation (1.169), the integral can be evaluated:

$$P_{\phi_M}(0) = \frac{1}{\pi\sqrt{\nu^2 + \beta^2\sigma^2}} E\left[\frac{\beta\sigma}{\pi/2,\ \sqrt{\nu^2 + \beta^2\sigma^2}}\right] \tag{1.170}$$

where $E[\pi/2, k]$ is the complete elliptic integral of the second kind.

It is possible to make some progress in solving for $P_{\phi_M}(x)$ if I make use of the convolution property of Fourier transforms or characteristic functions. For independent random variables [14],

$$M_{\phi_M}(\omega) = M_M(\omega) M_\phi(\omega) \tag{1.171}$$

where $M_x(\omega)$ is the Fourier transform or characteristic function of the pdf of random variable x [14]. $M_\phi(\omega)$ is given in the Appendix under Equation (A8), and for the sinusoidal density Equation (1.168) [24],

$$M_M(\omega) = J_o(\omega\beta\sigma)$$

where $J_o(z)$ is the Bessel's function of zeroth order.

Thus, by exploiting symmetry and taking the inverse transform of Equation (1.171),

$$P^{\cdot}_{\phi_M}(x) = \frac{\nu}{\pi} \int_0^{\infty} \omega K_1(\omega\nu) J_o(\omega\beta\sigma) \cos\ \omega x\ dx \qquad (1.172)$$

where $K_1(z)$ is the modified Bessel function of order one. Expanding the cosine and integrating term by term [24],

$$P^{\cdot}_{\phi_M}(x) = \frac{1}{\nu} \sum_{n=0}^{\infty} \frac{(-1)^n}{(2n)!} \left(\frac{x}{\nu}\right)^{2n} (n + \tfrac{1}{2}) [(2n-1)!!]^2$$

$$\cdot\ F\left[\frac{2n+3}{2}\ ,\ \frac{2n+1}{2}\ ;\ 1\ ;\ -\frac{\beta^2\sigma^2}{\nu^2}\right] \qquad (1.173)$$

where $(2n-1)!! = 1\cdot3\cdot5 \ldots (2n-1)$; $(-1)!! \equiv 1$, and $F(a,b;c;z)$ is Gauss's hypergeometric series [24]. Unfortunately, Equation (1.173) converges only for $\beta\sigma < \nu$ and $x < \nu$. When $\beta\sigma = \nu$,

$$P_{\dot{\phi}_M}(x) = \sqrt{\pi/2}\,\frac{1}{\nu}\sum_{n=0}^{\infty}\frac{(-1)^n}{2^n(2n)!}\left(\frac{x}{\nu}\right)^{2n}\left[(2n-1)!!\right]^2$$

$$\cdot\left\{\frac{1}{\Gamma(\frac{n}{2}+\frac{1}{4})\,\Gamma(\frac{1}{4}-\frac{n}{2})} - \frac{1}{\Gamma(\frac{n}{2}+\frac{3}{4})\,\Gamma(-\frac{n}{2}-\frac{1}{4})}\right\} \qquad (1.174)$$

As with Equation (1.173), Equation (1.174) converges only for $x < \nu$. $P_{\dot{\phi}}(\dot{\phi})$ is plotted in Figure 11 for the case of no modulation, Equation (A8), and for various values of $\beta\sigma$ relative to $\nu$ using Equation (1.169). Applying Equations (1.170), (1.173), and (1.174), when applicable, revealed that the error of the numerical integration of Equation (1.169) is approximately 1%.

For uniform frequency modulation, $M(t) = Mt$ and $\dot{M}(t) = M$, where M is a uniformly distributed random variable:

$$P_{\dot{M}}(M) = \begin{cases} 1/2A & |M| < A \\ 0 & \text{otherwise} \end{cases} \qquad (1.175)$$

and A is the maximum excursion from the carrier in Hz, thus, 2A is the bandwidth of the modulation. This characterization of $\dot{M}(t)$ would apply, for example, to a

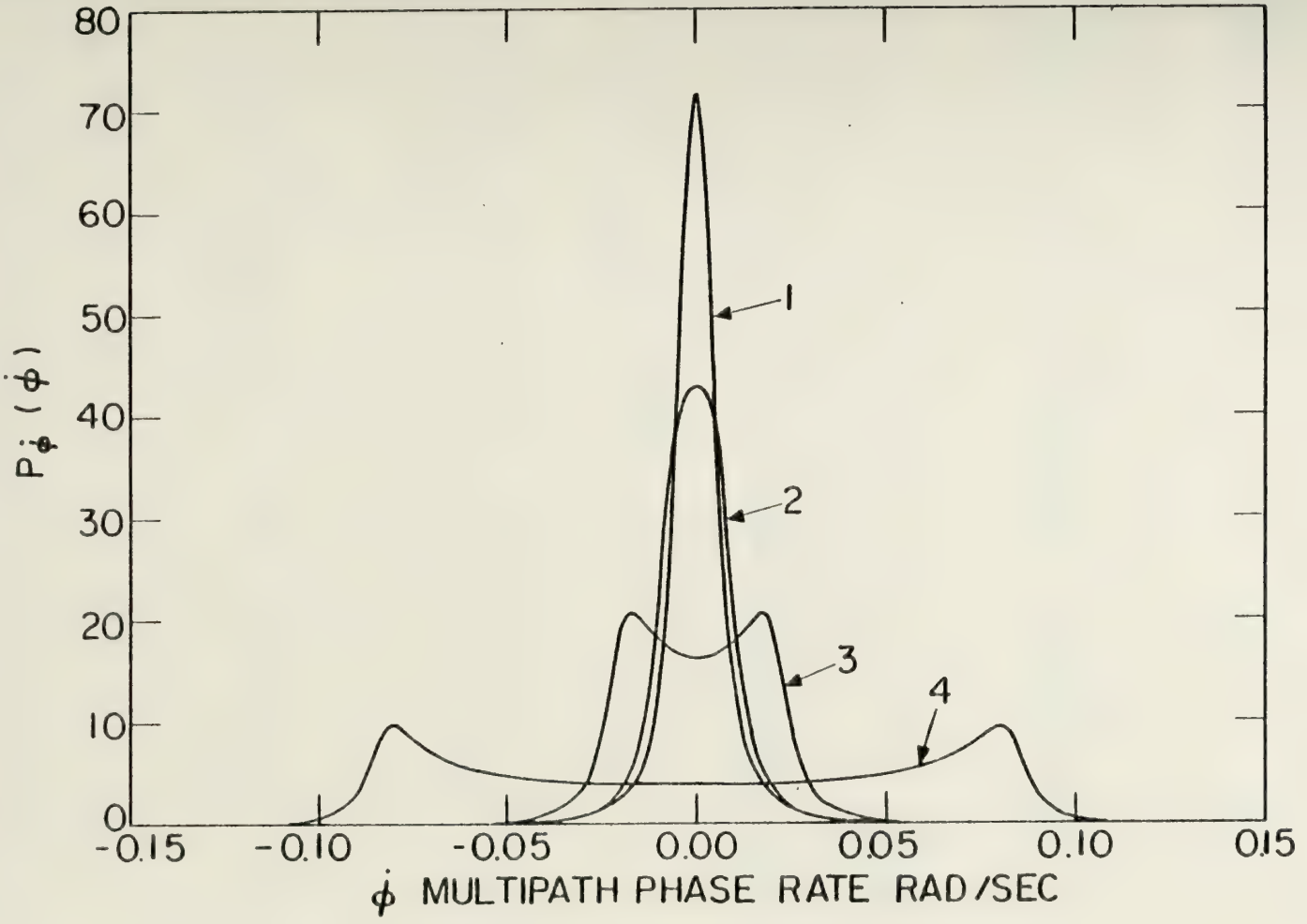


Fig.11 Comparative plot of $P_{\dot{\phi}}(\dot{\phi})$ for no modulation $\nu = .007$ (1), and sinusoidal phase modulation with $\nu = .007$ and $\beta\sigma = .007$ (2), $\beta\sigma = .021$ (3), and $\beta\sigma = .084$ (4).

deterministic $\dot{M}(t)$ such as a saw tooth. As before, I apply Equation (1.165) using Equation (1.175) and (A8), to obtain:

$$P_{\dot{\phi}_M}(x) = \frac{1}{4A}\left\{\frac{x+A}{\sqrt{\nu^2+(x+A)^2}} - \frac{x-A}{\sqrt{\nu^2+(x-A)^2}}\right\} \qquad (1.176)$$

Equation (1.176) is plotted in Figure 12 with no modulation (Equation A8) and for various values of A relative to $\nu$.

For the final example, Gaussian frequency modulation,

$$P_{\dot{M}}(\dot{M}) = \frac{1}{\sqrt{2\pi\sigma_G^2}} e^{-\frac{1}{2}\frac{\dot{M}^2}{\sigma_G^2}} \qquad (1.177)$$

where $\sigma_G^2$ is the variance of the modulation. As before, I convolve Equation (A8) this time with Equation (1.177) and

$$P_{\dot{\phi}_M}(x) = \frac{\nu^2}{2\sqrt{2\pi\sigma_G^2}} \int_{-\infty}^{\infty} (\nu^2+y^2)^{-\frac{3}{2}} \exp\left[-\frac{1}{2\sigma_G^2}(x-y)^2\right]dy \qquad (1.178)$$

As with sinusoidal phase modulation, I have been unable to solve the convolution integral analytically. However,

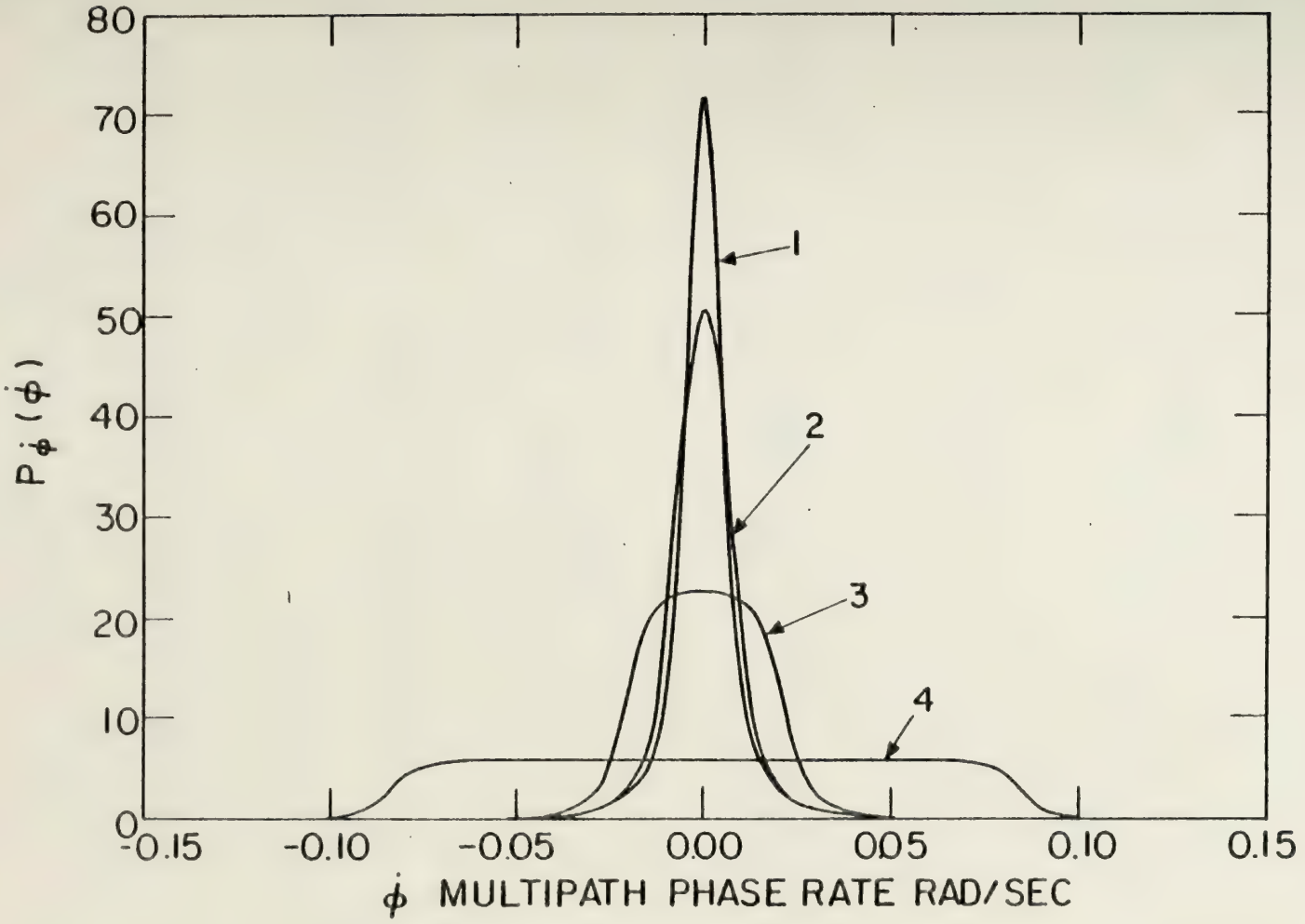


Fig.12 Comparative plot of $P_{\dot{\phi}}(\dot{\phi})$ for no modulation $\nu = .007$ (1), and uniform frequency modulation with $\nu = .007$, and A = .007 (2), A = .021 (3), and A = .084 (4).

applying the characteristic functions, I obtain an alternate expression of Equation (1.178):

$$P'_{\phi_M}(x) = \frac{\nu}{\pi} \int_0^\infty \omega e^{-\frac{1}{2}\omega^2\sigma_G^2} K_1(\omega\nu)\cos\ \omega x\ d\omega \qquad (1.179)$$

Expanding the cosine, I obtain,

$$P'_{\phi_M}(x) = \frac{1}{\sigma_G \pi\sqrt{2}} \sum_{n=0}^{\infty} \frac{(-2)^n}{(2n)!} \left(\frac{x}{\sigma_G}\right)^{2n} \Gamma\left(\frac{2n+3}{2}\right)\Gamma\left(\frac{2n+1}{2}\right)$$

$$\cdot \exp\left(\frac{\nu^2}{4\sigma^2}\right) W_{-n-\frac{1}{2},\frac{1}{2}}\left(\frac{\nu^2}{2\sigma_G^2}\right) \qquad (1.180)$$

Or, alternatively, expanding the exponential in Equation (1.179):

$$P'_{\phi_M}(x) = \frac{1}{\pi\nu} \sum_{n=0}^{\infty} \frac{1}{n!} \left(\frac{\sigma_G}{\nu}\right)^{2n} \Gamma\left(\frac{n+3}{2}\right)\Gamma\left(\frac{n+1}{2}\right)$$

$$\cdot F\left(\frac{n+3}{2}\ ,\ \frac{n+1}{2}\ ;\ \frac{1}{2}\ ;\ -\frac{x^2}{\nu^2}\right) \qquad (1.181)$$

where $W_{\nu,\mu}(z)$ is Whittaker's function, and $F(a,b;c;z)$ is Gauss's hypergeometric series.

Finally, Equation (1.176) will also model the effect of a nonmodulated, but finite bandwidth source if the conditions stated in the beginning of this section hold. It is clear that as long as the energy is uniformly distributed on the average between $f_c - A$ and $f_c + A$. Where $f_c$ is the carrier frequency, then Equation (1.176) applies, and the bandwidth, B, is given by $B = 2A$. A glance at Figure 12 reveals that the effects of the bandwidth on the pdf for $\dot{\phi}$ can be neglected if $B << 2\nu$. The above analysis also reveals that modulation coupled with bandwidth effects are additive. Thus,

$$P_{\dot{\phi}_{MB}}(\dot{\phi}) = P_{\dot{\phi}_M}(\dot{\phi}) * P_{\dot{\phi}_B}(\dot{\phi}) * P_{\dot{\phi}}(\dot{\phi}) \qquad (1.182)$$

where $P_{\dot{\phi}_B}(\dot{\phi})$ is the pdf of the bandwidth which we have assumed is uniform between $\pm B/2$, and $P_{\dot{\phi}_{MB}}(\dot{\phi})$ is the pdf for $\dot{\phi}$ when a narrowband signal is modulated and the criterion $B << 2\nu$ is not satisfied.

Taking the three examples of modulation used above, and coupling them with the bandwidth effect, I obtain for sinusoidal phase modulation,

$$P_{\dot{\phi}_{MB}}(x) = \frac{1}{2B\pi} \int_{-\beta\sigma}^{\beta\sigma} \frac{1}{\sqrt{\beta^2\sigma^2 - y^2}} \left\{ \frac{x + B/2 - y}{\sqrt{\nu^2 + (x + B/2 - y)^2}} \right.$$

$$\left. - \frac{x - B/2 - y}{\sqrt{\nu^2 + (x - B/2 - y)^2}} \right\} dy \qquad (1.183)$$

or,

$$P_{\dot{\phi}_{MB}}(x) = \frac{2\nu}{B\pi} \int_{o}^{\infty} K_1(\omega\nu) J_o(\omega\beta\sigma) \cos \omega x \sin \frac{\omega B}{2} \, d\omega \qquad (1.184)$$

For Gaussian frequency modulation,

$$P_{\dot{\phi}_{MB}}(x) = \frac{1}{2B\sqrt{2\pi}\sigma_G} \int_{-\infty}^{\infty} \exp\left[-\frac{1}{2\sigma_G^2}(x - y)^2\right]$$

$$\cdot \left\{ \frac{y + B/2}{\sqrt{\nu^2 + (x + B/2)^2}} - \frac{y - B/2}{\sqrt{\nu^2 + (x - B/2)^2}} \right\} dy \qquad (1.185)$$

or

$$P_{\dot{\phi}_{MB}}(x) = \frac{2\nu}{B\pi} \int_{o}^{\infty} e^{-\frac{1}{2}\omega^2\sigma_G^2} K_1(\omega\nu) \cos\omega x \sin \frac{\omega B}{2} \, d\omega \qquad (1.186)$$

and for uniform frequency modulation,

$$p_{\dot{\phi}_{MB}}(x) = \frac{1}{4AB}\left\{\sqrt{v^2 + (x+A+B/2)^2} - \sqrt{v^2 + (x+A-B/2)^2}\right.$$

$$\left. + \sqrt{v^2 + (x-A-B/2)^2} - \sqrt{v^2 + (x-A+B/2)^2}\right\}$$

. . .(1.187)

Finally, it should be noted at this point that because a finite bandwidth signal is indistinguishable from a "narrowband" signal which is experiencing extremely rapid uniform frequency modulation as indicated above, the effect of the bandwidth, as with modulation, is felt only by $\dot{\phi}$, the phase rate, and the amplitude variables remain unaffected.

### 1.3.3 Crossing Rate Statistics

For path independent source induced modulation, I have shown that the amplitude, amplitude rate, and joint densities of amplitude and amplitude rate are unaffected by the modulation. It follows, therefore, that $G(\rho_o)$ will be independent of the modulation and will be equivalent to the nonmodulated single source result given by

Equation (1.18).

For a modulated or finite bandwidth signal, $G(\phi_o)$ is as expected critically dependent on the parameters of the modulation and the bandwidth. To find $G(\phi_o)$ it is necessary first to solve for $P_{\phi,\dot{\phi}}(\phi,\dot{\phi})$ and this in turn is crucially dependent upon the exact nature of the modulation or bandwidth. For deterministic modulation, I consider Equations (1.162) and (1.163). The joint pdf for $\phi$ and $\dot{\phi}$ without modulation is given by [8,9]:

$$P_{\phi,\dot{\phi}}(\phi,\dot{\phi}) = \frac{1}{4\pi\nu} \frac{1}{[1 + \frac{\dot{\phi}^2}{\nu^2}]^{3/2}}, \quad \begin{matrix} 0 < \phi < 2\pi \\ |\dot{\phi}| < \infty \end{matrix} \tag{1.188}$$

Making the change of variables given by Equations (1.162) and (1.163) I obtain

$$H_{\phi,\dot{\phi}_M}(\phi,\dot{\phi}) = \frac{1}{4\pi\nu T_s} \int_0^{T_s} \frac{1}{[1 + \frac{(\dot{\phi} - \dot{M}(t))^2}{\nu^2}]^{3/2}} dt \tag{1.189}$$

For the interval 0 to $T_s$: $\min[M(t)] < \phi < 2\pi + \max[M(t)]$ and $|\dot{\phi}| < \infty$. Note again that the H function has all the properties of a pdf. To find the phase crossing rate

$G_M(\phi_o)$ I apply Equation (1.152) and

$$G_M(\phi_o) = \frac{1}{4\pi\nu T_s} \int_0^{T_s} \int_{-\infty}^{\infty} \frac{|\dot{\phi}|}{[1 + \frac{(\dot{\phi} - \dot{M}(t))^2}{\nu^2}]^{3/2}} \, dt \, d\dot{\phi} \qquad (1.190)$$

Rewriting Equation (1.190), I obtain

$$G_M(\phi_o) = \frac{\nu^2}{4\pi T_s} \int_0^{T_s} \left\{ \int_o^{\infty} \frac{\dot{\phi}}{[\nu^2 + \dot{M}(t)^2 + 2\dot{M}(t)\dot{\phi} + \dot{\phi}^2]^{3/2}} \, d\dot{\phi} \right.$$

$$\left. + \int_o^{\infty} \frac{\dot{\phi}}{[\nu^2 + \dot{M}(t)^2 - 2\dot{M}(t)\dot{\phi} + \dot{\phi}^2]^{3/2}} \, d\dot{\phi} \right\} dt \qquad (1.191)$$

Performing the integrations over $\dot{\phi}$:

$$G_M(\phi_o) = \frac{1}{2\pi T_s} \int_0^{T_s} \sqrt{\nu^2 + \dot{M}(t)^2} \, dt \qquad (1.192)$$

This is as far as one can proceed without the exact form of M(t). (Note that if $\dot{M}(t) \to 0$ I recover the no modulation result.) Equation (1.192) can also be used to

find the phase crossing rate when nonstationarities make $\nu$ a function of time as well. Obviously, however, $\nu(t)$ must be known. If $\dot{M}(t)$ is a random process or the modulation is periodic and exactly one or more integral number of periods are on the record (if there are many periods the number need not be integral), then the probabilistic approach used in the previous section can be applied here as well. From Equations (1.189), (1.165), and (1.166),

$$P_{\phi,\dot{\phi}_M}(\phi,\dot{\phi}) = \frac{1}{2\pi} P_{\dot{\phi}_M}(\dot{\phi}) \qquad (1.193)$$

For sinusoidal phase modulation, I use Equation (1.169) in Equations (1.193) and (1.151) to obtain

$$G_M(\phi_o) = \frac{\nu^2}{2\pi^2} \int_{-\beta\sigma}^{\beta\sigma} \frac{1}{\sqrt{\beta^2\sigma^2 - y^2}} \int_o^\infty \frac{x}{\sqrt{(\nu^2 + (x-y)^2)^3}} \, dxdy \qquad \ldots(1.194)$$

Integrating first over x I obtain

$$G_M(\phi_o) = \frac{\nu^2}{\pi^2} \int_o^{\beta\sigma} \frac{dy}{\sqrt{(\beta^2\sigma^2 - y^2)(\nu^2 + y^2)}} \qquad (1.195)$$

The remaining integral is a complete elliptic integral of the second kind:

$$G_M(\phi_o) = \frac{1}{\pi^2}\sqrt{\beta^2\overline{\sigma^2\overline{+\nu^2}^-}}\ E[\tfrac{\pi}{2}\ ,\ r] \qquad (1.196)$$

where

$$r = \frac{\beta\sigma}{\sqrt{\beta^2\overline{\sigma^2\overline{+\nu^2}^-}}}$$

For either $\beta$ or $\sigma \to 0$, $G_M(\phi_o)$ for no modulation is obtained.

To demonstrate the equivalence of the probabilistic approach and the deterministic approach given by Equation (1.192), I consider again sinusoidal phase modulation:

$$M(t) = \beta\sin(\sigma t + \phi_s)$$

and

$$\dot{M}(t) = \beta\sigma\cos(\sigma t + \phi_s)$$

Assuming I have exactly n cycles,

$$G_M(\phi_o) = \frac{1}{2\pi}\,\frac{\sigma}{2n\pi}\int_0^{\frac{2n\pi}{\sigma}} \sqrt{\nu^2\overline{+\beta^2\overline{\sigma^2\overline{\cos^2\sigma t}^-}^-}}\ dt \qquad (1.197)$$

I observe that the integral over one cycle of a $\cos^2 x$ is equal to four times the integral over 0 to $\pi/2$. Applying this observation to Equation (1.197),

$$G_M(\phi_o) = \frac{1}{2\pi} \frac{4n\sigma}{2n\pi} \int_o^{\pi/2\sigma} \sqrt{\nu^2 + \beta^2\sigma^2\cos^2\sigma t}\, dt$$

and therefore

$$G_M(\phi_o) = \frac{\sigma}{\pi^2} \int_o^{\pi/2\sigma} \sqrt{\nu^2 + \beta^2\sigma^2\cos^2\sigma t}\, dt \qquad (1.198)$$

I make the change of variables $x = \sigma t$ and apply the trigonometric identity $\cos^2 x = 1 - \sin^2 x$ in Equation (1.198) and simplifying,

$$G_M(\phi_o) = \frac{1}{\pi^2} \sqrt{\nu^2 + \beta^2\sigma^2} - \int_o^{\pi/2} \sqrt{1 - [\beta^2\sigma^2/(\nu^2 + \beta^2\sigma^2)]\sin^2 x}\, dx$$

. . . (1.199)

The integral in Equation (1.199) is the definitive form

of the complete elliptic integral of the second kind and Equation (1.196) is recovered exactly.

For Gaussian frequency modulation, Equation (1.178) is applied and

$$G_M(\phi_o) = \frac{\nu^2}{2\pi\sqrt{2\pi\sigma_G^2}} \int_{-\infty}^{\infty} \frac{1}{(\nu^2 + y^2)^{3/2}} \int_0^{\infty} x \exp[-\frac{1}{2\sigma_G^2}(x-y)^2]dxdy \quad \ldots(1.200)$$

Performing the integration over x yields

$$G_M(\phi_o) = \frac{\nu^2\sigma_G}{(2\pi)^{3/2}} \int_{-\infty}^{\infty} \frac{\exp(-\frac{y^2}{4\sigma_G^2})}{(\nu^2+y^2)^{3/2}} \left\{ D_{-2}(-\frac{y}{\sigma_G}) + D_{-2}(\frac{y}{\sigma_G}) \right\} dy \quad \ldots(1.201)$$

where $D_p(z)$ is the parabolic cylinder function [24]. I now apply the identity [24]

$$D_p(z) = 2^{\frac{p}{2}} e^{-\frac{z^2}{4}} \left\{ \frac{\sqrt{\pi}}{\Gamma(\frac{1-p}{2})} M(-\frac{p}{2},\frac{1}{2};\frac{z^2}{2}) - \frac{\sqrt{2\pi}\, z}{\Gamma(-\frac{p}{2})} M(\frac{1-p}{2},\frac{3}{2};\frac{z^2}{2}) \right\}$$

to Equation (1.193) and I have

$$G_M(\phi_o) = \frac{2\nu^2\sigma_G}{\pi\sqrt{2\pi}} \int_o^\infty \frac{\exp(-\frac{y^2}{2\sigma_G^2})}{(\nu^2+y^2)^{3/2}} M(1,\tfrac{1}{2},\tfrac{y^2}{2\sigma_G^2})dy \qquad (1.202)$$

where M(a,b,z) is the confluent hypergeometric function. The final integral in Equation (1.202) must be performed numerically.

For uniform frequency modulation, direct use of Equation (1.176) yields a value for $G(\phi_o) = \infty$. This result is not a physical characteristic, but rather a consequence only of the mathematical form of Equation (1.176). The integral leading to Equation (1.176) is

$$P^*_{\phi_M}(x) = \frac{\nu^2}{4A} \int_{-A}^{A} \frac{1}{(\nu^2 + (x-y)^2)^{3/2}} dy \qquad (1.203)$$

Applying Equation (1.203) to Equations (1.193) and (1.152) yields

$$G_M(\phi_o) = \frac{\nu^2}{4\pi A} \int_{-A}^{A} \int_o^\infty \frac{x}{(\nu^2 + (x-y)^2)^{3/2}} dxdy$$

I make the change of variables $t = x - y$ and

$$G_M(\phi_o) = \frac{\nu^2}{4\pi A} \int_{-A}^{A} \int_{-y}^{\infty} \frac{t+y}{\sqrt{(\nu^2 + t^2)^3}} \, dt \, dy$$

Performing the integration over t yields

$$G_M(\phi_o) = \frac{\nu^2}{4\pi A} \int_{-A}^{A} \left[ \frac{1}{\sqrt{\nu^2 + y^2}} + \frac{y^2}{\nu^2 \sqrt{\nu^2 + y^2}} \right] dy$$

and finally I obtain the result

$$G_M(\phi_o) = \frac{\nu^2}{4\pi A} \ln \left[ \frac{\nu}{\sqrt{\nu^2 + A^2} - A} \right] + \frac{1}{4\pi} \sqrt{\nu^2 + A} \qquad (1.204)$$

In the limit as $A \to 0$ Equation (1.204) converges to the no modulation result. Note if I let $A = B/2$ in Equation (1.204) then I have exactly the phase crossing rate for a finite bandwidth non-modulated source.

The crossing rates for modulated signals with bandwidth have not been solved; however, the procedure is quite

straightforward, though the integrals may not be.

I now consider the ratio of amplitude crossing rates to phase crossing rates. Dyer and Shepard [15] obtained this ratio for the narrowband, no modulation, single source:

$$\frac{G(\rho_o)}{G(\phi_o)} = (8\pi)^{\frac{1}{2}} \frac{\rho_o}{\sigma_1} \exp(-\frac{\rho_o^2}{2\sigma_1^2}) \tag{1.205}$$

Equation (1.205) is independent of $\nu$ and depends only upon $\sigma_1^2$ which, being a measure of the energy in the signal, is a controllable parameter unrelated to oceanic phenomena. However, non-stationary behavior of $\sigma_1^2$ due to ocean dynamics will affect the ratio given by Equation (1.205). Likewise, if the source is modulated or has a bandwidth which is not $<< 2\nu$ then the ratio given by Equation (1.205) will be affected. For these cases, the ratio $G(\rho_o)/G(\phi_o)$ will be a function of $\sigma_1^2$, $\nu^2$, and parameters of the modulation. Adopting the approach in Reference [15],. I obtain

$$\frac{G_M(\rho_o)}{G_M(\phi_o)} = (8\pi)^{\frac{1}{2}} C\sigma_1 P_\rho(\rho_o) \tag{1.206}$$

where, for sinusoidal phase modulation,

$$C = \frac{\nu\pi}{2\sqrt{\beta^2\sigma^2 + \nu^2}\, E[\frac{\pi}{2}, r]}, \quad r = \frac{\beta\sigma}{\sqrt{\beta^2\sigma^2 + \nu^2}} \tag{1.207}$$

for uniform frequency modulation,

$$C = \frac{2A\nu}{\nu^2 \ln[\frac{\nu}{\sqrt{\nu^2 + A^2} - A}] + A\sqrt{\nu^2 + A}} \tag{1.208}$$

for Gaussian frequency modulation,

$$C = [\frac{2\pi}{\nu} G_M(\phi_o)]^{-1} \tag{1.209}$$

where $G_M(\phi_o)$ is given by Equation (1.202), and finally for a finite bandwidth, non-modulated source C is given by Equation (1.208) with A = B/2. Except for the finite bandwidth result, great care should be taken in applying the formulas in this section to insure that the actual modulation fits the kinds of modulation assumed here. However, the procedure developed in this section can be applied on a case by case basis to any kind of frequency or phase modulation to determine the phase crossing rate factor.

# CHAPTER 2

# COMPUTER SIMULATION

A computer simulation of phase random multipath propagation was originally developed for two reasons. First, in the course of analysis of the multiple source cases it was felt that a computer simulation would provide confirmation of the rather complicated analysis when data were unavailable or difficult to obtain for the case in question. Second, when an analytical impasse was reached the simulation could provide insight into the nature of the solution, thus aiding in the analytical process. The simulation fulfilled these two objectives not only as originally intended in the area of multiple sources but in all aspects of the theoretical development presented in this thesis, as well as providing confirmation of some of the basic precepts of the phase random model of acoustic propagation.

## 2.1 Computer Model of Phase Random Multipath Propagation

A computer simulation which generates random samples from a phase-random multipath process has been developed. Currently there are two versions. The first, called RANDPHASE, simulates up to 50 equal intensity, equal $v^2$ components, including sinusoidal phase modulation, uniform

frequency modulation, and bandwidth effects on phase rate for a single source. The second, called BURMRAN, is capable of handling an arbitrary number of groups of unequal intensity but equal $\nu^2$, for the amplitude and amplitude rate variables. Both programs are written in FORTRAN IV and were run on an Interdata Model 80 computer with an IMLAC display processor. The FORTRAN listings for RANDPHASE and BURMRAN are contained in Reference [27].

The following algorithms are applied to generate samples for the amplitude and amplitude rate variables:

$$\chi_L = \sum_{i=1}^{L} r_i^2 \left\{ \left[ \sum_{n=1}^{N} \cos\theta_{n_i} \right]^2 + \left[ \sum_{n=1}^{N} \sin\theta_{n_i} \right]^2 \right\}$$

$$\dot{\chi}_L = \sum_{i=1}^{L} 2r_i^2 \left[ \sum_{n=1}^{N} \sin\theta_{n_i} \sum_{n=1}^{N} \dot{\theta}_{n_i} \cos\theta_{n_i} - \sum_{n=1}^{N} \cos\theta_{n_i} \sum_{n=1}^{N} \dot{\theta}_{n_i} \sin\theta_{n_i} \right]$$

$$\rho_L = \chi_L^{1/2}$$

$$\dot{\rho}_L = \frac{1}{2} \chi_L^{-1/2} \dot{\chi}_L$$

$$\Lambda_L = 10 \log_{10} \chi_L$$

$$\dot{\Lambda}_L = [10 \log_{10} e] \dot{\chi}_L / \chi_L \qquad (2.1a\text{-}f)$$

where $r_i$ is the single path amplitude for the ith source, L is the number of sources, $N$ is the number of paths, $\theta_{n_i}$ the single path phase, and $\dot{\theta}_{n_i}$ the single path phase rate. For L=1, the single source, samples of the multipath phase $\phi$ and the multipath phase rate $\dot{\phi}$ are generated. Equation (1.164) is used to generate the samples of $\dot{\phi}$. The input parameters to the program are $\nu^2$, L, $N$, A (or equivalently, B/2), $\beta$, $\sigma$, and I, the number of samples desired. For RANDPHASE the $r_i$ are equal and are set to one for convenience, though initialization to some other value is straightforward. For BURMRAN the array r must be specified.

Each program uses two random number generators employing a machine independent congruence technique [28]. One is used to generate uniformly distributed random numbers between 0 and $2\pi$ for $\theta_n$, and the other is used to generate samples of $\dot{\theta}_n$. It is assumed that $\dot{\theta}_n$ is uniformly distributed between $\pm \sqrt{3}\, \nu$, thus in the limit as $N \to \infty$, $E[\dot{\theta}_n] = 0$ and $E[\dot{\theta}_n^2] = \nu^2$. Application of the

program revealed that if the number of paths is greater than three, phase random multipath properties are obtained. Because of the central limit assumptions inherent in the phase random model [9] (e.g. $N > 3$), the exact nature of the density for $\dot{\theta}_n$ is unimportant. RANDPHASE was run with $\dot{\theta}_n$ distributed normally without any change in the results.

The number of independent samples of $\theta_n$ and $\dot{\theta}_n$ required for any given simulation is given by the product of L, $N$, and I. For most of the simulation runs I ≈ 600 samples. Where L and $N$ are large, the number of independent samples of $\theta_n$ and $\dot{\theta}_n$ can become quite large. One run of BURMRAN simulating the $N = 15$ problem of Reference [4] required ∿ 400,000 independent samples of $\theta_n$ and $\dot{\theta}_n$. The maximum integer that can be accommodated on the Interdata 80 is 32,767. I performed a run test on the system random number generator (which employs the linear congruence method) and for some primes the maximum string of unrepeated numbers was 8192, clearly inadequate. In order to increase the cycle lengths the machine independent congruence method is used. This technique artificially increases the maximum allowable integer number with factors appropriately segmented so that numerical overflows can be computed without machine

overflows. The cycle length is greater than $10^7$, and for $1.5 \times 10^6$ samples generated by this method, the Chi-square goodness of fit test [29] for uniformity was passed at the $\alpha = .05$ level of significance, though only by a small margin. It is true that the leftmost digits are the most random and that for large numbers of samples some correlation occurs as more of the rightmost digits are repeated. Table IV, reproduced from Reference [28], gives the repeat characteristics for the two sequences or generators used. Table IV indicates the randomness of the generator as a function of cycle length or number of samples. As more and more samples are taken, i.e., the cycle length becomes larger, more and more of the rightmost digits are repeated which can result in a correlation that will introduce some error in the overall simulation results. Because the repeat cycle length is so large, however, for most simulation runs this error is small.

When modulation or finite bandwidth effects are simulated, the Interdata 80 random number generator is used in addition to the two described above. Because L=1 for these simulations the large number of samples for $\theta_n$ and $\dot{\theta}_n$ is not required.

When the programs are executed, histograms are

TABLE IV

Repeat characteristics of the random number generater for the two sequences used.

| Cycle | Sequence One | Sequence Two |
|---|---|---|
| 0 | $735776465527_8$ | $311037552421_8$ |
| $8^1$ | $062221556427_8$ | $113326416521_8$ |
| $8^2$ | $650107434527_8$ | $655503553421_8$ |
| $8^3$ | $617512155527_8$ | $514633562421_8$ |
| $8^4$ | $65527_8$ | $52421_8$ |
| $8^5$ | $465527_8$ | $552421_8$ |
| $8^6$ | $6465527_8$ | $7552421_8$ |

produced by separating the range of samples for each of the variables specified by Equations (2.1) and (1.164) into 25 equally spaced bins. In RANDPHASE each histogram is then plotted along with its respective theoretical density and the Chi-square goodness of fit test is applied. The area under the theoretical curve is computed numerically using the trapezoidal rule, each of the twenty five bins being further subdivided into 16 intervals each. The expected frequency is then equal to the number of samples times the area. Bins in the tails are grouped such that the minimum expected frequency is 7. Thus the number of independent class intervals (a function of the variable, number of sources, paths, etc.) usually varies between 15 and 25 which is close to the criteria specified by Bendat and Piersol [29] for $\sim$ 600 samples. The Chi-square statistic ($\chi^2$) is computed and compared to the pass/fail value ($\chi^2_n$: .05), where n indicates the number of degrees of freedom of the statistic and .05 is the level of significance. The hypothesis is accepted if $\chi^2 < \chi^2_n$: .05. The number of degrees of freedom n is obtained by taking the number of class intervals and subtracting $1 + \beta$ where $\beta$ is the number of independent parameters that are varied to fit the pdf to the histogram (e.g. $\beta = 0$ for the uniform pdf and $\beta = 1$

for the Rayleigh, Gaussian, and Longuet-Higgins pdf's).

It should be noted that the theoretical densities were not least-squares fit to the histograms. Given the input parameters, we know $\sigma_1^2$ from Equation (1.2), and $\nu$ is obtained by taking the expected value of $\dot{\theta}_n^2$ from the computer generated $\dot{\theta}_n$'s (which is always within a few percent of the input value of $\nu$). The theoretical densities are plotted and the samples fall where they may.

In addition to the output on the graphics display a printout for each variable for each run of the simulation includes: the variable simulated, the number of sources, paths, samples, number of expected and observed frequencies for each bin, including an overflow bin, the observed and theoretical mean and variance, the range of values obtained, and the actual Chi-square statistic and the pass/fail value.

## 2.2 Simulation Results for a Single Narrowband Source

Examples of the results of the computer simulation RANDPHASE for a single, narrowband, non-modulated source are given in Figures 13-36. The figures are plotted by variable for $N$ = 4, 5, and 12 paths. For all these runs, the input value of $\nu$ is .007 rad/sec and I = 700 samples. Table V compiles the Chi-square statistics ($\chi^2$) for each of

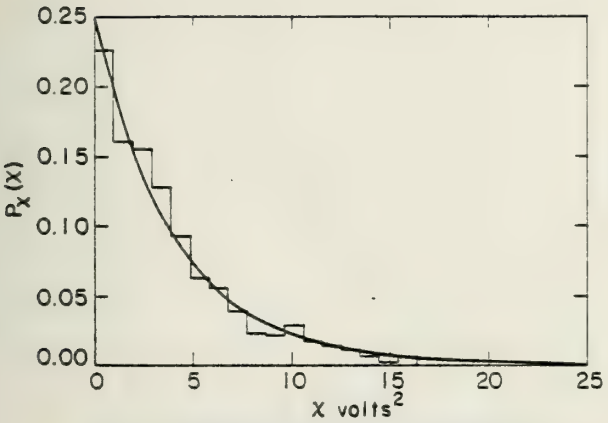


Fig. 13 Computer generated histogram of X, the sta mean square pressure for N=4 paths compared with equ. (A2).

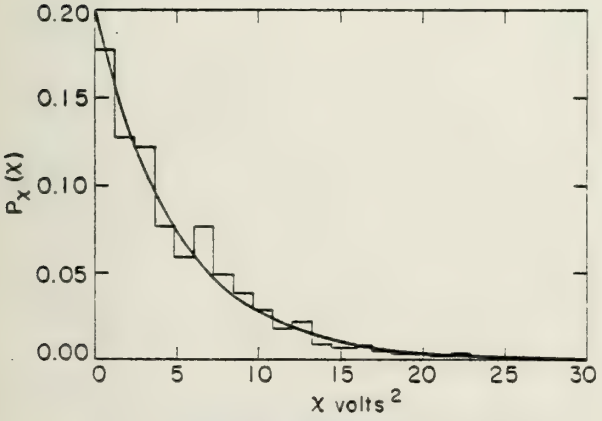


Fig. 14 Computer generated histogram of X for N=5 paths and equ. (A2).

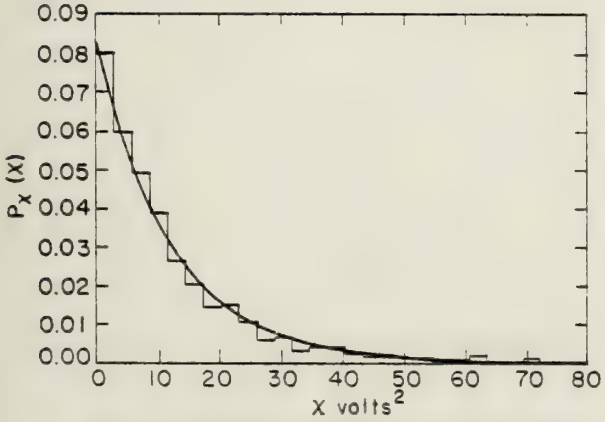


Fig. 15 Computer generated histogram of X for N=12 paths and equ. (A2).

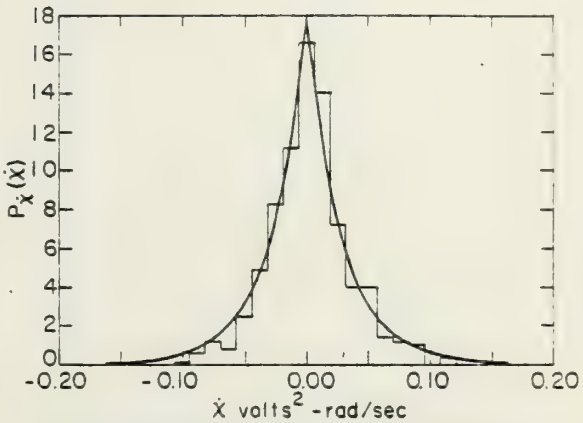


Fig. 16 Computer generated histogram of $\dot{X}$ with N=4 paths and equ. (1.4).

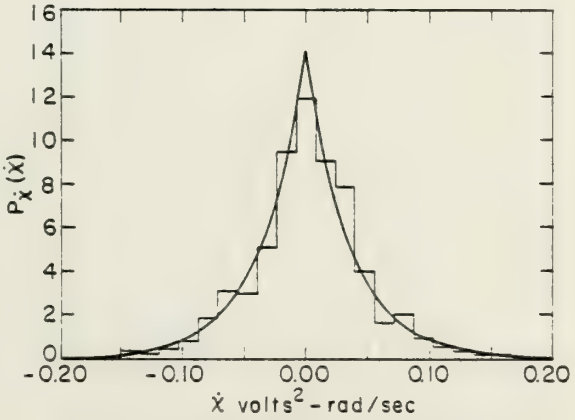


Fig. 17 Computer generated histogram of $\dot{X}$ for N=5 paths and equ. (1.4).

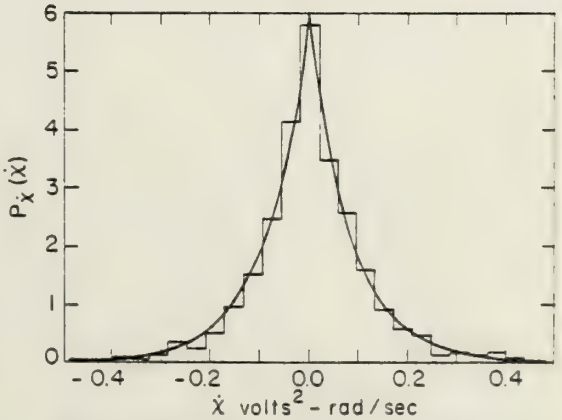


Fig. 18 Computer generated histogram of $\dot{X}$ for N=12 paths and equ. (1.4).

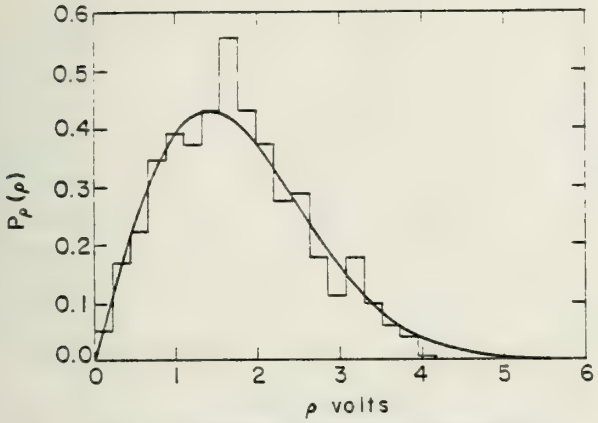


Fig. 19 Computer generated hisogram of $\rho$, the sta rms pressure for N = 4 paths compared with equ. (A1).

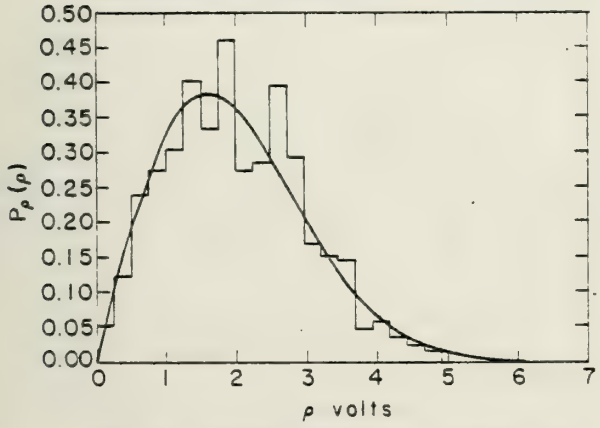


Fig. 20 Computer generated histogram of $\rho$ with N = 5 paths and equ. (A1).

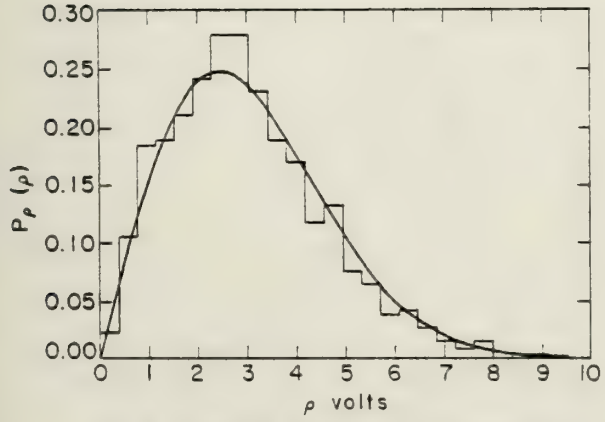


Fig. 21 Computer generated histogram of $\rho$ with N=12 paths and equ. (A1).

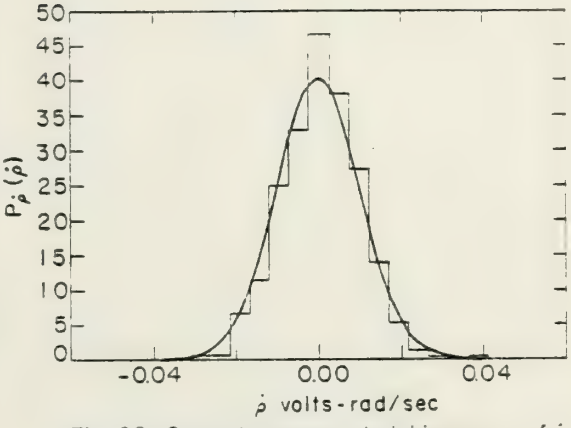


Fig. 22 Computer generated hisogram of $\dot\rho$ with N=4 paths and equ. (A5).

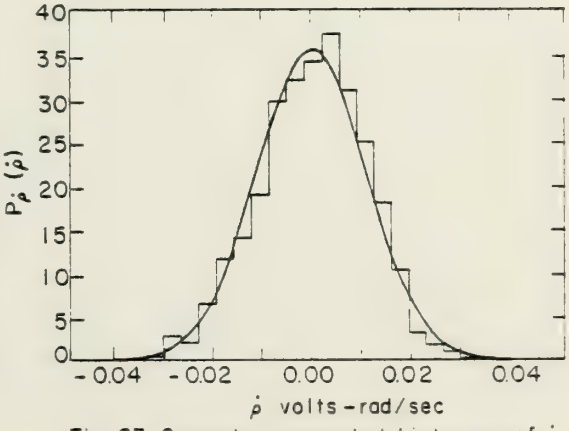


Fig. 23 Computer generated histogram of $\dot\rho$ with N= 5 paths and equ. (A5).

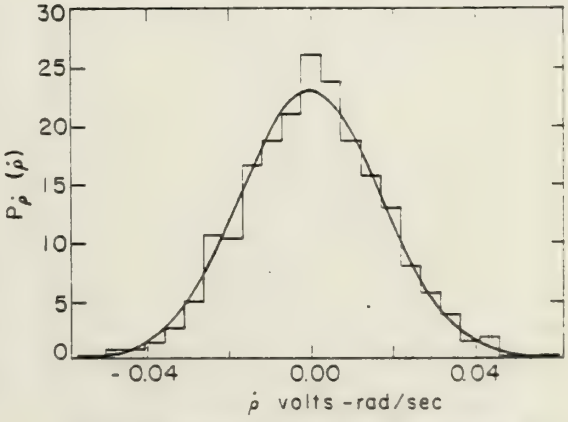


Fig. 24 Computer generated histogram of $\dot\rho$ with N=12 paths and equ. (A5).

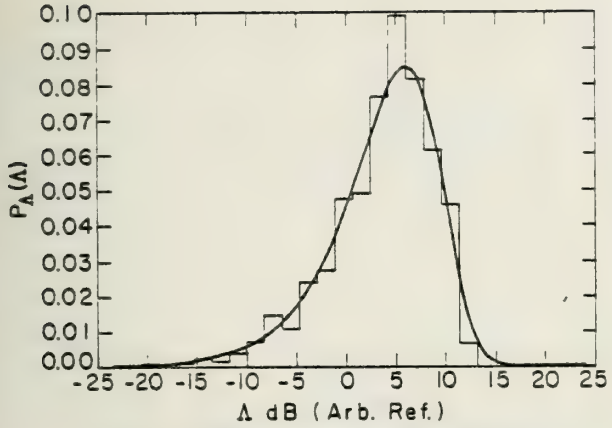


Fig. 25 Computer generated histogram of $\Lambda$, the level in dB's of the sta mean square pressure for N=4 paths compared with equ, (A3).

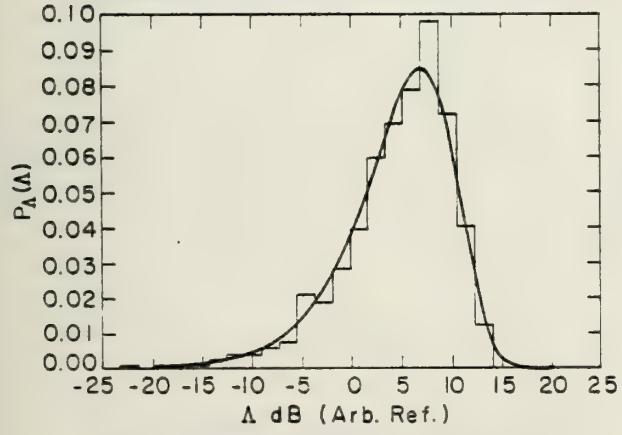


Fig. 26 Computer generated histogram of $\Lambda$ with N=5 paths and equ. (A3).

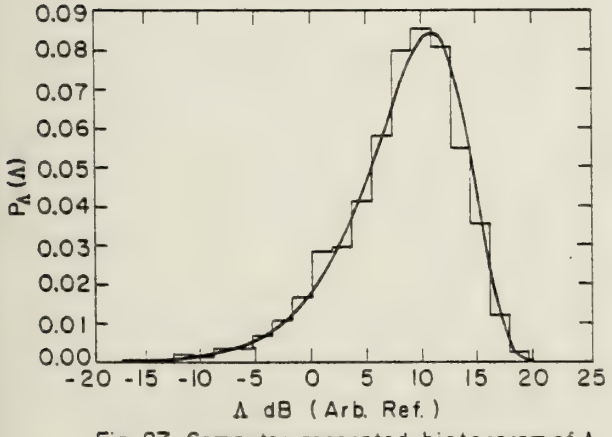


Fig. 27 Computer generated historgram of $\Lambda$ with N=12 paths and equ. (A3).

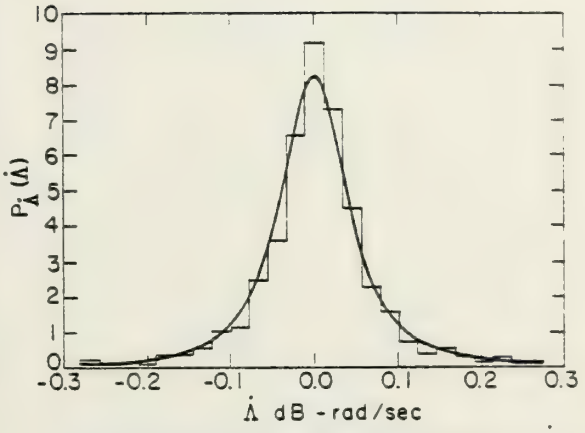


Fig. 28 Computer generated histogram of $\dot\Lambda$, with N=4 paths and equ. (1.7).

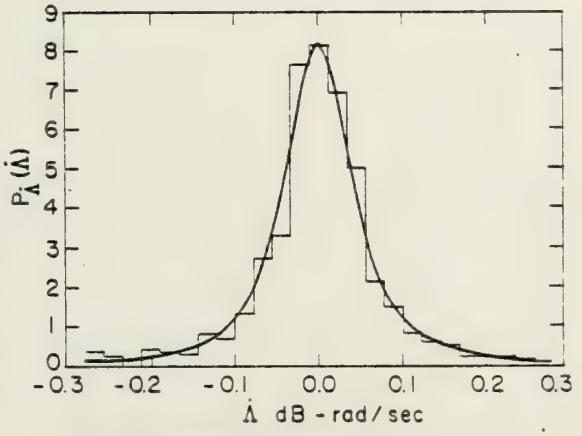


Fig. 29 Computer generated histogram of $\dot\Lambda$ with N=5 paths and equ (1.7).

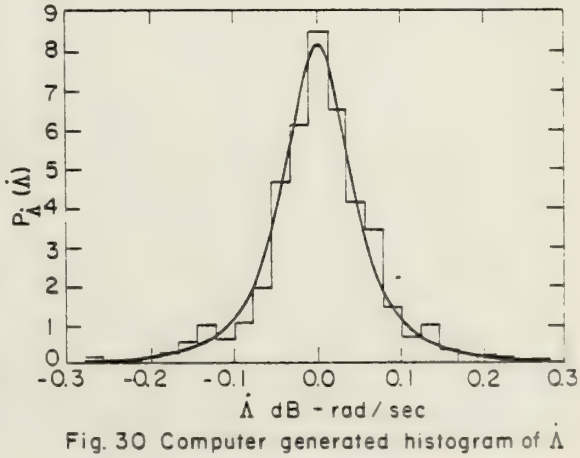


Fig. 30 Computer generated histogram of $\dot\Lambda$ with N = 12 paths and equ. (1.7).

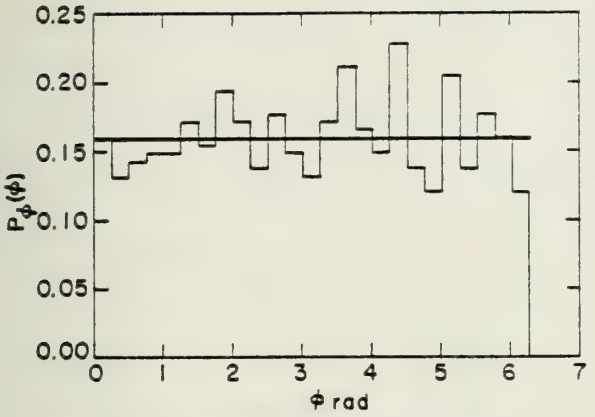


Fig. 31 Computer generated histogram of $\phi$, the multipath phase, for N = 4 paths compared with equ. (A4).

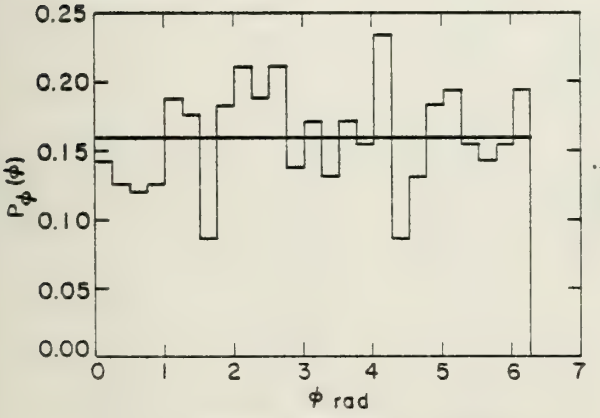


Fig. 32 Computer generated histogram of $\phi$, with N = 5 paths and equ. (A4).

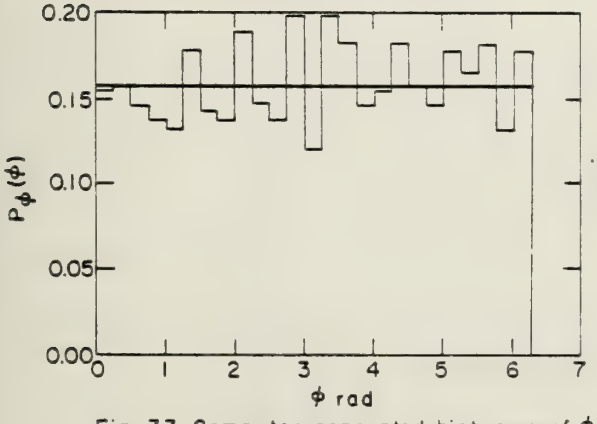


Fig. 33 Computer generated histogram of $\phi$, with N = 12 paths and equ. (A4).

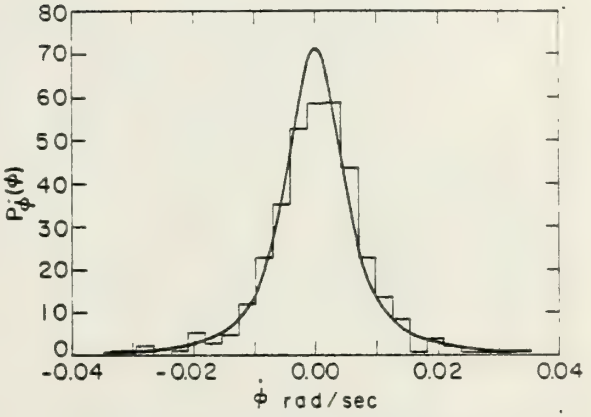


Fig. 34 Computer generated histogram of $\dot\phi$, with N = 4 paths and equ. (A8).

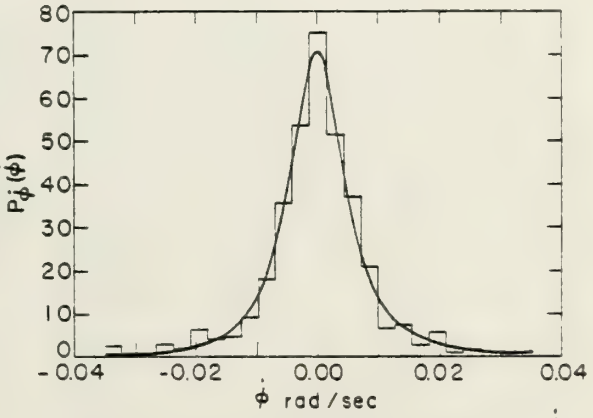


Fig. 35 Computer generated histogram of $\dot\phi$, with N = 5 paths and equ. (A8).

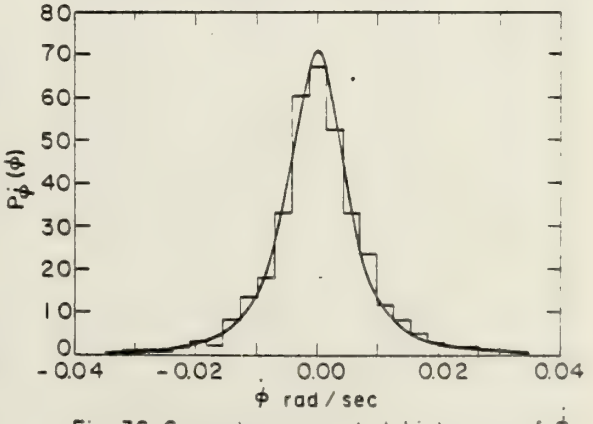


Fig. 36 Computer generated histogram of $\dot\phi$ with N = 12 paths and equ. (A8).

TABLE V

Results of the hi-square test for the RANDPHASE simulation of a single narrowband, non-modulated source. For $\chi^2 < \chi^2_n$: .05 the theoretical pdf passes the test at the .05 level of significance. The units are the same as in the figures.

| Fig. | Variable | $\chi^2$ | $\chi^2_n$: .05 | $N$ | Mean | | Std. Dev. | |
|---|---|---|---|---|---|---|---|---|
| | | | | | Theory | Data | Theory | Data |
| 13 | $\chi$ | 19.36 | 25.00 | 4 | 4.00 | 3.64 | 4.00 | 3.24 |
| 14 | $\chi$ | 18.59 | 25.00 | 5 | 5.00 | 4.85 | 5.00 | 4.31 |
| 15 | $\chi$ | 8.62 | 25.00 | 12 | 12.00 | 11.19 | 12.00 | 11.34 |
| 16 | $\dot{\chi}$ | 27.44 | 23.68 | 4 | 0.00 | 0.00 | 0.04 | 0.03 |
| 17 | $\dot{\chi}$ | 19.93 | 23.68 | 5 | 0.00 | 0.00 | 0.50 | 0.46 |
| 18 | $\dot{\chi}$ | 7.84 | 23.68 | 12 | 0.00 | 0.00 | 0.12 | 0.11 |
| 19 | $\rho$ | 24.02 | 28.87 | 4 | 1.77 | 1.71 | 0.93 | 0.84 |
| 20 | $\rho$ | 27.68 | 28.87 | 5 | 1.98 | 1.98 | 1.04 | 0.97 |
| 21 | $\rho$ | 12.85 | 28.87 | 12 | 3.07 | 2.96 | 1.60 | 1.56 |
| 22 | $\dot{\rho}$ | 14.37 | 18.31 | 4 | 0.00 | 0.00 | 0.01 | 0.01 |
| 23 | $\dot{\rho}$ | 9.79 | 23.68 | 5 | 0.00 | 0.00 | 0.01 | 0.01 |
| 24 | $\dot{\rho}$ | 6.50 | 26.30 | 12 | 0.00 | 0.00 | 0.02 | 0.02 |
| 25 | $\Lambda$ | 21.29 | 22.36 | 4 | 3.51 | 3.30 | 5.57 | 5.63 |
| 26 | $\Lambda$ | 11.24 | 22.36 | 5 | 4.48 | 4.55 | 5.57 | 5.43 |
| 27 | $\Lambda$ | 9.00 | 22.36 | 12 | 8.28 | 7.99 | 5.57 | 5.46 |
| 28 | $\dot{\Lambda}$ | 10.61 | 26.30 | 4 | 0.00 | 0.01 | $\infty$ | 0.20 |
| 29 | $\dot{\Lambda}$ | 15.36 | 26.30 | 5 | 0.00 | 0.00 | $\infty$ | 0.11 |
| 30 | $\dot{\Lambda}$ | 25.96 | 26.30 | 12 | 0.00 | -0.01 | $\infty$ | 0.11 |
| 31 | $\phi$ | 20.64 | 36.42 | 4 | $\pi$ | 3.16 | 1.81 | 1.76 |
| 32 | $\phi$ | 37.43 | 36.42 | 5 | $\pi$ | 3.21 | 1.81 | 1.78 |
| 33 | $\phi$ | 13.07 | 36.42 | 12 | $\pi$ | 3.20 | 1.81 | 1.80 |
| 34 | $\dot{\phi}$ | 23.64 | 26.30 | 4 | 0.00 | 0.00 | $\infty$ | 0.01 |
| 35 | $\dot{\phi}$ | 24.60 | 26.30 | 5 | 0.00 | 0.00 | $\infty$ | 0.01 |
| 36 | $\dot{\phi}$ | 9.36 | 26.30 | 12 | 0.00 | 0.00 | $\infty$ | 0.02 |

the figures and the $\chi^2_n$: .05 in which n is the number of degrees of freedom, which is equal to the number of class intervals minus one (recall that the densities were not fit), and .05 is the level of significance. For $\chi^2 < \chi^2_n$: .05 the theoretical density passes the Chi square test. Also shown in Table V is the theoretical value of the mean and standard deviation and the measured values from the computer generated "data".

First, note that all the theoretical densities match the histograms very well as indicated by results of the Chi-square test. Particularly note that the pdf's for $\dot{\chi}$ and $\dot{\Lambda}$ given by Equations (1.4) and (1.7) respectively are indeed supported by computer simulation. Of the 24 examples shown, only two fail the Chi-square test. All the pdf's in Figures 13-36 are the limiting densities as $N \to \infty$. The results of the simulation for $N = 2$ and 3 paths (including further analysis of this case) are given in Appendix C. Upon comparison with the results of Appendix C, it is quite acceptable to assume that for $N \geq 4$ paths phase random multipath propagation is obtained. It is true that $\dot{\chi}$ for $N = 4$ paths did fail the Chi-square test but this is only one out of eight variables. It should be noted that for $N = 2$ and 3 paths the limiting densities for seven out of eight of the

ariables (the multipath phase $\phi$ is always uniform)
ailed the Chi-square test (see Reference [27]), thus the
ustification for choosing $N \geq 4$ as the required number of
aths is evident. The failure of $\phi$ for the 5 path case
ndicates perhaps a lack of randomness or a correlation
or that particular cycle length in the random number
enerator. Though the results on the average get better
s N becomes large, as indicated in Table V, (except
uriously enough for $\dot{\Lambda}$), after 12 paths the results
re approximately constant indicating that the
orrelation in each of the random number generators is
ow the limiting factor. This assertion follows from
onsideration of $N = 30$ [27] in which by the way $\chi^2$ for
is 4.49, and $\chi^2_n$: .05 = 26.30. In addition to
ontaining the other simulations not shown in the figures
or mentioned above Reference [27] also includes the
ore detailed printout mentioned earlier. It is
nteresting to note that even when phase random conditions
re met for the single source the pdf for $\rho$ always appears
o be among the worst performers while $\dot{\rho}$ is always among
ne best. This result was first noted by Hamblen [9]
nen he investigated ocean acoustic data. Because this
esult is repeated in the simulation, it appears to be
function of the statistical nature of the variables, as

well as the non-stationarity of $\sigma_1^2$ when analyzing real data.

## 2.3 Simulation Results for Multiple Sources

Figures 37-42 are the results of a simulation run with 20 equal intensity, equal $\nu^2$ receptions, 5 paths, and I = 600 samples. The theoretical densities are given by Equations (1.19), (1.67), (1.79), (1.80), (1.83), and (1.84) respectively. The results of the Chi-square test are tabulated in Table VI. Also shown are the means and standard deviations as predicted by the theory and observed in the simulation. With one exception, the computer simulation agrees well with the theoretical predictions. One of the important results of the analysis of the equal intensity, equal $\nu^2$ case (Section 1.2.2.1) is that $P_{\dot{\rho}}(\dot{\rho})$ is independent of the number of sources. Figures 24, 43, 44, and 40 are examples of $P_{\dot{\rho}}(\dot{\rho})$ for 1, 3, 4, and 20 equal intensity ($\sigma_1^2 = 2.5$), equal $\nu^2$ ($\nu = .007$ rad/sec) sources. Figures 43 and 44 passed the Chi-square test, and the histograms clearly support this prediction as well.

As a final example of multiple source simulations, I treated the N = 15 group problem of Reference [4]. As was noted in Section 1.2.1.4, and illustrated in Table I,

TABLE VI

Results of the chi-square test for RANDPHASE simulation of 20 equal intensity ($\sigma_j^2 = 2.5$), equal $\nu^2$ sources with $N = 5$ for each. The input $\nu$ was .00700. Actual $\nu$ was .00699 rad/sec. The units are the same as in the figures.

| Fig. | Variable | $\chi^2$ | $\chi_n^2$: .05 | Mean | | Std. Dev. | |
|---|---|---|---|---|---|---|---|
| | | | | Theory | Data | Theory | Data |
| 37 | $\chi$ | 9.26 | 26.30 | 100.00 | 99.86 | 22.36 | 20.81 |
| 38 | $\dot{\chi}$ | 17.01 | 23.68 | 0.00 | -0.01 | 0.22 | 0.20 |
| 39 | $\rho$ | 11.08 | 26.30 | 9.94 | 9.94 | 1.11 | 1.40 |
| 40 | $\dot{\rho}$ | 19.62 | 18.31 | 0.00 | 0.00 | 0.01 | 0.01 |
| 41 | $\Lambda$ | 15.26 | 25.00 | 19.89 | 19.90 | 0.98 | 0.93 |
| 42 | $\dot{\Lambda}$ | 13.53 | 26.30 | 0.00 | 0.00 | 0.01 | 0.01 |

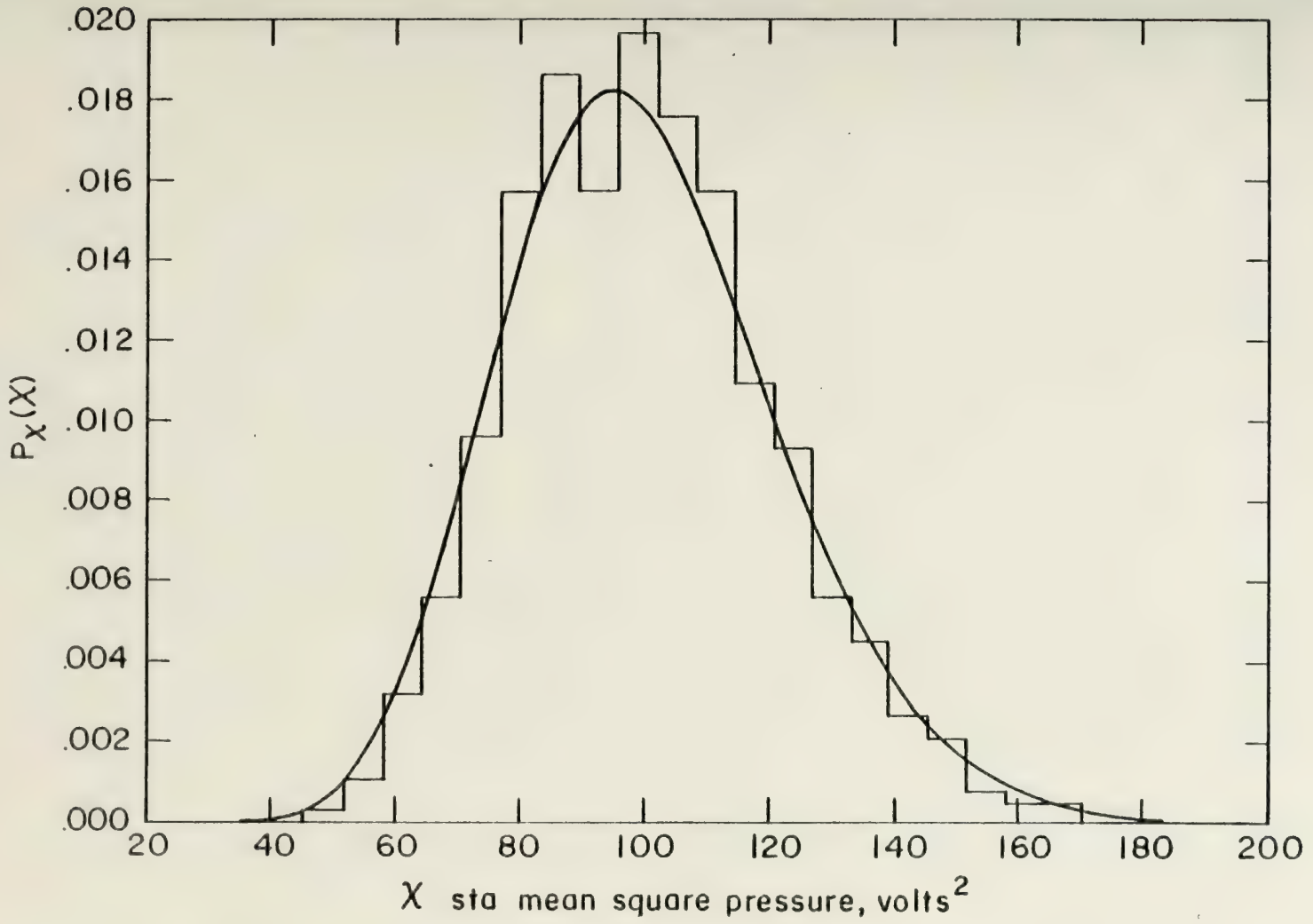


Fig. 37 Computer generated histogram of $X$ for L = 20 sources and equ. (1.19)

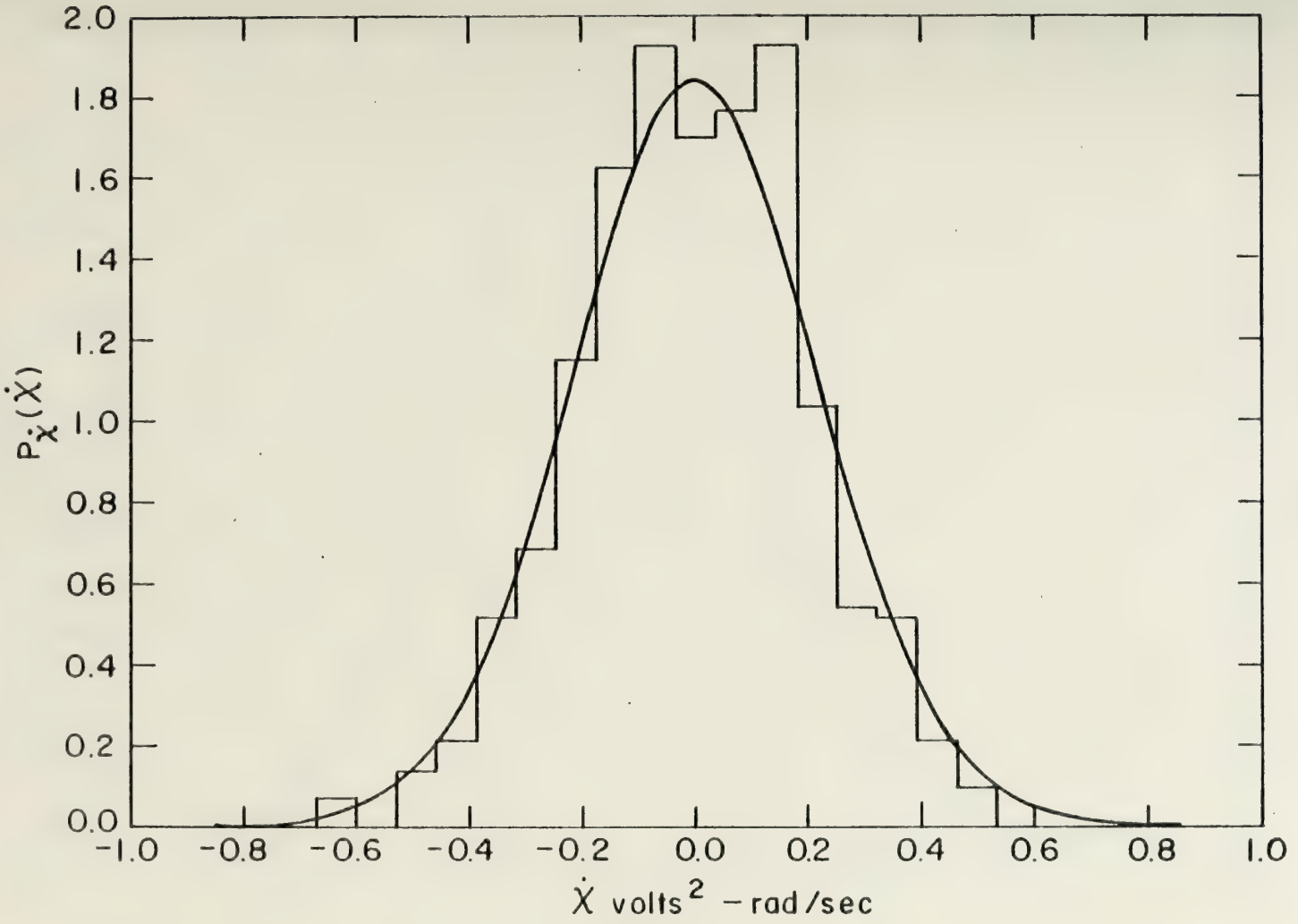


Fig. 38 Computer generated histogram of $\dot{X}$ for L = 20 sources and equ. (1.67).

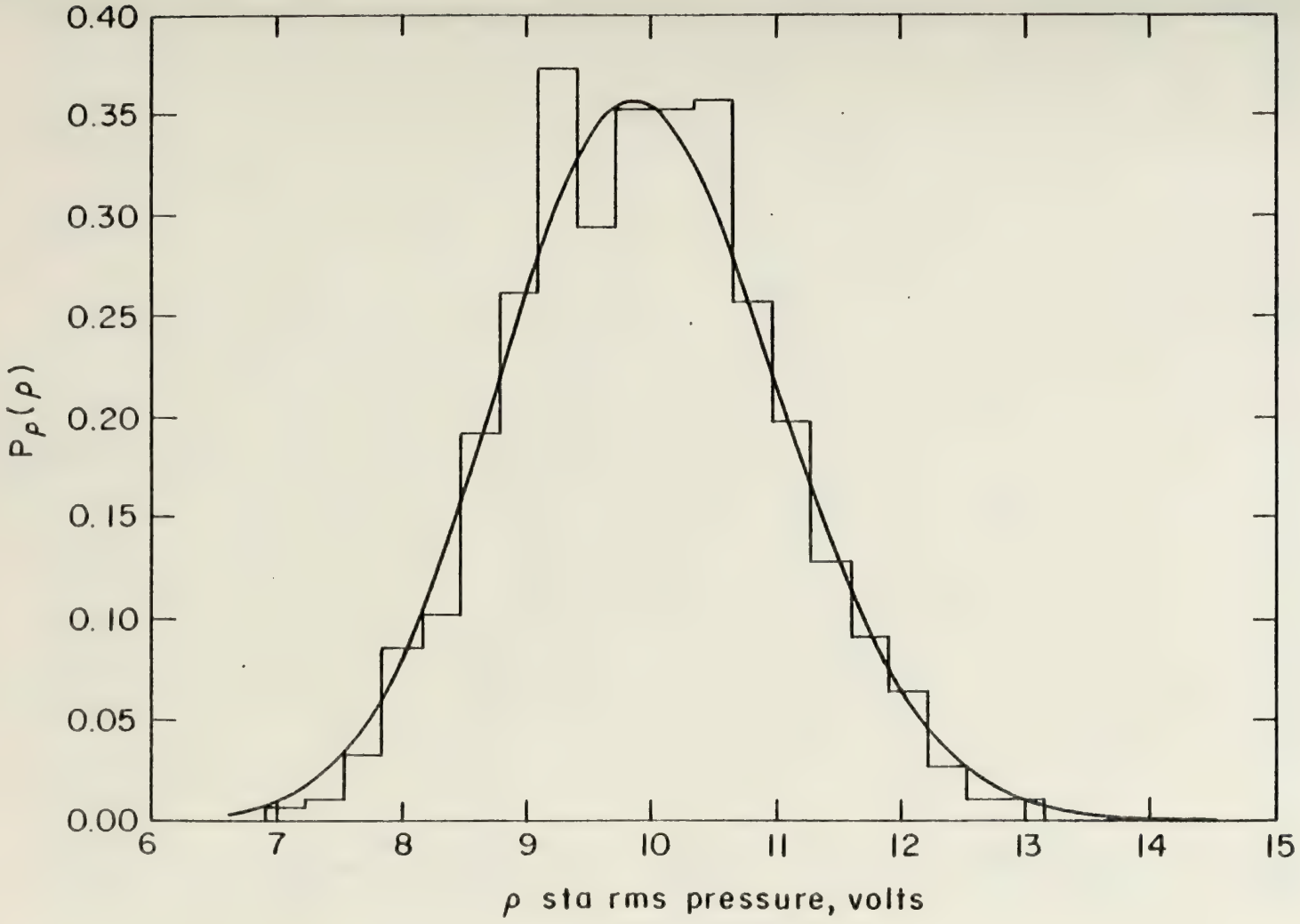


Fig. 39 Computer generated histogram of $\rho$ for L = 20 sources and equ. (1.79).

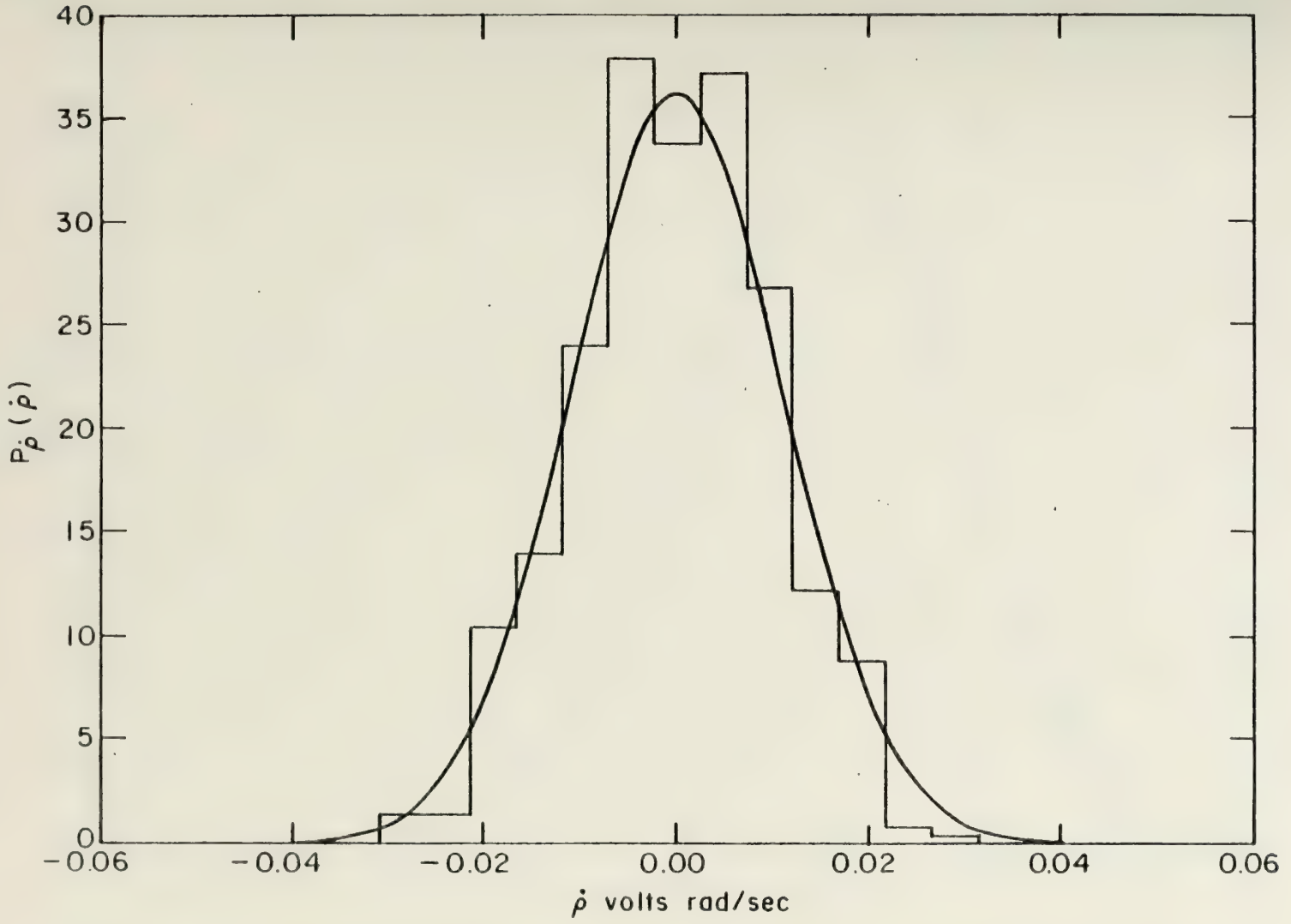


Fig. 40 Computer generated histogram of $\dot{\rho}$ for L = 20 sources and equ. (1.80).

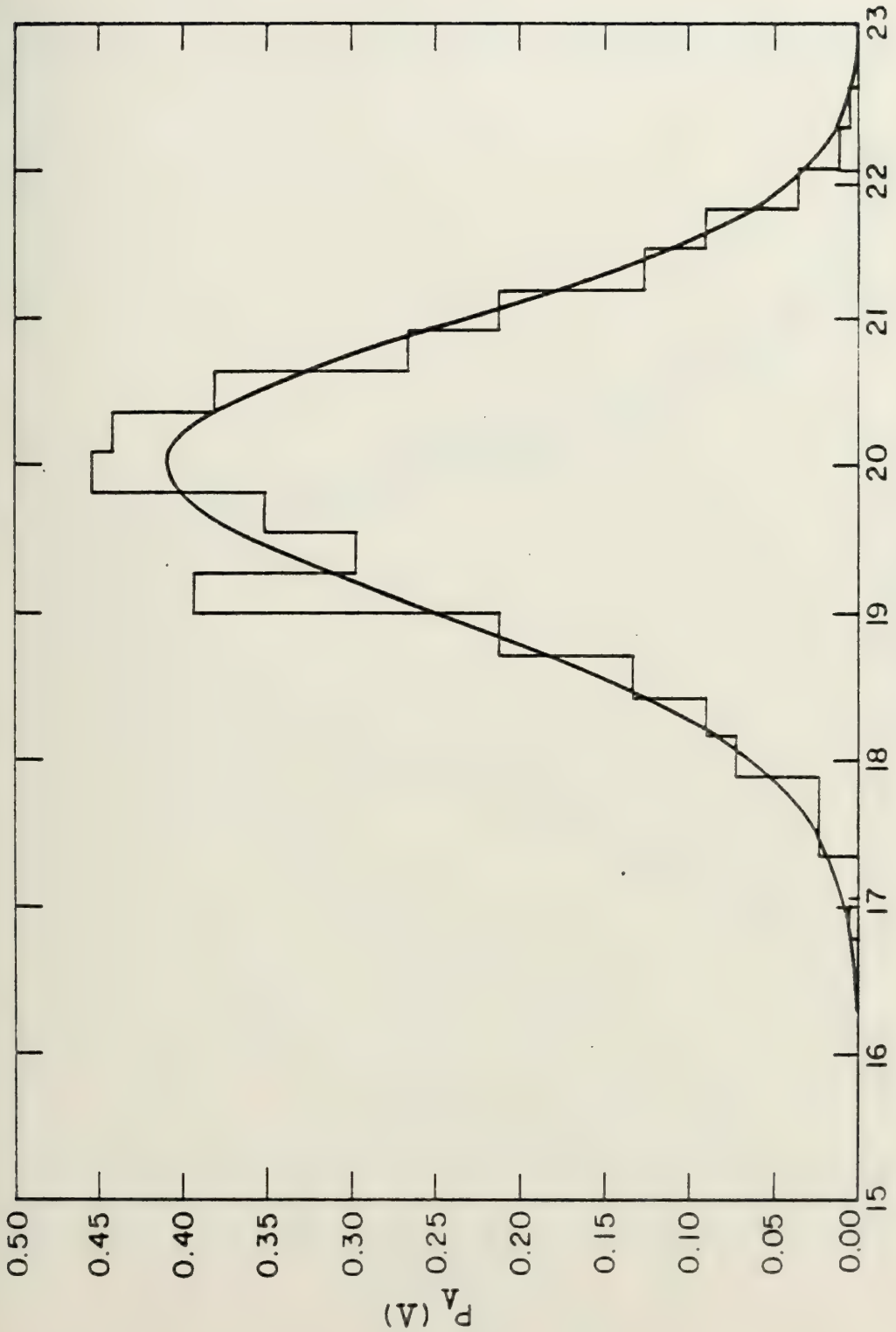


Fig. 41 Computer generated histogram of $\Lambda$ for L = 20 sources and equ. (1.83)

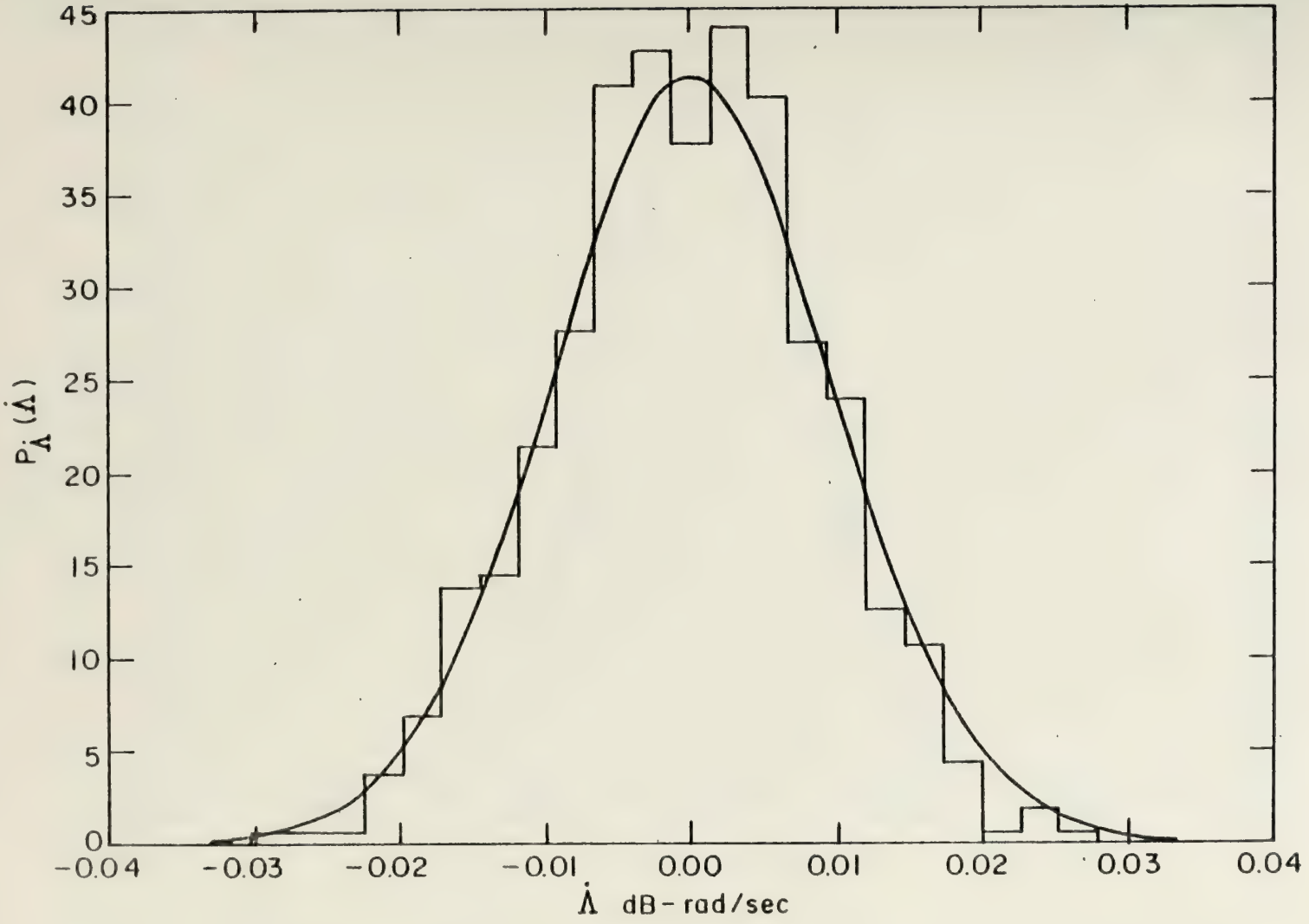


Fig. 42 Computer generated histogram of $\dot{\Lambda}$ for L = 20 sources and equ. (1.84).

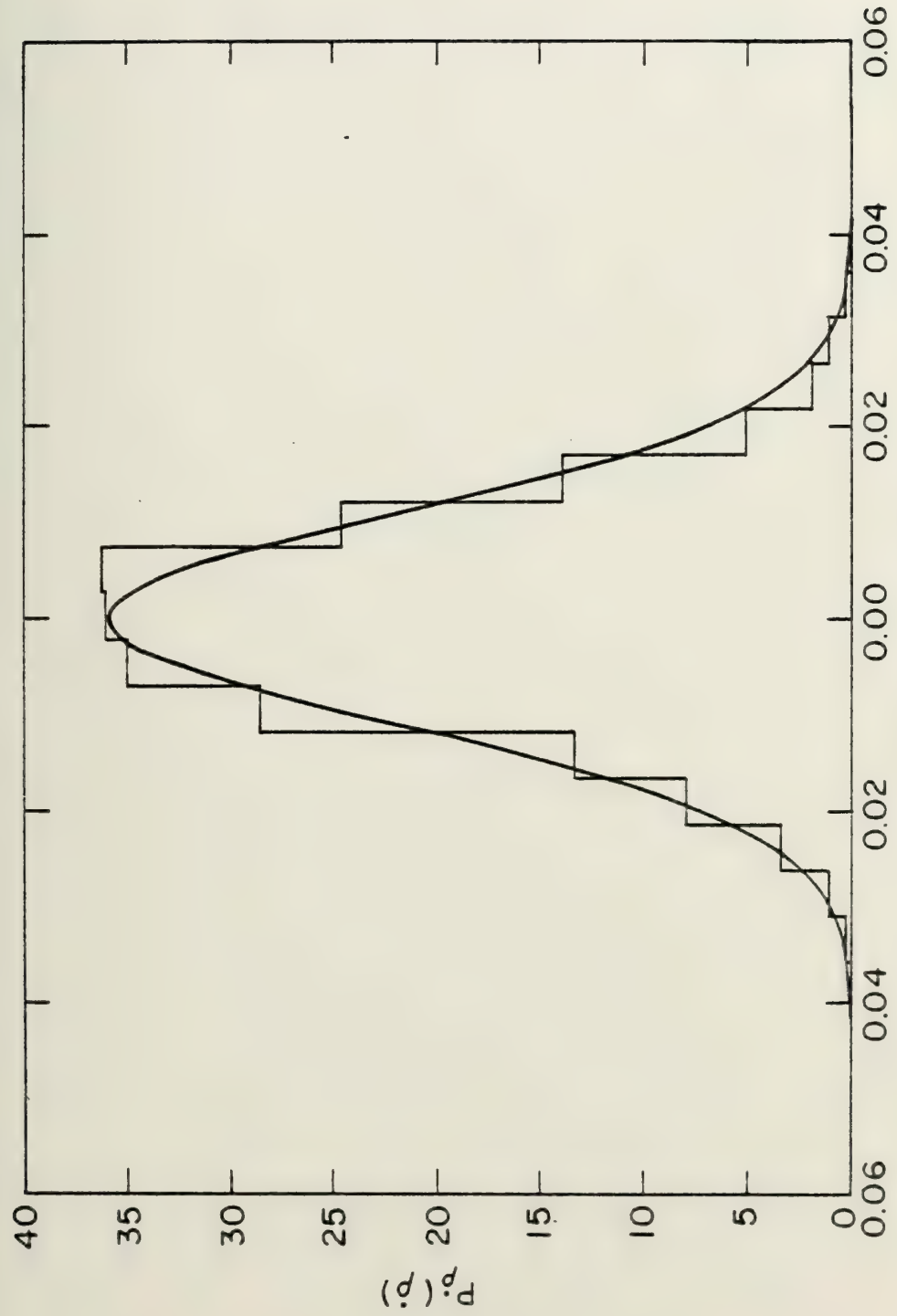


Fig. 43 Computer generated histogram of $\dot{\rho}$ for L = 3 sources and equ. (1.80)

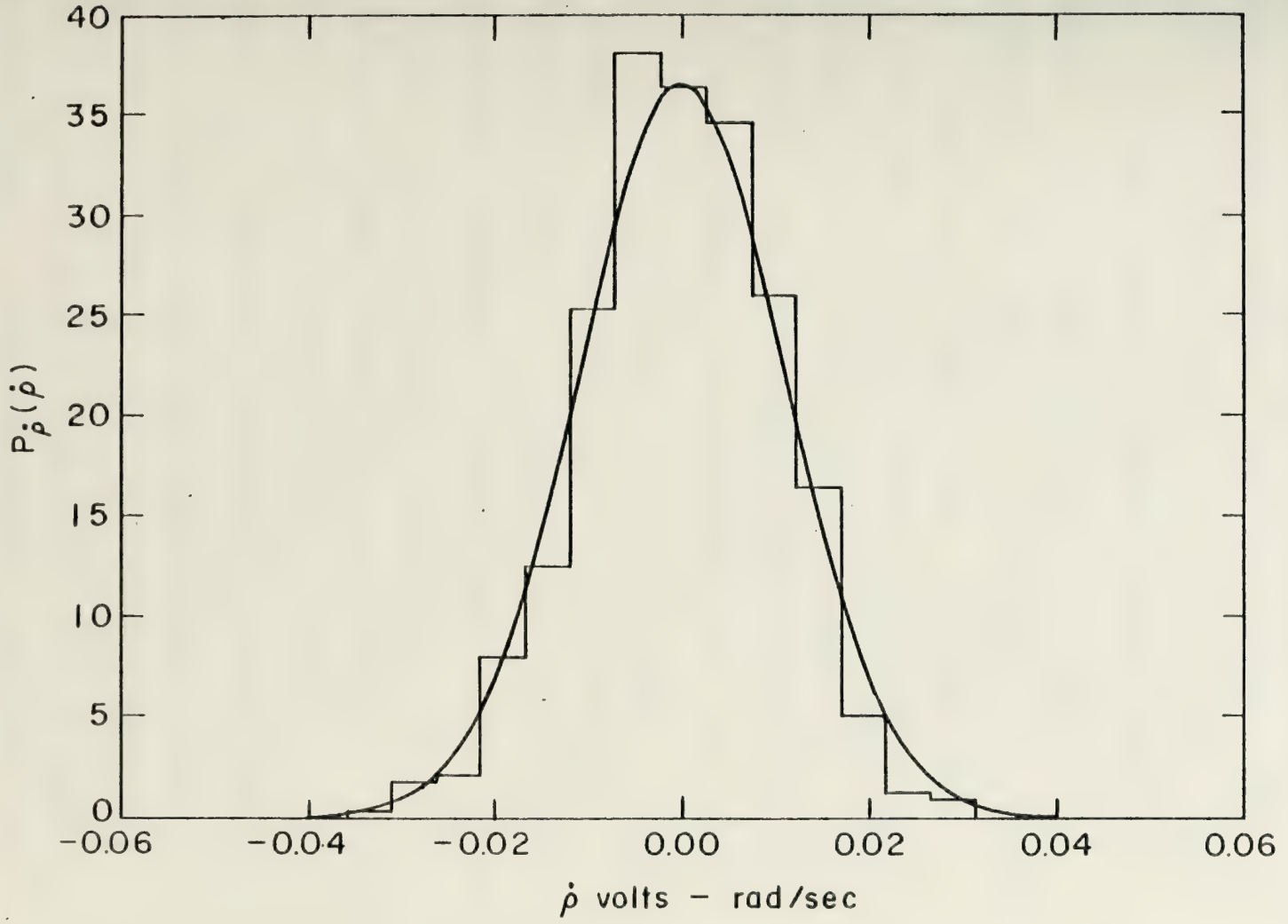


Fig. 44 Computer generated histogram of $\dot{\rho}$ for L = 4 sources and equ. (1.80).

the first eight groups are the most energetic. I applied BURMRAN therefore, with 123 sources, the appropriate r array, 5 paths, I = 600 samples, and an input $\nu$ of .007 rad/sec. The results are shown in Figures 45, 46, 47, and 47a for $\chi$, $\dot{\chi}$, $\Lambda$, and $\dot{\rho}$ respectively. In Table VII I have listed the Chi-square results and other pertinent data. The theoretical densities are given by the Edgeworth's series approximations Equations (1.45), (1.108), and (1.53) for $\chi$, $\dot{\chi}$, and $\Lambda$ respectively. For $\dot{\rho}$ I have plotted the Gaussian using the variance obtained from the data (the curve was not fit). The excellent performance confirms the assertion made in Section 1.2 that even for the most complicated realizations of Case (c) the pdf for $\dot{\rho}$ will be Gaussian in which the variance is in fact = $E[\dot{\rho}^2]$. The results for $\chi$ and $\Lambda$ are not very good (once again the rate variables out-perform the amplitude variables). The error appears to be in underpredicting the mean as indicated in Table VII. However, these results should be interpreted in light of the very large number of samples required for $\theta_n$ and $\dot{\theta}_n$ (369,000 for each) certainly introduced some correlation error due to the repeat characteristics of the random number generator (see Table IV). Both $\theta_n$ and $\dot{\theta}_n$ barely passed the Chi-square

TABLE VII

Results of the chi-square test for BURMRAN simulation of 123 different source problem. The units are the same as in the figures.

| Fig. | Variable | $\chi^2$ | $\chi^2_n$: .05 | Mean | | Std. Dev. | |
|---|---|---|---|---|---|---|---|
| | | | | Theory | Data | Theory | Data |
| 45 | $\chi$ | 36.46 | 23.68 | 5.72 | 5.80 | 1.65 | 1.43 |
| 46 | $\dot{\chi}$ | 18.72 | 23.68 | 0.00 | 0.00 | 0.02 | 0.01 |
| 47 | $\Lambda$ | 36.34 | 27.59 | 7.36* | 7.51 | 1.46* | 1.07 |
| 47a | $\dot{\rho}$ | 13.05 | 30.14 | 0.00 | 0.00 | -- | 0.003 |

*From equ. (1.60a) which is the Gaussian assumption. Note that these numbers should not be compared with those given in Section 1.2.1 because this simulation included only the first 8 groups so there will be a slight difference in the mean values (see Table I).

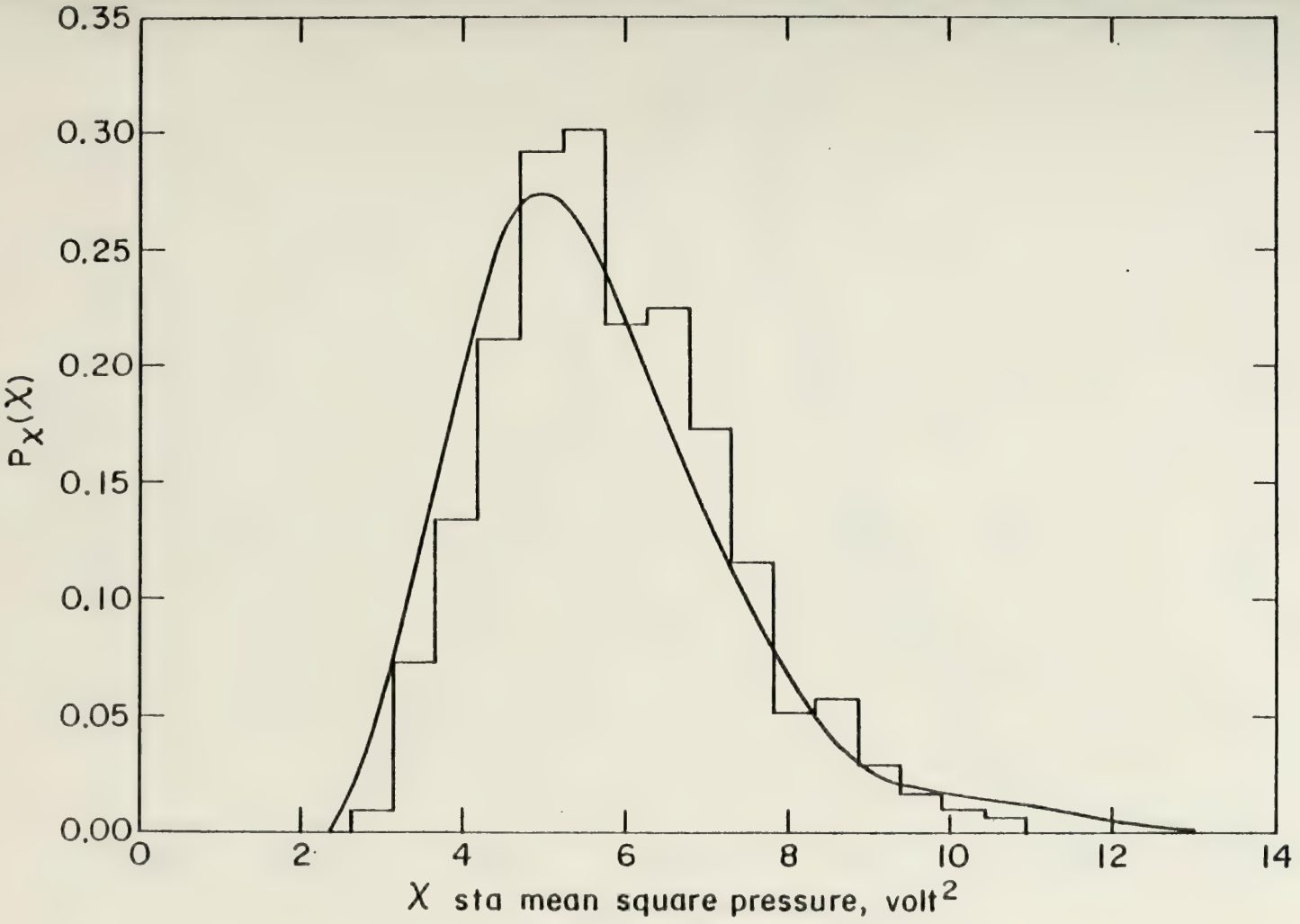


Fig. 45 Computer generated histogram of $X$ for the 123 different source problem modelling distant shipping noise off Bermuda, and equ. (1.45).

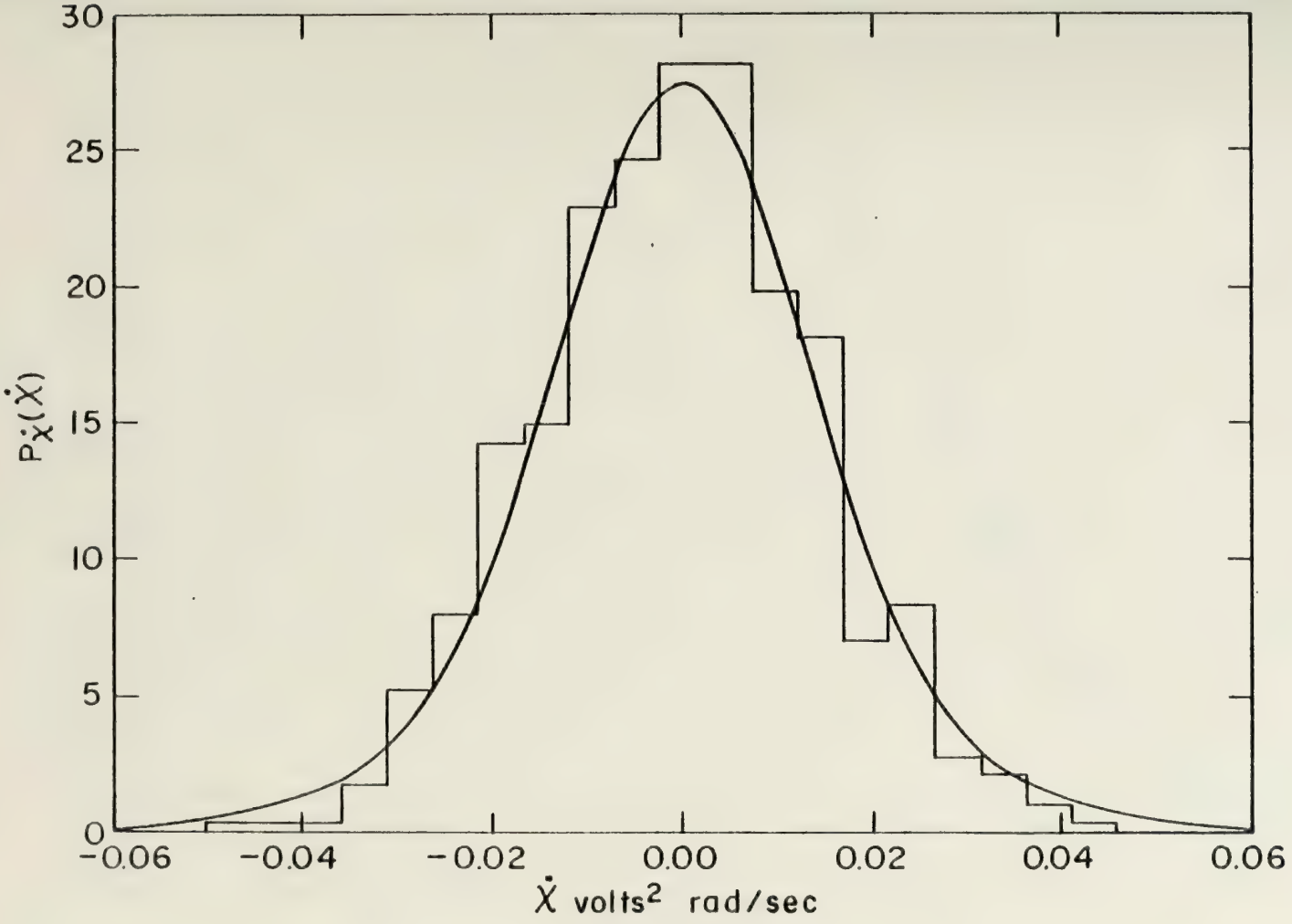


Fig. 46 Computer generated histogram of $\dot{X}$ for the L = 123 different source problem modelling distant shipping noise off Bermuda, and equ. (1.108).

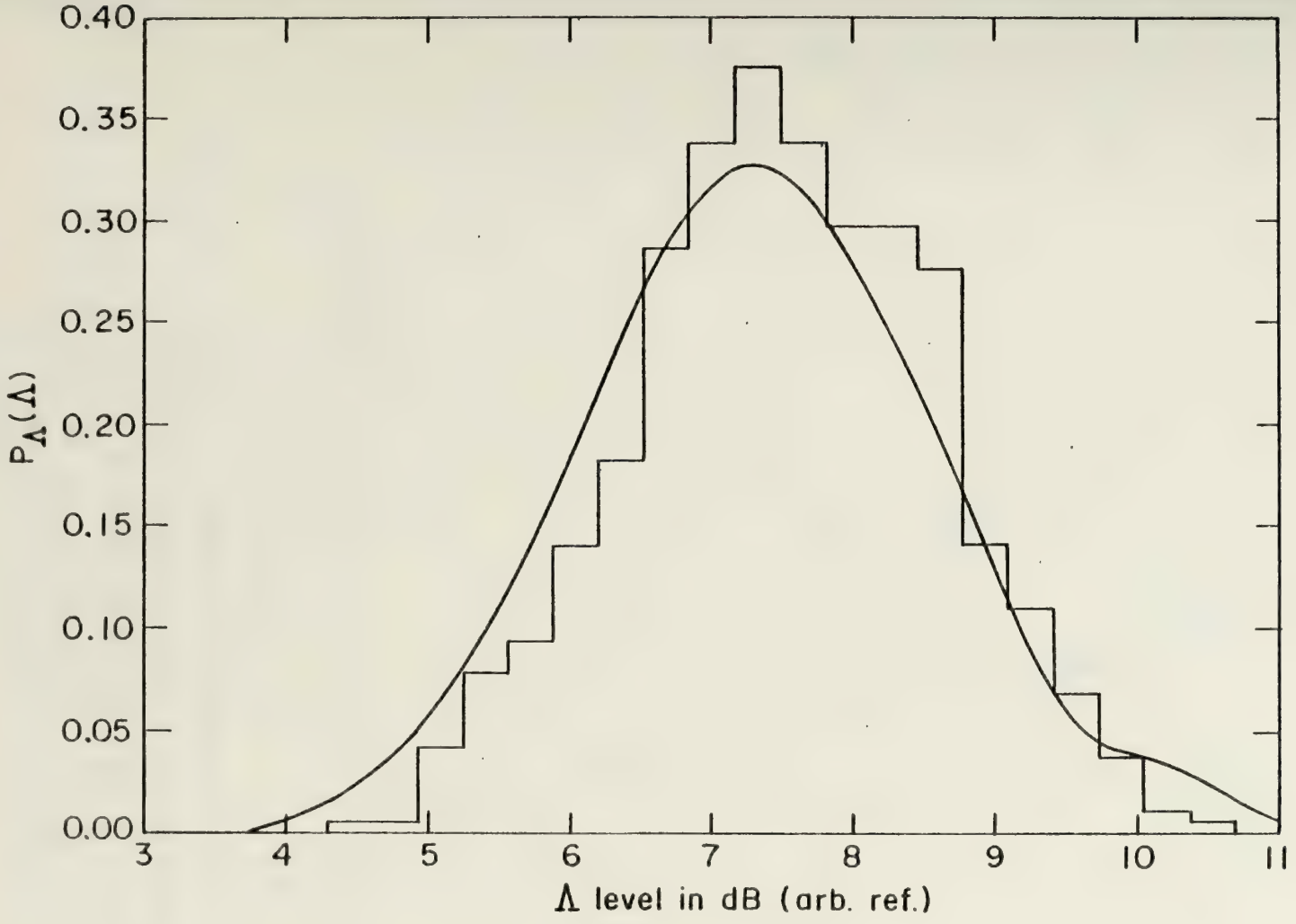


Fig. 47 Computer generated histogram of the level for the L = 123 different source problem modelling distant shipping noise off Bermuda, and equ. (1.53).

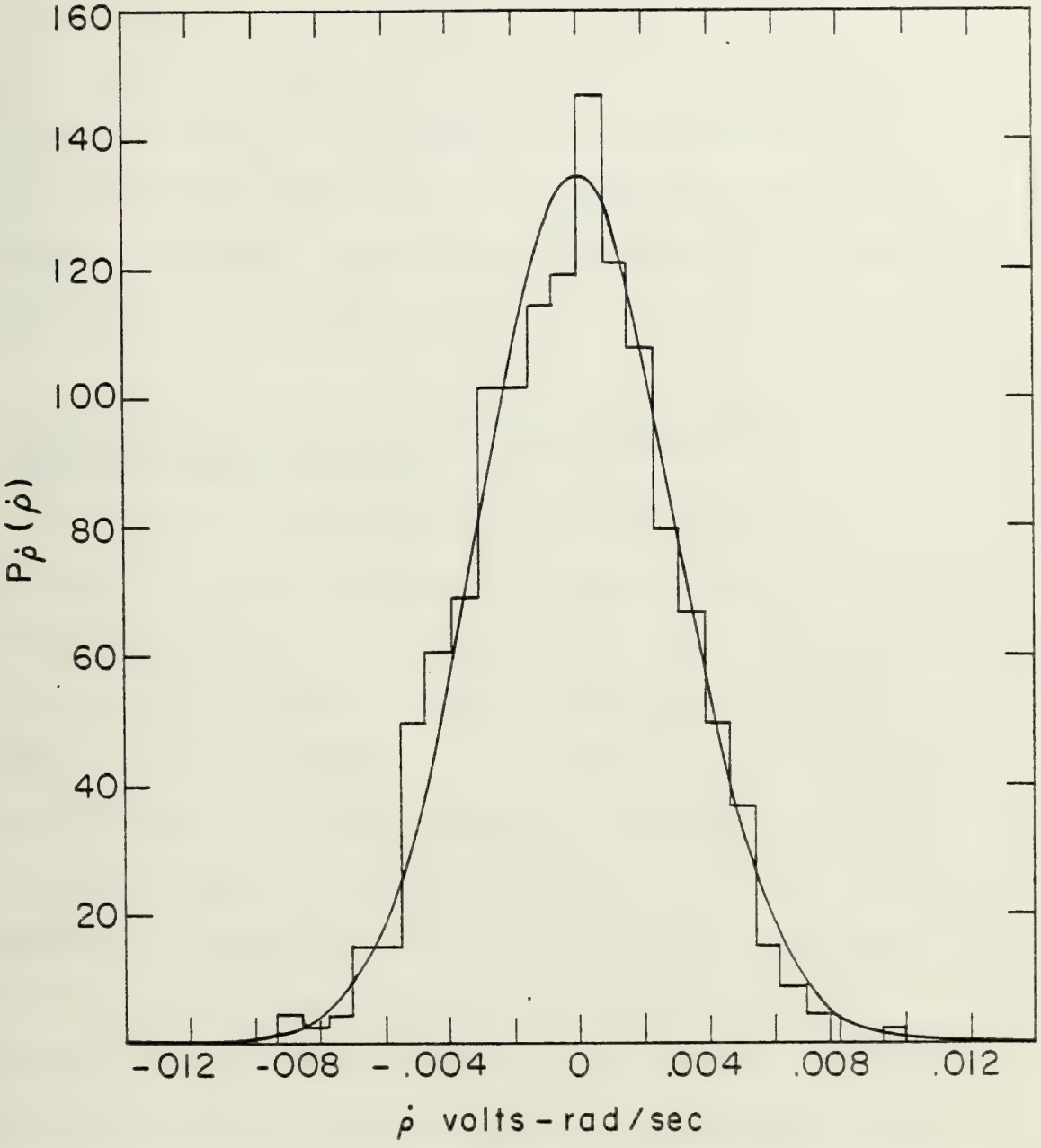


Fig. 47a Computer generated histogram of $\dot{\rho}$ for the L=123 different source problem modelling distant shipping noise off Bermuda, and the Gaussian using a variance given by $E[\dot{\rho}^2]$ obtained from the computer generated samples.

test with results of $\chi^2$ = 994.16 and 981.53 respectively, and $\chi^2_n$: .05 = 1019.94. In any case, the non-Gaussian skew is certainly evident in the histogram in Figure 45, once again dissuading the Gaussian assumption in favor of the Edgeworth's series.

## 2.4 Simulation Results for a Finite Bandwidth and/or Modulated Source

Figures 43-51 are examples of the RANDPHASE simulation of $\dot{\phi}_M$ when the source is undergoing varying degrees of sinusoidal phase modulation. The histograms are plotted with Equation (1.169) (Note that $\nu$ and $\beta\sigma$ are both given in rad/sec). Figures 52-55 are examples of varying degrees of uniform frequency modulation, or alternatively varying amounts of bandwidth on $\dot{\phi}_M$. The histograms are plotted with Equation (1.176) (Note that $\nu$ and A are both given in rad/sec). In Table VIII I have compiled the results of the Chi-square test, and the values of $\beta\sigma$, A, or B, as appropriate. All these simulations were run with an input value of $\nu$ = .007 rad/sec, 5 paths, and I = 700 samples. With the use of Table VIII compare Figure 52 (for B = $\nu$) and Figure 53 (for B = 2$\nu$), with Figure 28, the non-modulated pdf for $\dot{\phi}$. This shows quite clearly again that only for B << 2$\nu$ can bandwidth effects be neglected. As with the other simulation

TABLE VIII

Results of Chi-square test and other data for the RANDPHASE simulation of $\dot{\phi}_M$ for varying degrees of modulation and bandwidth with $N = 5$ paths.

| Fig. | $\chi^2$ | $\chi^2_n$: .05 | $\nu$ rad/sec | A rad/sec | B rad/sec | $\beta\sigma$ rad/sec |
|---|---|---|---|---|---|---|
| 48 | 19.30 | 23.68 | .0070 | - | - | .0011 |
| 49 | 31.55 | 23.68 | .0070 | - | - | .0070 |
| 50 | 12.13 | 23.68 | .0070 | - | - | .0210 |
| 51 | 22.39 | 28.87 | .0070 | - | - | .0840 |
| 52 | 25.82 | 26.30 | .0070 | .0035 | .0070 | - |
| 53 | 12.72 | 23.68 | .0070 | .0070 | .0140 | - |
| 54 | 17.62 | 23.68 | .0070 | .0210 | .0420 | - |
| 55 | 22.76 | 28.87 | .0070 | .0700 | .1400 | - |

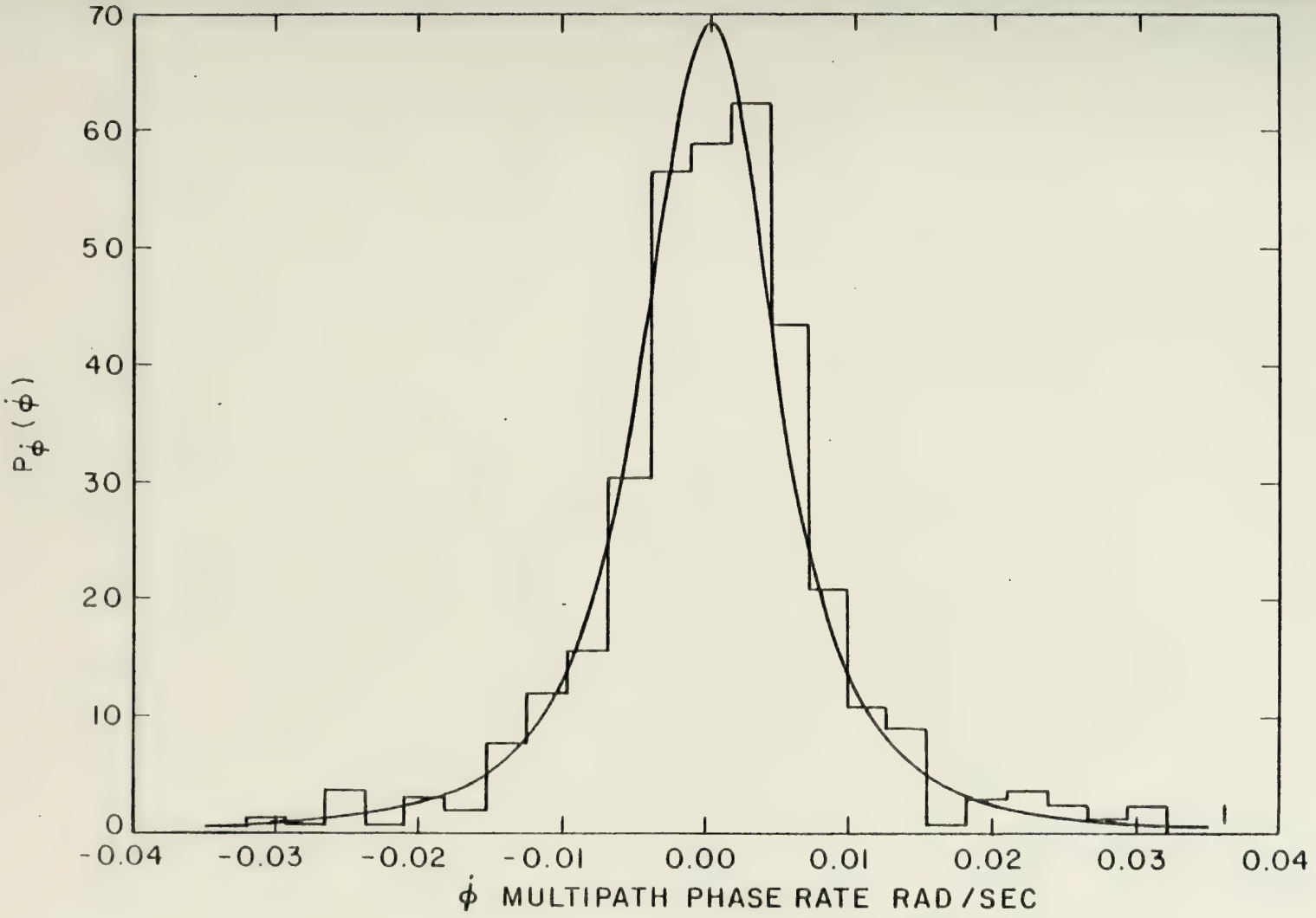


Fig. 48 Histogram of computer generated samples of $\dot{\phi}$ with sinusoidal phase modulation of the source, $\nu = .007$ , $\beta\sigma = .0011$ and equ. (1.169)

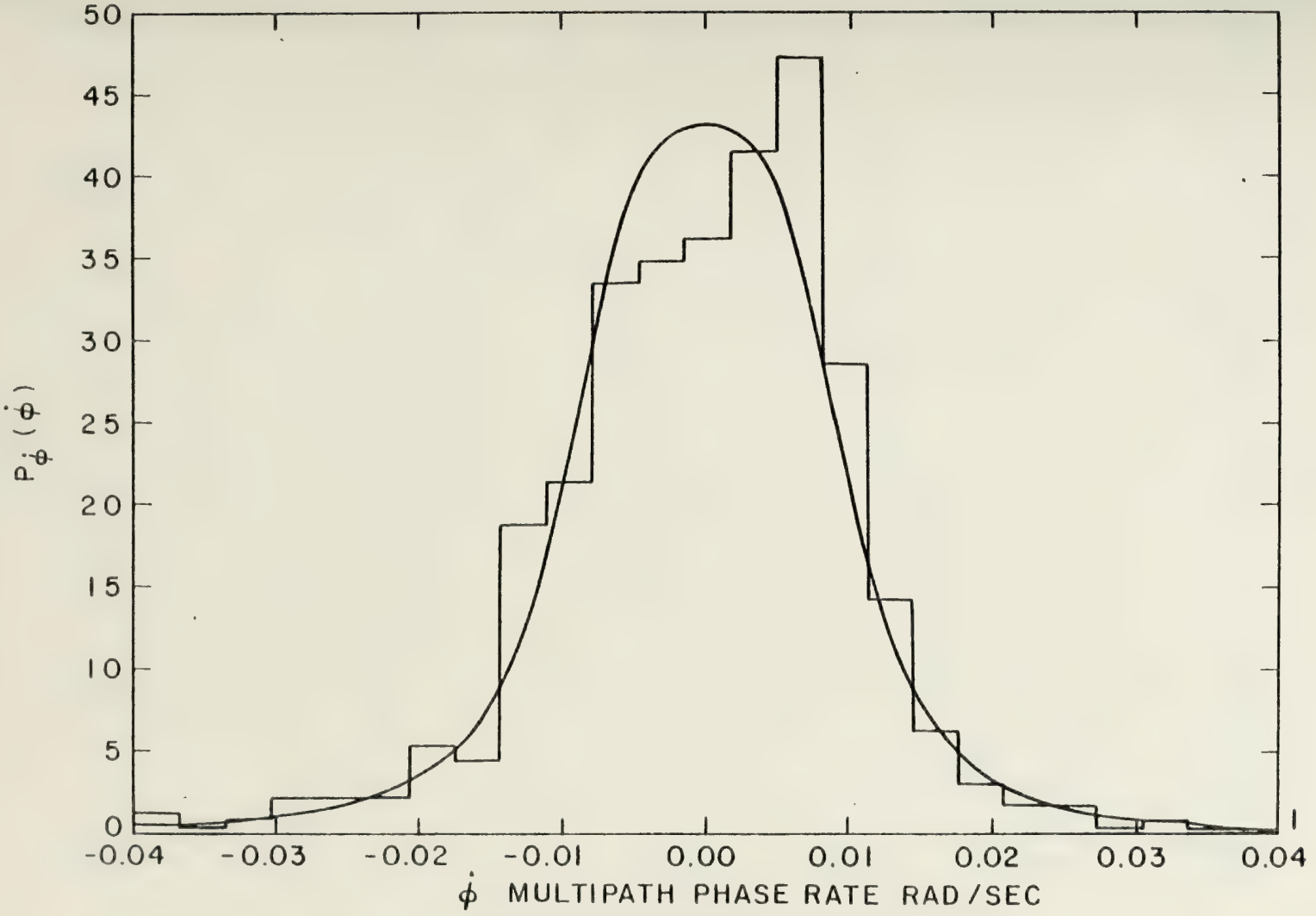


Fig. 49 Histogram of computer generated samples of $\dot{\phi}$ with sinusoidal phase modulation of the source, $\nu = .007$, $\beta\sigma = .007$ and equ. (1.169)

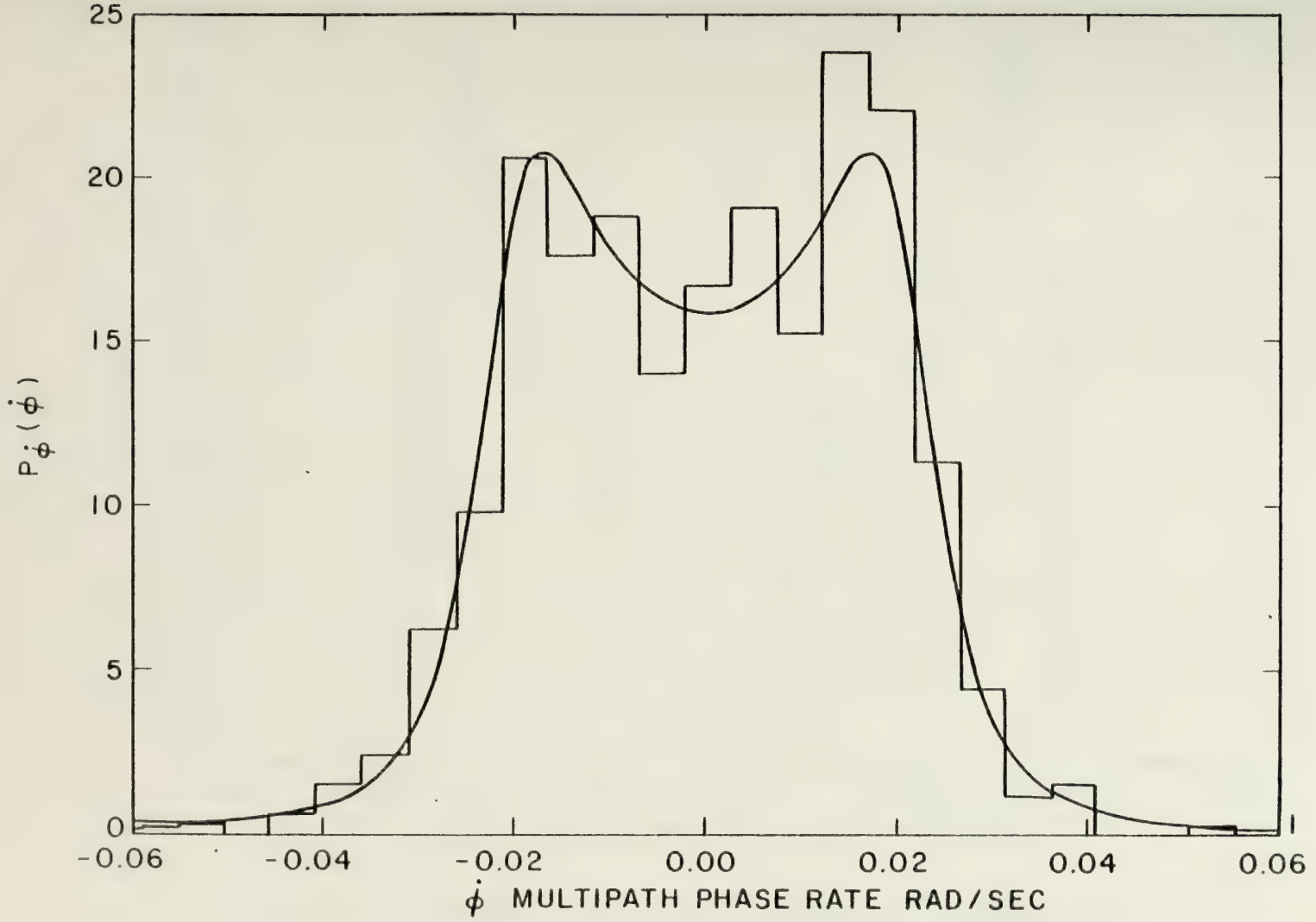


Fig. 50 Histogram of computer generated samples of $\dot{\phi}$ with sinusoidal phase modulation of the source, $\nu = .007$, $\beta\sigma = .021$ and equ. (1.169)

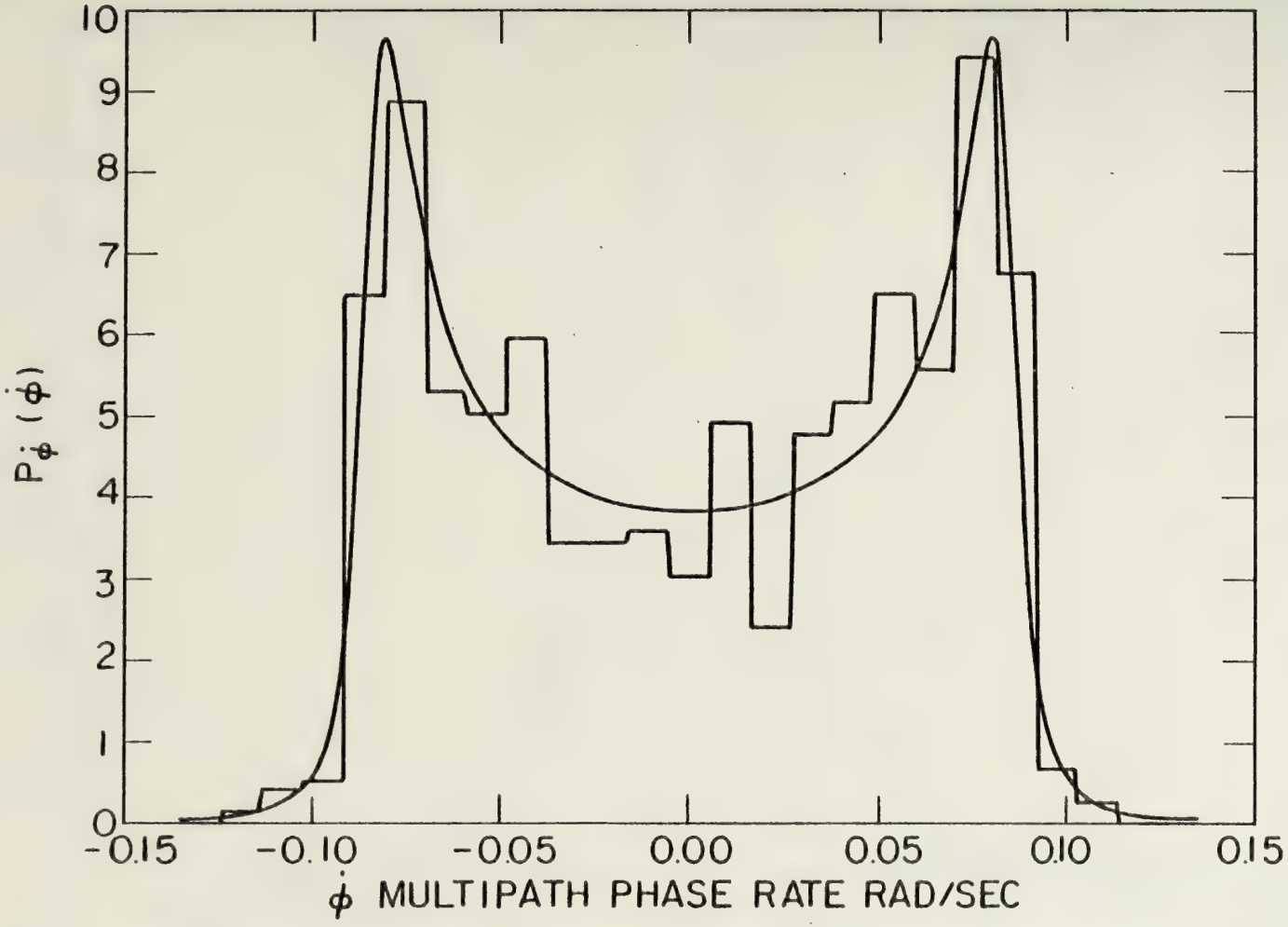


Fig. 51 Histogram of computer generated samples of $\dot{\phi}$ with sinusoidal phase modulation of the source, $\nu = .007$, $\beta\sigma = .084$ and equation (1.169)

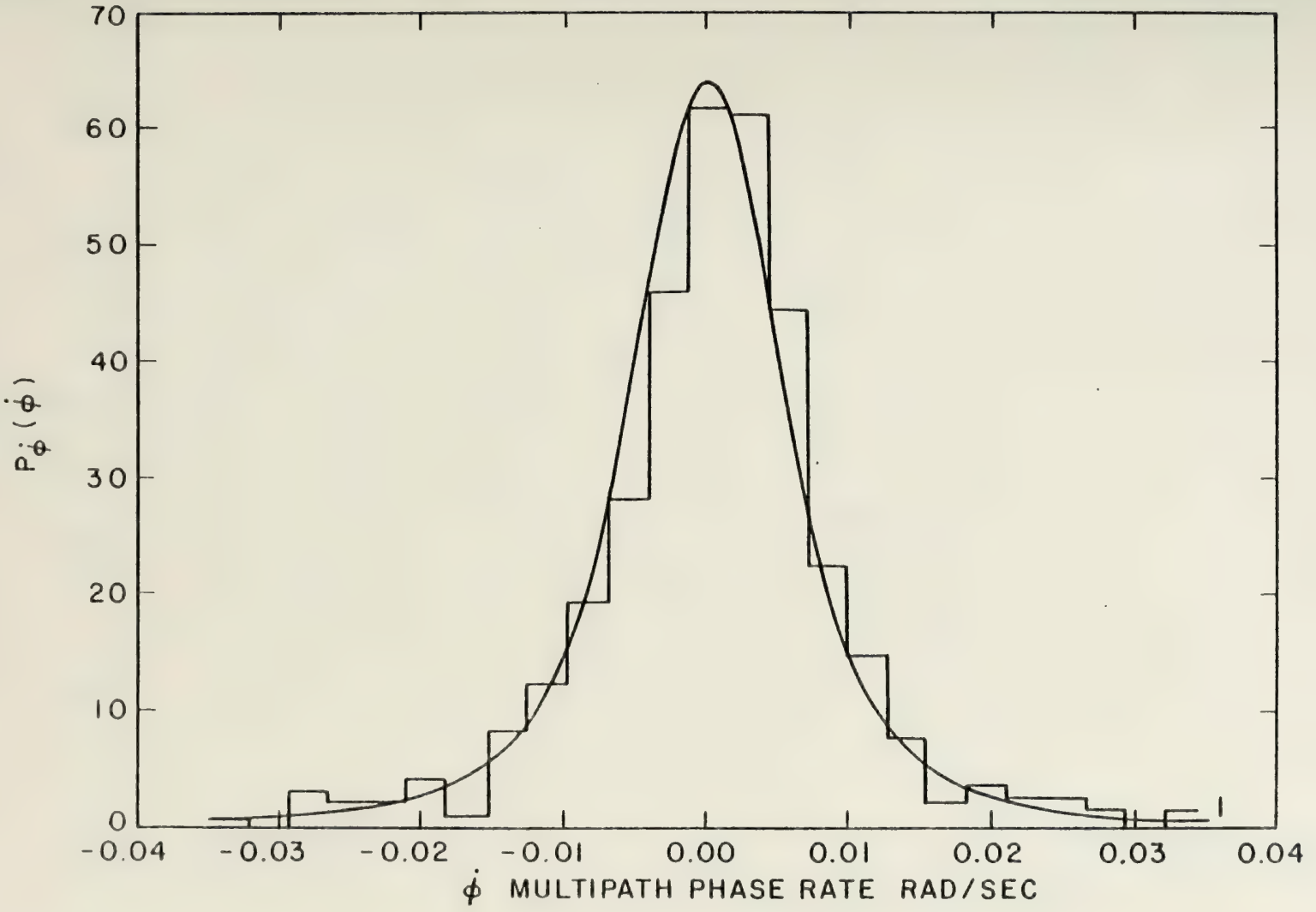


Fig. 52 Histogram of computer generated samples of $\dot\phi$ with uniform frequency modulation of the source, $\nu = .007$, $A = .0035$ and equ. (1.176)

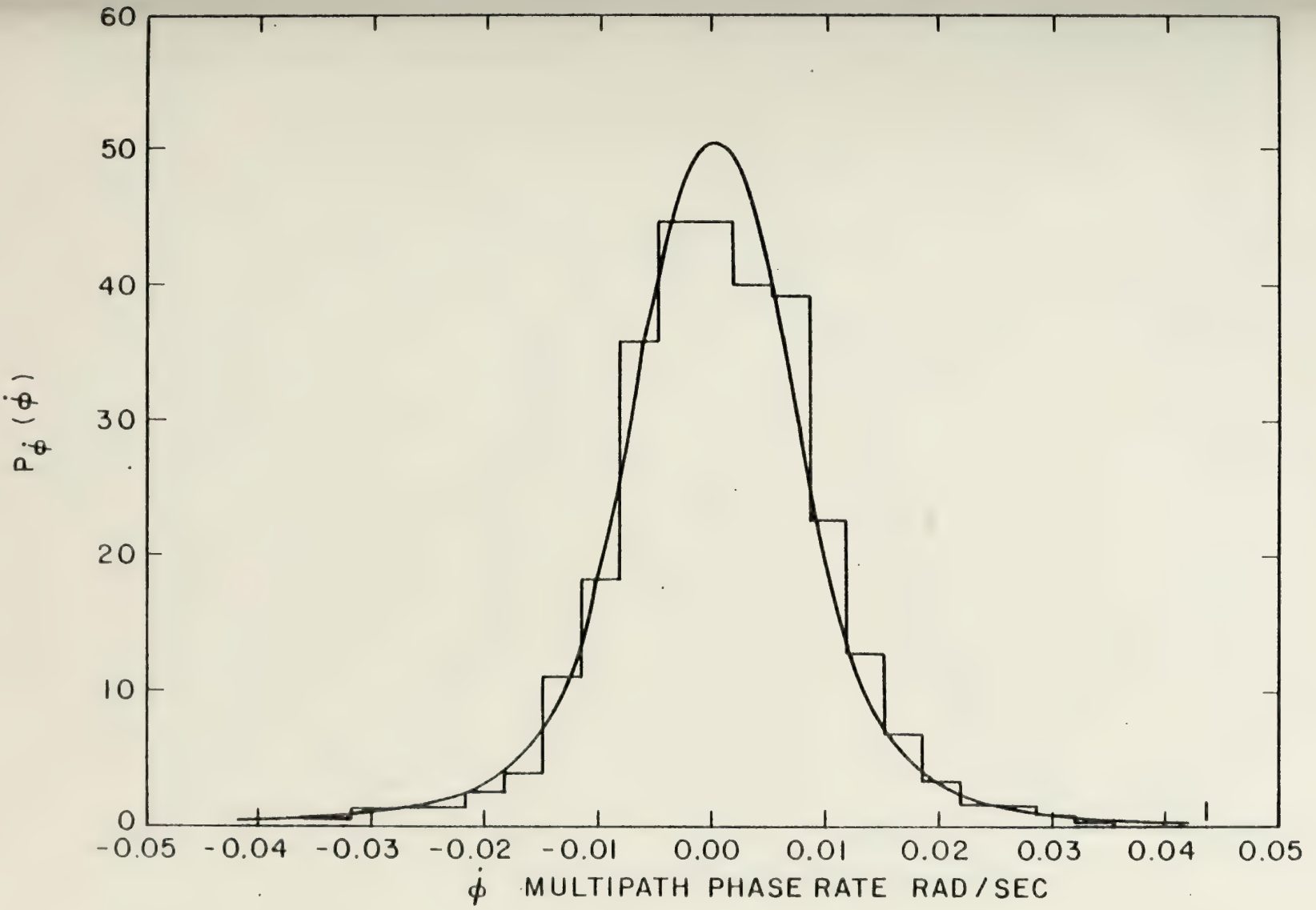


Fig. 53 Histogram of computer generated samples of $\dot{\phi}$ with uniform frequency modulation of the source, $\nu = .007$, $A = .007$ and equ. (1.176)

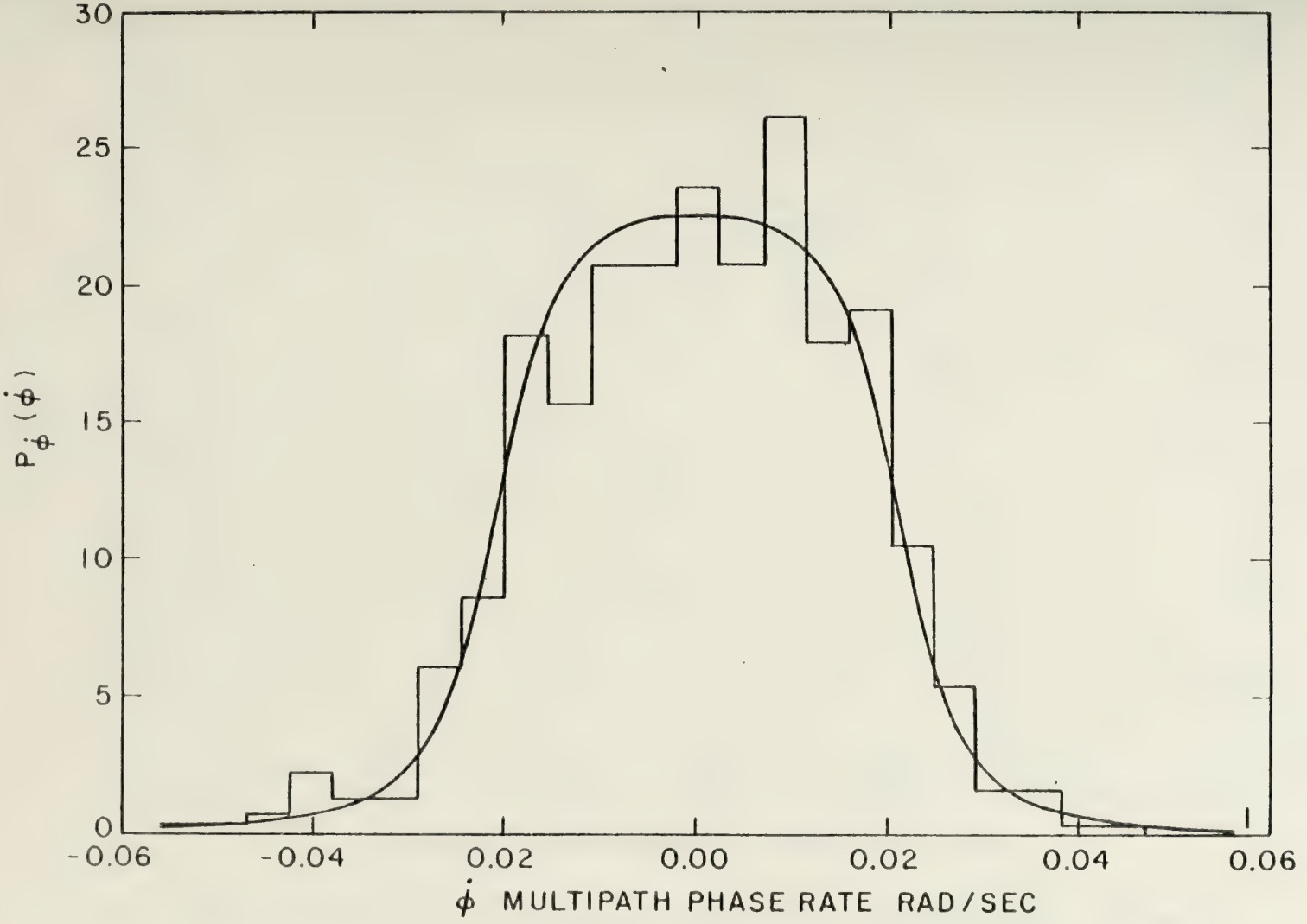


Fig. 54 Histogram of computer generated samples of $\dot{\phi}$ with uniform frequency modulation of the source, $\nu = .007$, $A = .021$ and equ. (1.176)

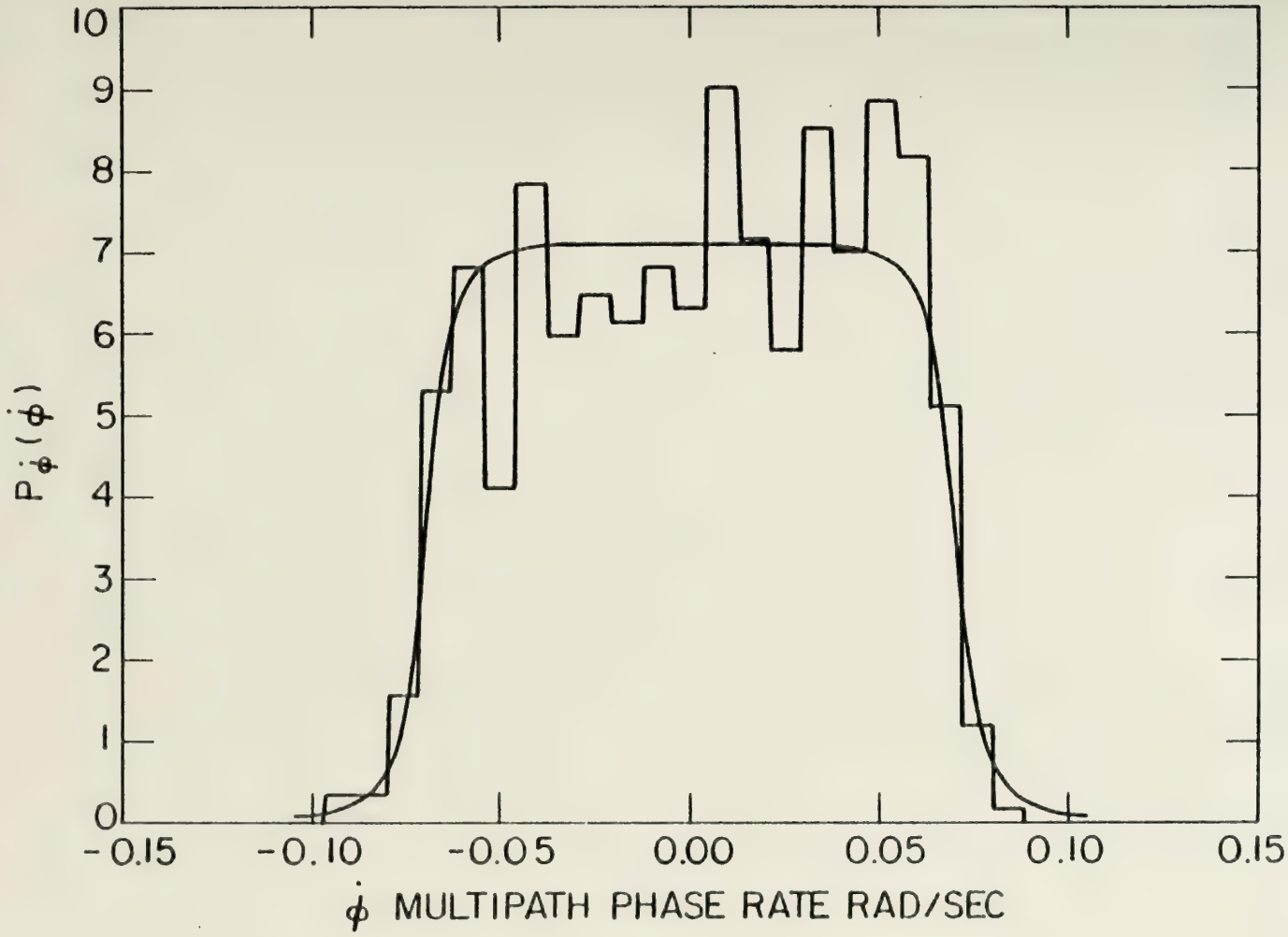


Fig. 55 Histogram of computer generated samples of $\dot{\phi}$ with uniform frequency modulation of the source, $\nu = .007$, $A = .07$ and equation (1.176).

results, the fit of the theory to the computer data is quite good with only one of the eight runs failing the Chi-square test.

# CHAPTER 3

# DATA ANALYSIS

I have analyzed two sets of data from acoustic experiments in the ocean. These data are compared with the theory presented in Chapter 1. In Section 3.1, data from an experiment performed by R. Porter and R. Spindel, near Eleuthera [12] are shown among other successful comparisons to support the theoretical pdf's for amplitude rate and level rate derived for the first time in this thesis. Also, the analytical results of the modulation theory derived in Section 1.3 explain heretofore unobserved phenomena of the Eleuthera data accurately. In Section 3.2, data from the CASE experiment [13] conducted in the Pacific are investigated in general, with special emphasis in light of the modulation theory of Chapter 1. Furthermore, these data provide more insight into the parameter $\nu^2$ and reveal, as well, shortcomings of our current understanding of this vital ocean acoustic parameter and its driving mechanisms.

## 3.1 The Eleuthera Experiment

Data made available by the Woods Hole Oceanographic Institution were acquired during a long-range acoustic propagation experiment conducted near Eleuthera [12].

The data analyzed consisted of four records (see Table IX) in which two cw signals, one at 220 Hz, and one at 406 Hz, for each record were transmitted from Eleuthera to drifting sonobuoys approximately 300 km northeast towards Bermuda. A Doppler position-tracking system [30] was used to remove mean multipath phase-rates due to sonobuoy motion. These data were also analyzed by Dyer and Shepard [15] and Hamblen [9].

TABLE IX

Log of the W.H.O.I. Fluctuation Data

| Record | Date | Time (GMT) | Record Length (h) |
|---|---|---|---|
| 447 | 13 Sept. 74 | 1900 - 0310 | 8.16 |
| 448 | 12 Sept. 74 | 0402 - 1204 | 8.05 |
| 449 | 11 Sept. 74 | 1800 - 0145 | 7.75 |
| 424 | 11 Sept. 74 | 0644 - 1527 | 8.72 |

### 3.1.1 Analysis of the Single Source

From the original digitized time series of $\rho\cos\phi$ and $\rho\sin\phi$, time series of $\dot{\Lambda}$, $\dot{\chi}$, and $\dot{\phi}$ for the two frequencies are produced for each record. The phase data were analyzed previously by Dyer and Shepard [15] and Hamblen [9]. Details of the phase unwrapping routine can be found in Reference [15]. Histograms are then generated from these time series. For the histograms of $\dot{\Lambda}$ and $\dot{\chi}$, Equations (1.7) and (1.4), respectively, are fit such that the value of $\nu^2$ and $\sigma_1^2\nu$, respectively, minimize the Chi-square statistic. The value of $\nu^2$ for each run is also obtained by fitting Equation (A8) to the histograms of $\dot{\phi}$. The values of $\nu^2$ obtained from $\dot{\phi}$ agree closely, as expected, with those obtained previously by Hamblen [9]. However, the value of $\nu^2$ obtained from $\dot{\Lambda}$ by fitting Equation (1.7) is smaller by a factor of almost 2 in every case. This can be understood as follows. As the analysis of Section 1.3 shows, any finite bandwidth effects or carrier instabilities, or in this particular case, any errors in the Doppler position-tracking system, would manifest themselves in "spreading" or increasing the variance of $\dot{\phi}$ while leaving $\dot{\Lambda}$ unmolested.

To test this explanation further, $\nu^2$ is obtained for

each record by taking the ratio of $\sigma_1^2\nu^2$ to $\sigma_1^2$, parameters which were found previously [9] by fitting Equation (A1) and (A5) to histograms of $\rho$ and $\dot{\rho}$, respectively. Also, $\nu^2$ is obtained by taking the value of $\sigma_1^2\nu$ from the fit of Equation (1.4) to the histograms of $\dot{\chi}$ and dividing by the previously found values of $\sigma_1^2$ [9]. If the reasoning is correct, then these values of $\nu^2$ should agree with the values of $\nu^2$ obtained from $\dot{\Lambda}$ for each record as they are all derived from densities which are insensitive to angle modulation or finite bandwidth effects. The results are tabulated in Table X, which shows that without exception these values of $\nu^2$ agree to within 33% or less and, furthermore, they are all as hypothesized less than the values of $\nu^2$ obtained from $\dot{\phi}$.

Except for Record 424, the values for $\nu$ obtained from $\dot{\Lambda}$, noting the square root range dependence predicted by Dyson, Munk, and Zetler [11], are reasonably consistent with the values for $\nu$ obtained previously by them for the Eleuthera to Mid-station and the Eleuthera to Bermuda transmissions for the 406 Hz source, while the values of $\nu$ obtained from $\dot{\phi}$ are not as consistent (see Table XI). Why run 424 exhibited the larger values for $\nu$ in all cases (see Table X again) is unknown.

In order to obtain a measure of the bandwidth of the

TABLE X

The values of $\nu^2$ obtained from the time series and histograms of the amplitude densities are compared with the values of $\nu^2$ obtained in fitting Equation (A8) to the histograms of $\dot{\phi}$. The values of A, the half-bandwidth measure of the "modulation" is tabulated for each run in the last column.

| Record | Freq. (Hz) | $\nu^2$ rad$^2$/sec$^2$ (x $10^{-4}$) | | | | A, mHz | $\sigma_G$, mHz |
|---|---|---|---|---|---|---|---|
| | | $\sigma_1^2\nu^2/\sigma_1^2$ | $(\sigma_1^2\nu/\sigma_1^2)^2$ | $\dot{\Lambda}$ | $\dot{\phi}$ | | |
| 447 | 220 | 1.8 | 1.5 | 2.0 | 4.7 | 3.3 | 2.0 |
| | 406 | 3.5 | 3.6 | 4.1 | 7.9 | 4.3 | 2.6 |
| 448 | 220 | 6.7 | 8.3 | 6.1 | 8.7 | 2.2 | 1.3 |
| | 406 | 2.9 | 2.4 | 3.0 | 7.1 | 4.4 | 2.7 |
| 449 | 220 | 2.4 | 2.4 | 2.7 | 4.4 | 2.6 | 1.6 |
| | 406 | 3.1 | 2.4 | 3.6 | 7.6 | 4.4 | 2.7 |
| 424 | 220 | 10 | 12 | 11 | 15 | 2.8 | 1.7 |
| | 406 | 11 | 11 | 15 | 24 | 5.8 | 3.6 |

TABLE XI

The average values of $\nu$ in mHz for the 406Hz source for Records 447, 448, and 449 obtained from $\dot{\phi}$ and $\dot{\Lambda}$ are compared to the values of $\nu$ obtained by Dyson, Munk, and Zetler (DMZ).

| | $\dot{\phi}$ | $\dot{\Lambda}$ | DMZ Mid-Station | | | DMZ Bermuda |
|---|---|---|---|---|---|---|
| Range (km) | 300 | 300 | | 550 | | 1250 |
| $\nu$ in mHz | 4.4 | 3.0 | Measured 2.8 | Equ. (18) 2.2 | Ray Mix 2.6 | Measured 4.0 |

modulation in these data, I fit Equation (1.176) to the histograms of $\dot{\phi}$ using the values of $\nu^2$ obtained from the histograms of $\dot{\Lambda}$. I determine the value of A, the half-bandwidth of the modulation, that minimizes the Chi-square statistic. I likewise fit Equation (1.178) which assumes a Gaussian rather than a uniform modulation function and find $\sigma_G$, the standard deviation of the carrier fluctuations. Note that the half-bandwidth of the modulation as given by 1/e of the best fit of Equation (1.178) is approximately equal to the value of A obtained from fitting Equation (1.176). The values of $\nu^2$ from the $\dot{\Lambda}$ histograms are used because $\dot{\Lambda}$, as revealed by Equation (1.7), is independent of $\sigma_1^2$ and is less sensitive to its non-stationary behavior. In Table X, the least Chi-square value of A and $\sigma_G$ are given for each run. Because the frequency stability of both sources is many orders of magnitude less than $\nu$, the modulation as measured by A or $\sigma_G$ can be attributed to the error in the Doppler position-tracking system. An error of ±.017 m/sec in measuring the velocity of the receiving hydrophone itself results in a half-bandwidth value for the modulation of 2.5 mHz at 220 Hz and 4.5 mHz at 406 Hz, consistent with the values tabulated in Table X. The velocity error is consistent with the experimental setup

and the performance characteristics of the Doppler position-tracking system [31].

In Figures 56-59, the histograms of $\dot{\chi}$, $\dot{\Lambda}$, and $\dot{\phi}$ and the least squares fit of Equations (1.4), (1.7), and (1.176), respectively, are shown for all the records. Table XII lists the Chi-square statistics for $\dot{\Lambda}$ and $\dot{\chi}$ and Table XIII lists the Chi-square statistics for $\dot{\phi}$ when fit by Equation (A8) (which assumes no modulation), Equation (1.176), and Equation (1.178). With a few exceptions, the fit of the theory to the data is excellent. Of the three runs that failed the Chi-square test, two were the result of fitting the no-modulation density, Equation (A8), to $\dot{\phi}$ which, in light of the foregoing analysis, is suspect from the start. As Table XIII shows, while Equation (1.176) performed better than Equation (A8) in five out of the eight runs, Equation (1.178) performed better than both Equations (A8) and (1.176) for all cases except Run 424 where performance was better than Equation (1.176) but slightly worse than Equation (A8). In fact, a Gaussian-like error in extracting the mean phase rate is characteristic of the Doppler position-tracking system [31].

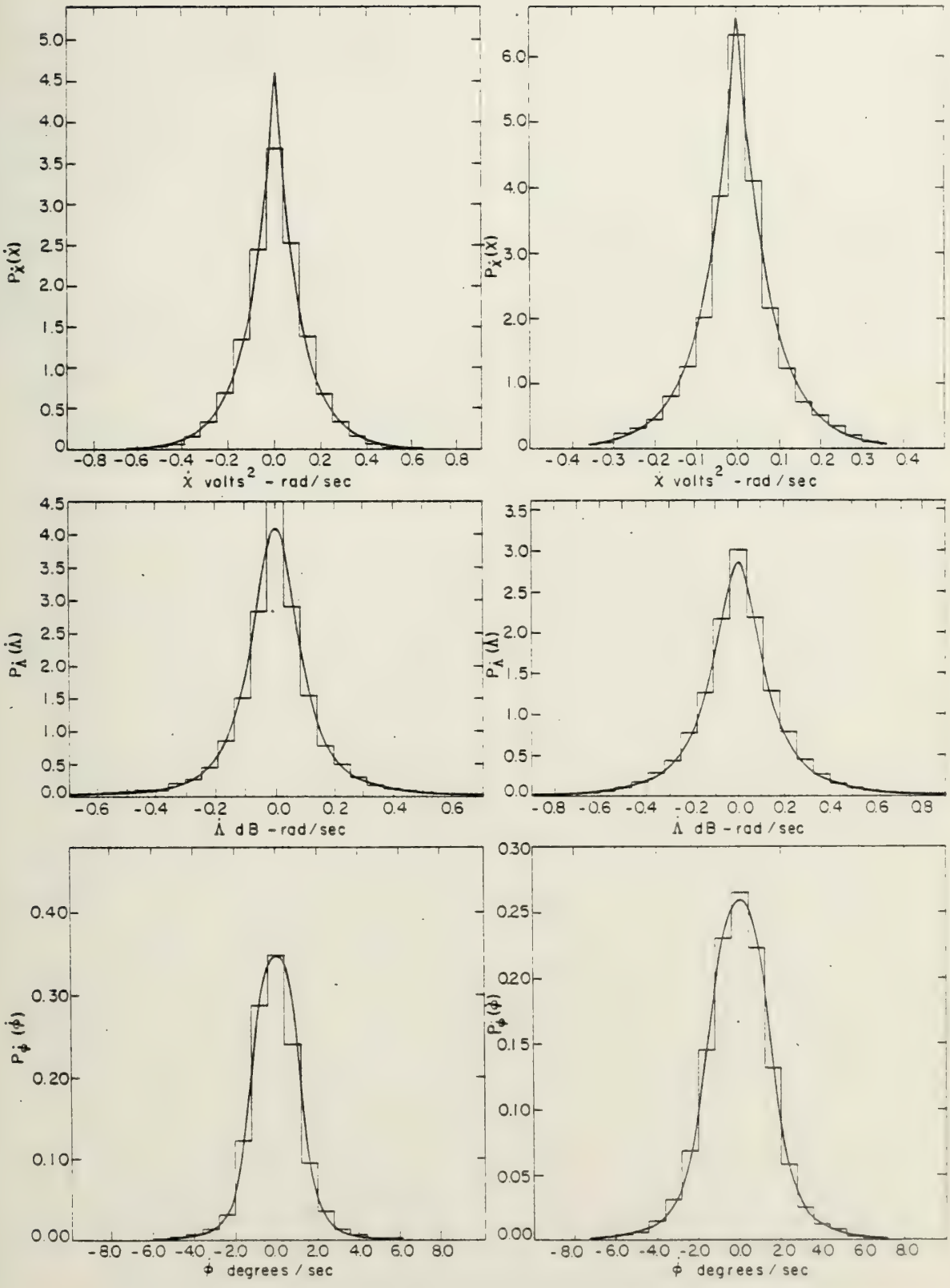


Fig. 56 Histograms from record 447 for $\dot{X}$, $\dot{\Lambda}$, and $\dot{\phi}$, and the least chi-square fit of eqns (1.4), (1.7), and (1.176), respectively. Results for 220 Hz are on the left, and 406 Hz on the right.

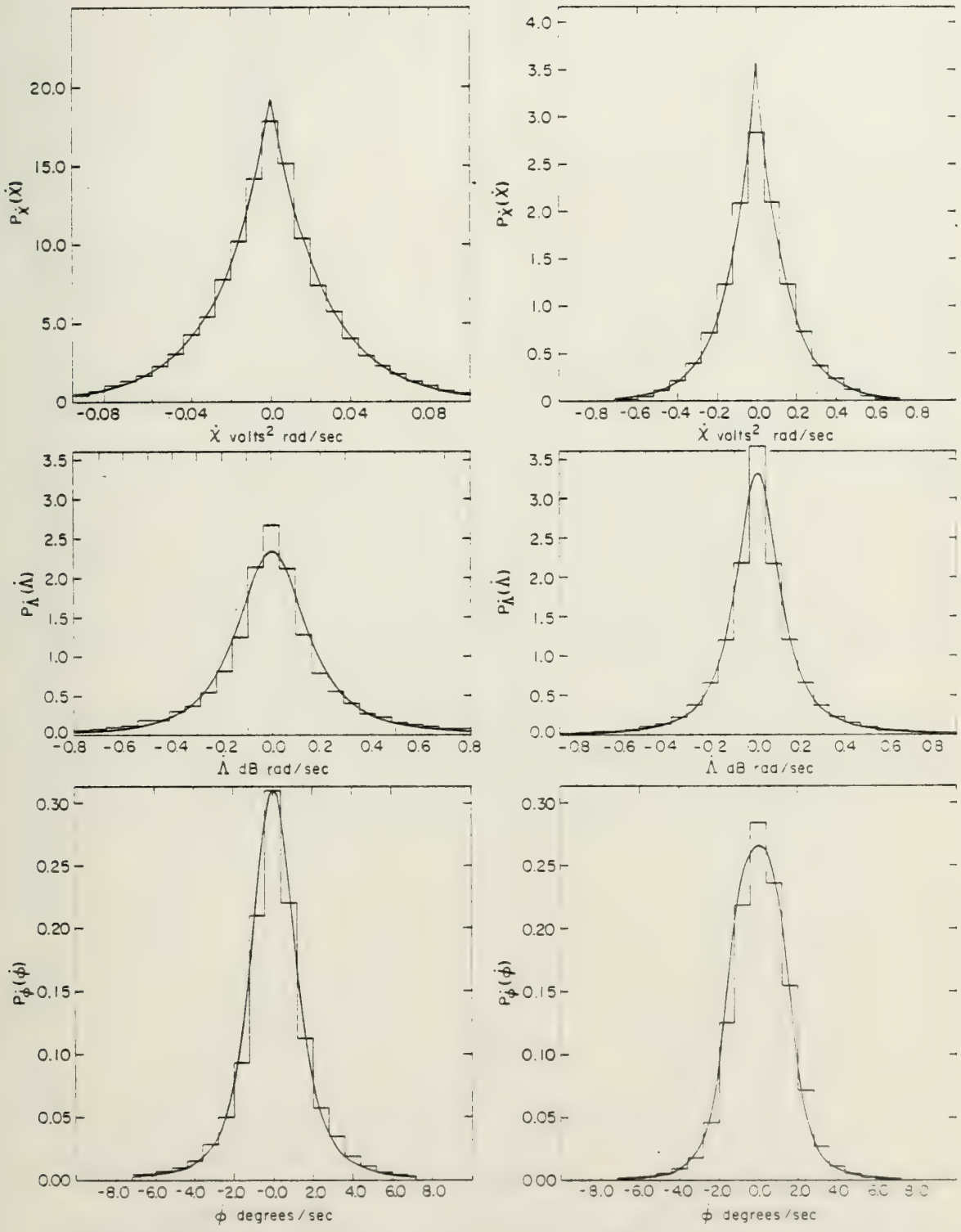


Fig 57 Histograms from Record 448 for $\dot{X}$, $\dot{\Lambda}$, and $\dot{\phi}$, and the least chi-square fit of eqns (I.14), (I.?), and (I.176), respectively. Results for 220 Hz are on the left, and 406 Hz on the right

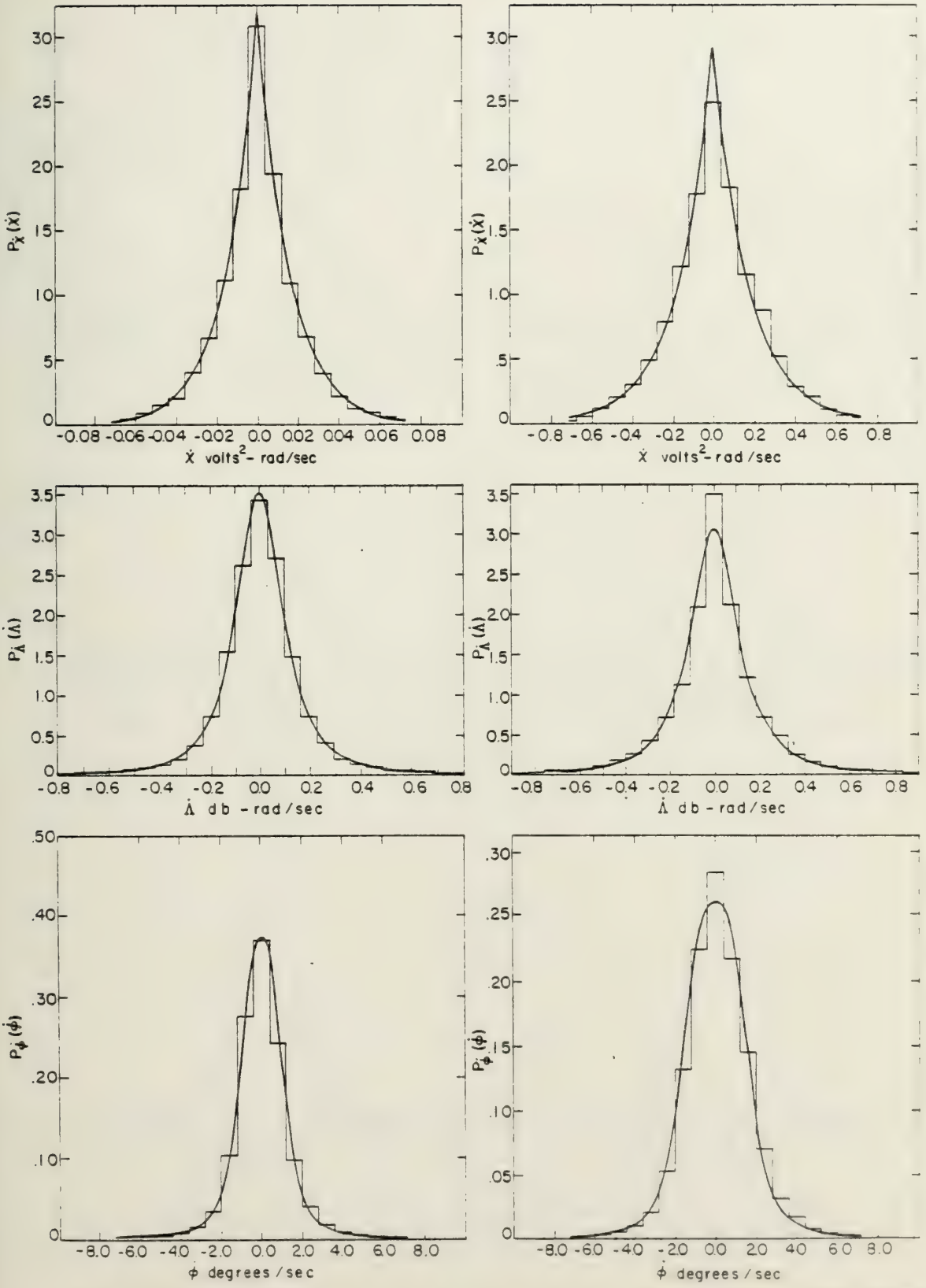


Fig. 58 Histograms from Record 449 for $\dot{X}$, $\dot{\Lambda}$, and $\dot{\phi}$, and the least chi-square fit of equs (1.4), (1.7), and (1.176), respectively. Results for 220 Hz are on the left, and 406 Hz on the right

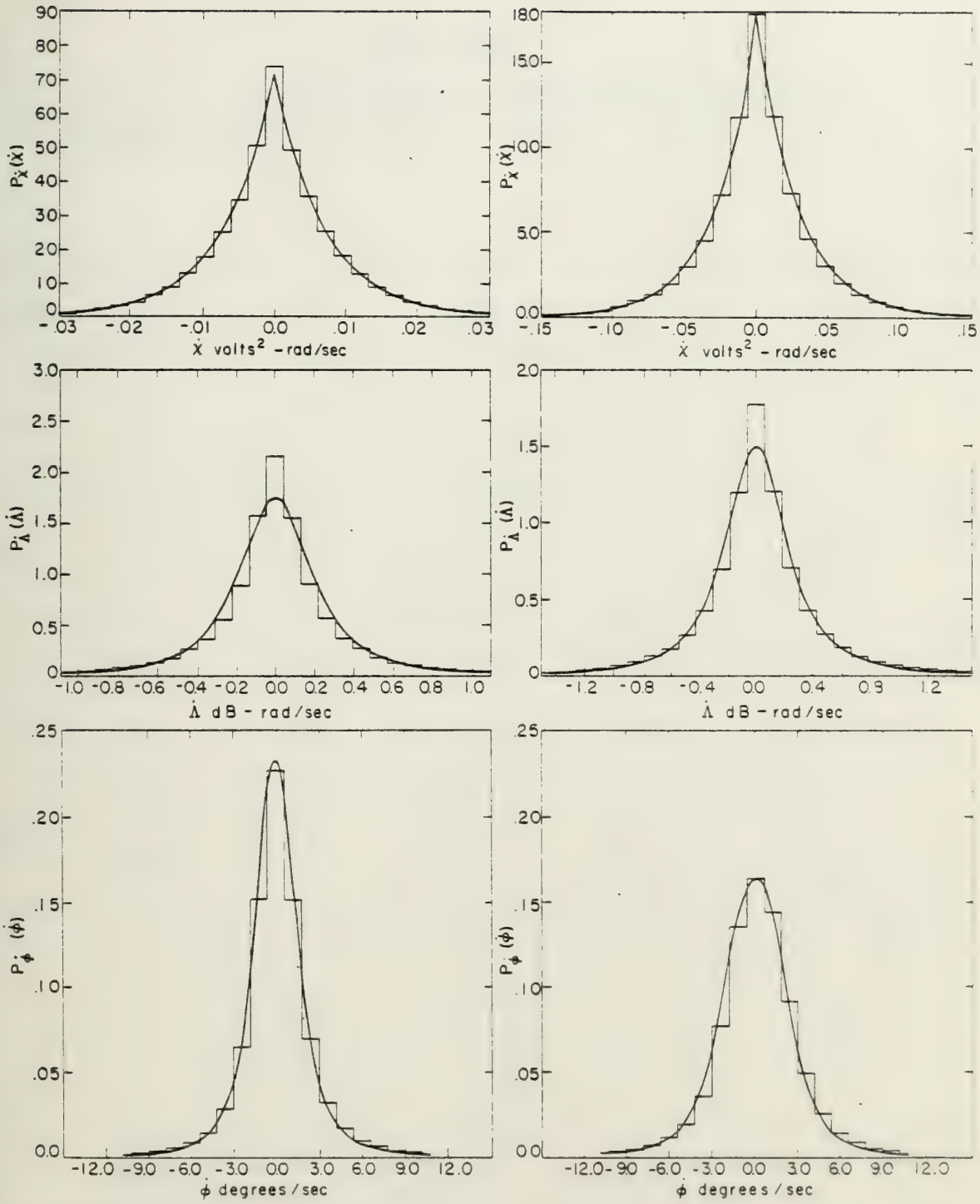


Fig. 59 Histograms from Record 424 for $\dot{X}$, $\dot{\Lambda}$, and $\dot{\phi}$, and the least chi-square fit of equs (14), (17) and (1.176), respectively. Results for 220 Hz are on the left, and 406 Hz on the right.

TABLE XII

Results of the Chi-square goodness-of-fit test of $\dot{\chi}$ and $\dot{\Lambda}$ to Equations (1.4) and (1.7), respectively.

| Record | Freq. Hz | $\dot{\chi}:\chi^2$ | $\chi_n^2$:.05 | $\dot{\Lambda}:\chi^2$ | $\chi_n^2$:.05 |
|---|---|---|---|---|---|
| 447 | 220 | 1.81 | 16.92 | 3.45 | 21.03 |
| | 406 | 3.52 | 23.68 | 1.86 | 23.68 |
| 448 | 220 | 1.45 | 31.41 | 11.61 | 28.87 |
| | 406 | 2.61 | 19.68 | 4.51 | 23.68 |
| 449 | 220 | 1.65 | 21.03 | 1.20 | 23.68 |
| | 406 | 2.96 | 21.03 | 6.44 | 23.68 |
| 424 | 220 | 2.30 | 31.41 | 32.31 | 28.87 |
| | 406 | 6.04 | 31.41 | 16.38 | 28.87 |

TABLE XIII

Results of the Chi-square goodness-of-fit test of $\dot{\phi}$ to Equations (A8), (1.176), and (1.178).

| Record | Freq. Hz | Eq. (A8): $\chi^2$ | Eq. (1.176): $\chi^2$ | Eq. (1.178): $\chi^2$ | $\chi^2_n$:.05 |
|---|---|---|---|---|---|
| 447 | 220 | 16.24 | 3.19 | 2.78 | 15.51 |
| | 406 | 16.54 | 4.13 | 1.19 | 21.03 |
| 448 | 220 | 10.57 | 21.10 | 7.06 | 23.68 |
| | 406 | 22.95 | 6.84 | 3.68 | 21.03 |
| 449 | 220 | 5.43 | 3.26 | 2.67 | 21.03 |
| | 406 | 14.87 | 7.02 | 3.67 | 21.03 |
| 424 | 220 | 10.45 | 23.84 | 12.07 | 26.30 |
| | 406 | 9.78 | 14.61 | 12.71 | 26.30 |

### 3.1.2 Multiple Sources

Because the 220 Hz and 406 Hz sources were transmitted and recorded simultaneously for each record and were each quadrature demodulated about their respective center frequencies and summed incoherently, this affords an opportunity to check the equations derived in Section 1.2.2.2 for two different sources. For each record, the 220 Hz source was designated Source one, and the 406 Hz, Source two. The values for $\sigma_{11}^2$ and $\sigma_{12}^2$ were obtained from Hamblen's [9] previous analysis. The values for $\nu_1^2$ and $\nu_2^2$ in $rad^2/sec^2$ are obtained from Table X. In Figures 60-63, I have plotted representative results. In Figure 60 the histograms for $\chi$ and $\rho$ are plotted with the following equations:

$$P_{\chi_{2D}}(\chi) = \frac{1}{2\sigma_{11}^2 - 2\sigma_{12}^2}\left[\exp\left(-\frac{\chi}{2\sigma_{11}^2}\right) - \exp\left(-\frac{\chi}{2\sigma_{12}^2}\right)\right] \quad (3.1)$$

$$P_{\rho_{2D}}(\rho) = \frac{\rho}{\sigma_{11}^2 - \sigma_{12}^2}\left[\exp\left(-\frac{\rho^2}{2\sigma_{11}^2}\right) - \exp\left(-\frac{\rho^2}{2\sigma_{12}^2}\right)\right] \quad (3.2)$$

Equation (3.1) was first derived by Dyer [4], and Equation (3.2) is simply the transformation $\rho = \chi^{1/2}$ of Equation (3.1). In Table XIV, I have listed the results of

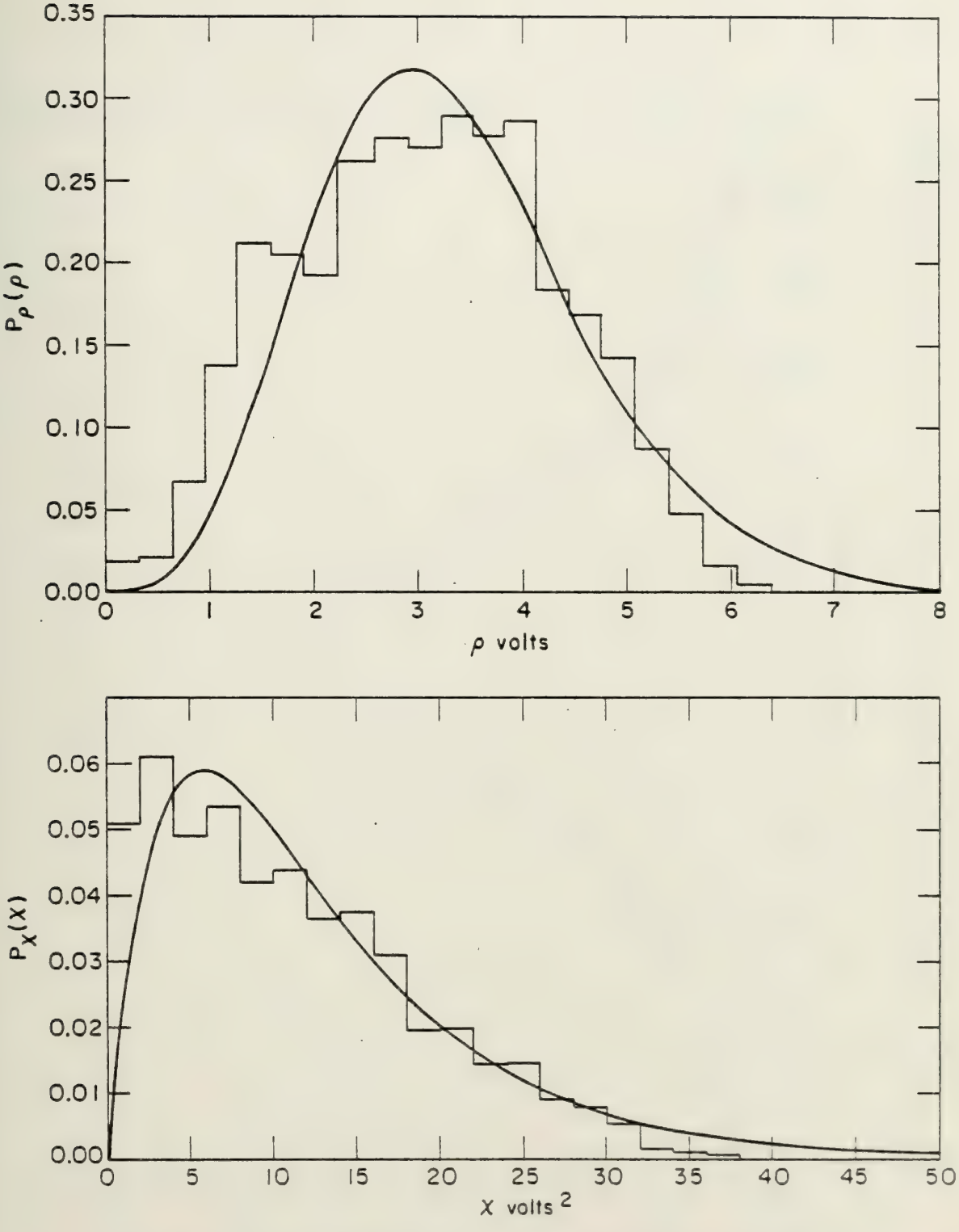


Fig. 60 The histograms of $X$ and $\rho$ for two different sources from Record 447, plotted with equs (3.1) and (3.2) respectively.

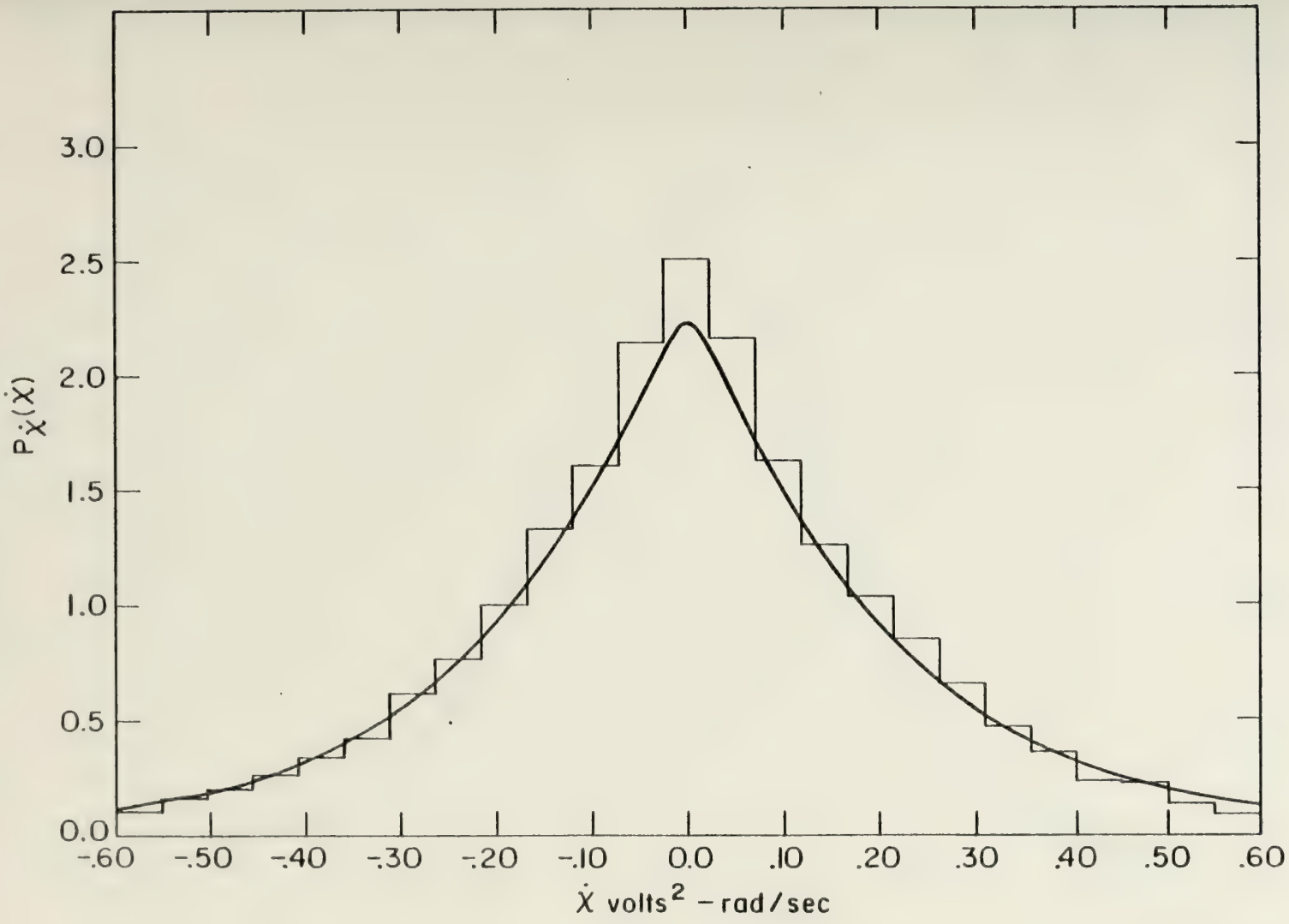


Fig. 61 The histogram of $\dot{X}$ for two different sources from Record 449, plotted with equ. (1.95) with L = 2.

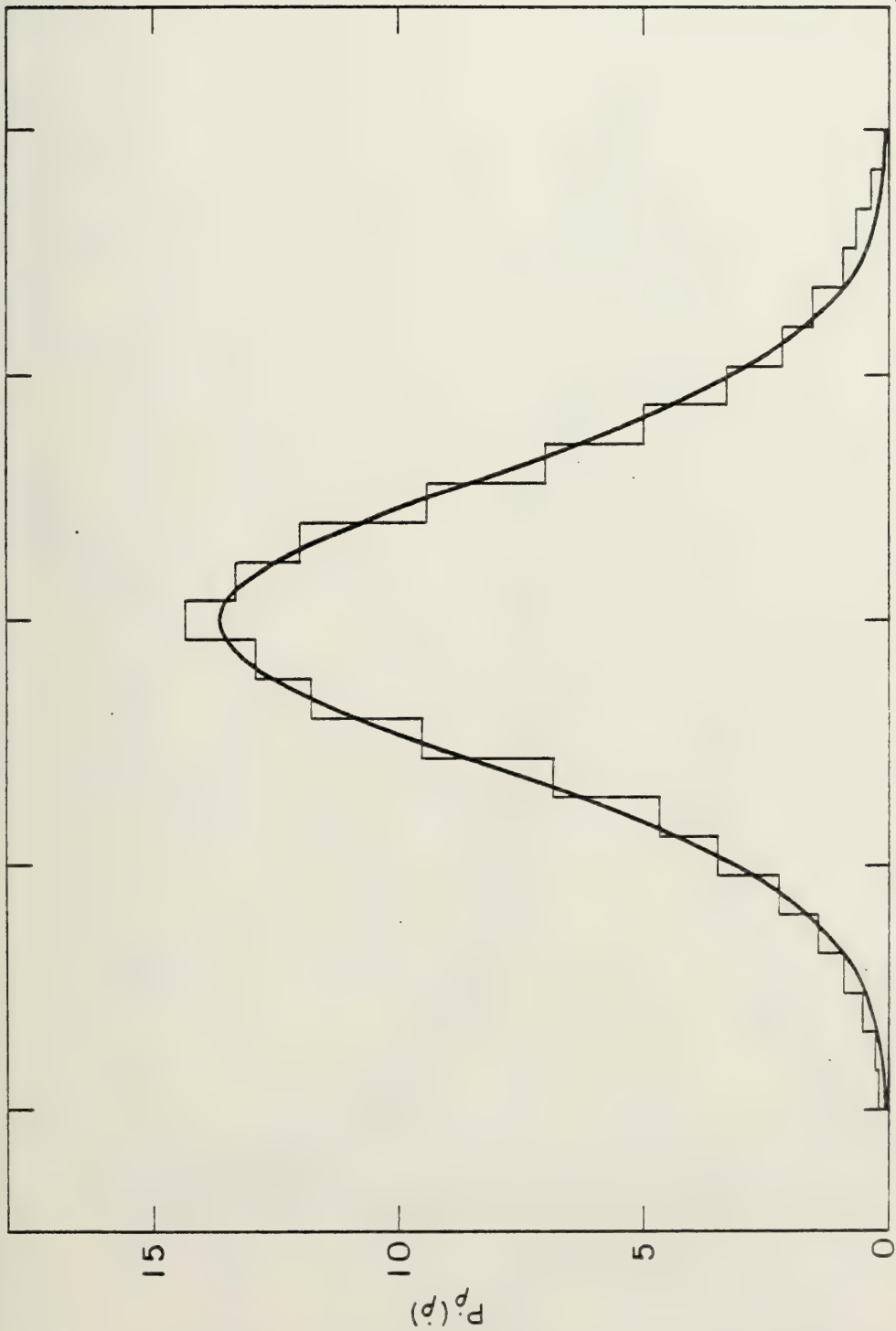


Fig. 62 The histogram of $\dot{\rho}$ for two different sources from Record 447, plotted with equ. (1.114).

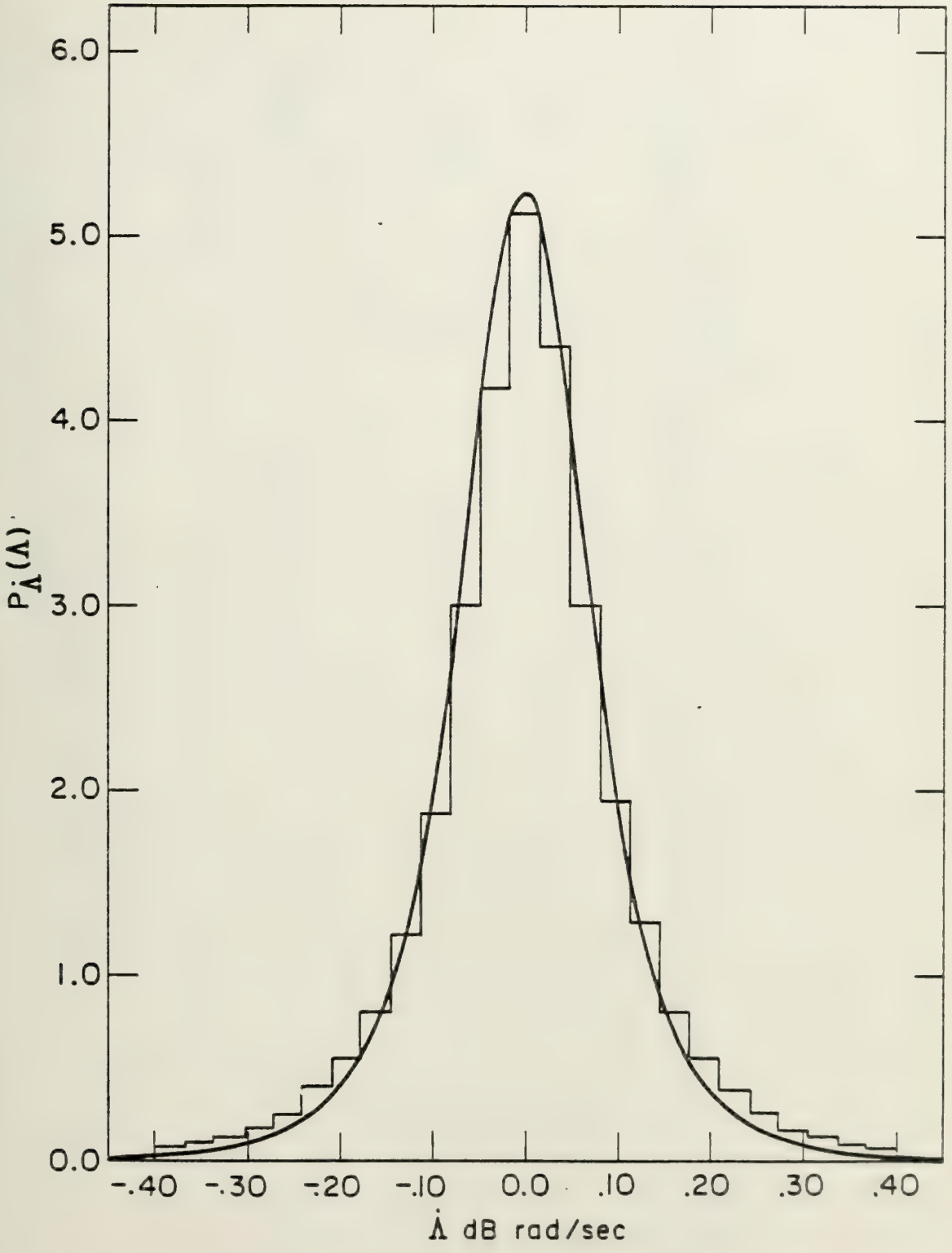


Fig. 63 The histogram of $\dot{\Lambda}$ for two different sources from Record 447 plotted with equ. (1.123).

TABLE XIV

Results of Chi-square test for multiple source densities. Also shown are the values of $\sigma_i^2$ and $\nu^2$ obtained from the single source analysis.

| Fig. | Variable | Record | $\chi^2$ | $\chi_n^2$: .05 | $\sigma_{li}^2$ (volts$^2$) | | $\nu_i^2$ (rad$^2$/sec$^2$) | |
|---|---|---|---|---|---|---|---|---|
| | | | | | i=1,(220Hz) | i=2,(406Hz) | i=1,(220Hz) | i=2,(406Hz) |
| 60 | $\rho$ | 447 | 38.82 | 27.59 | 4.4 | 2.0 | $2.0 \pm 4$ x10 | $4.1 \pm 4$ x10 |
| | $\chi$ | 447 | 31.83* | 25.00 | | | | |
| 61 | $\dot{\chi}$ | 449 | 4.29 | 33.92 | 0.5 | 5.5 | $2.7 \pm 4$ x.10 | $3.6 \pm 4$ x10 |
| 62 | $\dot{\rho}$ | 447 | 3.84 | 26.30 | 4.4 | 2.0 | $2.0 \pm 4$ x10 | $4.1 \pm 4$ x10 |
| 63 | $\dot{\Lambda}$ | 447 | 12.65 | 25.00 | | | | |

*In performing the Chi-square test [29] a contribution of 21.96 came from the first class interval only (there were a total of 16 class intervals). If class interval #1 were dropped $\chi^2$ = 9.87 and $\chi_n^2$: .05 = 23.68.

the Chi-square test and listed the values of $\sigma_{1i}^2$ and $\nu_i^2$ used. Note that the theoretical pdf's for these plots were not fit to the histograms. Also in determining the Chi-square statistic, I have approximated the area under the theoretical pdf for each class interval by taking the value of the pdf at the center of the interval times the width of the interval. Figures 61-63 are the histograms for $\dot{\chi}$, $\dot{\rho}$, and $\dot{\Lambda}$, plotted with Equations (1.95), (1.114), and (1.123), respectively.

In general, the amplitude densities perform rather poorly as expected, while the rate densities perform exceptionally well supporting the theory in Section 1.2.2.2. As noted earlier, the non-stationarity in $\sigma_1^2$ discovered by Hamblen [9] in these data, as well as the apparent statistical stability of the rate variables accounts for the difference in performance of the amplitude and amplitude rate variables.

### 3.1.2 Crossing Rate Statistics

Following Dyer and Shepard [15], I have analyzed the crossing rate statistics for each of the frequencies of the four records of the Eleuthera experiment. Even though the "modulation" in these data are very small (see Table X), the effect on the crossing rate statistics

is dramatic. From Equation (1.18), I have [15],

$$G(\rho_o) = \frac{2\nu\rho_o}{\sigma_1\sqrt{2\pi}} \exp[-\frac{\rho_o^2}{2\sigma_1^2}] \tag{3.3}$$

and [15],

$$G(\phi_o) = \frac{\nu}{2\pi} \tag{3.4}$$

Equation (3.4) assumes no modulation. When the ratio of Equation (3.3) to Equation (3.4) is taken, $\nu$ cancels, i.e. [15],

$$\frac{G(\rho_o)}{G(\phi_o)} = (8\pi)^{\frac{1}{2}} P_\rho(\rho_o)\,\sigma_1 \tag{3.5}$$

However, if the source is modulated or has a finite bandwidth (i.e., $B \gtrsim 2\nu$), then in fact $\nu$ does not cancel when the ratio of the two is taken:

$$\frac{G(\rho_o)}{G(\phi_o)} = (8\pi)^{\frac{1}{2}} \frac{\nu_A}{\nu_{\dot\phi}} P_\rho(\rho_o)\,\sigma_1 \tag{3.6}$$

where $\nu_A$ signifies the value of $\nu$ obtained from the amplitude densities, and $\nu_{\dot\phi}$ the value of $\nu$ obtained from fitting Equation (A8) (which assumes no modulation) to the histogram of $\dot\phi$ of a modulated source. This is tantamount

to assuming that the pdf for $\dot{M}$ is such that Equation (1.165) yields the Longuet-Higgins density with a larger $\nu \equiv \nu_{\dot{\phi}} > \nu_A$. If there is no modulation of the source and $B << 2\nu$, then $\nu_A = \nu_{\dot{\phi}}$ (as will be shown in Section 3.2). For the data of the Eleuthera experiment, however, $\nu_A \neq \nu_{\dot{\phi}}$ because of the error in the Doppler position/tracking system. The ratio $\nu_A/\nu_{\dot{\phi}}$ can be considered a correction factor to account for modulation effects in crossing rate statistics. However, because the error in extracting the mean phase rate is more Gaussian than Longuet-Higgins, as demonstrated quite convincingly by the performance of Equation (1.178) on the histograms of $\dot{\phi}$, I have also computed the correction factor, using the analysis of Section 1.3.3, given by Equation (1.209). In Table XV, I have compiled the correction factors given by $\nu_A/\nu_{\dot{\phi}}$, and Equation (1.209). I obtain $\nu_A/\nu_{\dot{\phi}}$ by taking the ratio of $\nu$ from $\dot{\Lambda}$ to $\nu$ from $\dot{\phi}$ given in Table X. For Equation (1.209) $\sigma_G$, and $\nu$ (from $\dot{\Lambda}$, converted to mHz) are likewise obtained from Table X. In Figures 64-67 reproduced in part from Reference [15] I have plotted the new curves applying the $\nu_A/\nu_{\dot{\phi}}$, and Equation (1.209) correction factors. Note that because the correction factors are a function of $\nu$ and parameters of the modulation there is one curve for each frequency. The

TABLE XV

The correction factors to the unmodulated value of $G(\rho_o)/G(\phi_o)$ for the Eleuthera experiment, based on the ratio of $\nu_A$ (from $\dot{\Lambda}$, Table X), to $\nu_{\dot{\phi}}$ (from $\dot{\phi}$, Table X), and a Gaussian frequency modulation assumption.

| Record | Frequency | $\nu_A/\nu_{\dot{\phi}}$ | Eq. (1.209) |
|---|---|---|---|
| 447 | 220 | .65 | .41 |
| | 406 | .72 | .44 |
| 448 | 220 | .84 | .56 |
| | 406 | .65 | .40 |
| 449 | 220 | .78 | .47 |
| | 406 | .69 | .42 |
| 424 | 220 | .86 | .58 |
| | 406 | .79 | .54 |

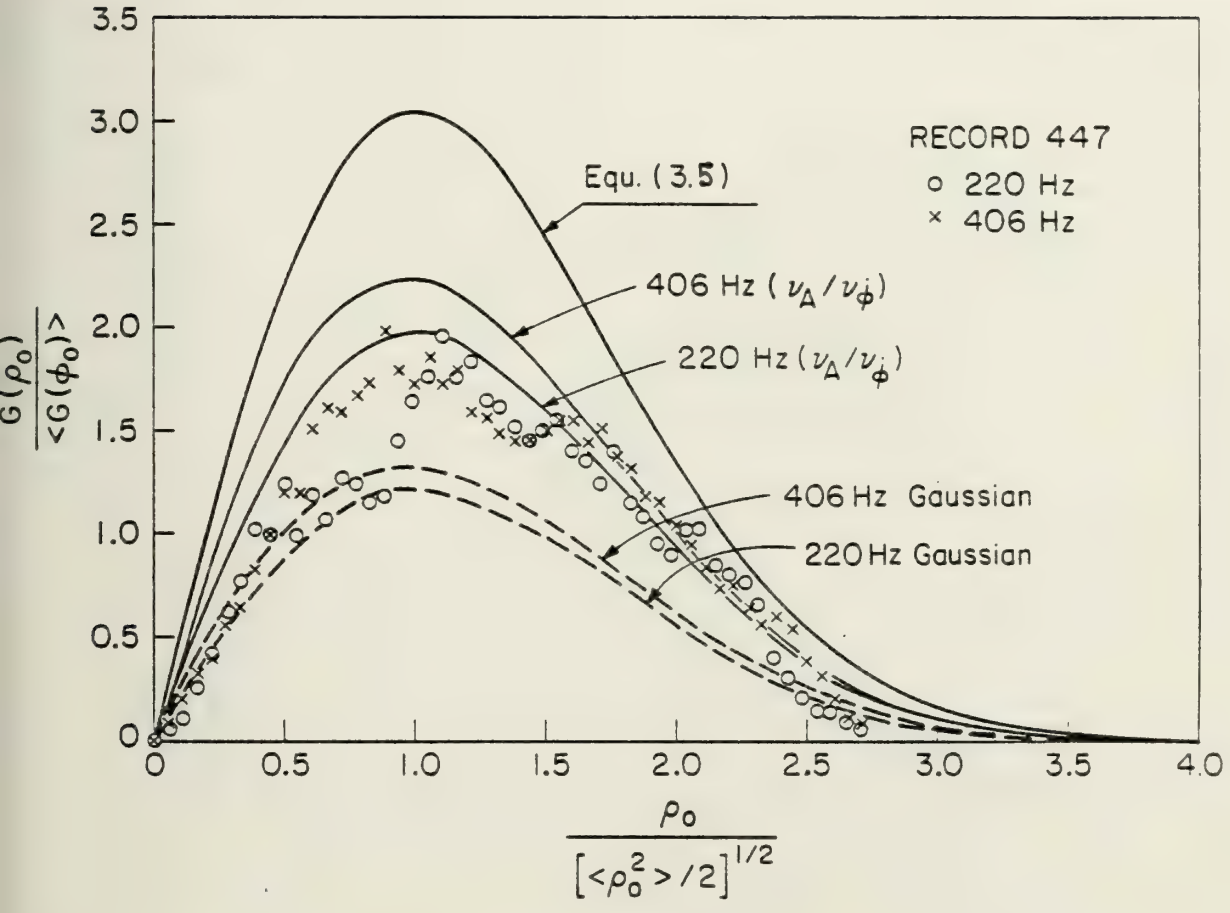


Fig.64 Ratio of phase period to amplitude period, versus amplitude, for record 447. Equ. (3.5) is the theoretical ratio for a non-modulated narrowband source. The correction factors $\nu_A/\nu_\phi$ (Table XV), and Equ. (1.209) (Gaussian modulation) have been applied to obtain the corrected curves for 220 Hz and 406 Hz accounting for the modulation.

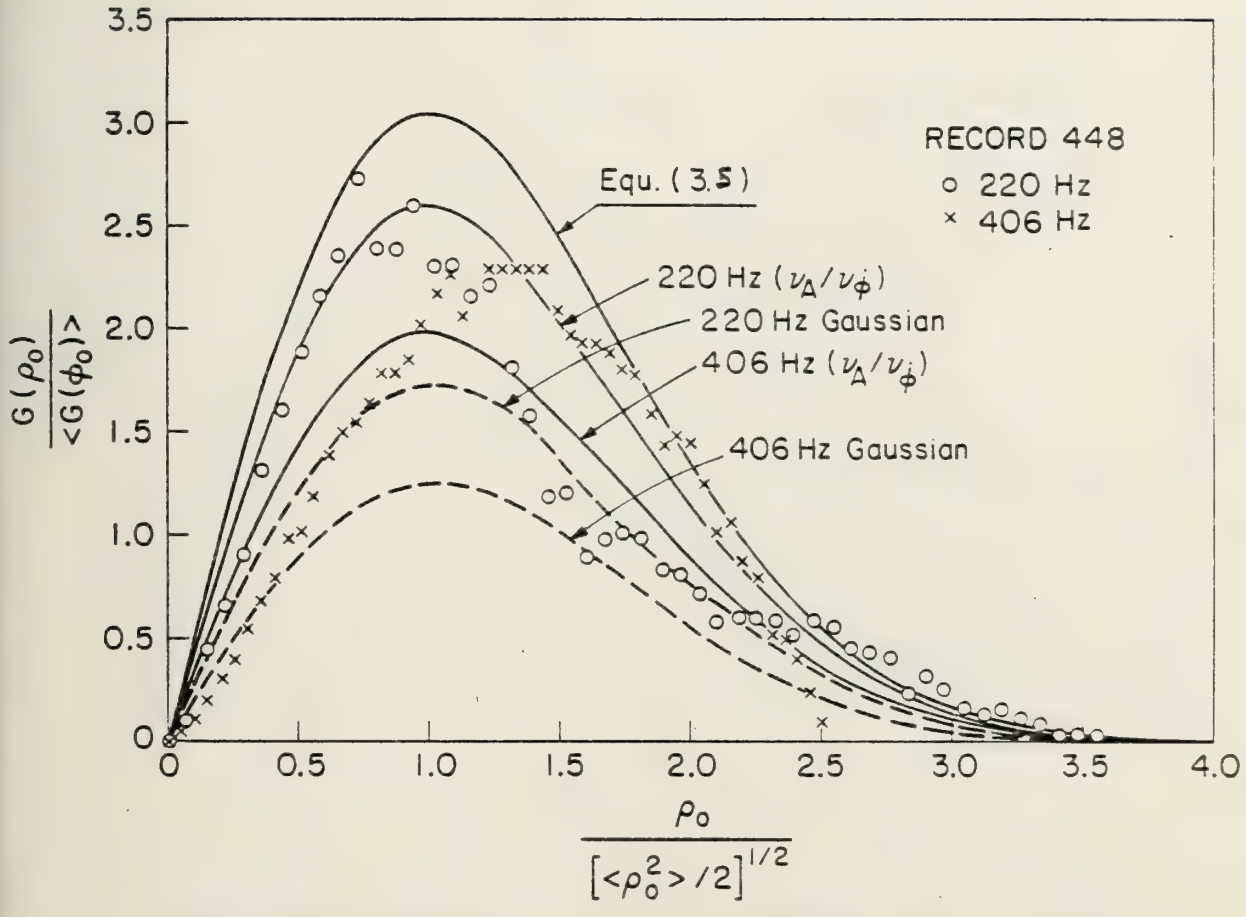


Fig. 65 Ratio of phase period to amplitude period, versus amplitude, for record 448. Equ. (3.5) is the theoretical ratio for a non-modulated narrowband source. The correction factors $\nu_A/\nu_\phi$ (Table XV), and Equ. (1.209) (Gaussian modulation) have been applied to obtain the corrected curves for 220 Hz and 406 Hz accounting for the modulation.

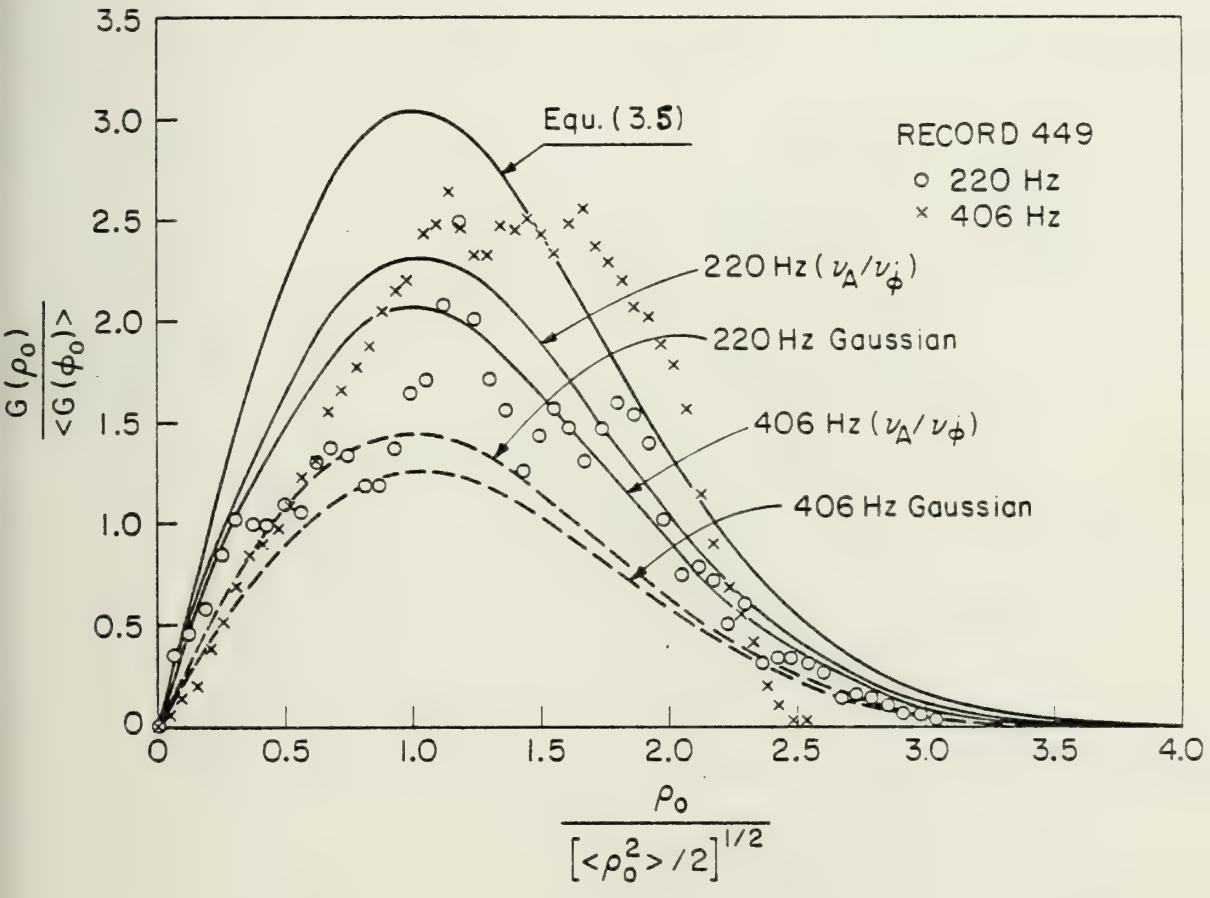


Fig. 66 Ratio of phase period to amplitude period, versus amplitude, for record 449. Equ. (3.5) is the theoretical ratio for a non-modulated narrowband source. The correction factors $\nu_A/\nu_\phi$ (Table XV), and Equ. (1.209) (Gaussian modulation) have been applied to obtain the corrected curves for 220 Hz and 406 Hz accounting for the modulation.

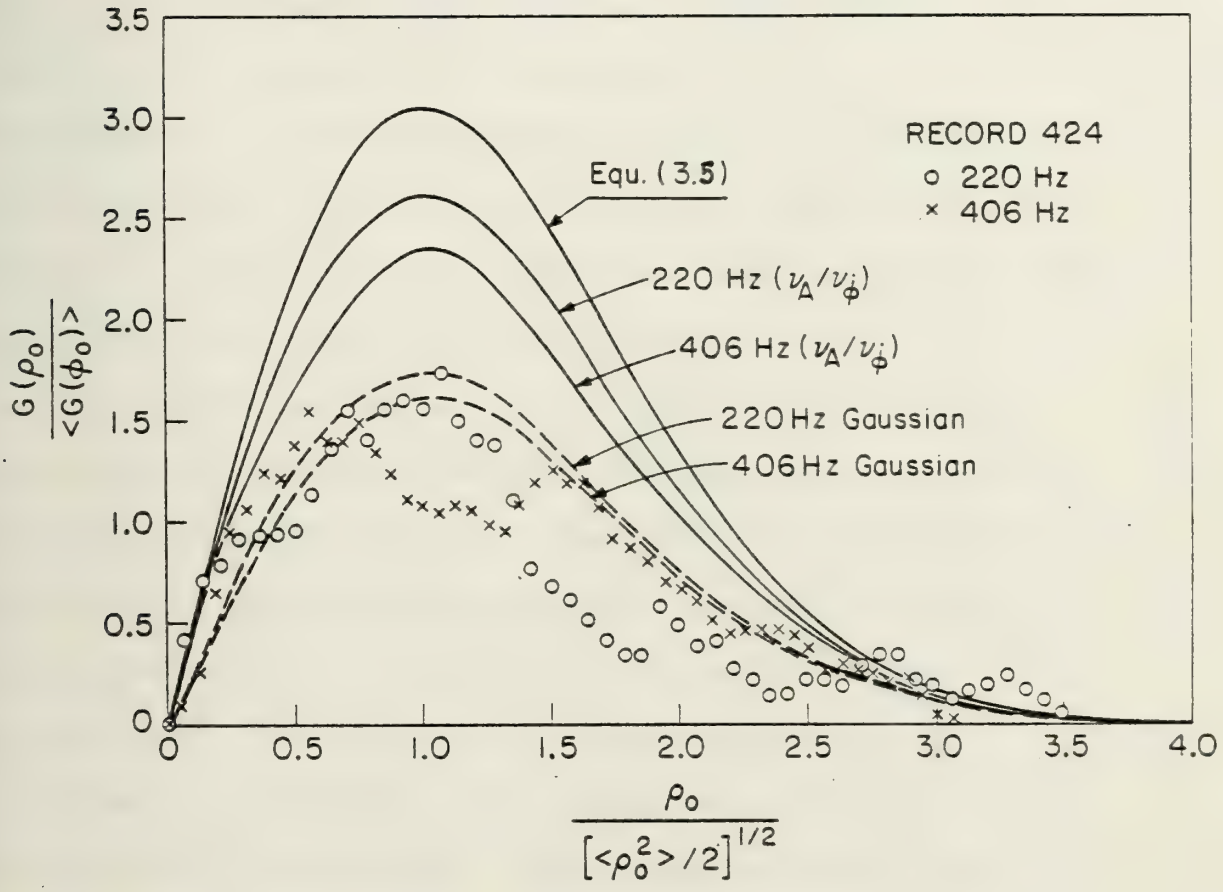


Fig. 67 Ratio of phase period to amplitude period, versus amplitude, for record 424. Equ. (3.5) is the theoretical ratio for a non-modulated narrowband source. The correction factors $\nu_A/\nu_\phi$ (Table XV), and Equ. (1.209) (Gaussian modulation) have been applied to obtain the corrected curves for 220 Hz and 406 Hz accounting for the modulation.

bracketed $\langle G(\phi_o) \rangle$ indicates that an average value of $G(\phi_o)$ has been used. The range of values results from restrictions placed on the maximum value of $\dot{\phi}$ as a consequence of phase unwrapping routines. As indicated in the figures, $\rho_o$ has been normalized such that the $E[\rho_o^2] = 2$. Details of the above and other aspects of the data reduction can be found in Reference [15].

The corrected curves are a dramatic improvement over the Dyer, Shepard theory. Except for run 424 where the Gaussian performs much better, the Longuet-Higgins and Gaussian curves perform about the same with the former tending to be slightly high and the latter slightly low. The variance in these results only indicates our uncertainty in the exact nature of the modulation in these data. The important results are as follows: (1) The modulation theory discovered the heretofore unnoticed modulation in these data, (2) accounted for its effects on the histograms of $\dot{\phi}$, and (3) correctly predicted the crossing rate statistics completely explaining the consistent over prediction of the Dyer, Shepard theory.

## 3.2 The CASE Experiment

Data from the CASE experiment [13] were analyzed in

order to compare the theory to data in which the modulation is known and controlled. Three configurations were used: (1) fixed source on a seamount, (2) source towed by a surface ship, and (3) source mounted on a submersible. The signals were monitored at four widely separated fixed deep water receivers at ranges varying from 200 to 400 km. Runs from one of the receivers had to be subsequently rejected due to an extremely low signal to noise ratio. Two carrier frequencies were employed, one at 15 and the other at 33 Hz. The signals were frequency modulated by a pseudo-random function generator with an average period of 107 sec and an overall pattern that repeats itself every 640 sec (see Figure 68). The bandwidth of the modulation is pre-selected, and for the runs analyzed is either 0 (no modulation), 1/8, 1/4, or 1/2 Hz.

A total of 88 runs of 15 min duration each was analyzed. From the filtered digitized complex data, time series and histograms were generated for $\dot{\Lambda}$ and $\dot{\phi}$. As before, Equations (1.7) and (A8) are fit, respectively, such that the value of $\nu^2$ obtained minimizes the Chi-square statistic.

Of the 88 runs, 12 were not modulated and the values of $\nu$ obtained from $\dot{\Lambda}$ and $\dot{\phi}$ for those runs agree (run by run)

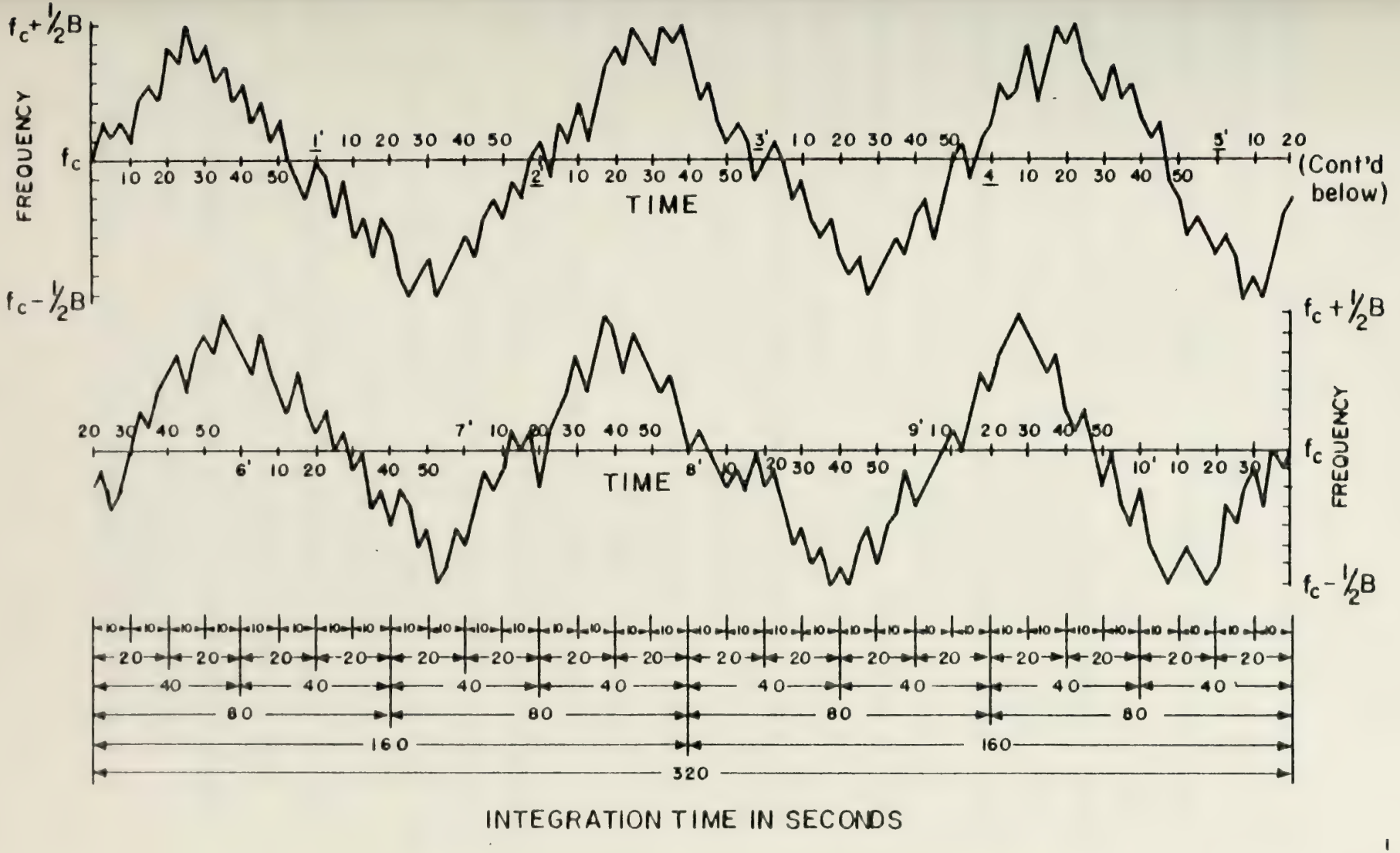


Fig. 68 The source frequency function for the modulation induced in the CASE experiment., reproduced from Reference [32].

to within approximately 10%. In Table XVI, I have listed these values as well as the range frequency and receiver number for each run. For all of these runs, the source was fixed on the seamount. For 9 of these 12 runs, the quadrature components exhibit significant nonzero means. During the data reduction these means for all the runs analyzed regrettably were removed. However, runs 76-77 had no significant means and the values of $\nu$ are consistent with those from runs 66-68 which are at the same frequency. It appears that extracting the means even when significant (and this was true only for runs 66-68, 71-73, and 113-115) is a negligible factor. However, runs 113-115 do in fact contain the largest three values of $\nu$ obtained for all the 15 Hz runs and are perhaps suspect, though other runs with insignificant means also exhibit values of $\nu$ approaching and exceeding 1.

For the remaining 76 runs, 24 were modulated with a 1/8 Hz bandwidth, 35 with a 1/4 Hz bandwidth, and 17 with a 1/2 Hz bandwidth. As expected with modulation, the value of $\nu^2$ obtained from fitting Equation (A8) to the histograms of $\dot{\phi}$ were larger than those obtained from $\dot{\Lambda}$ by large factors depending upon the bandwidth of the modulation. Because the modulation pattern (Figure 68) is approximately a saw-tooth and the spectrum of the

TABLE XVI

The values of $\nu$ obtained from the 12 non-modulated runs analysed in the CASE experiment. In addition to being non-modulated the source was fixed on a seamount.

| Case Record # | Freq. (Hz) | $\nu$ (rad/sec) $\dot{\phi}$ | $\nu$ (rad/sec) $\dot{\Lambda}$ | Range (km) | RCVR |
|---|---|---|---|---|---|
| 66* | 33 | .094 | .104 | 250 | 1 |
| 67* | 33 | .353 | .354 | 320 | 2 |
| 68* | 33 | .191 | .194 | 450 | 3 |
| 71* | 15 | .407 | .421 | 250 | 1 |
| 72* | 15 | 1.186 | .982 | 320 | 2 |
| 73* | 15 | .741 | .727 | 450 | 3 |
| 76 | 33 | .042 | .044 | 250 | 1 |
| 77 | 33 | .154 | .147 | 320 | 2 |
| 78 | 33 | .106 | .096 | 450 | 3 |
| 113* | 15 | 1.349 | 1.208 | 250 | 1 |
| 114* | 15 | 1.495 | 1.272 | 320 | 2 |
| 115* | 15 | 1.279 | 1.084 | 450 | 3 |

*These runs showed significant means in the quadrature components.

modulation (Figure 69) is approximately uniform, the analysis of Section I.B is applied.

Equation (1.176) is fit to the histograms of $\dot{\phi}$ using the value of $\nu^2$ obtained from fitting $\dot{\Lambda}$ and varying A such that the Chi-square statistic is minimized. The value of A is then compared to the actual signal bandwidth set by the experimenter. In Figure 70 the error in percent is plotted against the number of runs that exhibit a given error. For the 76 runs with modulation, the average error in determining the bandwidth of the modulation by this method is 8%. Predictive ability appears to be degraded somewhat when the oceanic fluctuations are of the same order as the bandwidth of the modulation, i.e., when $\nu \approx A$ the average error was 17%. It should be remembered, however, that the modulation is not exactly uniform and, therefore, using Equation (1.176) is an approximation to begin with, and this approximation is worst when $\nu \approx A$. Finally, I note that the error is consistently negative, i.e., the foregoing method underpredicts. The reason for this is unknown.

Performance on the Chi-square test was also quite good. All 88 runs passed at the $\alpha = .10$ level of significance when Equation (1.7) is fitted to the histograms of $\dot{\Lambda}$. In fitting Equation (1.176) to the

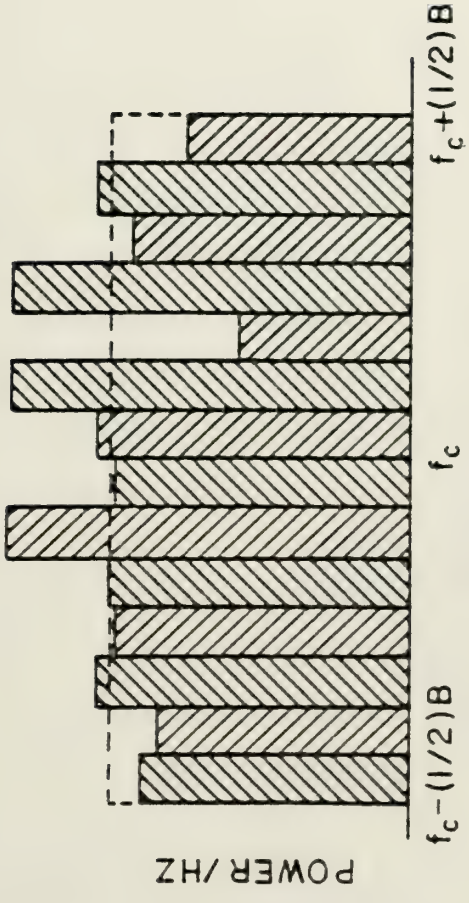


Fig. 69 The source signal power spectrum of the modulation used in the CASE experiment, reproduced from Reference [32].

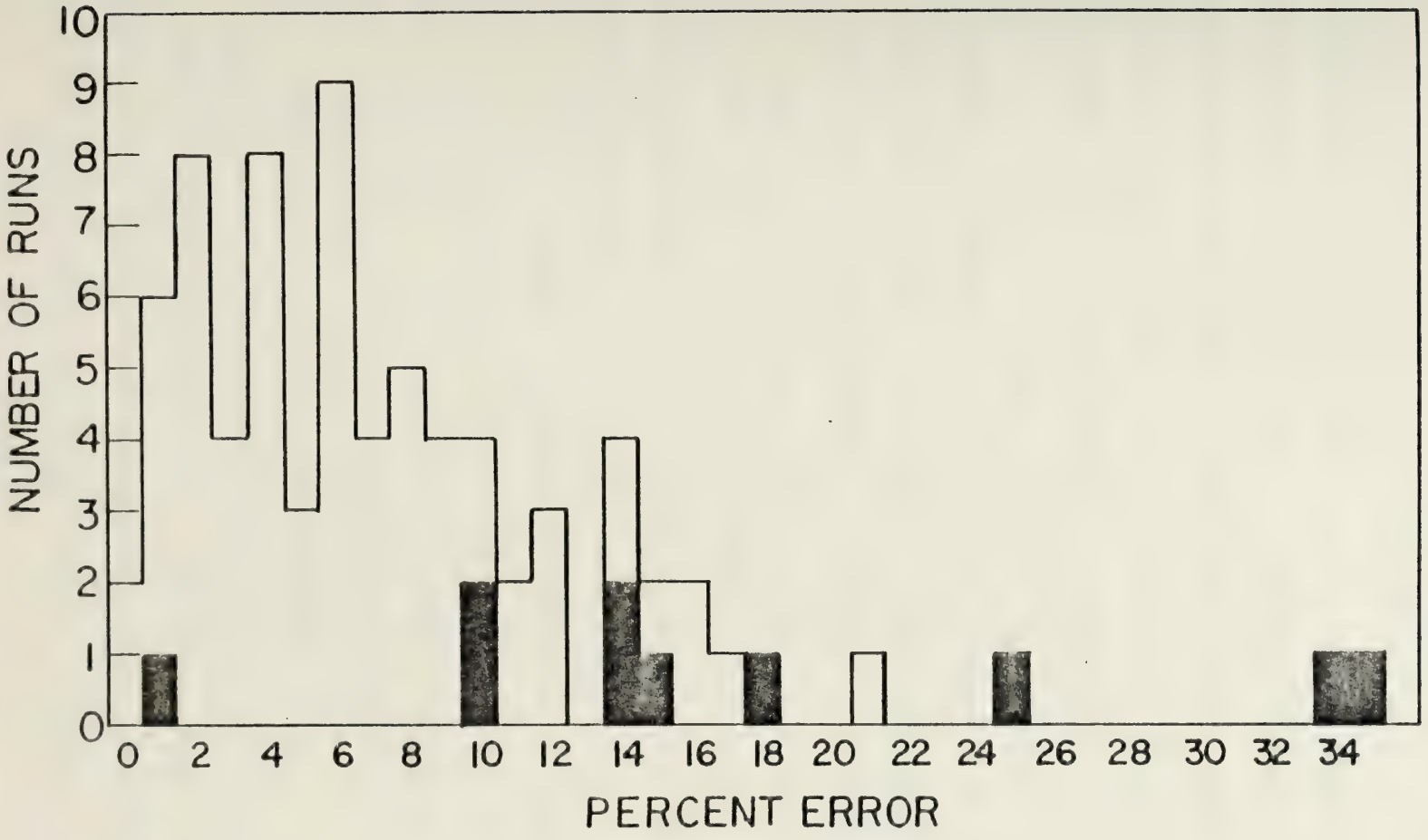


Fig. 70 The error in percent versus number of runs in determining the bandwidth of the modulation of the CASE data. The shaded portions represent those runs in which $\nu \approx A$.

histograms of $\dot{\phi}$ for 76 runs with modulation, only 2 runs fail. For the 12 runs without modulation, only 1 run fails when Equation (A8) is fit to the histograms of $\dot{\phi}$. The fit of Equation (A8) to the 76 modulated runs is as anticipated extremely poor; 29 of the 76 runs failed and those that passed did so by a very small margin.

In Table XVII, I have compiled the values of $\nu$ (from $\dot{\Lambda}$), A, actual A, range, range rate, source configuration, frequency, and receiver number for each of the 76 modulated runs. Under source configuration C indicates fixed on the seamount, T indicated towed by a surface ship, and S indicates mounted on a submersible.

Figures 71 and 72 are representative of the modulated runs when A >> $\nu$. Figure 71 shows the time series and histogram of $\dot{\Lambda}$ and the best fit of Equation (1.7). Figure 72 includes the time series and histogram of $\dot{\phi}$ and the best fit of Equation (A8) and Equation (1.176). Reference [33] contains the plots for all the runs as well as the FORTRAN listing of the data analysis program for the CASE experiment.

Comparison of $\nu^2$ from the CASE experiment with the Dyson, Munk, and Zetler model [11] is unfavorable. The values of $\nu^2$ obtained at 15 Hz are, in fact, greater than those obtained at 33 Hz, contrary to the frequency scaling

TABLE XVII

Data for each of the 75 modulated runs. Under source configuration, C indicates fixed on the sea mount, T-towed by a surface ship, and S-mounted on a submersible.

| Case Record # | Freq. (Hz) | $\nu$ (rad/sec) | A (Hz) | Actual A (Hz) | Range (km) | Range Rate (kts) | Source Configuration | RCVR # |
|---|---|---|---|---|---|---|---|---|
| 2 | 15 | .105 | .119 | .125 | 350 | 1.0 | T | 1 |
| 3 | 15 | .109 | .123 | .125 | 340 | 0.2 | T | 2 |
| 4 | 15 | .117 | .119 | .125 | 420 | -0.8 | T | 3 |
| 6 | 15 | .114 | .109 | .125 | 350 | 0.7 | T | 1 |
| 7 | 15 | .131 | .119 | .125 | 340 | 1.5 | T | 2 |
| 8 | 15 | .148 | .118 | .125 | 420 | 1.9 | T | 3 |
| 10 | 15 | .090 | .055 | .062 | 350 | 0.0 | T | 1 |
| 11 | 15 | .095 | .057 | .062 | 340 | 0.7 | T | 2 |
| 12 | 15 | .113 | .058 | .062 | 420 | 1.4 | T | 3 |
| 14 | 15 | .051 | .059 | .062 | 300 | -0.4 | T | 1 |
| 15 | 15 | .142 | .057 | .062 | 290 | 0.8 | T | 2 |
| 16 | 15 | .240 | .053 | .062 | 380 | 1.5 | T | 3 |
| 18 | 15 | .074 | .115 | .125 | 300 | 2.0 | T | 1 |
| 19 | 15 | .186 | .111 | .125 | 290 | 1.7 | T | 2 |
| 20 | 15 | .215 | .107 | .125 | 380 | 1.0 | T | 3 |

TABLE XVII
(continued)

| Case Record # | Freq. (Hz) | $\nu$ (rad/sec) | A (Hz) | Actual A (Hz) | Range (km) | Range Rate (kts) | Source Configuration | RCVR # |
|---|---|---|---|---|---|---|---|---|
| 22 | 15 | .101 | .118 | .125 | 300 | -0.1 | T | 1 |
| 23 | 15 | .160 | .117 | .125 | 290 | 1.1 | T | 2 |
| 24 | 15 | .241 | .111 | .125 | 380 | 1.7 | T | 3 |
| 26 | 33 | .118 | .123 | .125 | 350 | 10.0 | S | 1 |
| 27 | 33 | .068 | .125 | .125 | 340 | 8.7 | S | 2 |
| 28 | 33 | .075 | .124 | .125 | 420 | 8.0 | S | 3 |
| 31 | 33 | .101 | .061 | .062 | 350 | 9.8 | S | 1 |
| 32 | 33 | .025 | .062 | .062 | 340 | 9.4 | S | 2 |
| 33 | 33 | .036 | .064 | .062 | 420 | 7.3 | S | 3 |
| 36 | 33 | .327 | .062 | .062 | 350 | -1.7 | S | 1 |
| 37 | 33 | .057 | .062 | .062 | 340 | 3.4 | S | 2 |
| 38 | 33 | .038 | .061 | .062 | 420 | 6.9 | S | 3 |
| 41 | 33 | .064 | .129 | .125 | 350 | 9.8 | S | 1 |
| 42 | 33 | .065 | .129 | .125 | 340 | 9.4 | S | 2 |
| 43 | 33 | .074 | .131 | .125 | 420 | 7.2 | S | 3 |
| 51 | 33 | .039 | .118 | .125 | 300 | 2.0 | T | 1 |
| 52 | 33 | .047 | .119 | .125 | 280 | 1.7 | T | 2 |
| 53 | 33 | .231 | .117 | .125 | 340 | 1.0 | T | 3 |

TABLE XVII
(continued)

| Case Record # | Freq. (Hz) | $\nu$ (rad/sec) | A (Hz) | Actual A (Hz) | Range (km) | Range Rate (kts) | Source Configuration | RCVR # |
|---|---|---|---|---|---|---|---|---|
| 61 | 15 | .156 | .115 | .125 | 340 | 0.1 | T | 1 |
| 62 | 15 | .154 | .120 | .125 | 340 | 2.6 | T | 2 |
| 63 | 15 | .433 | .121 | .125 | 440 | 4.0 | T | 3 |
| 81 | 33 | .166 | .064 | .062 | 250 | 0.0 | C | 1 |
| 82 | 33 | .204 | .054 | .062 | 320 | 0.0 | C | 2 |
| 83 | 33 | .079 | .061 | .062 | 450 | 0.0 | C | 3 |
| 85 | 33 | .176 | .119 | .125 | 250 | 0.0 | C | 1 |
| 86 | 33 | .290 | .118 | .125 | 320 | 0.0 | C | 2 |
| 87 | 33 | .100 | .120 | .125 | 450 | 0.0 | C | 3 |
| 93 | 33 | .077 | .059 | .062 | 300 | -0.6 | T | 1 |
| 94 | 33 | .046 | .060 | .062 | 260 | 0.7 | T | 2 |
| 95 | 33 | .057 | .058 | .062 | 340 | 1.6 | T | 3 |
| 105 | 15 | .185 | .105 | .125 | 250 | 0.0 | C | 1 |
| 106 | 15 | .491 | .103 | .125 | 320 | 0.0 | C | 2 |
| 107 | 15 | .237 | .105 | .125 | 450 | 0.0 | C | 3 |
| 109 | 15 | .095 | .054 | .062 | 250 | 0.0 | C | 1 |
| 110 | 15 | .307 | .056 | .062 | 320 | 0.0 | C | 2 |
| 111 | 15 | .201 | .056 | .062 | 450 | 0.0 | C | 3 |

TABLE XVII
(continued)

| Case Record # | Freq. (Hz) | $\nu$ (rad/sec) | A (Hz) | Actual A (Hz) | Range (km) | Range Rate (kts) | Source Configuration | RCVR # |
|---|---|---|---|---|---|---|---|---|
| 117 | 33 | .135 | .232 | .250 | 250 | 0.0 | C | 1 |
| 118 | 33 | .266 | .241 | .250 | 320 | 0.0 | C | 2 |
| 119 | 33 | .106 | .250 | .250 | 450 | 0.0 | C | 3 |
| 121 | 15 | .284 | .198 | .250 | 250 | 0.0 | C | 1 |
| 122 | 15 | .751 | .166 | .250 | 320 | 0.0 | C | 2 |
| 123 | 15 | .399 | .212 | .250 | 450 | 0.0 | C | 3 |
| 125 | 15 | .136 | .117 | .125 | 340 | 5.0 | T | 1 |
| 126 | 15 | .084 | .123 | .125 | 340 | 4.2 | T | 2 |
| 127 | 15 | .228 | .124 | .125 | 440 | 2.9 | T | 3 |
| 129 | 15 | .115 | .226 | .250 | 340 | 5.0 | T | 1 |
| 130 | 15 | .157 | .234 | .250 | 340 | 4.2 | T | 2 |
| 131 | 15 | .729 | .187 | .250 | 440 | 2.9 | T | 3 |
| 133 | 15 | .072 | .060 | .062 | 340 | -0.8 | T | 1 |
| 134 | 15 | .155 | .057 | .062 | 340 | 1.9 | T | 2 |
| 135 | 15 | .837 | .071 | .062 | 440 | 3.5 | T | 3 |
| 137 | 33 | .169 | .246 | .250 | 250 | 0.0 | C | 1 |
| 138 | 33 | .386 | .235 | .250 | 320 | 0.0 | C | 2 |
| 139 | 33 | .126 | .252 | .250 | 450 | 0.0 | C | 3 |

TABLE XVII
(continued)

| Case Record # | Freq. (Hz) | $\nu$ (rad/sec) | A (Hz) | Actual A (Hz) | Range (km) | Range Rate (kts) | Source Configuration | RCVR # |
|---|---|---|---|---|---|---|---|---|
| 141 | 15 | .183 | .208 | .250 | 250 | 0.0 | C | 1 |
| 142 | 15 | 1.100 | .163 | .250 | 320 | 0.0 | C | 2 |
| 143 | 15 | .292 | .225 | .250 | 450 | 0.0 | C | 3 |
| 145 | 15 | .178 | .231 | .250 | 300 | -0.1 | T | 1 |
| 147 | 15 | .175 | .221 | .250 | 380 | 1.7 | T | 3 |
| 149 | 33 | .049 | .124 | .125 | 300 | -0.2 | T | 1 |
| 150 | 33 | .027 | .121 | .125 | 260 | 1.0 | T | 2 |

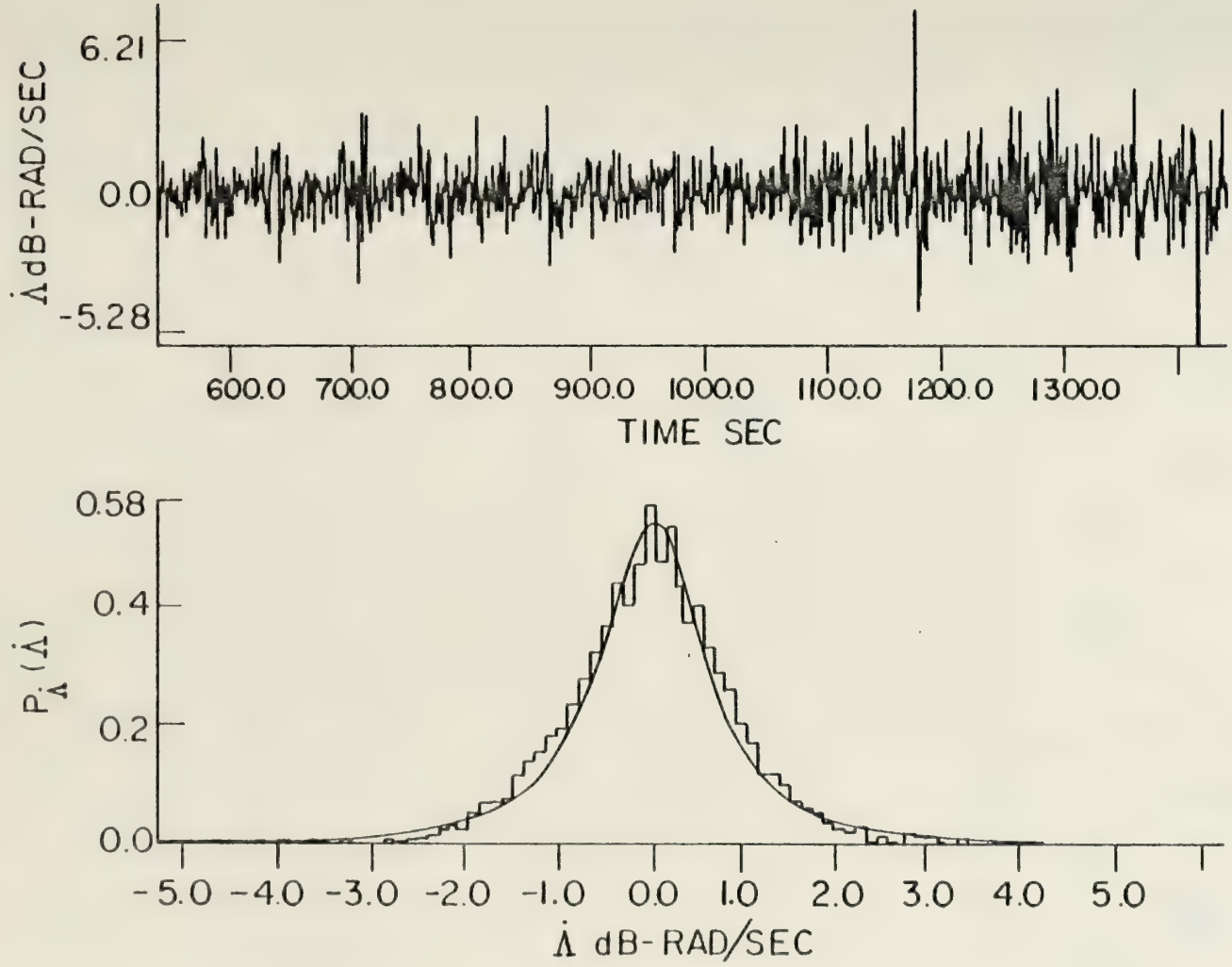


Fig. 71 The time series and histogram of $\dot{\Lambda}$ is plotted with the best fit of equation (1.7) for a representative run of the CASE experiment in which $A >> \nu$.

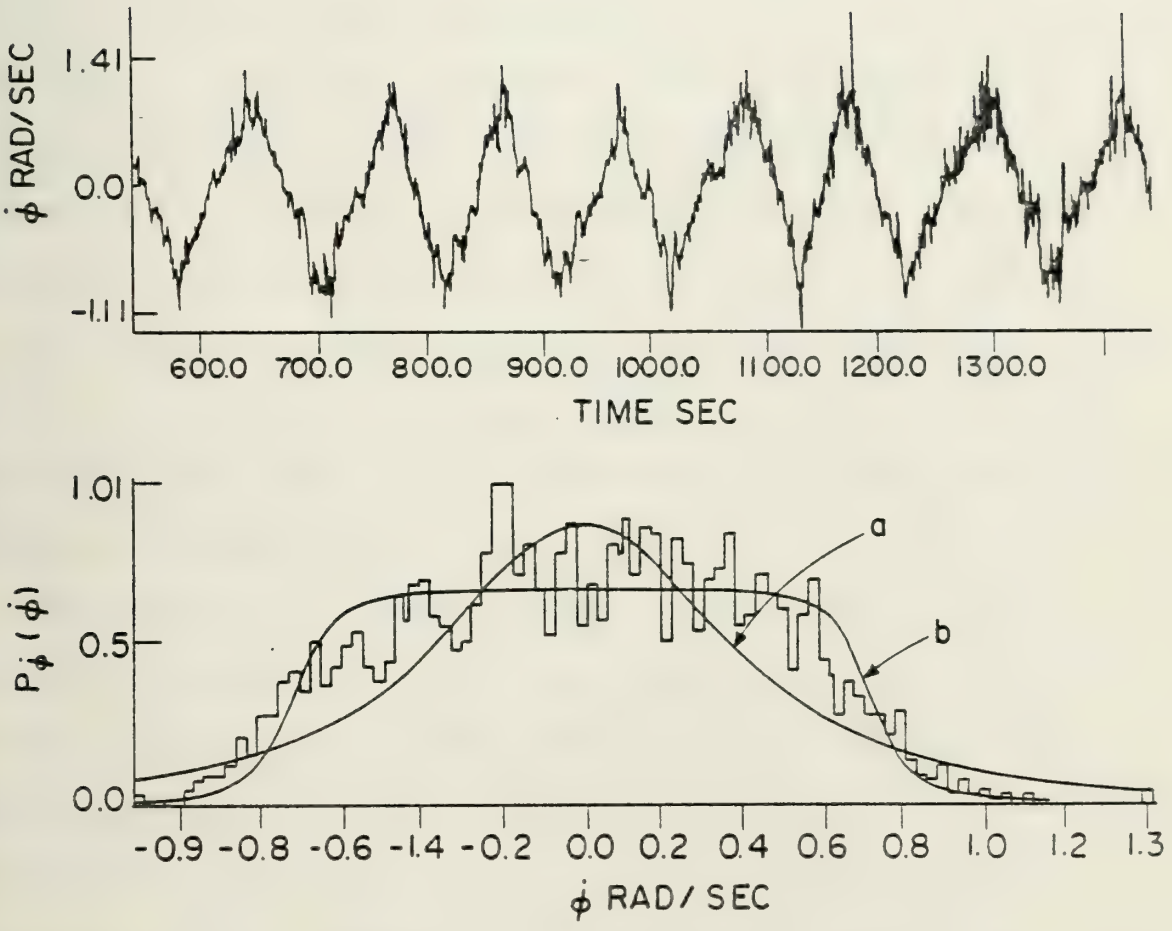


Fig. 72 The time series and histogram of $\dot{\phi}$ for the same run shown in Fig. 71 is plotted along with the best fit of equation (A8) which assumes no modulation (a) and the best fit of equation (1.176) which includes the effect of source induced modulation (b).

proposed in their model, and these values are in turn several orders of magnitude greater than the values predicted by the model (see Table XVIII and Figure 73). However, the rms single path phase fluctuation for the frequencies and ranges of the CASE experiment as predicted by an internal wave model only, appear to be $<< 2\pi$, and if so, the model would not be applicable to the CASE data. In order to obtain a very rough estimate of applicability, Equation (118) (for small $\beta$), Reference [34], has been plotted in Figure 74 for $\langle\phi^2\rangle = (2\pi)^2$, for range in km vs. frequency in Hz. That portion of the figure above and to the right of the line indicates that phase fluctuations due to internal waves are $> 2\pi$. The dotted lines represent the CASE experiment, the circles represent the Eleuthera data. Despite the assumptions involved, the good results of DMZ with the Eleuthera data (Table XI), and the poorer results with CASE, could be explained by Figure 74. It is apparent that some other mechanism must account for the fully saturated phase random process evident in the CASE experiment. Other possible mechanisms could include range rate, other ocean dynamic phenomena such as Rossby waves or meso-scale eddies, tidal currents magnified by bottom interaction at the receiver location, or rough scattering effects.

TABLE XVIII

Comparison of the average values of $\nu$ obtained from the CASE experiment to the predictions of the DMZ internal wave model. Also shown are the variances for the values of $\nu$ obtained from CASE.

| | | $\nu$ (mHz) | | | Variance of Case $\nu$ (mHz) | |
|---|---|---|---|---|---|---|
| | | DMZ | CASE | | | |
| Freq. (Hz) | 15 | .08 | 38* | 53 | 35* | 55 |
| | 33 | .18 | 19+ | 20 | 14+ | 15 |

*These values were computed leaving out runs 71-73 and 113-115 that exhibited significant non-zero means in the quadrature components.

+These values were computed leaving out runs 66-68 that exhibited significant non-zero means in the quadrature components.

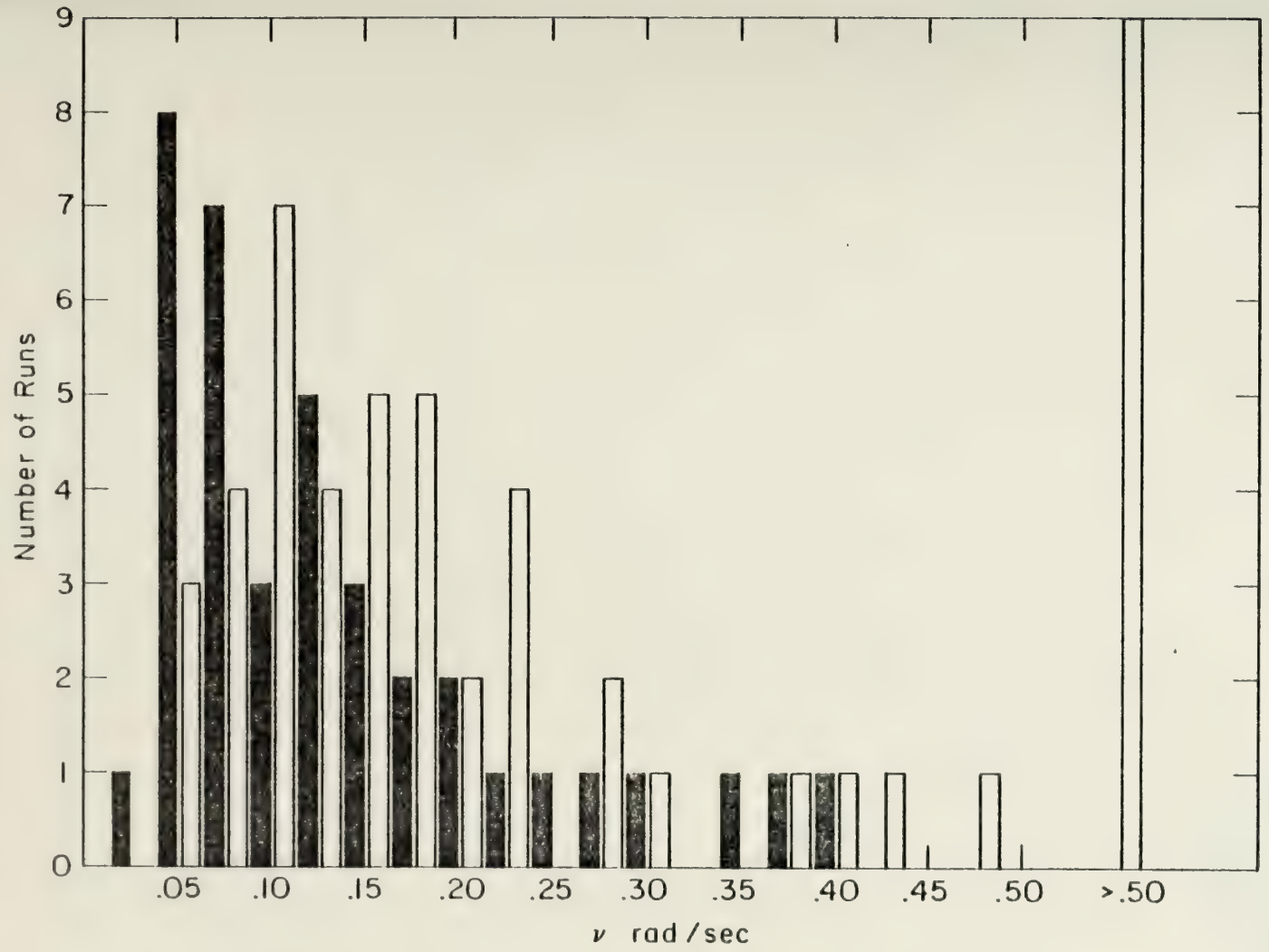


Fig. 73 Histogram of $\nu$ for all the runs analyzed in the CASE experiment. The interval is .025 rad/sec and the black bars are 33 Hz, the clear bars 15 Hz.

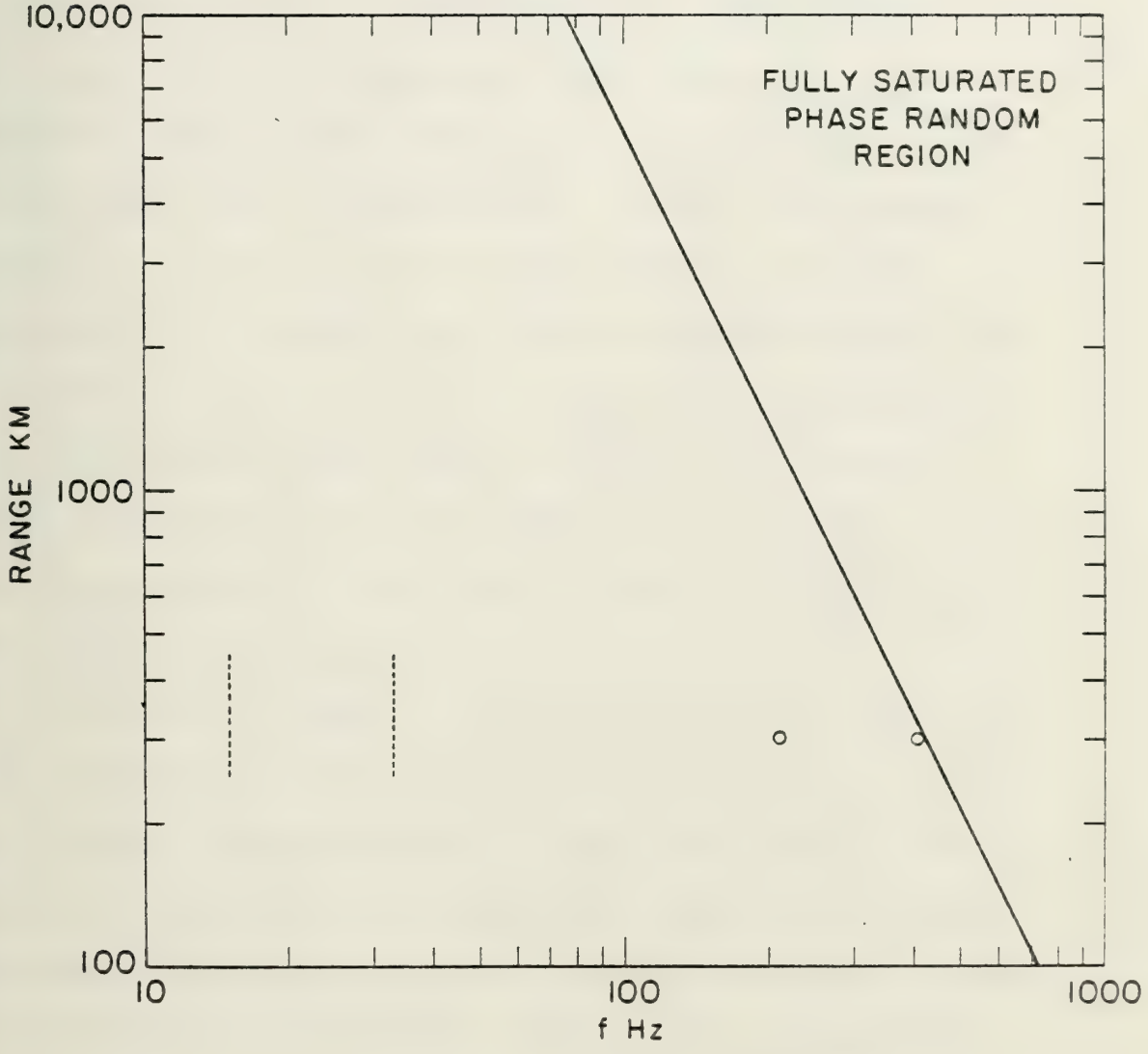


Fig. 74 Range vs. Frequency for $\langle \phi^2 \rangle^{1/2} = 2\pi$. The portion of the graph above and to the right of the line is the fully saturated region based on internal wave models. The CASE experiment is indicated by the dotted lines and the Eleuthera data by the circles.

Although no strong correlation was found between $\nu$ and range rate, it is apparent from Figure 75 that the larger values of $\nu$ were obtained at 0 range rate. I also investigated other correlations. I found none between $\nu$ and range, or time of day (see Figures 76 and 77 respectively). Because the CASE experiment was run over approximately one and one-half months with experimental runs occurring on many different days, tidal effects cannot be inferred from the times. At the present time, the dates of each of the runs are unavailable, making tidal checks impossible.

In Figures 78 and 79 I have plotted the values of $\nu$ vs. receiver for 15 Hz and 33 Hz respectively. Because each receiver was monitoring a given experimental run simultaneously I have connected the values of $\nu$ at each receiver by lines for each run. The time of day is noted to the left of the receiver 1 values. An "N" next to the time indicates that there was no range rate, either the source was fixed on the seamount or motionless for that run. For 15 Hz (Figure 78), receiver 2 consistently sees a higher value for $\nu$ than receiver 1, and receiver 3 consistently sees a larger value than receiver 1. Between receivers 2 and 3 the results are mixed. For 33 Hz (Figure 79), receiver 2 consistently sees a $\nu$ greater than

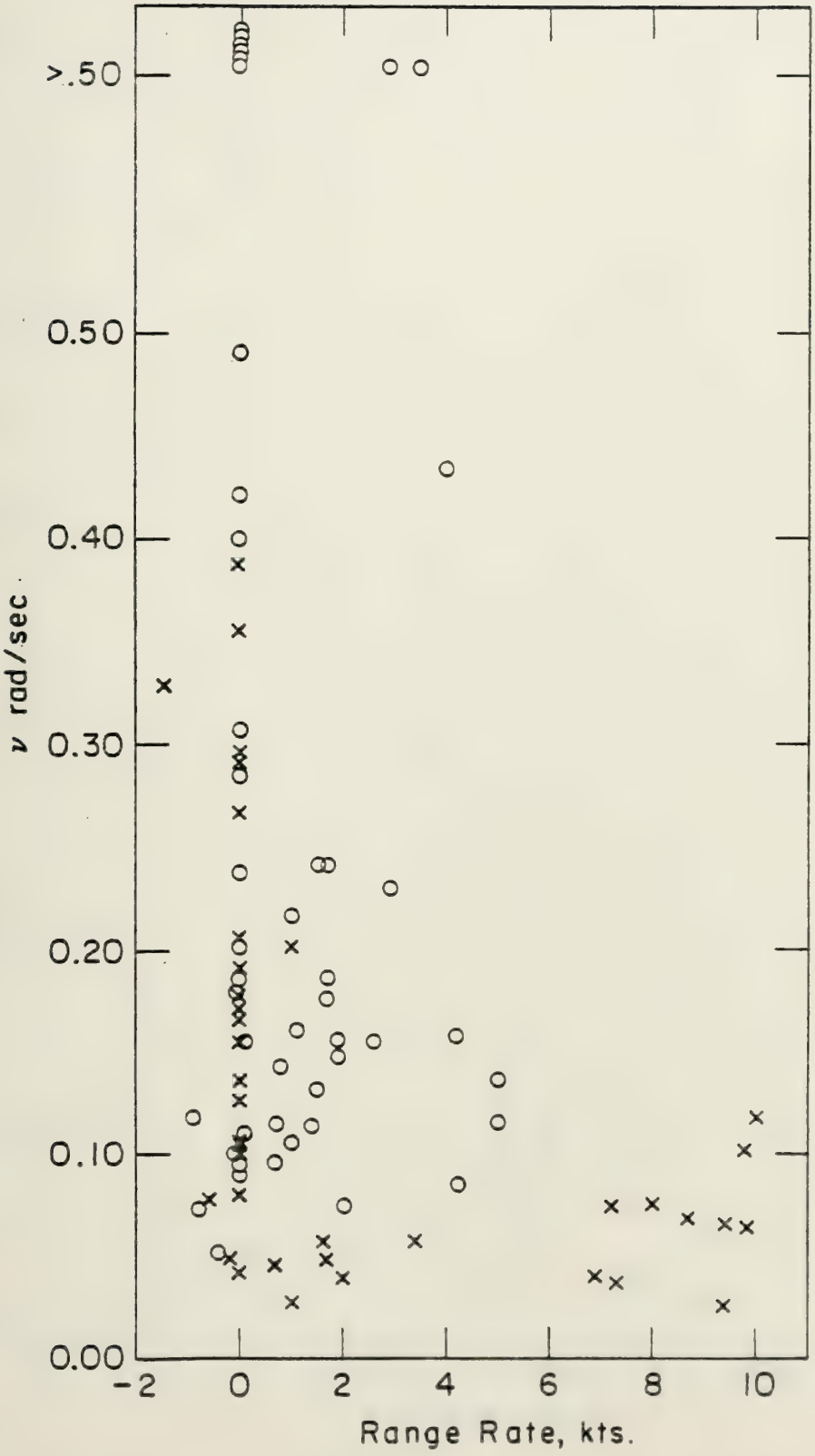


Fig. 75 A plot of $\nu$ vs. range rate. The circles represent 15 Hz, the x's 33 Hz.

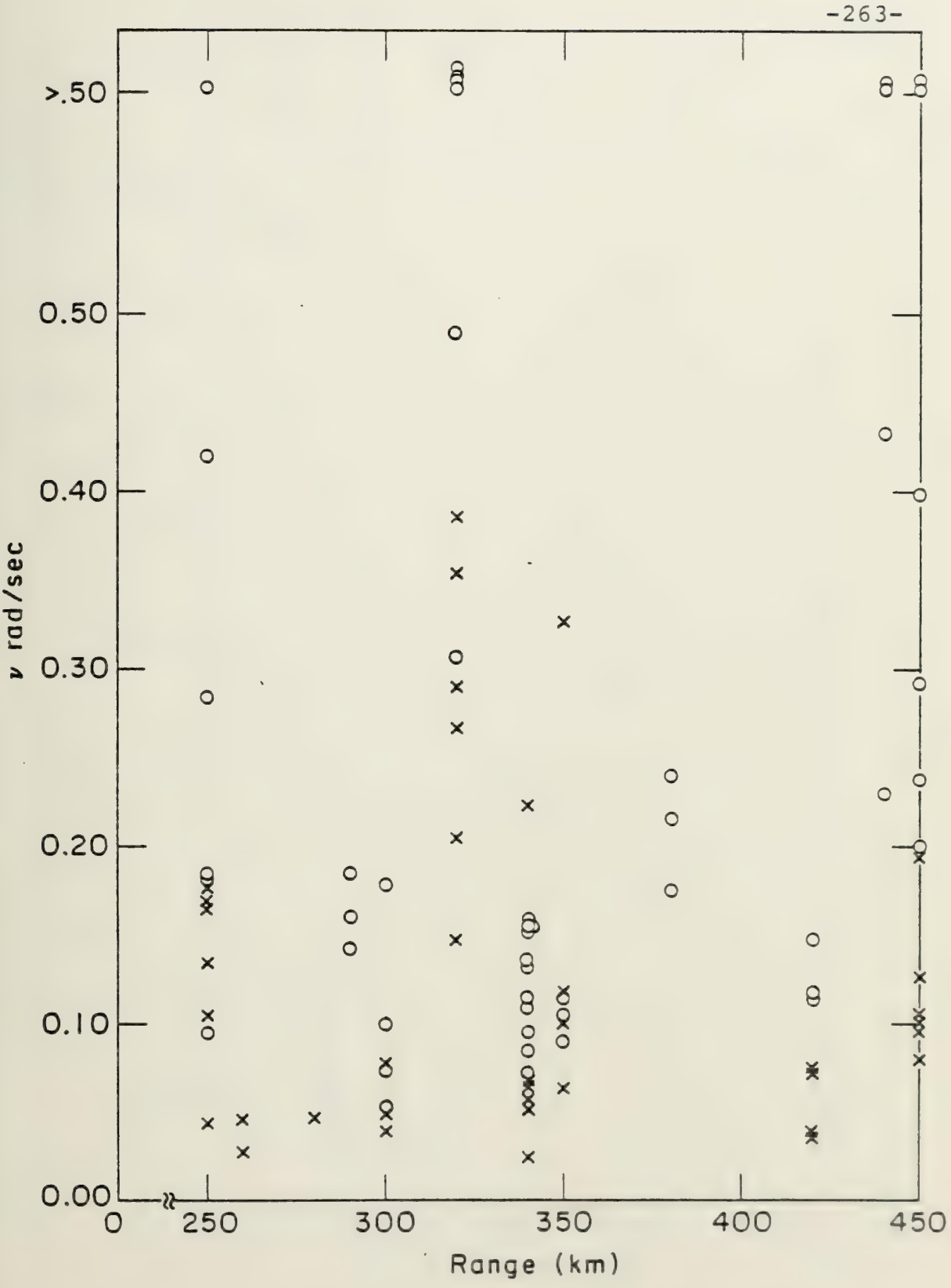


Fig. 76 A plot of $\nu$ vs. range. The circles represent 15 Hz, the x's 33 Hz.

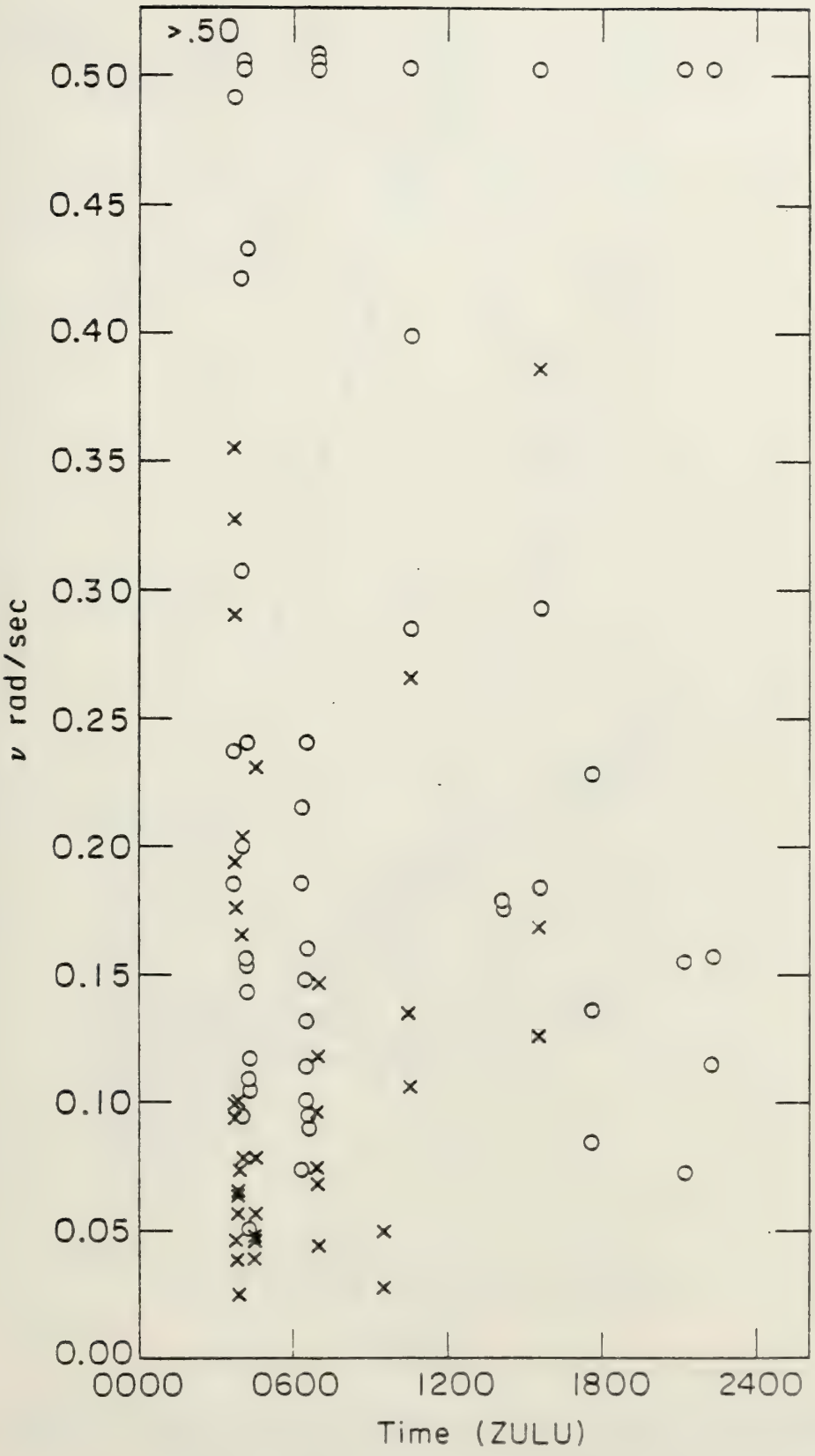


Fig. 77 A plot of $\nu$ vs. time of day. The circles represent 15 Hz, the x's 33 Hz.

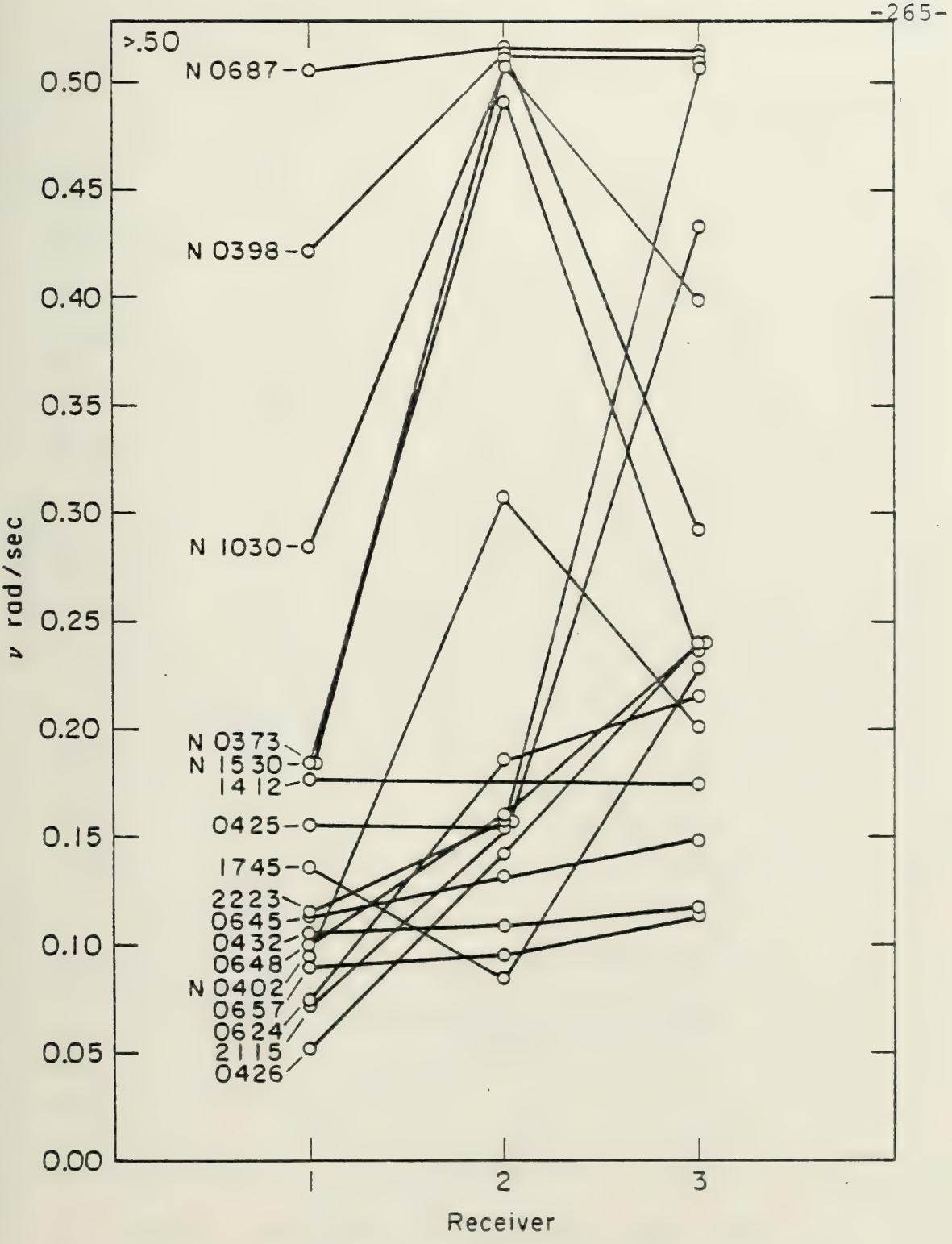


Fig. 78 Plot of $\nu$ vs. receiver for 15 Hz. The lines connect values of $\nu$ obtained simultaneously at each receiver. The start times for each run (ZULU) are indicated to the left of the receiver 1 values. The N indicates a zero range rate run.

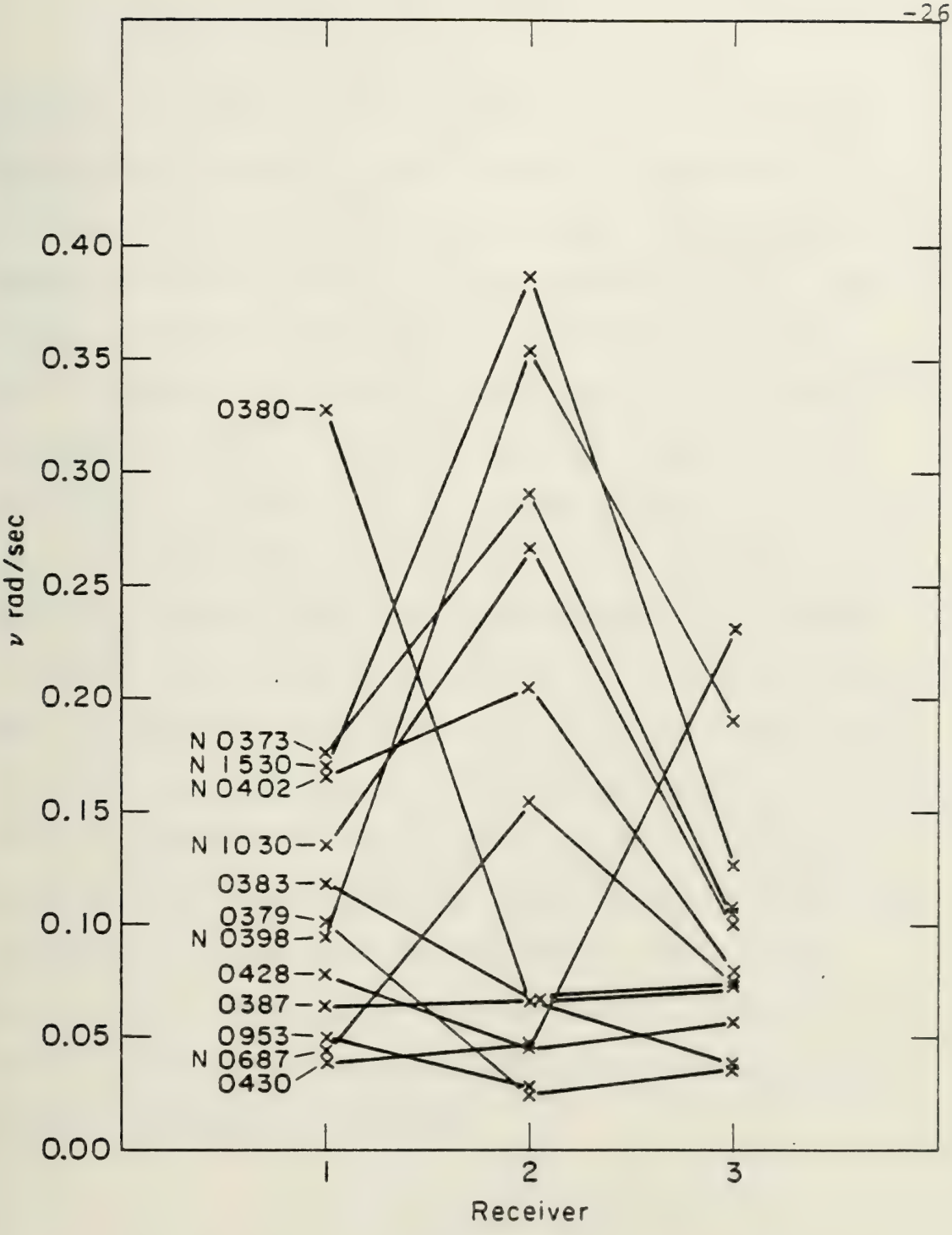


Fig. 79 Plot of $\nu$ vs. receiver for 33 Hz. The lines connect values of $\nu$ obtained simultaneously at each receiver. The start times for each run (ZULU) are indicated to the left of the receiver 1 values. The N indicates a zero range rate run.

receiver 3. For 8 of the 12 runs, smaller values of $\nu$ are seen at receiver 3 than are seen at receiver 1. Between 1 and 2 the results are mixed. These results suggest the possibility of rough scattering or a tidal current phenomena which would be receiver dependent. Note, however, that the no range rate runs ("N") for both frequencies all exhibit the same pattern, with low values at receiver 1, the highest values at receiver 2, and low values again at receiver 3. For all receivers range rate groups $\nu$ at lower values than the no range rate runs, the latter having a consistently higher mean. Thus, as observed earlier (Figure 75), there does appear to be some small correlation with range rate to the extent that either there is range rate in which case $\nu$ is independent of the amount, or there isn't, in which case $\nu$ exhibits a higher mean and variance. This is more graphically illustrated in Figures 80-85 in which I have plotted $\nu$ vs. range rate now separating the values by receiver as well as frequency.

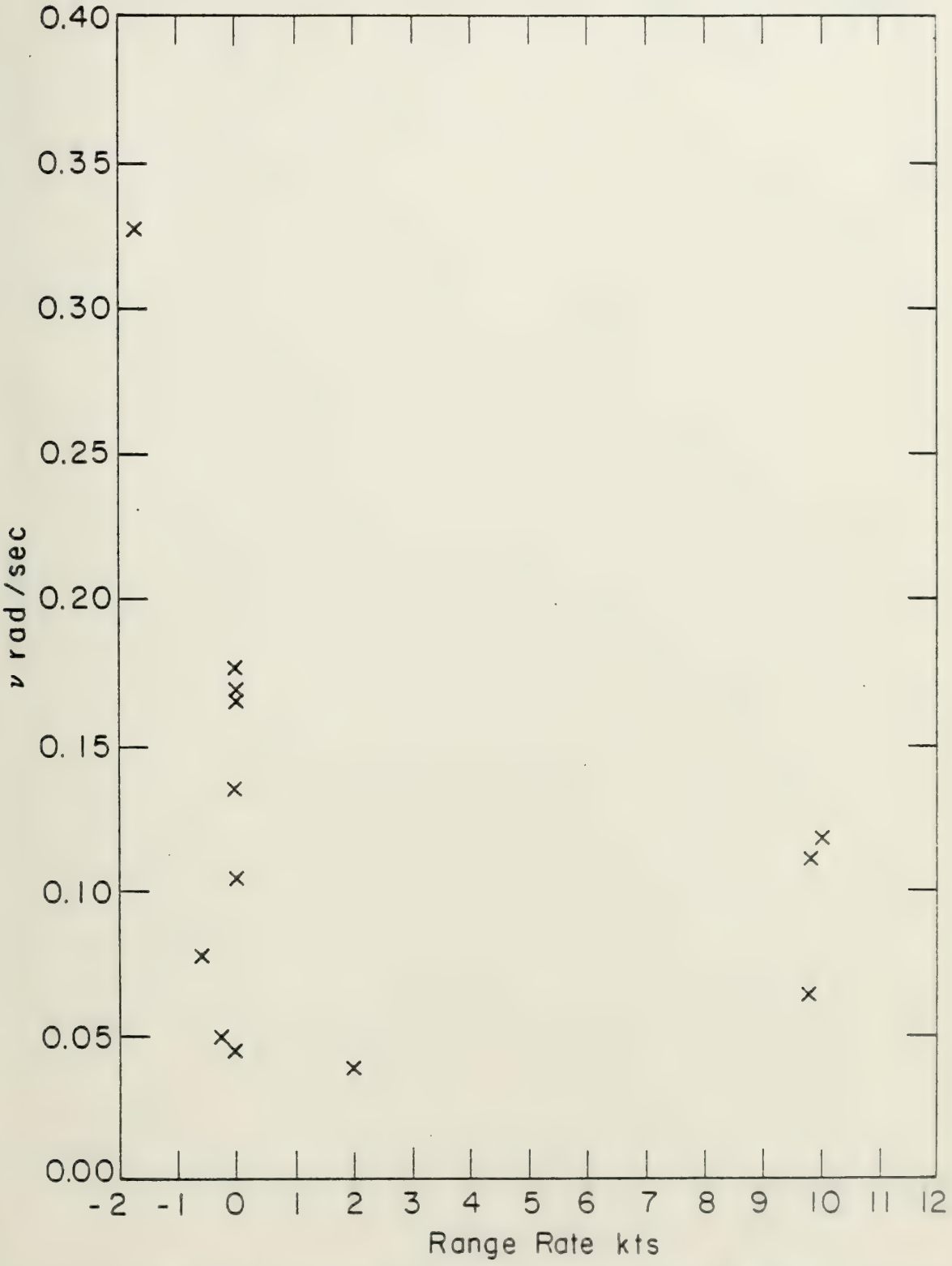


Fig. 80 A plot of $\nu$ vs. range rate for the 33 Hz signal measured at receiver 1.

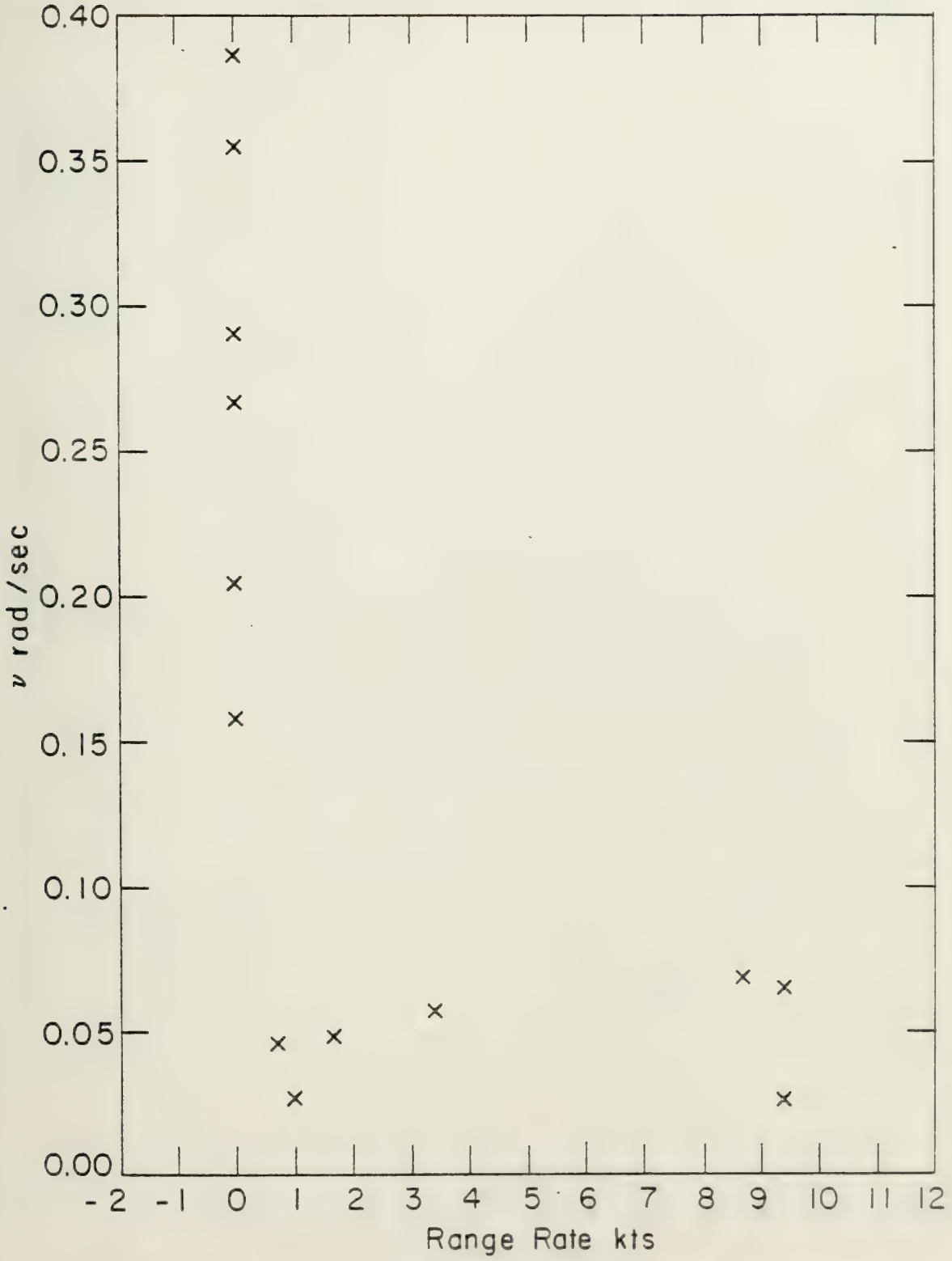


Fig. 81 A plot of $\nu$ vs. range rate for the 33Hz signal measured at receiver 2.

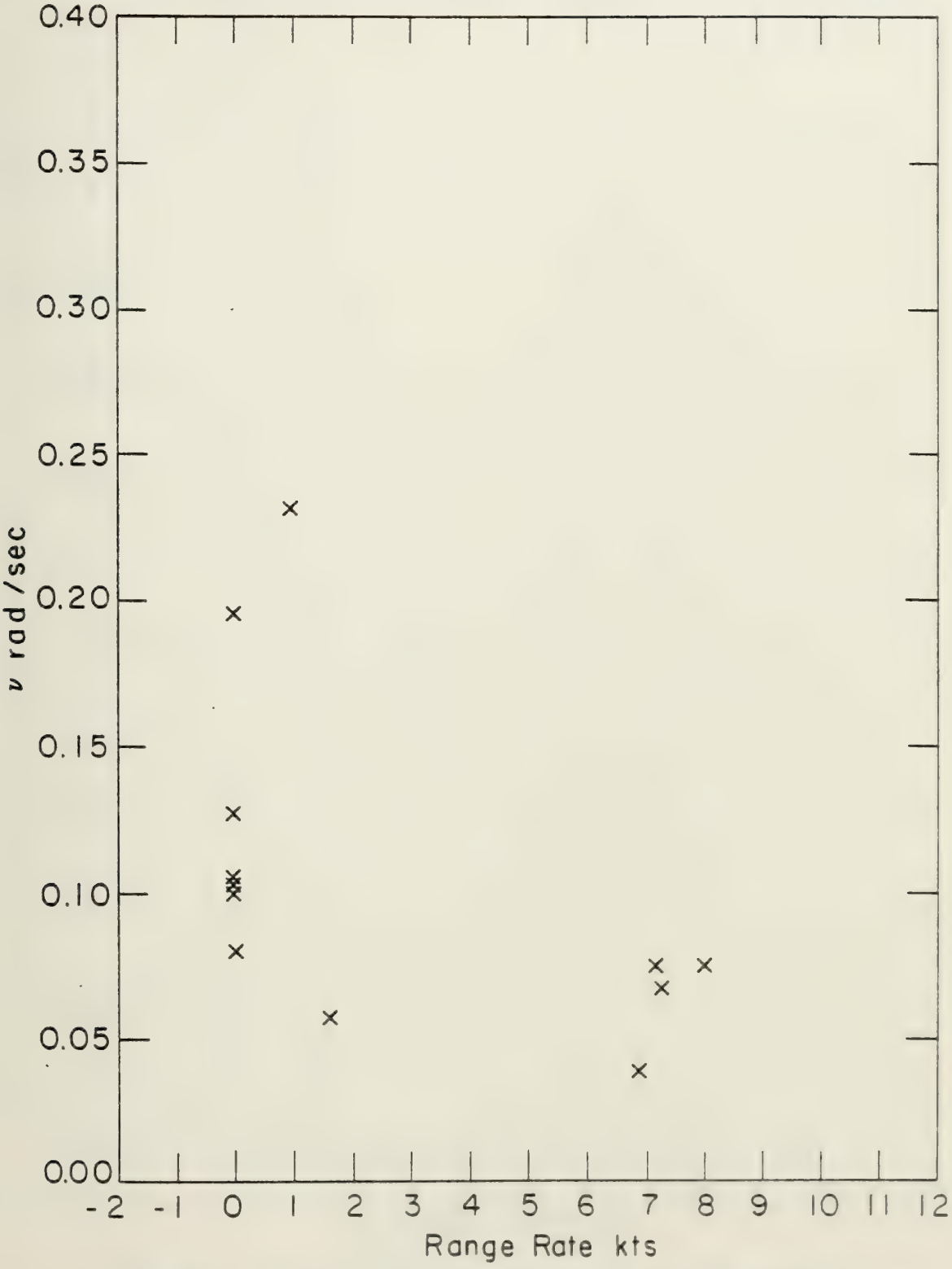


Fig. 82 A plot of $\nu$ vs. range rate for the 33 Hz signal measured at receiver 3.

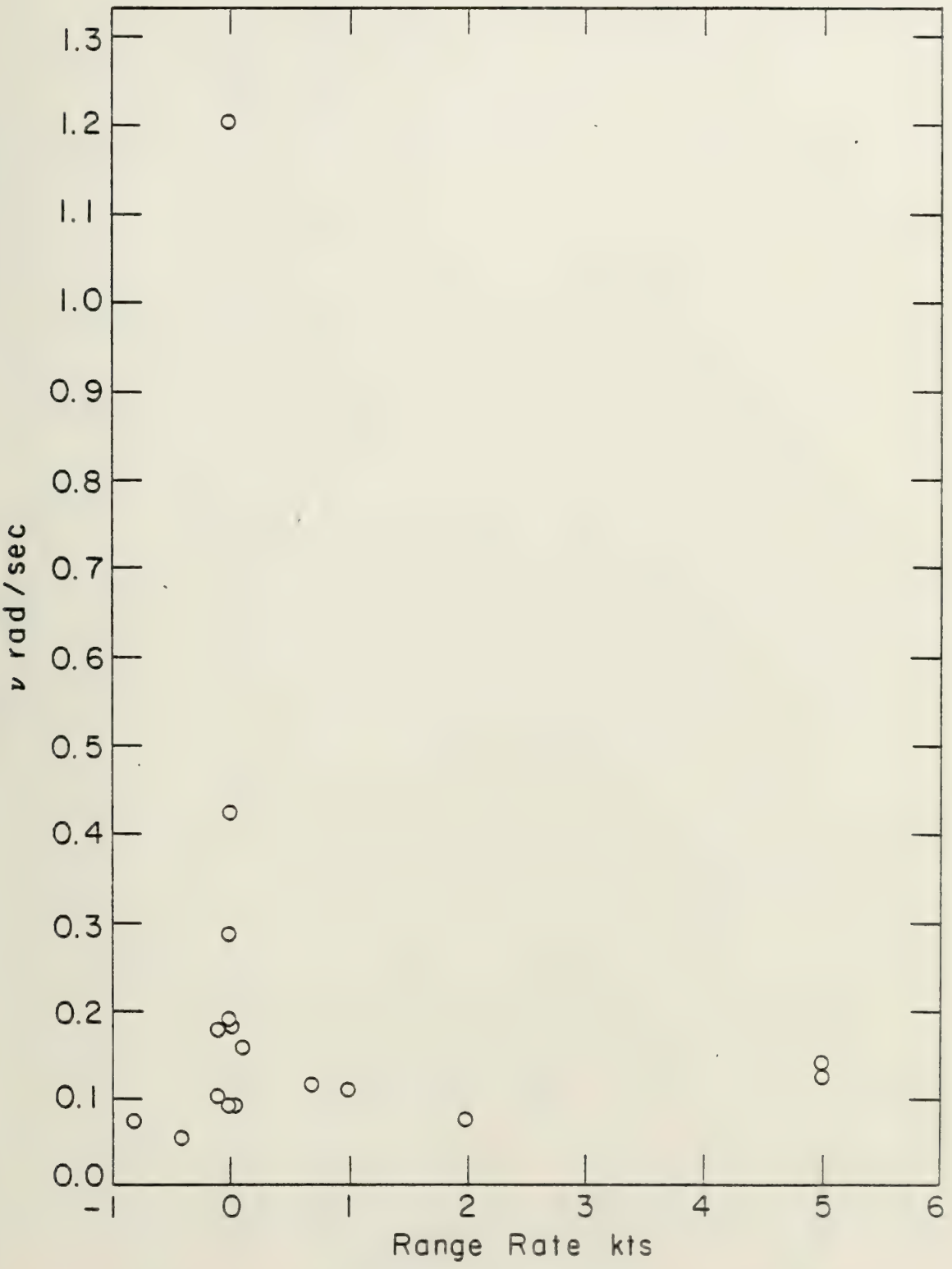


Fig. 83 A plot of $\nu$ vs. range rate for the 15 Hz signal measured at receiver 1.

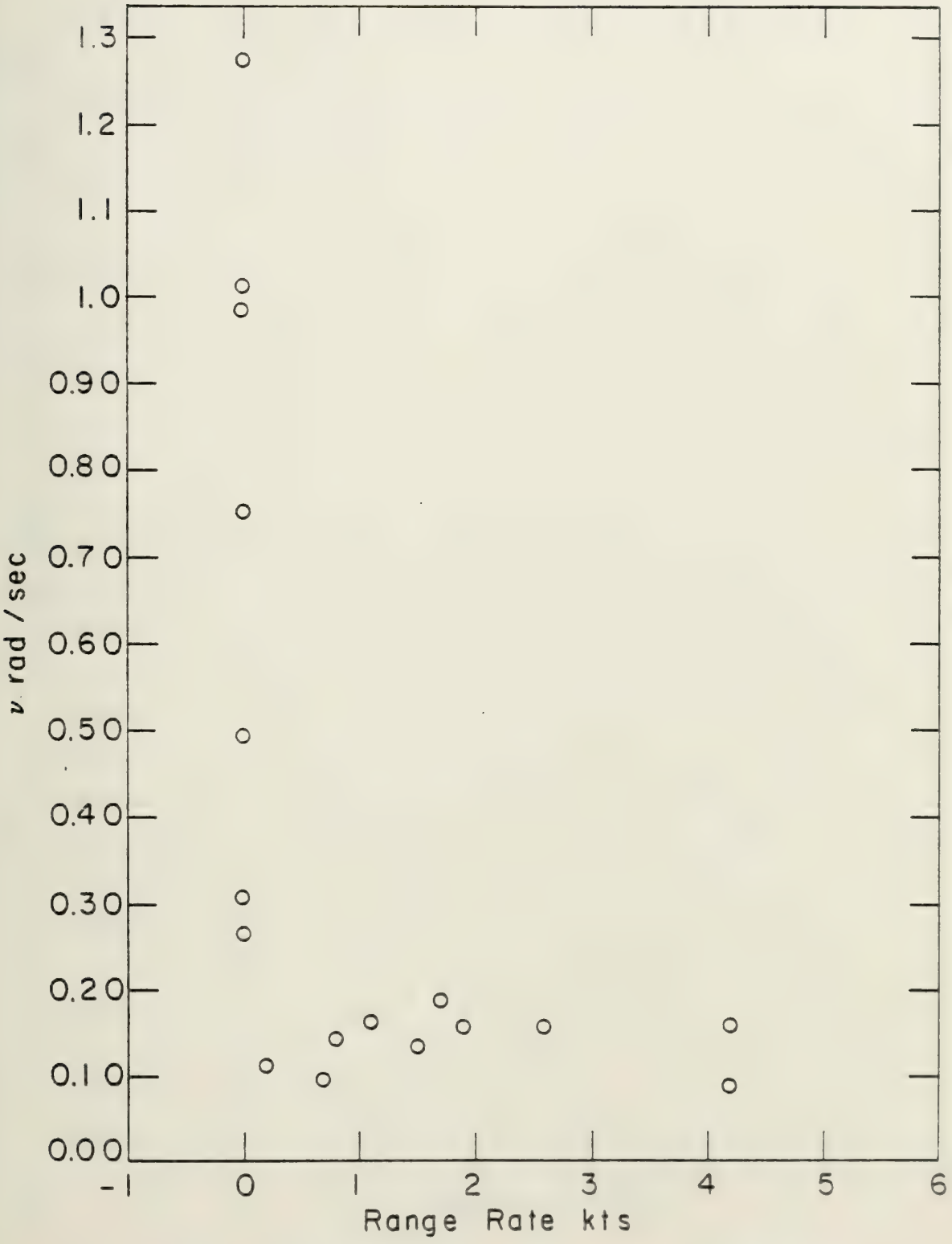


Fig. 84 A plot of $\nu$ vs. range rate for the 15 Hz signal measured at receiver 2.

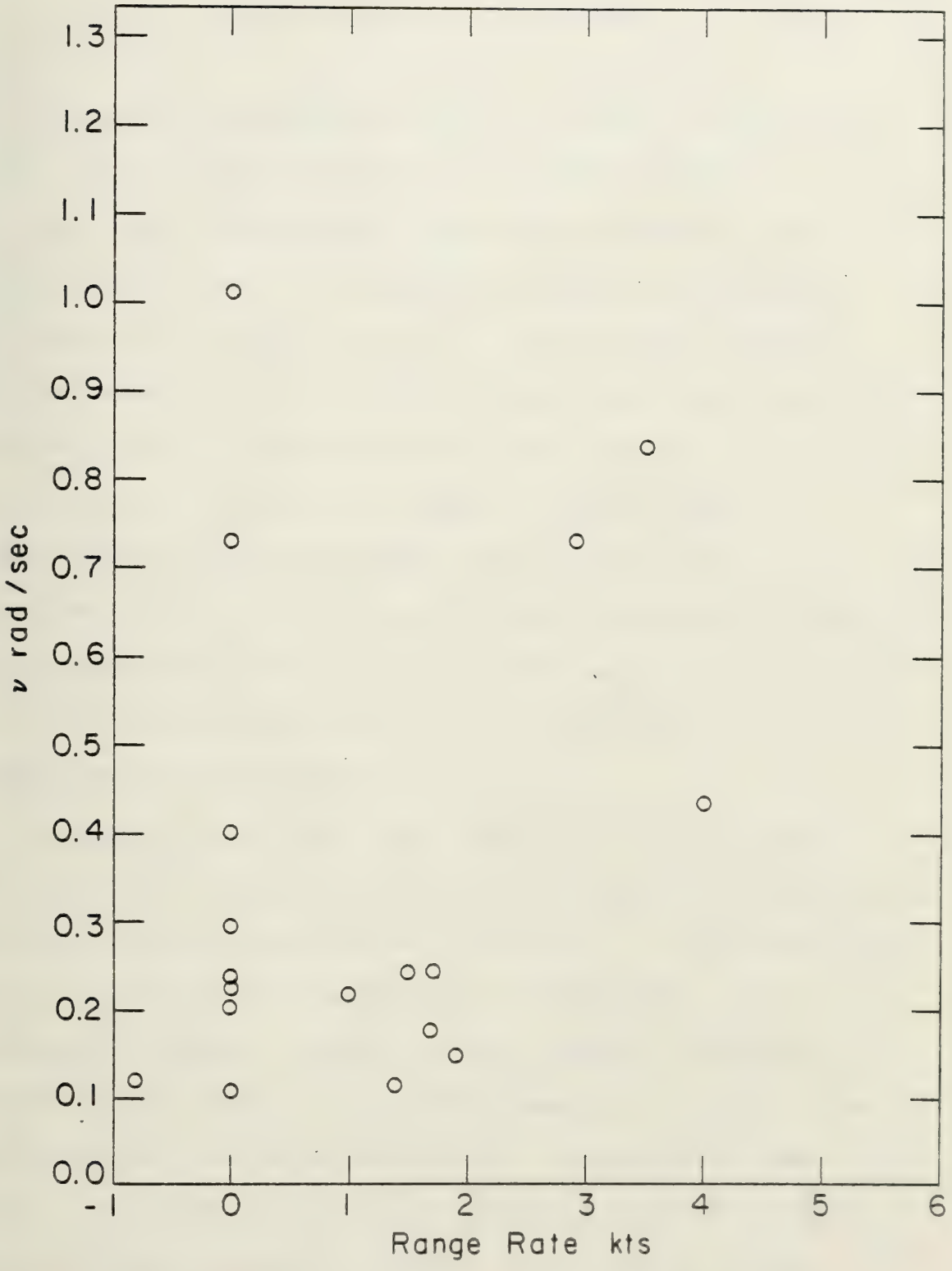


Fig. 85 A plot of $\nu$ vs. range rate for the 15 Hz signal measured at receiver 3.

# DISCUSSION AND CONCLUSIONS

The major contributions of this thesis are twofold. First, on the theoretical front the understanding of the statistics of acoustic signals propagated to long ranges in the ocean has been significantly advanced by the derivation of many new pdf's, particularly for the rate variables and joint pdf's of amplitude and amplitude rate, as well as the theoretical development of the effects of modulation. Second, the application of this new theory to ocean acoustic data has revealed new understanding of the effects of finite bandwidths and/or modulation on the statistics, as well as a clearer picture of the limitations of current models relating $\nu^2$ to ocean or experimental phenomena.

To be more specific, the completion of the family of pdf's for the single source and particularly the derivation of $P_{\dot{\Lambda}}(\dot{\Lambda})$ has permitted direct measure of $\nu^2$ from amplitude quantities which are independent of bandwidth and/or modulation effects. However, more research is needed to understand the effects of non-stationarities in $\sigma_1^2$ on the amplitude and amplitude rate pdf's. Although $\sigma_1^2$ does not appear explicitly in $P_{\dot{\Lambda}}(\dot{\Lambda})$, non-stationarities in $\sigma_1^2$ will possibly have some small effect. The effect, however, will be related to the rate of change of $\sigma_1^2$ and not to the

absolute change which would affect those variables in which $\sigma_1^2$ appears explicitly, so that measurement of $\nu^2$ via $\dot{\Lambda}$ is the preferred method.

The Eleuthera data analysis reveals that for measuring $\nu^2$ use of the time series and histograms of $\dot{\phi}$ and Equation (A8) apply only when $B << 2\nu$, $A << \nu$, and the Doppler shift due to relative source/receiver motion is $<< 2\nu$. It is true that relative source/receiver motion induces Doppler modulation, which is path dependent as each path has a different arrival angle at the receiver. However, in forming $\dot{\Lambda}$, or, in fact, any of the amplitude or amplitude rate variables, the mean Doppler is removed and it is only the path to path differential Doppler that remains. For $\dot{\phi}$, however, the mean Doppler as well as the differential Doppler contribute, and naive use of Equation (A8) on $\dot{\phi}$ will result in error. Even when the mean phase-rate is removed, as was done with the Eleuthera data, we discover that a new criterion must be met, namely that the error in removing the mean phase rate must be $<< 2\nu$.

Recognition of the $\dot{\Lambda}$ method of measuring $\nu^2$ is alone one of the major contributions of this research. However, a more thorough analysis is in order to determine the effect of the differential Doppler on the pdf's of

amplitude, amplitude rate, and phase rate when there is relative source/receiver motion. Because arrival angles are small for long-range propagation, it is anticipated that this effect will be small if not negligible in most cases. For the Eleuthera data, the mean drift rate along the transmission path was on the average 100 m/hr [12]. Assuming a maximum arrival angle of 14° the maximum differential Doppler shift is $1 \times 10^{-4}$Hz at 220Hz and $2 \times 10^{-4}$Hz at 406Hz, an order of magnitude less than $\nu$ for these data. For the CASE data, the differential Doppler was also negligible for all the runs analyzed.

In addition to range rate, other mechanisms which affect the value of $\nu^2$ must be researched. Analysis of the CASE data revealed that some mechanism other than internal waves must account for the fully saturated phase random nature of the data. My preliminary correlations indicate that a receiver related phenomenon such as slope-influenced tidal currents, or rough scattering, would be a good place to start. However, other mechanisms including Rossby waves, meso-scale eddies, etc. cannot be counted out. I must confess to some feeling of uneasiness surrounding the great run to run variance of the measured values of $\nu^2$ in the CASE experiment. Clearly a mechanism of some temporally varying nature must be

accountable. This again points toward a tidal phenomena. The Eleuthera data reveal a temporally stable $\nu^2$, even more so than Hamblen [9] discovered, because his analysis includes what is now recognized as a Doppler error.

The analysis of effects of finite bandwidth and/or modulated signals coupled with the new confidence in obtaining $\nu^2$ minus these effects has revealed a potentially powerful technique for separating source and ocean effects in the received signal. This technique uncovered the effect of the Doppler error in the Eleuthera data with great improvement in crossing rate predictions, and predicted the bandwidth of the modulation of the CASE data with an average error of 8%. This technique could be refined by use of more sensitive statistical tests such as the Kolmogorov-Smirnov test. Also the pdf's for many different kinds of modulation could be tried, not only to determine such parameters of the modulation as its bandwidth, but also the nature of the modulation itself when it is unknown, by comparing the performance of the selected densities on the histograms.

Aside from the applications of the amplitude statistics to distant shipping noise problems [4,5] the analysis of the statistics of multiple source cases is a

relatively untapped reservoir especially for the rate statistics. In order to improve predictions in the tails of the densities whose exact solutions remain unknown, the Chernov bound or "tilted" density [25] approach mentioned earlier should be investigated. I believe, however, that the analysis presented is complete enough, and the problems remaining few enough to warrant investigation into the applications of this analysis. The coherent source analysis may be a reasonable model for determining the statistics for the signal plus ocean noise. The multiple source cases analyzed may well be applicable to other noise problems. Table III provides a comprehensive summary of the state of this analysis at the present time.

The analysis contained in Appendix C, relying on some results of earlier investigators in fields other than acoustics, completes the solution of the statistics for the amplitude for $N \leq 3$ paths. For $N \geq 4$ I have shown with the computer simulation that limiting pdf's suffice. More research is needed into the exact nature of $P_{\dot{\theta}_n}(\dot{\theta}_n)$, the pdf for the single path phase. As previously noted by Hamblen [9] and as supported by the analysis in Appendix C, the rate densities of amplitude and multipath phase for $N$ small cannot be found unless $P_{\dot{\theta}_n}(\dot{\theta}_n)$

is known. No investigators to date have related, to my knowledge, any knowledge, experimental or theoretical, about $P_{\dot{\theta}_n}(\dot{\theta}_n)$ aside from the usual Gaussian or uniform assumptions as I have done. In Appendix C I have solved for $P_{\dot{\chi}}(\dot{\chi})$ when $N = 2$ paths making these assumptions.

In summary, the theoretical analysis of long range acoustic propagation presented in this thesis has been supported by both computer simulation and comparison with data from ocean acoustic experiments with extremely satisfactory results. I hope that the analysis presented and the conclusions reached will be of use to other researchers in the future.

REFERENCES

[1] Lord Rayleigh, Phil. Mag., p. 75, (Aug. 1880).

[2] P. G. Bergmann, "Intensity Fluctuations", Physics of Sound in the Sea, National Defense Research Committee, 158-172, (1946).

[3] I. Dyer, J. Acoust. Soc. Am., 48, 337-345 (1970).

[4] I. Dyer, J. Acoust. Soc. Am., 53, 564-570 (1973).

[5] P. Mikhalevsky, and I. Dyer, J. Acoust. Soc. Am., 63, 732-738, (1978).

[6] W. Mark, J. Acoust. Soc. Am., 52, 413-425, (1972).

[7] M. Nakagami in W. C. Hoffman, Ed., Statistical Methods in Wave Propagation, Pergammon Press, NY, (1960).

[8] M. S. Longuet-Higgins, J. Geophy. Res., 80, 2688-2694, (1975).

[9] W. Hamblen, Ph.D. Thesis, M.I.T., Camb., MA, (1977) (unpublished).

[10] S. O. Rice, Bell Syst. Tech. J., 23, 282-332, (1944); 24, 46-156, (1945).

[11] F. Dyson, W. Munk, B. Zetler, J. Acoust. Soc. Am., 59, 1121-1133, (1976).

[12] R. Porter, and R. Spindel, J. Acoust. Soc. Am., 61, 943-958, (1977).

[13] J. J. Anton, "A Fluctuation Data Base for the CASE Experiment," Systems Control, Inc., Tech. Rep. 5204-2, April 1978.

[14] H. Cramer, Mathematical Methods of Statistics, Princeton University, Princeton, NJ, (1946).

[15] I. Dyer and G. W. Shepard, J. Acoust. Soc. Am., 61, 937-942, (1977).

[16] L. Slater, Confluent Hypergeometric Functions, Cambridge University Press, (1960).

[17] Erdelyi, Ed., Higher Transcendental Functions, Volume I, McGraw-Hill, NY, (1953).

[18] M. Abramowitz, Ed., Handbook of Mathematical Functions, National Bureau of Standards, Washington, D.C., (1970).

[19] N. Pran, Sankyha: The Indian Journal of Statistics, 2, 153-166, (1951).

[20] S. Rushton, Sankyha: The Indian Journal of Statistics, 13, 369-411, (1952).

[21] P. Morse and H. Feshback, Methods of Theoretical Physics, Part I, McGraw-Hill, NY, (1953).

[22] J. O'Connor, Statistics of Sea Noise, M.S. Thesis, M.I.T., Cambridge, MA, (1973) (unpublished).

[23] K. Pearson, Tables of the Incomplete Gamma Function, Cambridge University Press, (1965).

[24] I. S. Gradshteyn, and I. W. Ryzhik, Table of Integrals Series and Products, Academic Press, NY, (1965).

[25] H. Van Trees, Detection, Estimation, and Modulation Theory, Part I, John Wiley and Sons, Inc., NY (1963).

[26] J. Jao, and M. Elbaum, Proc. I.E.E.E., 66, 781-789, (1978).

[27] P. Mikhalevsky, "Computer Simulation - Phase Random Model", M.I.T., Camb., MA, (1978) (unpublished).

[28] R. Bucy, C. Hecht, and K. D. Senne, "An Engineer's Guide to Building Nonlinear Filters", Vol. I, Appendix, Frank J. Seiler Research Laboratory Report SRL-TR-72-0004, May, (1972).

[29] J. S. Bendat and A. G. Piersol, Random Data: Analysis and Measurement Procedures, John Wiley and Sons, (1971).

[30] R. Porter, R. Spindel, and R. Jaffee, J. Acoust. Soc. Am., 53, 1691-1699, (1973).

[31] Private communication with R. Spindel.

[32] A. Gerlach, "Random Frequency Function Generation", NRL Report 7697, (1973).

[33] P. Mikhalevsky, "Collection of Graphics From the CASE Experiment", 2 Vols., M.I.T., Camb., MA, (1978), (unpublished).

[34] W. Munk, F. Zachariasen, J. Acoust. Soc. Am., 59, 818-838, (1976).

[35] See, for example, A. Drake, Fundamentals of Applied Probability Theory, McGraw-Hill, NY, (1951).

[36] Lord Rayleigh, Phil. Mag., p. 246, (Feb. 1899).

[37] J. Kluyver, "A Local Probability Problem," Proc. Roy. Acad. Amsterdam VIII, (1906).

[38] K. Pearson, and J. Blakeman, Drapers' Company Research Memoirs, Biometric Series, (1906).

# APPENDIX A

## FIRST ORDER DENSITIES FOR THE SINGLE NARROWBAND SOURCE

Assembled below are the pdf's associated with a single narrowband source and their characteristic functions [14].

Notation:

$P_\chi(\chi)$ is the pdf of random variable $\chi$

$M_\chi(\omega)$ is the characteristic function of $\chi$

$\mu_\chi$ is the expected value or mean of $\chi$

$\sigma_\chi^2$ is the variance of $\chi$

$\varepsilon = 10 \log_{10} e = 4.34...$

### A. Amplitude Densities

(1) $$P_\rho(\rho) = \frac{\rho}{\sigma_1^2} \exp[-\frac{\rho^2}{2\sigma_1^2}] \quad , \rho > 0 \; ; \quad \text{Rayleigh} \qquad \text{(A1)}$$

$$\mu_\rho = \sigma_1\sqrt{\pi/2} \quad , \quad \sigma_\rho^2 = \sigma_1^2(2 - \pi/2)$$

$$M_\rho(\omega) = \exp(-\frac{\omega^2\sigma_1^2}{4}) \; D_{-2}(-i\omega\sigma_1)$$

where $D_p(z)$ is the parabolic cylinder function [24].

(2) $P_\chi(\chi) = \frac{1}{2\sigma_1^2} \exp[-\frac{\chi}{2\sigma_1^2}]$ , $\chi > 0$ ; Exponential (A2)

$$\mu_\chi = 2\sigma_1^2, \ \sigma_\chi^2 = 4\sigma_1^4$$

$$M_\chi(\omega) = \frac{1}{1 - i2\sigma_1^2\omega}$$

(3) $P_\Lambda(\Lambda) = \frac{1}{2\varepsilon\sigma_1^2} \exp[\frac{\Lambda}{\varepsilon} - \frac{1}{2\sigma_1^2} \exp(\frac{\Lambda}{\varepsilon})]$ , $-\infty<\Lambda<\infty$;

Log-Rayleigh (A3)

$$\mu_\Lambda = \varepsilon[\ln 2\sigma_1^2 - \gamma] \ , \ \sigma_\Lambda^2 = \varepsilon^2 \frac{\pi^2}{6}$$

$$M_\Lambda(\omega) = (2\sigma_1^2)^{i\varepsilon\omega}\Gamma(1 + i\varepsilon\omega)$$

where $\gamma$ = Euler's constant = .5772...

$\Gamma(z)$ is the gamma function [24].

$$(4)\quad P_{\phi}(\phi) = \begin{cases} 1/2\pi & 0<\phi<2\pi \\ 0 & \text{otherwise} \end{cases} \quad ; \text{ Uniform} \qquad (A4)$$

$$\mu_{\phi} = \pi \ , \ \sigma_{\phi}^2 = \frac{\pi^2}{3}$$

$$M_{\phi}(\omega) = \frac{1}{\omega\pi} \exp(-i\omega\pi)\sin\omega\pi$$

B. Amplitude Rate Densities

$$(5)\quad P_{\dot{\rho}}(\dot{\rho}) = \frac{1}{\sqrt{2\pi\sigma_1^2\nu^2}} \exp[-\frac{\dot{\rho}^2}{2\sigma_1^2\nu^2}] \ , \ -\infty<\rho<\infty \ ; \text{ Gaussian}$$

(A5)

$$\mu_{\dot{\rho}} = 0 \ , \ \sigma_{\dot{\rho}}^2 = \sigma_1^2\nu^2$$

$$M_{\dot{\rho}}(\omega) = \exp(-\frac{1}{2}\omega^2\sigma_1^2\nu^2)$$

(6) $$P_{\dot{\chi}}(\dot{\chi}) = \frac{1}{4\nu\sigma_1^2} \exp[-\frac{|\dot{\chi}|}{2\sigma_1^2\nu}] \ , \ -\infty<\dot{\chi}<\infty \ ; \quad \text{Laplace} \qquad \text{(A6)}$$

$$\mu_{\dot{\chi}} = 0, \ \sigma_{\dot{\chi}}^2 = 8\sigma_1^4\nu^2$$

$$M_{\dot{\chi}}(\omega) = \frac{1}{1 + 4\omega^2\sigma_1^4\nu^2}$$

(7) $$P_{\dot{\Lambda}}(\dot{\Lambda}) = \frac{1/2\nu}{2\varepsilon[1 + \frac{\dot{\Lambda}^2}{4\varepsilon^2\nu^2}]^{3/2}} \ , \ -\infty<\dot{\Lambda}<\infty \ ; \ \text{Longuet-Higgins}$$

(A7)

$$\mu_{\dot{\Lambda}} = 0 \ , \ \sigma_{\dot{\Lambda}}^2 = \infty$$

$$M_{\dot{\Lambda}}(\omega) = 2\varepsilon\nu|\omega|K_1(2\varepsilon\nu|\omega|)$$

where $K_1(z)$ is the modified Bessel function of order one.

(8) For no modulation only:

$$P_{\dot{\phi}}(\dot{\phi}) = \frac{1/\nu}{2\left[1 + \frac{\dot{\phi}^2}{\nu^2}\right]^{3/2}} \quad , \quad -\infty<\dot{\phi}<\infty \quad ; \text{ Longuet-Higgins} \qquad (A8)$$

$$\mu_{\dot{\phi}} = 0 \quad , \quad \sigma^2_{\dot{\phi}} = \infty$$

$$M_{\dot{\phi}}(\omega) = \nu|\omega| K_1(\nu|\omega|)$$

# APPENDIX B

## THE ERLANG AND RELATED PDF's

The Erlang pdf (Equation 1.19, Section 1.2.1.1) was derived by A. K. Erlang in the early 1900's in connection with waiting times in telephone operations. It is the probability of the time until the $n^{th}$ arrival in a Poisson process, or the density of the $n^{th}$ order interarrival time [35]. Note that the first order interarrival time (L=1) is an exponential pdf. L can be extended to include noninteger values by merely replacing the factorial of the Erlang with the $\Gamma$ function and hence the name gamma pdf. Although mathematically valid, the simple physical interpretation of the Erlang breaks down when noninteger values of L are introduced. In the case of distant-shipping noise, L is an integer.

In the language of queing theory, it is interesting to note that determination of the pdf of $\chi$ for Case (c) of Section 1.2.1 in all its generality is the same as the solution for the pdf of the $n^{th}$ order interarrival time in a renewal process in which the first order interarrival times are independent random variables distributed according to Equation (1.19) with different $\mu_i$ and $L_i$.

Though originally derived independently, the slightly less general chi-square pdf with n degrees of

freedom can be derived from Equation (1.19) by merely letting a = 1/2 and L = n/2 [14].

If we let $a = m/\mu_x$ and L = m, and make the transformation $R = \chi^{1/2}$ in Equation (1.19), we have the density of the short time rms pressure:

$$P_R(R) = \frac{2m^m R^{2m-1}}{\Gamma(m)\mu_x^m} e^{-(m/\mu_x)R^2} \qquad (B1)$$

In terms of the statistics for $\chi$, $m = (\mu_x/\sigma_x)^2$, which is the inverse of the normalized variance of $\chi$. Equation (A1) was first proposed by M. Nakagami in 1943 [7] to describe the envelope of long range h.f. radio wave propagation undergoing rapid fading and is known as the "m" distribution. When m=1, Equation (B1) is the Rayleigh distribution as expected. One can note that the phase-random model of long range acoustic propagation is analogous to the rapid fading of long range h.f. propagation. Thus, the connection between the "m" and Erlang, or gamma pdf, is more than just a functional similarity; they describe in alternative language the same process.

# APPENDIX C

## THE STATISTICS FOR $N \leq 3$ PATHS

The solution for the pdf of the amplitude of a vector which is the sum of many vectors added with random phases has been a problem of long standing interest. Lord Rayleigh was probably the first to investigate this problem in two papers, the first published in 1880 [1], and the second in 1899 [36]. He was, however, concerned with the limit when the number of summed vectors is large, and he derived the density of the amplitude for this limiting case which bears his name. The first investigators to tackle the problem of small $N$ (note that the characterization of summed paths as random vectors is mathematically identical) was Kluyver (1905) [37], and Pearson (1906) [38], the latter in connection with mosquito migration!

For arbitrary $N$ and unequal amplitudes, $A_i$, Kluyver [37] obtained the general solution in integral form as follows:

$$ {}_N P_\rho(\rho) = \rho \int_0^\infty u \quad J_o(u\rho) \prod_{i=1}^{N} J_o(uA_i)\,du \qquad \text{(C1)} $$

For the problem of sums of independent multipaths, we have that $A_i = r$ for all i and thus:

$$ {}_{N}P_{\rho}(\rho) = \rho \int_{o}^{\infty} u\, J_{o}(u\rho)[J_{o}(ur)]^{N}\, du \qquad (C2) $$

Pearson [38] obtains solutions of this equation for $N = 2,3$ and for $N \geq 4$ he obtains solutions in terms of series of Bessel functions.

C.1 Solution for $N = 2$

Though I derived this solution independently, it was Pearson [38] who obtained it first. For two paths I have for the quadrature components:

$$ \begin{aligned} X &= r(\cos\theta_1 + \cos\theta_2) \\ Y &= r(\sin\theta_1 + \sin\theta_2) \end{aligned} \qquad (C3) $$

where $\theta_1$ and $\theta_2$ are independent random variables distributed uniformly between 0 and $2\pi$. Forming the sta mean square pressure $\chi$ from Equations (C3),

$$ \begin{aligned} \chi = r^2(&\cos^2\theta_1 + 2\cos\theta_1\cos\theta_2 + \cos^2\theta_2 + \sin^2\theta_1 \\ &+ 2\sin\theta_1\sin\theta_2 + \sin^2\theta_2) \end{aligned} \qquad (C4) $$

Using some trigonometric identities I have

$$ \chi = 2r^2 + 2r^2\cos(\theta_1 - \theta_2) \qquad (C5) $$

Taking advantage of the symmetry of the cosine the random variable defined by $\theta_1 - \theta_2$ behaves as if it were uniformly distributed between 0 and $\pi$. Thus, forming the cumulative distribution function:

$$2^{P_{<\chi}}(\chi) = \frac{1}{\pi} \int_{o}^{\cos^{-1}\left(\frac{\chi-2r^2}{2r^2}\right)} d\theta, \quad 0 < \theta < \pi \qquad (C6)$$

and

$$2^{P_{\chi}}(\chi) = \frac{\partial}{\partial\chi}\, 2^{P_{<\chi}}(\chi) \qquad (C7)$$

I obtain the final solution:

$$2^{P_{\chi}}(\chi) = \frac{1}{\pi} \quad \frac{1}{\sqrt{4r^2\chi-\chi^2}} \qquad 0 < \chi < 4r^2 \qquad (C8)$$

where,

$$\mu_{\chi} = 2r^2, \quad \sigma_{\chi}^2 = 2r^4$$

Making the transformation to $\rho$ and $\Lambda$:

$$2^{P_{\rho}}(\rho) = \frac{2}{\pi} \frac{1}{\sqrt{4r^2-\rho^2}}, \qquad 0 \leq \rho < 2r \qquad (C9)$$

$$\mu_{\rho} = 4r/\pi, \quad \sigma_{\rho}^2 = r^2(2 - 16/\pi^2)$$

and,

$$2^{P_{\Lambda}}(\Lambda) = \frac{e^{\Lambda/2\varepsilon}}{\varepsilon\pi} \quad \frac{1}{\sqrt{4r^2-e^{\Lambda/\varepsilon}}}, \quad -\infty < \Lambda < 2\varepsilon\ell n2r$$

$$\mu_{\Lambda} = 2\varepsilon\ell nr, \; \sigma_{\Lambda}^2 = \varepsilon^2[\pi^2/6 - 2(\ell nr)^2] \qquad (C10)$$

From Equation (C5) I have

$$\dot{\chi} = 2r^2(\dot{\theta}_2 - \dot{\theta}_1) \sin(\theta_1 - \theta_2) \qquad (C11)$$

It is clear from Equation (C11) that for small $N$ exact knowledge of $P_{\dot{\theta}_n}(\dot{\theta}_n)$ is required before rate densities, or joint densities of amplitude and amplitude rate can be found.

I will now perform the calculations required to find ${}_2P_{\dot{\chi}}(\dot{\chi})$ assuming $P_{\dot{\theta}_n}(\dot{\theta}_n)$ is Gaussian and then assuming $P_{\dot{\theta}_n}(\dot{\theta}_n)$ is uniform. For the former:

$$P_{\dot{\theta}_n}(\dot{\theta}_n) = \frac{1}{\sqrt{2\pi\nu^2}} \, e^{-\frac{\dot{\theta}_n^2}{2\nu^2}}, \quad |\dot{\theta}_n| < \infty \tag{C12}$$

The pdf for $t = \sin(\theta_1 - \theta_2)$ is given by

$$P_t(t) = \frac{1}{\pi} \, \frac{1}{\sqrt{1-t^2}}, \quad |t| < 1 \tag{C13}$$

The pdf for $z = \dot{\theta}_2 - \dot{\theta}_1$ is by inspection

$$P_z(z) = \frac{1}{\sqrt{4\pi\nu^2}} \, e^{-\frac{z^2}{4\nu^2}}, \quad |z| < \infty \tag{C14}$$

Because z and t are independent random variables the joint density of z and t is the product of Eqns. (C13) and (C14). I seek the pdf for the product $u = zt$, and explorting symmetry,

$$P_u(u) = \frac{\partial}{\partial u} \int_0^1 \int_0^{u/t} P_{z,t}(z,t) \, dzdt \tag{C15}$$

Differentiating under the integral sign I obtain

$$P_u(u) = \frac{1}{\pi\nu\sqrt{\pi}} \int_0^1 \frac{\exp\left(-\frac{u^2}{4t^2\nu^2}\right)}{t(1-t^2)^{1/2}}\, dt \qquad (C16)$$

I now make the change of variable $u_1 = u^2$ and then integrate and make the final change of variables $\dot{\chi} = 2r^2u_1$ to obtain:

$$2P_{\dot{\chi}}(\dot{\chi}) = \frac{1}{4r^2\pi\nu\sqrt{\pi}} \exp\left[-\frac{\dot{\chi}^2}{32r^4\nu^2}\right] K_o\left[\frac{\dot{\chi}^2}{32r^4\nu^2}\right],$$

$$|\dot{\chi}| < \infty \qquad (C17)$$

where $K_o(z)$ is the Modified Bessel function of order 0.

For $\dot{\theta}_n$ uniformly distributed

$$P_{\dot{\theta}_n}(\dot{\theta}_n) = \begin{cases} \frac{1}{2\sqrt{3}\nu} & |\dot{\theta}_n| < \sqrt{3}\,\nu \\ 0 & \text{elsewhere} \end{cases} \qquad (C18)$$

Note the factors in Eqn. (C18) insure $E[\dot{\theta}_n^2] = \nu^2$ as required. Now the density for $z = \dot{\theta}_2 - \dot{\theta}_1$ is

$$P_z(z) = \begin{cases} \frac{1}{2\sqrt{3}\nu}\left[1 - \frac{|z|}{2\sqrt{3}\nu}\right], & |z| < 2\sqrt{3}\nu \\ 0 & \text{elsewhere} \end{cases} \qquad (C19)$$

The pdf for $t = \sin(\theta_1 - \theta_2)$ is given by Eqn. (C13). Defining $u = zt$ I integrate over the joint density as before. The integration is non trivial and requires

careful concern for the limits:

$$P_u(u) = \frac{\partial}{\partial u}\int_{\frac{u}{2\sqrt{3}\nu}}^{1}\int_{0}^{u/t} P_{z,t}(z,t)\,dzdt$$

$$+ \frac{\partial}{\partial u}\int_{0}^{u/2\sqrt{3}\nu}\int_{0}^{2\sqrt{3}\nu} P_{z,t}(z,t)\;dzdt \qquad \text{(C20)}$$

In each case I perform the integration over z first and then differentiate under the remaining integral, and integrate. After making the final change of variables $\dot{\chi} = 2r^2u$ I have:

$$2P_{\dot{\chi}}(\dot{\chi}) = \frac{1}{4r^2\sqrt{3}\nu\pi}\left\{\ell n\left[\frac{1+\sqrt{1-\left(\frac{\dot{\chi}}{4r^2\sqrt{3}\nu}\right)^2}}{1-\sqrt{1-\left(\frac{\dot{\chi}}{4r^2\sqrt{3}\nu}\right)^2}}\right] - 2\sqrt{1-\frac{|\dot{\chi}|}{4r^2\sqrt{3}\nu}}\right\}, \quad |\dot{\chi}| < 4r^2\sqrt{3}\nu \qquad \text{(C21)}$$

C.2 Solution for $N = 3$

For this case following Pearson [38],

$$P_\rho(\rho) = \begin{cases} \dfrac{\sqrt{\rho}}{\pi^2 r^{3/2}} \alpha K\left(\frac{\pi}{2}, \alpha\right), & 0 < \rho < r \\ \dfrac{\sqrt{\rho}}{\pi^2 r^{3/2}} K\left(\frac{\pi}{2}, \frac{1}{\alpha}\right), & r < \rho < 3r \\ 0, & \text{elsewhere} \end{cases} \qquad (C22)$$

where

$$\alpha^2 = \frac{16 r^3 \rho}{(\rho+r)^3 (3r-\rho)} ,$$

and $K(\frac{\pi}{2}, \alpha)$ is the complete elliptic integral of the first kind. Note that numerical integration is now required to obtain the moments.

Transforming to $\chi$ and $\Lambda$:

$$3P_\chi(\chi) = \begin{cases} \dfrac{1}{2\pi^2 r^{3/2} \chi^{1/4}} \beta K\left(\frac{\pi}{2}, \beta\right), & 0 < \chi < r^2 \\ \dfrac{1}{2\pi^2 r^{3/2} \chi^{1/4}} K\left(\frac{\pi}{2}, \frac{1}{\beta}\right), & r^2 < \chi < 9r^2 \\ 0, & \text{elsewhere} \end{cases} \qquad \ldots (C23)$$

where

$$\beta^2 = \frac{16 r^3 \chi^{1/2}}{(\chi^{1/2} + r)^3 (3r - \chi^{1/2})}$$

and lastly,

$$
{}_3P_{\Lambda}(\Lambda) = \begin{cases} \dfrac{\exp(\frac{3\Lambda}{4\varepsilon})}{2\varepsilon\pi^2 r^{3/2}} \; \gamma K\left(\frac{\pi}{2}, \gamma\right), & -\infty < \Lambda < 2\varepsilon \ell n r \\ \dfrac{\exp(\frac{3\Lambda}{4\varepsilon})}{2\varepsilon\pi^2 r^{3/2}} \; K\left(\frac{\pi}{2}, \frac{1}{\gamma}\right), & 2\varepsilon \ell n r < \Lambda < 2\varepsilon \ell n 3r \\ 0, & \text{elsewhere} \end{cases} \qquad \text{(C24)}
$$

where

$$
\gamma^2 = \frac{16 r^3 \exp(\frac{\Lambda}{2\varepsilon})}{[\exp(\frac{\Lambda}{2\varepsilon}) + r]^3 [3r - \exp(\frac{\Lambda}{2\varepsilon})]}
$$

The rate density for $\dot{\chi}$, $\dot{\rho}$, or $\dot{\Lambda}$ assuming a $P_{\dot{\theta}_n}(\dot{\theta}_n)$, are sufficiently more complicated than $N = 2$ that I have not solved for them.

## C.3 Computer Simulation

Figures C1-C9 are histograms of the computer generated samples of the amplitude variables for $N = 2,3$, and 4 paths. The exact pdf for $N = 2$, and 3 is shown with the limiting pdf. Note that for $N = 4$ the performance of the limiting pdf is good enough (see Table V for Chi-square

test results) to warrant use of the limiting forms for $N \geq 4$. In Figure C10, I have plotted Equation (C21) with the histogram of $\dot{\chi}$ for $N = 2$ (recall that the computer simulation assumes $P_{\dot{\theta}_n}(\dot{\theta}_n)$ is uniform), as well as the limiting pdf, Equation (1.4).

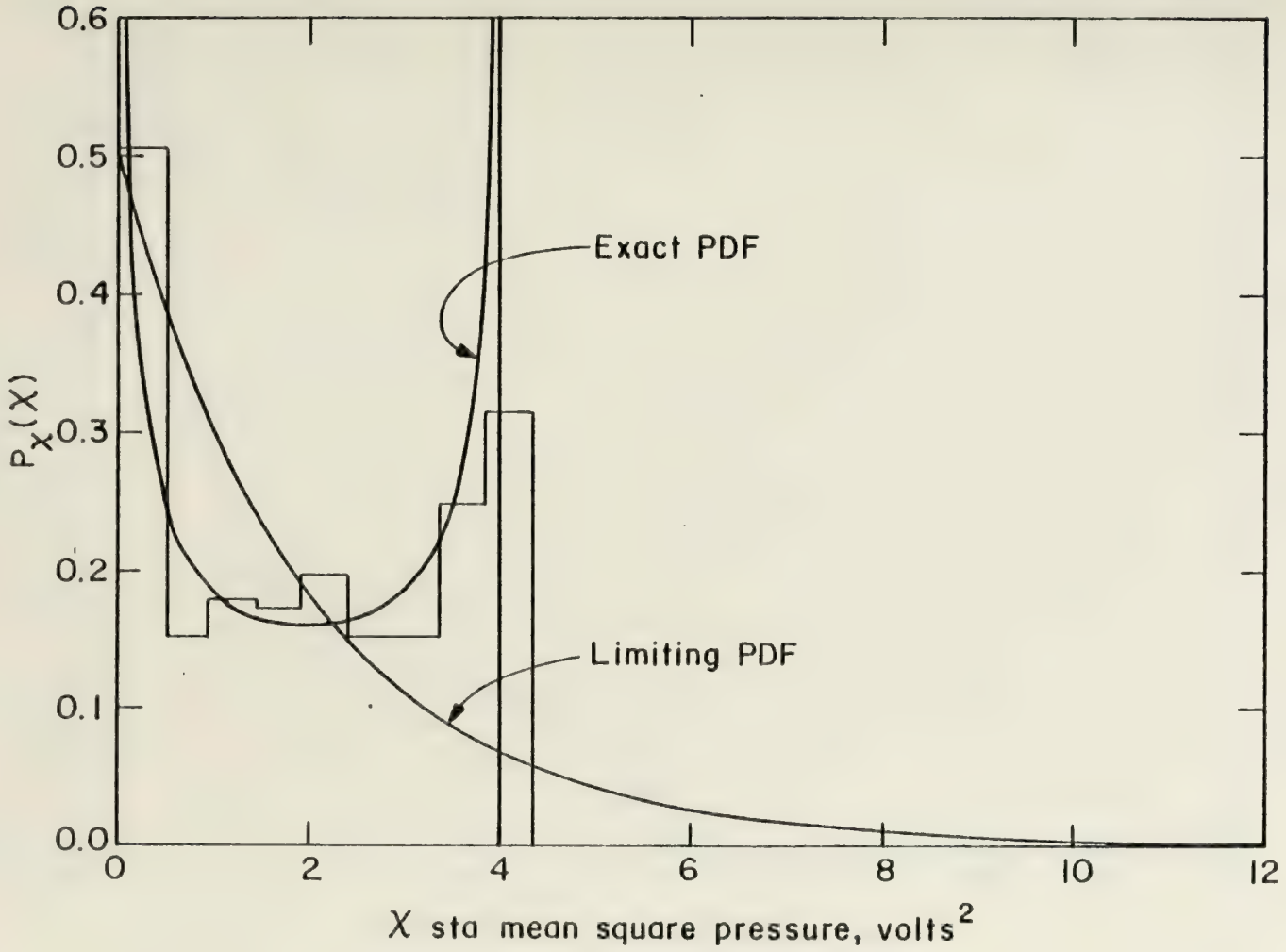


Fig. C1 The computer generated histogram for N = 2 paths, plotted with the exact pdf, equ. (C8), and the limiting pdf ($N \to \infty$), equ. (A2).

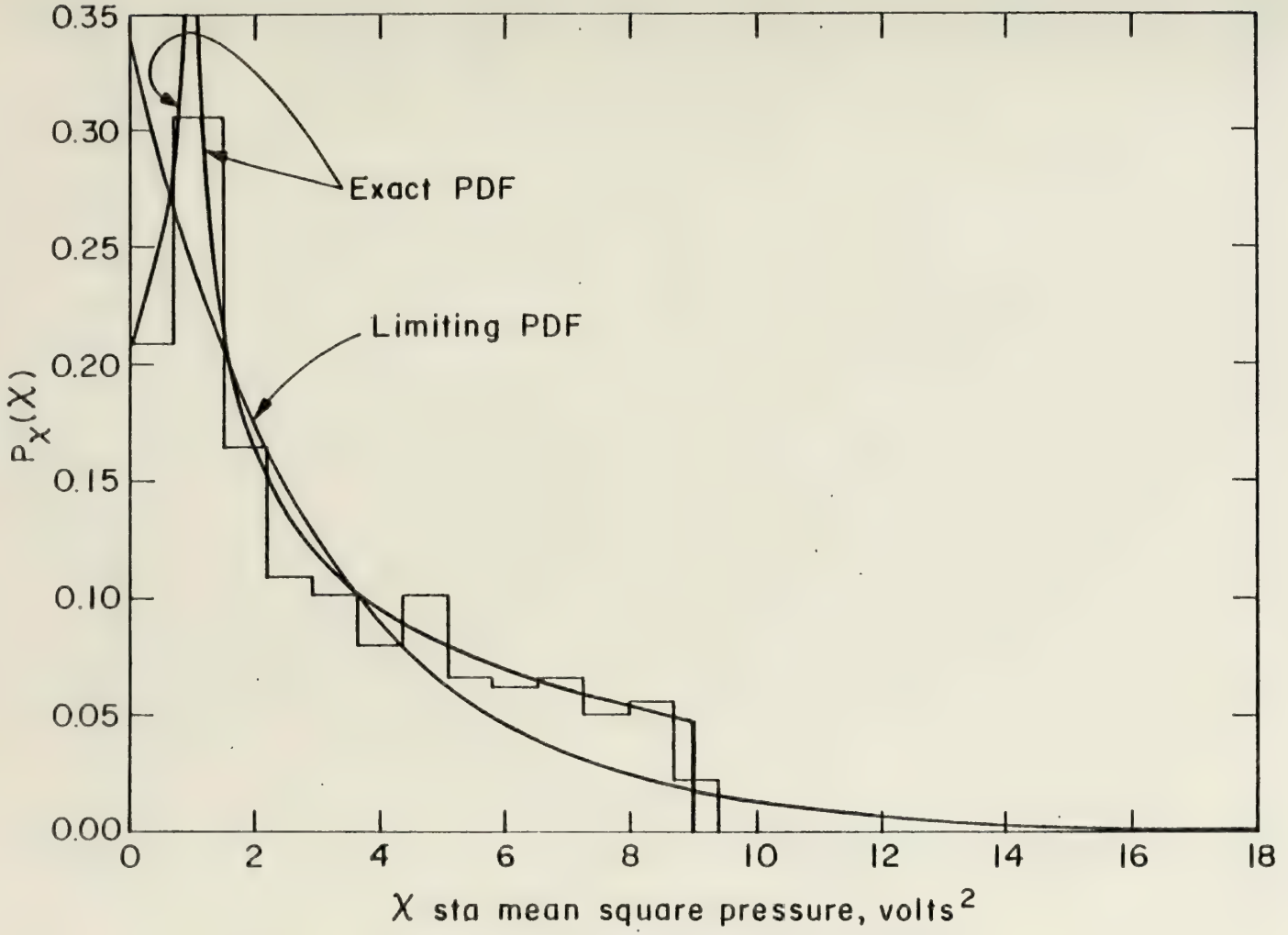


Fig. C2 The computer generated histogram for N = 3 paths, plotted with the exact pdf, equ. (C23), and the limiting pdf ($N \to \infty$), equ. (A2).

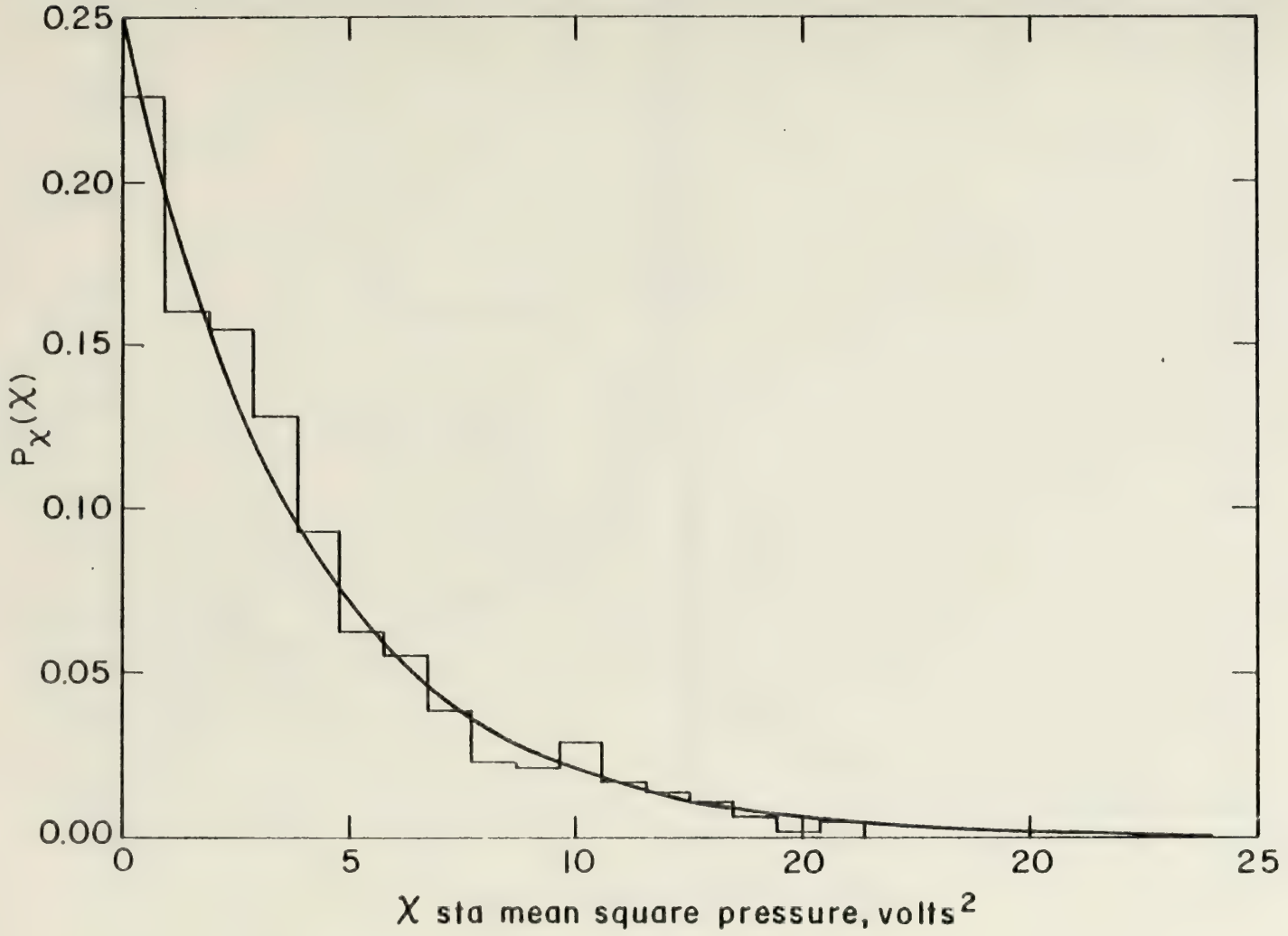


Fig. C3 The computer generated histogram for N = 4 paths plotted with the limiting pdf equ. (A2).

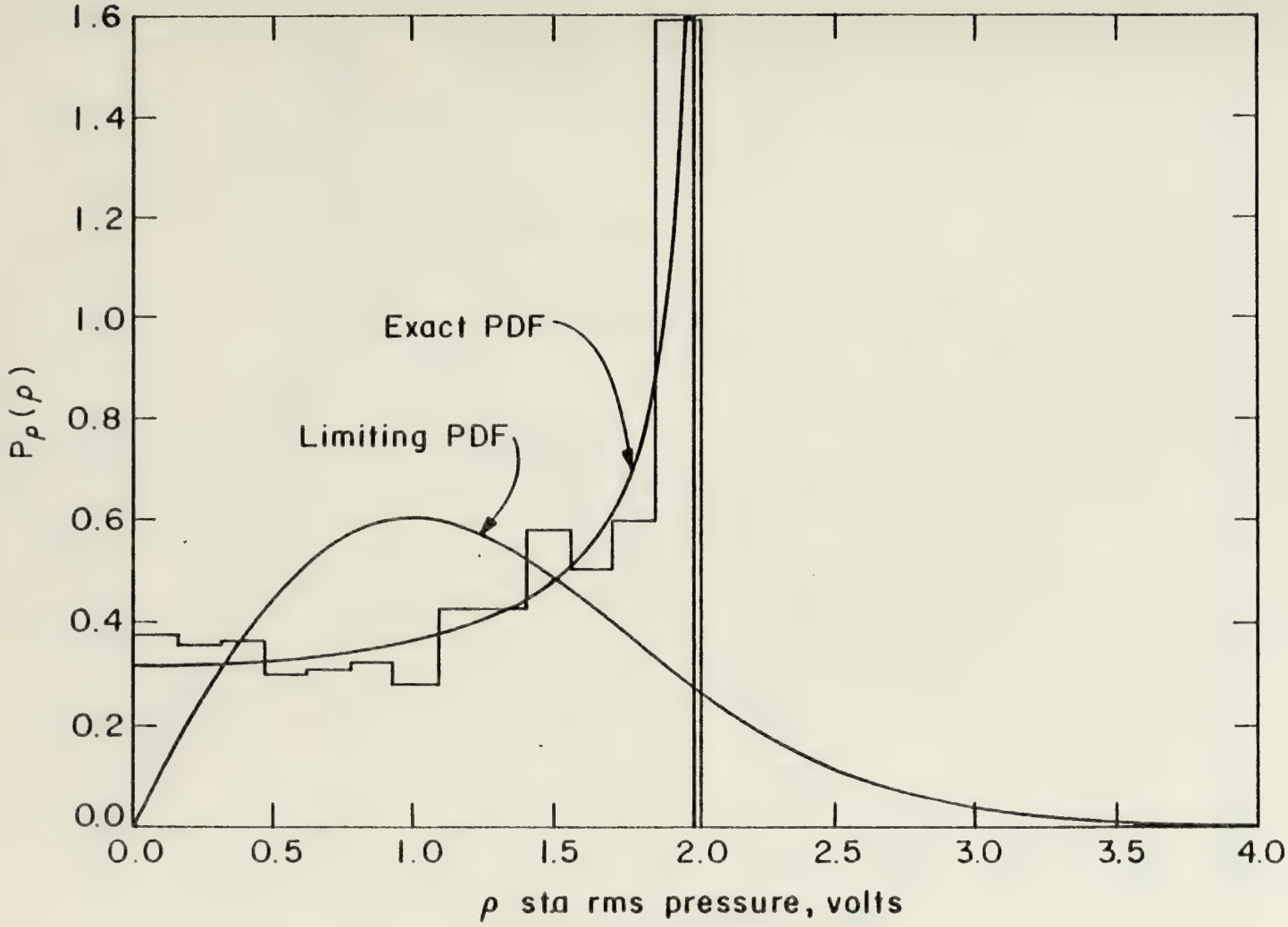


Fig. C4 The computer generated histogram for N = 2 paths, plotted with the exact pdf, equ. (C9), and the limiting pdf ( $N \rightarrow \infty$), equ. (A1).

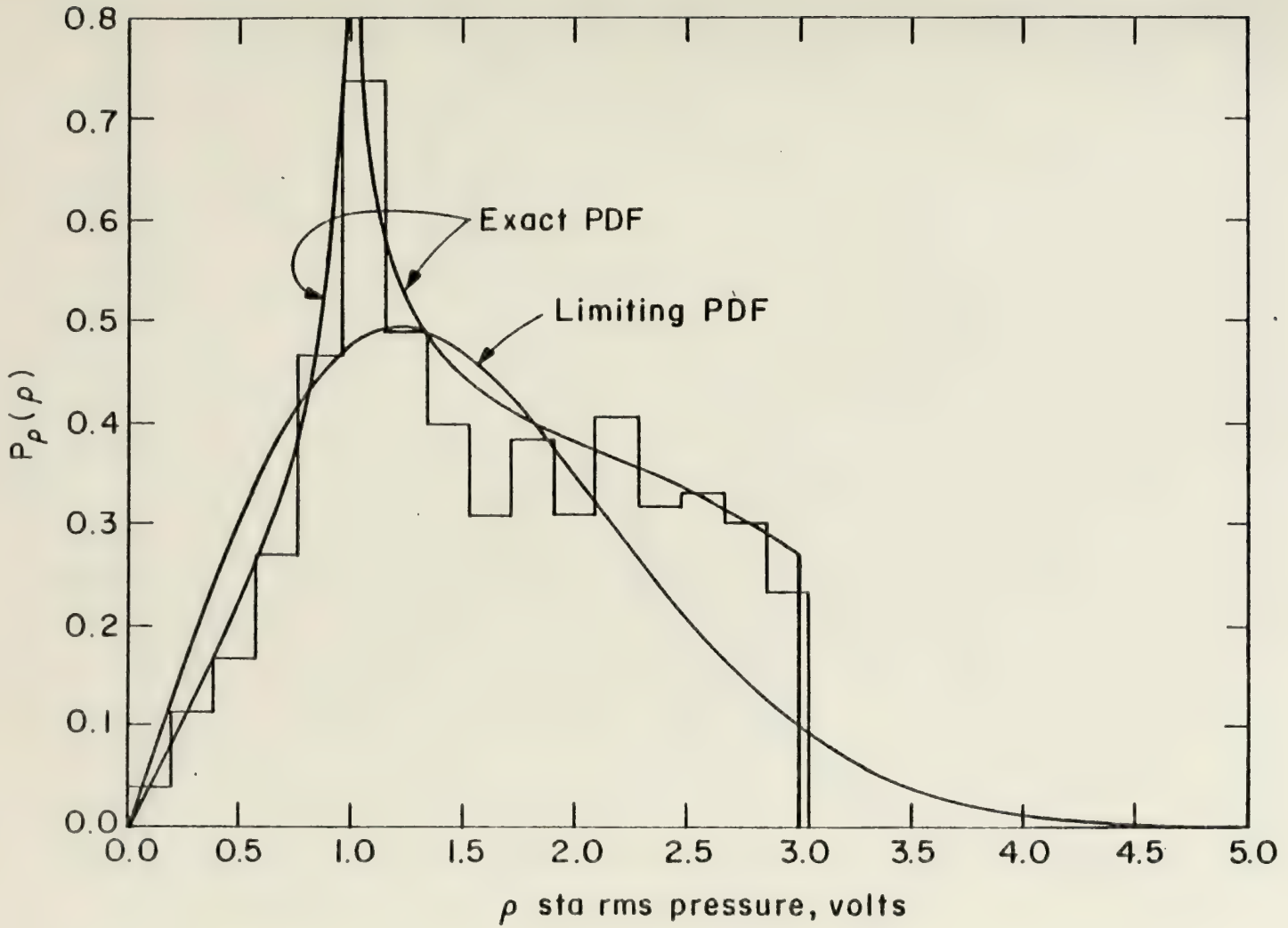


Fig. C5 The computer generated for histogram for N = 3 paths, plotted with the exact pdf, equ. (C22), and the limiting pdf ($N \rightarrow \infty$), equ. (A1).

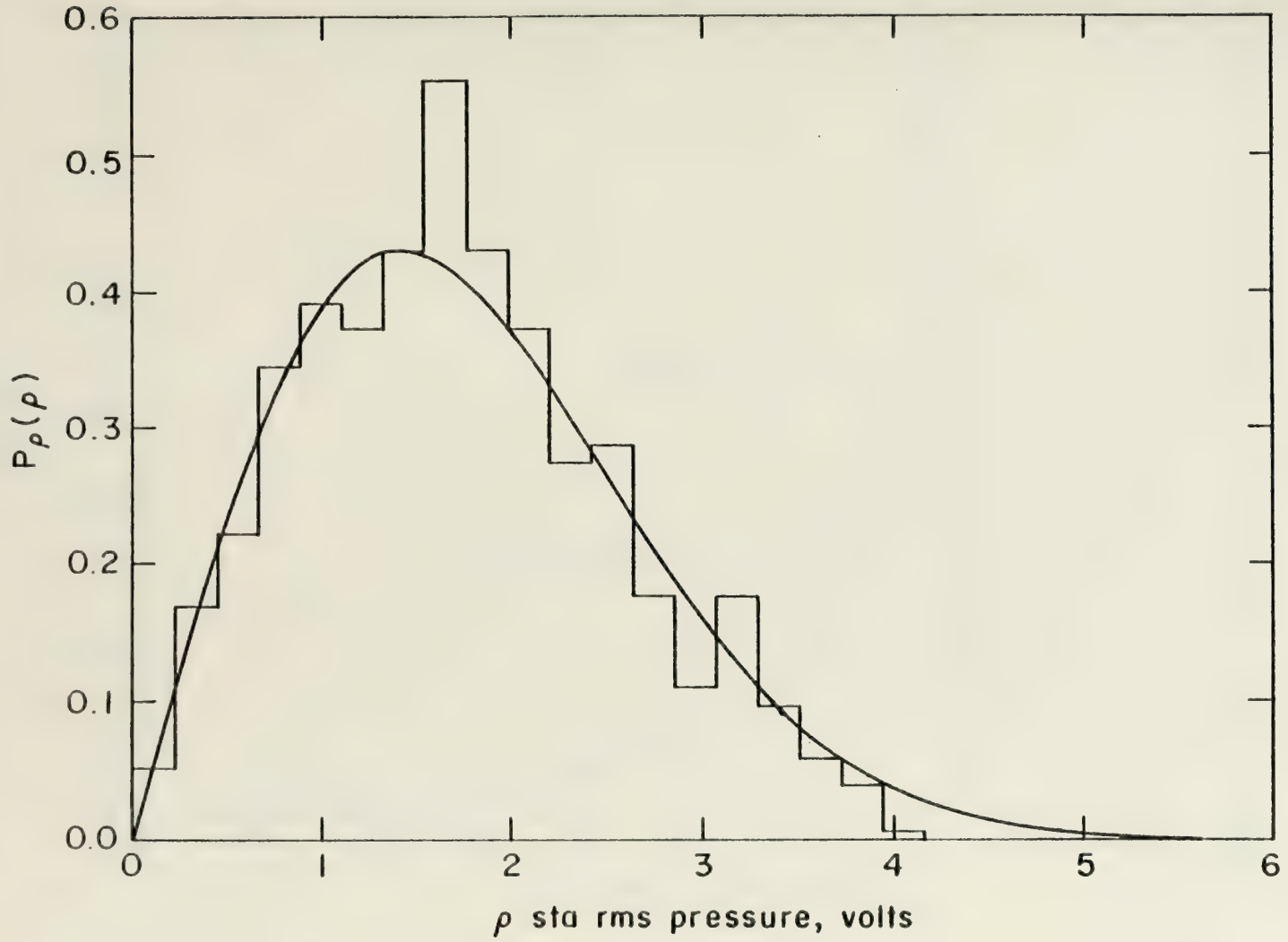


Fig. C6 The computer generated histogram for N = 4 paths, plotted with the limiting pdf, equ. (A1).

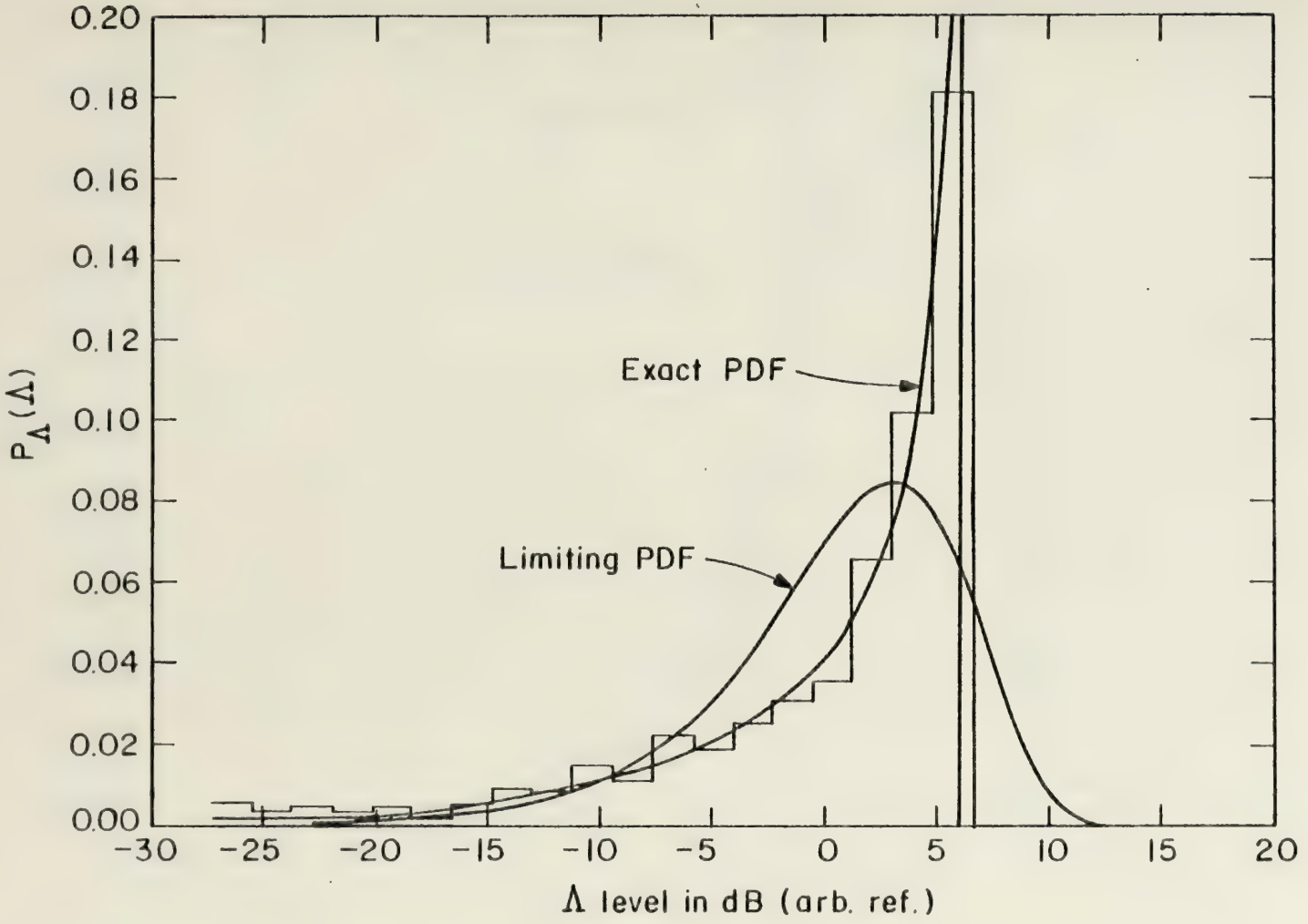


Fig. C7 The computer generated histogram for N = 2 paths, plotted with the exact pdf, equ. (C10), and the limiting pdf ($N \to \infty$), equ. (A3).

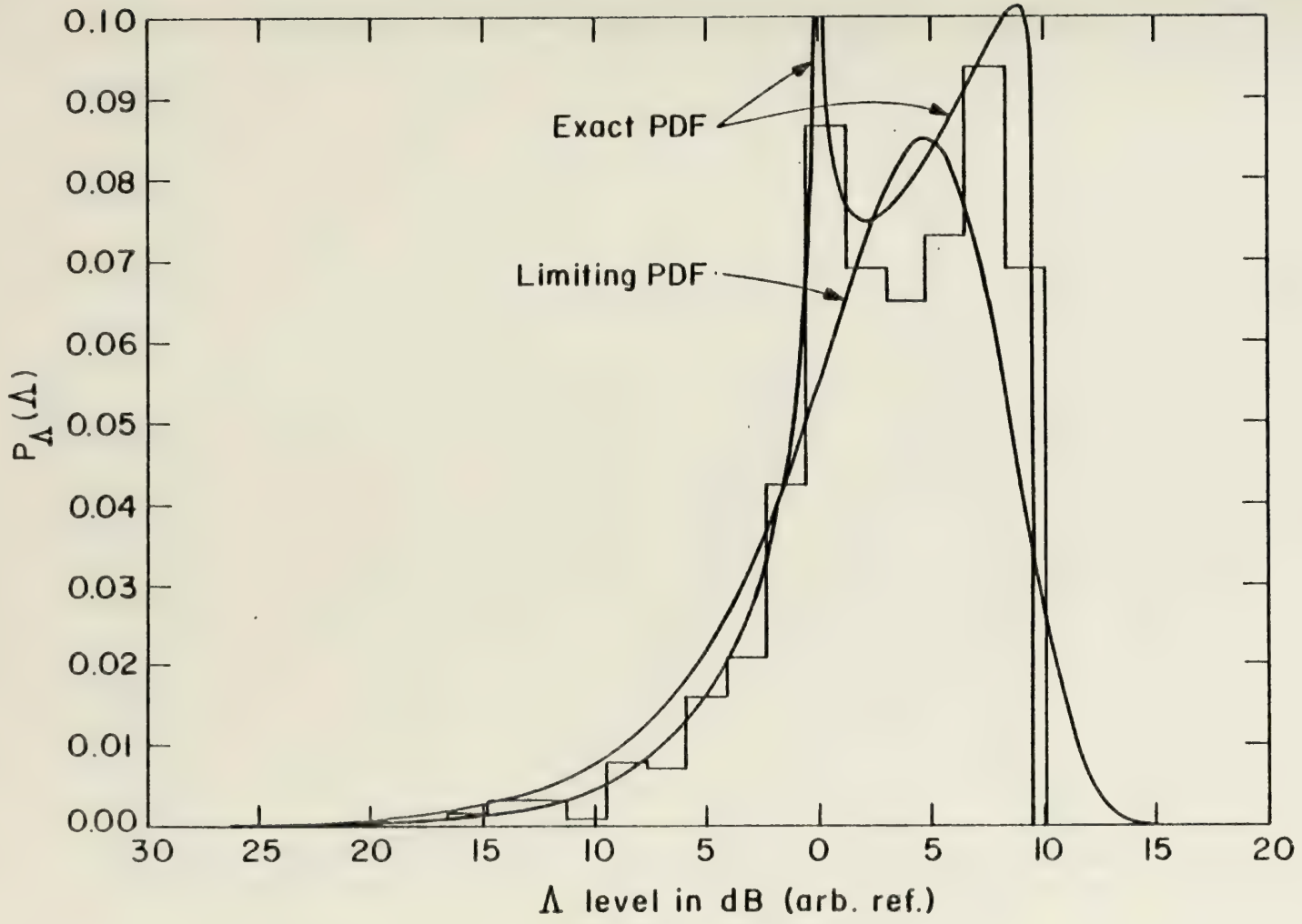


Fig. C8 The computer generated histogram for N = 3 paths, plotted with the exact pdf, equ. (C24), and the limiting pdf ($N \to \infty$) equ. (A3).

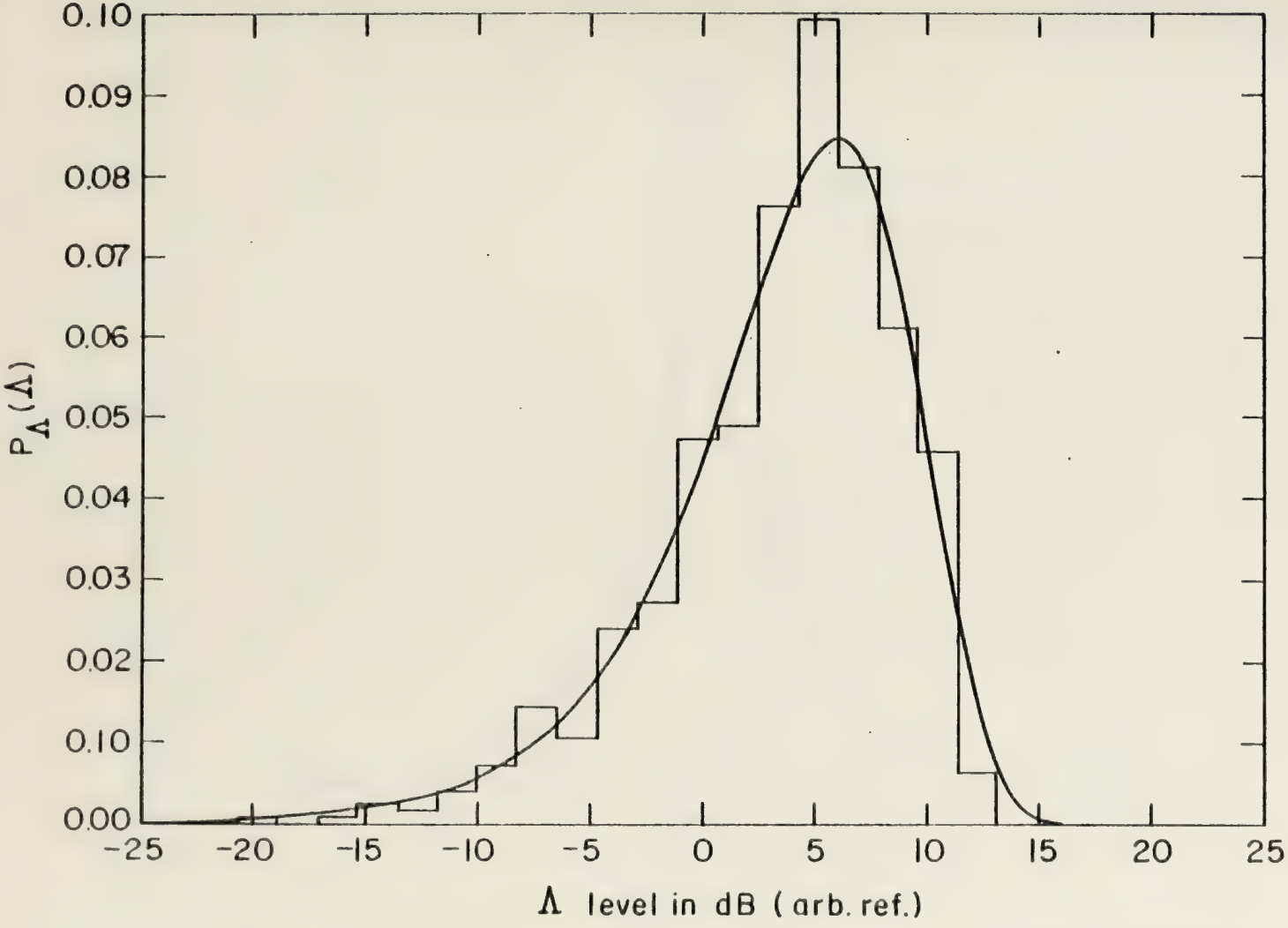


Fig. C9 The computer generated histogram for N = 4 paths, plotted with limiting pdf, equ. (A3).

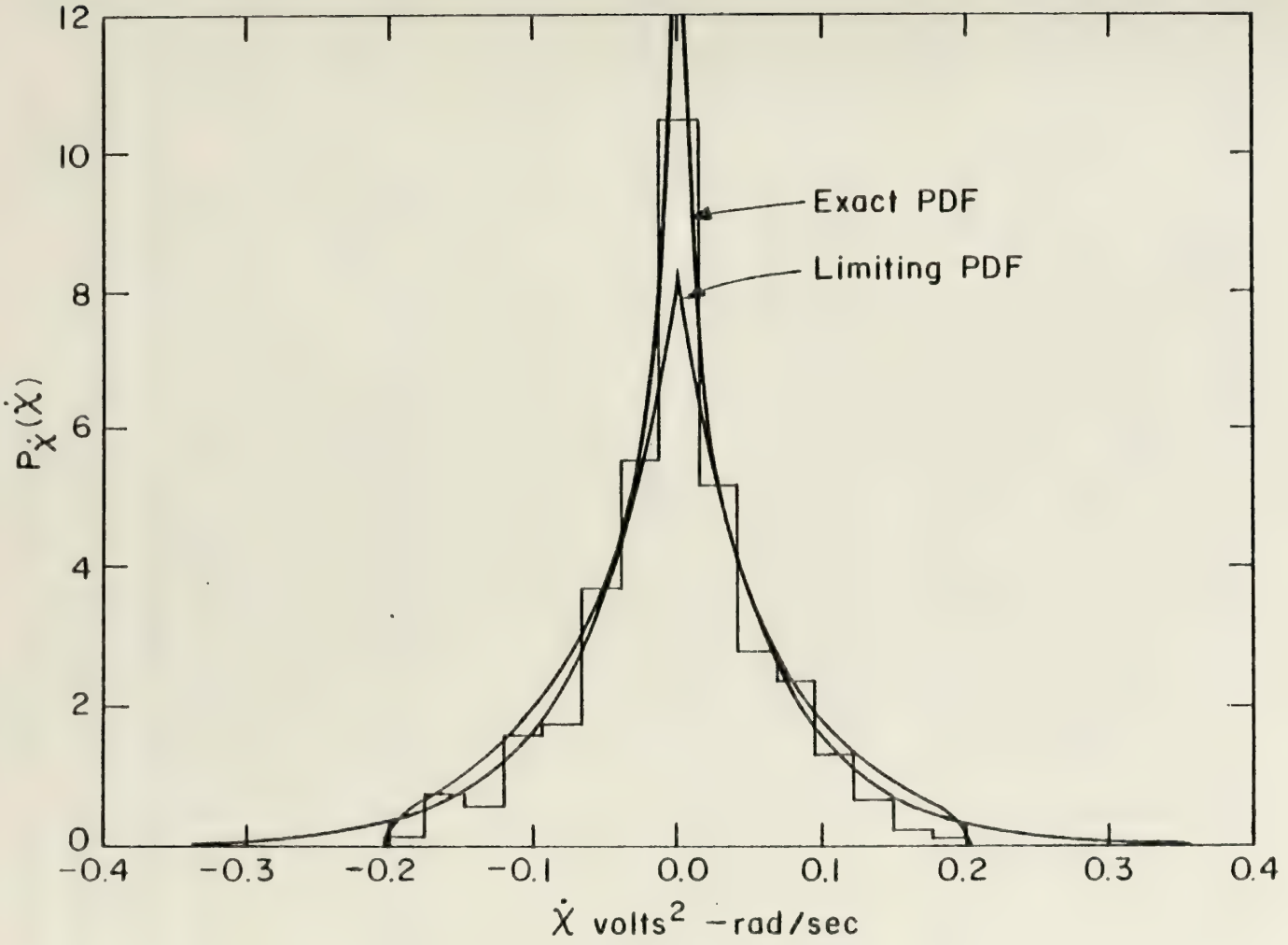


Fig. C10 Computer generated histogram for N = 2 paths, plotted with the exact pdf, equ. (C21), and the limiting pdf ($N \to \infty$), equ. (1.4).

# APPENDIX D

## AMPLITUDE PARAMETER VARIATION

In this appendix I will briefly introduce the analysis involved in amplitude parameter variation. This analysis is the first step towards understanding the statistics of received signals that are either nonstationary in r or $\sigma_1^2$, or when r or $\sigma_1^2$ is purposely modulated at the source.

For the first case, I consider that r is a random variable distributed uniformly between a lower limit of $b \geq 0$, and an upper limit of $a > b$. It is evident from Equation (2.1c) with $L = 1$ that

$$\rho_{AV} = r\rho \tag{D1}$$

where now $\rho$ can be considered a random variable, distributed Rayleigh according to Equation (A1) but in which $\sigma_1^2 = N/2$. Note, however, that there is an implied assumption that $N \geq 4$. From Equation (D1) and the fact that r is a measure of the gain of the signal which can be controlled at the source, or of the change in pathwise signal strength, it is true that r and $\rho$ are independent random variables. This assumes of course that during the experiment the number of paths remains constant. Thus,

forming the joint density of r and $\rho$ I obtain the cumulative distribution function,

$$P_{<\rho_{AV}}(\rho_{AV}) = \frac{1}{(a-b)\sigma_1^2}\int_{\frac{\rho_{AV}}{a}}^{\frac{\rho_{AV}}{b}}\int_{b}^{\frac{\rho_{AV}}{\rho}} \rho \exp(-\frac{\rho^2}{2\sigma_1^2})\,dr\,d\rho$$

$$+ \frac{1}{(a-b)\sigma_1^2}\int_{0}^{\frac{\rho_{AV}}{a}}\int_{b}^{a} \rho \exp(-\frac{\rho^2}{2\sigma_1^2})\,dr\,d\rho \qquad \text{(D2)}$$

Performing the integration and taking $\frac{\partial}{\partial\rho_{AV}} P_{<\rho_{AV}}(\rho_{AV})$ I obtain the final result:

$$P_{\rho_{AV}}(\rho_{AV}) = \frac{1}{(a-b)\sigma_1^2} \frac{\pi}{2}\left[\text{Erf}(\frac{\rho_{AV}}{b\sigma_1\sqrt{2}}) - \text{Erf}(\frac{\rho_{AV}}{a\sigma_1\sqrt{2}})\right] \qquad \text{(D3)}$$

$$\mu_{\rho_{AV}} = (a+b)\frac{\sigma_1}{2}\sqrt{\frac{\pi}{2}}\,,\quad \sigma_{\rho_{AV}} = \frac{a+b}{2}\sigma_1\sqrt{\frac{8}{3}-\frac{\pi}{2}-\frac{8ab}{3(a+b)^2}}$$

Note that when $a = b = r$, $\mu_{\rho_{AV}}$ and $\sigma_{\rho_{AV}}$ assume their no variation values (see Equation A1, Appendix A), and

likewise,

$$\lim_{\substack{a\to r \\ b\to r}} P_{\rho_{AV}}(\rho_{AV}) \to P_{\rho}(\rho)$$

With the appropriate transformations, I get:

$$P_{\chi_{AV}}(\chi_{AV}) = \frac{(\chi_{AV})^{-1/2}}{2\sigma_1(a-b)} \frac{\pi}{2} \left[ \mathrm{Erf}\left(\frac{\sqrt{\chi_{AV}}}{b\sigma_1\sqrt{2}}\right) - \mathrm{Erf}\left(\frac{\sqrt{\chi_{AV}}}{a\sigma_1\sqrt{2}}\right) \right] \tag{D4}$$

$$P_{\Lambda_{AV}}(\Lambda_{AV}) = \frac{1}{\varepsilon} \frac{\exp\left(\frac{\Lambda_{AV}}{2\varepsilon}\right)}{2\sigma_1(a-b)} \frac{\pi}{2} \left\{ \mathrm{Erf}\left[ \frac{\exp\left(\frac{\Lambda_{AV}}{2\varepsilon}\right)}{b\sigma_1\sqrt{2}} \right] - \mathrm{Erf}\left[ \frac{\exp\left(\frac{\Lambda_{AV}}{2\varepsilon}\right)}{a\sigma_1\sqrt{2}} \right] \right\} \tag{D5}$$

Note: $\sigma_1^2 = N/2$ in Equations (D2-D5).

In order to compare the effect of certain levels of uncertainty in r on the pdf for $\rho$, the following procedure must be employed. Given that r is uniformly distributed between b and a, its average value is a+b/2. Plot Equation (A1) with $\sigma_1^2 = \frac{N}{2}\left(\frac{a+b}{2}\right)^2$ and then plot Equation (D3). If this is not done, then one may

erroneously conclude that the effect of uncertainty in r is quite dramatic when in fact it is not!

I have taken various values of a and b such that $\frac{a+b}{2} = 1$ and plotted Equation (A1) with Equation (D3) in Figure D1. Note that with 50% (3dB) uncertainty in r, the variation from Equation (A1) is not terribly significant; however, for uncertainty > 50%, the effect becomes very noticeable in the pdf. In Figure D2 I have plotted Equation (A3) with Equation (D5). As before with 3dB of uncertainty, the effect is small. However, for $\sim$ 7dB or greater uncertainty, the effect is large and in fact is very close to the limiting form (100% or $\infty$dB uncertainty). Nakagami [7] obtains a similar result in relation to uncertainty of the mean intensity in dB of multipath RF propagation. In obtaining the limiting pdf (i.e., 100% uncertainty), it is necessary to let b = 0 and a = 2r in Equations (D2-D5) (note, Erf($\infty$) = 1) and rewrite the equations analytically first, otherwise considerable computer time and/or overflows will result.

Next, I assume r varies sinusoidally about a mean given by a and an amplitude of b. Thus,

$$P_r(r) = \frac{1}{\pi} \frac{1}{\sqrt{b^2 - (r-a)^2}} \quad , \; |r-a| < b$$

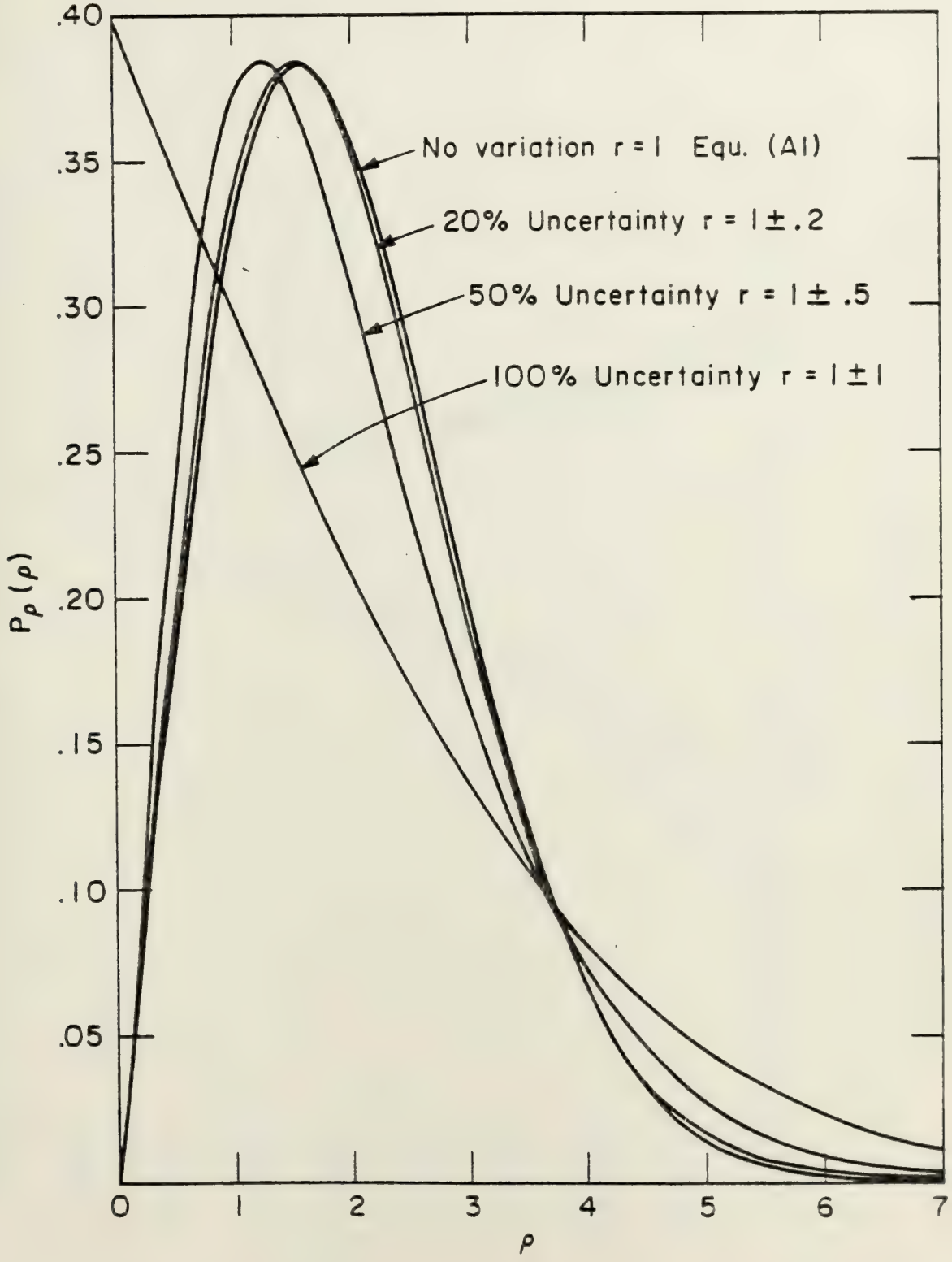


Fig. D1 Comparison plot of the effect of amplitude variation on the pdf for $\rho$. Equ (A1) is plotted with equ (D3) with various levels of uncertainty. N = 5 paths.

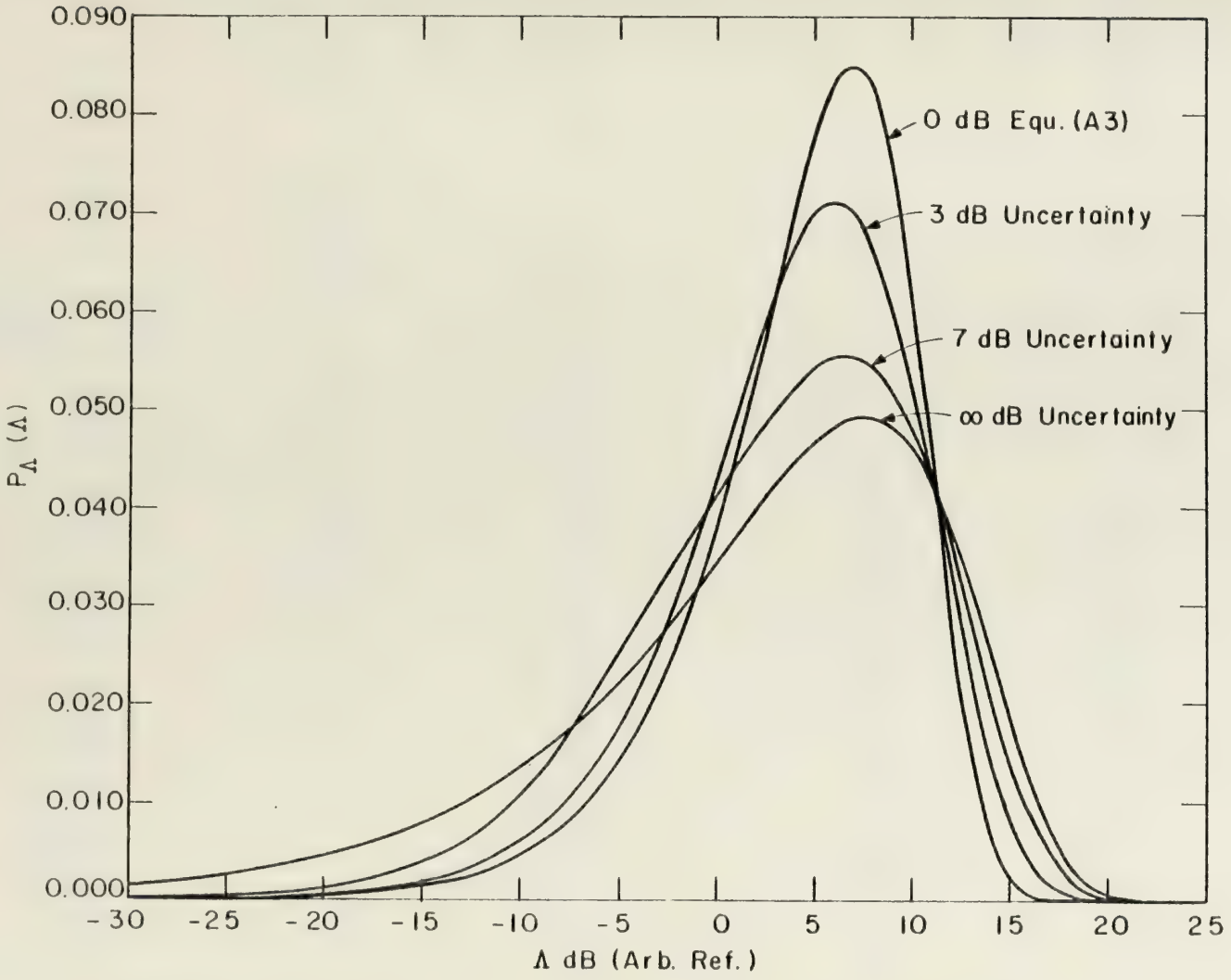


Fig. D2 A comparative plot of the effects of uncertainty in the single path amplitude on the density of the level. Equ (A3) no uncertainty, is plotted with equ (D5) with various values of uncertainty.

The cumulative distribution function is given by

$$P_{<\rho_{AV}}(\rho_{AV}) = \frac{1}{\pi\sigma_1^2}\int_{\frac{\rho_{AV}}{a+b}}^{\frac{\rho_{AV}}{a-b}}\int_{a-b}^{\frac{\rho_{AV}}{\rho}} \frac{\rho}{\sqrt{b^2-(r-a)^2}}\exp(-\frac{\rho^2}{2\sigma_1^2})\,dr\,d\rho$$

$$+\frac{1}{\pi\sigma_1^2}\int_{0}^{\frac{\rho_{AV}}{a+b}}\int_{a-b}^{a+b}\frac{\rho}{\sqrt{b^2-(r-a)^2}}\exp(-\frac{\rho^2}{2\sigma_1^2})\,dr\,d\rho$$

. . .(D6)

Integrating, and differentiating with respect to $\rho_{AV}$ and simplifying as much as possible, I obtain

$$P_{\rho_{AV}}(\rho_{AV}) = \frac{\rho_{AV}}{(a-b)^2\sigma_1^2}\exp\left[\frac{\rho_{AV}^2}{2(a-b)^2\sigma_1^2}\right]$$

$$+\frac{1}{\pi\sigma_1^2}\int_{(\frac{\rho_{AV}}{a+b})^2}^{(\frac{\rho_{AV}}{a-b})^2}\exp(-\frac{y}{2\sigma_1^2})\frac{1}{\sqrt{y(b^2-a^2)+2a\rho_{AV}\sqrt{y}-\rho_{AV}^2}}\,dy$$

. . .(D7)

Unfortunately, the analytical solution to Equation (D7) has not been found. For the special case when a = b, however, the analysis can be concluded:

$$P_{\rho_{AV}}(\rho_{AV}) = \frac{1}{4a^2\sqrt{\pi}\ \sigma_1^2}\left(\frac{\rho_{AV}}{2a\sigma_1}\right)^{-\frac{1}{2}} \exp\left(-\frac{\rho_{AV}^2}{16a^2\sigma_1^2}\right)$$

$$\cdot \left\{a\sigma_1 D_{-\frac{3}{2}}\left(\frac{\rho_{AV}}{2a\sigma_1}\right) + \rho_{AV} D_{-\frac{1}{2}}\left(\frac{\rho_{AV}}{2a\sigma_1}\right)\right\} \qquad \text{(D8)}$$

where $D_\nu(z)$ is the parabolic cylinder function. As a check, the integral of Equation (D8) over $\rho_{AV}$ from 0 to $\infty$ is, in fact, 1.

As a final example, I consider the case in which we allow $\sigma_1^2$ to be a random variable and Equation (A1) to be the conditional pdf of $\rho$ given $\sigma_1^2$. Allowing $\sigma_1^2$ to be uniformly distributed between b and a, and applying Bayes Theorem, I get:

$$P_{\rho_{AV}}(\rho_{AV}) = \frac{1}{a-b}\int_b^a \frac{\rho_{AV}}{\sigma_1^2}\exp\left(-\frac{\rho_{AV}^2}{2\sigma_1^2}\right)d\sigma_1^2 \qquad \text{(D9)}$$

then:

$$P_{\rho_{AV}}(\rho_{AV}) = \frac{\rho_{AV}}{a-b}\left[E_1(\frac{\rho_{AV}^2}{2a}) - E_1(\frac{\rho_{AV}^2}{2b})\right] \qquad (D10)$$

where $E_1(z)$ is the exponential integral. Applying the identity [18]:

$$E_1(z) = -\gamma - \ln z - \sum_{n=1}^{\infty} \frac{(-1)^n z^n}{nn!}, \quad (|\arg z| < \pi)$$

where $\gamma$ is Euler's constant = .5772... I obtain

$$P_{\rho_{AV}}(\rho_{AV}) = \frac{\rho_{AV}}{a-b}\left\{\ln\frac{a}{b} + \sum_{n=1}^{\infty}(-1)^n(\frac{\rho_{AV}^2}{2b})^n\frac{1}{nn!} - \sum_{n=1}^{\infty}(-1)^n(\frac{\rho_{AV}^2}{2a})^n\frac{1}{nn!}\right\} \qquad (D11)$$

Although I did not plot Equation (D11), the numbers I obtained for relative levels of uncertainty in $\sigma_1^2$ agree

closely with the results of uncertainty in r, and the effect of $\sigma_1^2$ randomization (i.e., $\leq$ 3dB uncertainty) on the amplitude densities appears also to be small while limiting forms are obtained for uncertainty $\geq$ 7dB.

A more thorough investigation of this phenomena could uncover the statistical dependencies on identifiable non-stationarities, such as propagation loss due to changing ranges or other oceanic or experimental factors which result in the temporal dependence of r or $\sigma_1^2$. The effects on the statistics can then be analyzed using the procedures employed above.

# BIOGRAPHICAL NOTE

The author was born on February 2, 1950. He attended Harvard University (1968-72) where he received his Bachelor of Arts degree in Engineering and Applied Physics (1972), his Master of Science in Applied Mathematics (1972), and was commissioned an Ensign in the regular Navy (1972). He served two years as the Anti-Submarine Warfare Officer aboard the U.S.S. Joseph P. Hewes (FF-1078) which saw action in Vietnam and was in the Mediterranean during the Yom Kippur War (1973). He also served one year as the Staff Weapons Officer, Commander Destroyer Squadron 12 Staff, homeported in Athens, Greece. In September 1975, he enrolled at the Massachusetts Institute of Technology where he is currently a candidate for the degree of Doctor of Philosophy. The author is still on active duty in the United States Navy and is currently a Lieutenant. The author is married to the former Litsa Pentaskoufi of Patras, Greece, and they have one daughter, Lara, who is two years old.

188141

Thesis
M58145 Mikhalevsky
c.1 The statistics of finite bandwidth modulated acoustic signals propagated to long ranges in the ocean, including multiple source effects.

Thesis
M58145 Mikhalevsky
c.1 The statistics of finite bandwidth modulated acoustic signals propagated to long ranges in the ocean, including multiple source effects.

188141

thesM58145
The statistics of finite bandwidth, modu
3 2768 001 88330 9
DUDLEY KNOX LIBRARY